Long-Baseline Neutrino Experiment (LBNE) Project
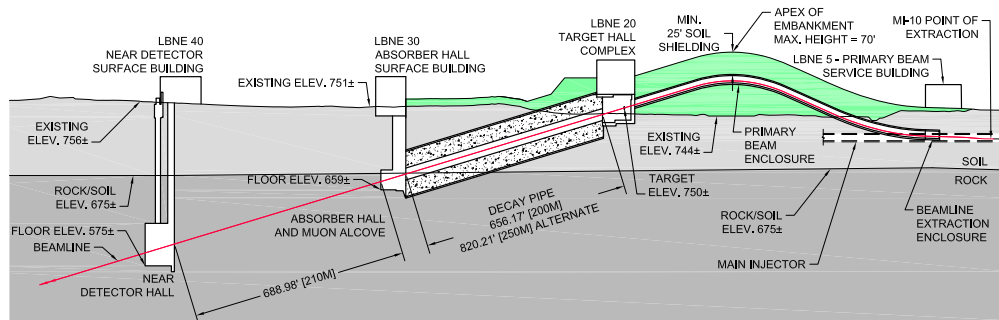
Conceptual Design Report

Volume 2: The Beamline at the Near Site

July 3, 2012

Contents

Acronyms, Abbreviations and Units

AC	alternating current
ACNET	Accelerator Controls NETwork
ASME	American Society of Mechanical Engineers
atm	atmosphere
AWG	American Wire Gauge
BLIP	Brookhaven Linac Isotope Producer
BLM	Beam-loss monitor
BNB	Booster Neutrino Beam
BNL	Brookhaven National Laboratory
BPM	Beam-position monitor
BuLB	Basic Micro Learning Box
CAMAC	Computer Automated Measurement and Control
CCD	charge-coupled device
CDC	Critical Device Controller
CDR	Conceptual Design Report
CORS	Continuously Observed Reference Station
CP	charge parity
CUB	Central Utilities Building
DAQ	data acquisition
DC	direct current

DCCT	DC current transformers
DI	de-ionization
DOE	Department of Energy
DS	downstream
DUSEL	Deep Underground Science and Engineering Laboratory
E-Net	Ethernet
ESS	Electrical Safety System
FEA	finite element analysis
FF	final focus
FFT	fast fourier transform
FODO	A repetitive configuration of focusing (F) and defocusing (D) magnetic elements separated by a fixed spacing of non-focusing elements (O)
FPGA	field programmable gate array
FRCM	Fermilab Radiological Control Manual
ft	foot or feet
gpm	gallons per minute
GPS	global positioning system
GRS	Geodetic Reference System
hBN	Hexagonal boron nitride
hp	horsepower
HRM	Hot-link Rack Monitor
HTO	tritiated water molecule
Hx	Heat Exchanger
ID	inner diameter
IHEP	Institute for high energy physics
IMU	Inertial Measuring Unit
INS	Inertial Navigation System

IPM	Ionization Profile Monitor
ITRF	International Terrestrial Reference Frame
L	used here to indicate the "level" underground, in feet
LC	inductive/capacitive
LCW	low-conductivity water
LHC	Large Hadron Collider
LOTO	lock-out/tag-out
MAD	Methodical Accelerator Design
MARS	a monte carlo code
MCC	Motor control centers
MECAR	Main Injector Excitation Controller and Regulator
MI	Main Injector
MI-10 (60, 64 etc)	Surface buildings above extraction point on Main
MIBS	Main Injector Beam Synchronous Clock
MPS	machine-protection system
MUX	multiplex
NAD	North American Datum
NGS	National Geodetic Survey
NuMI	Neutrinos at the Main Injector (Beamline facility at Fermilab)
OD	outer diameter
P5	Particle Physics Project Prioritization Panel
PLC	Programmable Logic Controller
POCO	name of graphite supplier (POCO Graphite)
POT	Protons on Target
Ppm	parts per million
PW	Pond Water

RAL	Rutherford Appleton Laboratory
RAW	Radioactive water
RF	radio frequency
RH	remote handling
RSS	Radiation Safety Interlock Systems
SCR	silicon-controlled rectifier
SEM	secondary emission monitor
SI	Systems Integration
TCLK	Tevatron Clock
TCV	Temperature control valve
TH	Target Hall
THI	Target Hall instrumentation
THSP	Target Hall shield pile
TLM	Total loss monitors
TLM	Total-loss monitor
UHV	Ultra High Vacuum
US	upstream
VA	Volt-Ampere (also kVA, MVA)
VAC	Volts AC (also mVAC, kVAC, MVAC)
VFD	variable-frequency drive
VME	VMEbus, VERSAmodule Eurocard bus, ANSI/IEEE 1014-1987; a computer bus standard
WBS	Work Breakdown Structure

List of Figures

List of Tables

1   Introduction

1.1   Introduction to the LBNE Project

The Long-Baseline Neutrino Experiment (LBNE) Project team has prepared this Conceptual Design Report (CDR) which describes a world-class facility to enable a compelling research program in neutrino physics. The ultimate goal in the operation of the facility and experimental program is to measure fundamental physical parameters, explore physics beyond the Standard Model and better elucidate the nature of matter and antimatter.

Although the Standard Model of particle physics presents a remarkably accurate description of the elementary particles and their interactions, it is known that the current model is incomplete and that a more fundamental underlying theory must exist. Results from the last decade, revealing that the three known types of neutrinos have nonzero mass, mix with one another and oscillate between generations, point to physics beyond the Standard Model. Measuring the mass and other properties of neutrinos is fundamental to understanding the deeper, underlying theory and will profoundly shape our understanding of the evolution of the universe.

1.1.1   About this Conceptual Design Report

The LBNE Conceptual Design Report is intended to describe, at a conceptual level, the scope and design of the experimental and conventional facilities that the LBNE Project plans to build to address a well-defined set of neutrino-physics measurement objectives. At this Conceptual Design stage the LBNE Project presents a *Reference Design* for all of the planned components and facilities, and alternative designs that are still under consideration for particular elements. The scope includes

- an intense neutrino beam aimed at a far site

- detectors located at the near site just downstream of the neutrino source

- a massive neutrino detector located at the far site

- construction of conventional facilities at both the near and far sites

The selected near and far sites are Fermi National Accelerator Laboratory (Fermilab), in Batavia, IL and Sanford Underground Laboratory at Homestake (Sanford Laboratory), respectively. The latter is the site of the formerly proposed Deep Underground Science and Engineering Laboratory (DUSEL) in Lead, South Dakota.

This CDR is organized into six stand-alone volumes, one to describe the overall LBNE Project and one for each of its component subprojects:

- Volume 1: The LBNE Project

- Volume 2: The Beamline at the Near Site

- Volume 3: Detectors at the Near Site

- Volume 4: The Liquid Argon Detector at the Far Site

- Volume 5: Conventional Facilities at the Near Site

- Volume 6: Conventional Facilities at the Far Site

Volume 1 is intended to provide readers of varying backgrounds an introduction to LBNE and to the following volumes of this CDR. It contains high-level information and refers the reader to topic-specific volumes and supporting documents, also listed in Section 1.1.5. Each of the other volumes contains a common, brief introduction to the overall LBNE Project, an introduction to the individual subproject and a detailed description of its conceptual design.

1.1.2   LBNE and the U.S. Neutrino-Physics Program

In its 2008 report, the Particle Physics Project Prioritization Panel (P5) recommended a world-class neutrino-physics program as a core component of the U.S. particle physics program [1]. Included in the report is the long-term vision of a large detector at the Sanford Laboratory and a high-intensity neutrino source at Fermilab.

On January 8, 2010, the Department of Energy (DOE) approved the Mission Need for a new long-baseline neutrino experiment that would enable this world-class program and firmly establish the U.S. as the leader in neutrino science. The LBNE Project is designed to meet this Mission Need.

With the facilities provided by the LBNE Project, the LBNE Science Collaboration proposes to mount a broad attack on the science of neutrinos with sensitivity to all known parameters in a single experiment. The focus of the program will be the explicit demonstration of leptonic CP violation, if it exists, by precisely measuring the asymmetric oscillations of muon-type neutrinos and antineutrinos into electron-type neutrinos and antineutrinos.

The experiment will result in the most precise measurements of the three-flavor neutrino-oscillation parameters over a very long baseline and a wide range of neutrino energies, in particular, the CP-violating phase in the three-flavor framework. The unique features of the experiment – the long baseline, the broad-band beam, and the high resolution of the detector – will enable the search for new physics that manifests itself as deviations from the expected three-flavor neutrino-oscillation model.

The configuration of the LBNE facility, in which a large neutrino detector is located deep underground, could also provide opportunities for research in other areas of physics, such as nucleon decay and neutrino astrophysics, including studies of neutrino bursts from supernovae occuring in our galaxy. The scientific goals and capabilities of LBNE are outlined in Volume 1 of this CDR and described fully in the LBNE Case Study Report (Liquid Argon TPC Far Detector) [2] and the 2010 Interim Report of the Long-Baseline Neutrino Experiment Collaboration Physics Working Groups [3].

1.1.3   LBNE Project Organization

The LBNE Project Office at Fermilab is headed by the Project Manager and assisted by the Project Engineer, Project Systems Engineer and Project Scientist. Project Office support staff include a Project Controls Manager and supporting staff, a Financial Manager, an Environment, Safety and Health (ES&H) Manager, a Computing Coordinator, Quality Assurance and Risk Managers, a documentation team and administrative support. The Beamline, Liquid Argon Far Detector and Conventional Facilities subprojects are managed by the Project Office at Fermilab, while the Near Detector Complex subproject is managed by a Project Office at Los Alamos National Laboratory (LANL).

More information on Project Organization can be found in Volume 1 of this CDR. A full description of LBNE Project management is contained in the LBNE Project Management Plan [4].

1.1.4   Principal Parameters of the LBNE Project

The principal parameters of the major Project elements are given in Table 1–1.

Table 1–1: LBNE Principal Parameters

Project Element Parameter	Value
Near- to Far-Site Baseline	1,300 km
Primary Proton Beam Power	708 kW, upgradable to 2.3 MW
Protons on Target per Year	6.5×10^{20}
Primary Beam Energy	60 – 120 GeV (tunable)
Neutrino Beam Type	Horn-focused with decay volume
Neutrino Beam Energy Range	0.5 – 5 GeV
Neutrino Beam Decay Pipe Diameter × Length	4 m × 200 m
Near Site Neutrino Detector Type	Liquid Argon Time Projection Chamber (LArTPC) Tracker
Near Site Neutrino Detector Active Mass	18 ton
Far Detector Type	LArTPC
Far Detector Active (Fiducial) Mass	40 (33) kton
Far Detector Depth	1480 m

1.1.5 Supporting Documents

A host of information related to the CDR is available in a set of supporting documents. Detailed information on risk analysis and mitigation, value engineering, ES&H, costing, project management and other topics not directly in the design scope can be found in these documents, listed in Table 1–2. Each document is numbered and stored in LBNE's document database, accessible via a username/password combination provided by the Project. Project documents stored in this database are made available to internal and external review committees through Web sites developed to support individual reviews.

Table 1–2: LBNE CD-1 Documents

Title	LBNE Doc Number(s)
Acquisition Plan	5329
Alternatives Analysis	4382
Case Study Report; Liquid Argon TPC Detector	3600
Configuration Management Plan	5452
DOE Acquisition Strategy for LBNE	5442
Integrated Environment, Safety and Health Management Plan	4514
LAr-FD Preliminary ODH Analysis	2478
Global Science Objectives, Science Requirements and Traceback Reports	4772
Preliminary Hazard Analysis Report	4513

Preliminary Project Execution Plan	5443
Preliminary Security Vulnerability Assessment Report	4826
Project Management Plan	2453
Project Organization Chart	5449
Quality Assurance Plan	2449
Report on the Depth Requirements for a Massive Detector at Homestake	0034
Requirements, Beamline	4835
Requirements (Parameter Tables), Far Detector	3747 (2843)
Requirements, Far Site Conventional Facilities	4408
Requirements, Near Detectors	5579
Requirements, Near Site Conventional Facilities	5437
Risk Management Plan	5749
Value Engineering Report	3082
Work Breakdown Structure (WBS)	4219

1.2   Introduction to the LBNE Beamline

1.2.1   Overview and General Layout

The LBNE Beamline at Fermilab will be designed to provide a neutrino beam of sufficient intensity and energy to meet the goals of the LBNE experiment with respect to long-baseline neutrino-oscillation physics. The design is a conventional, horn-focused neutrino beamline. The components of the beamline will be designed to extract a proton beam from the Fermilab Main Injector (MI) and transport it to a target area where the collisions generate a beam of charged particles. This secondary beam, aimed toward the Far Detector, is followed by a decay-pipe tunnel where the particles of the secondary beam decay to generate the neutrino beam. At the end of the decay pipe, an absorber pile removes the residual hadrons.

The facility is designed for initial operation at proton-beam power of 708 kW, with the capability to support an upgrade to 2.3 MW. In the reference design, extraction of the proton beam occurs at MI-10, a new installation. After extraction, this primary beam establishes a horizontally straight compass heading west-northwest toward the Far Detector, but will be bent upward to an apex before being bent downward at the appropriate angle, 101 milliradians (5.79°) as shown in Figure 1–1. The primary beam will be above grade for about 700 feet; this design minimizes expensive underground construction and significantly

enhances capability for ground-water radiological protection. The design requires, however, construction of an earthen embankment, or hill, whose dimensions are commensurate with the bending strength of the dipole magnets required for the beamline. The embankment will need to be approximately 1100 feet long and 70 feet high above grade at its peak.
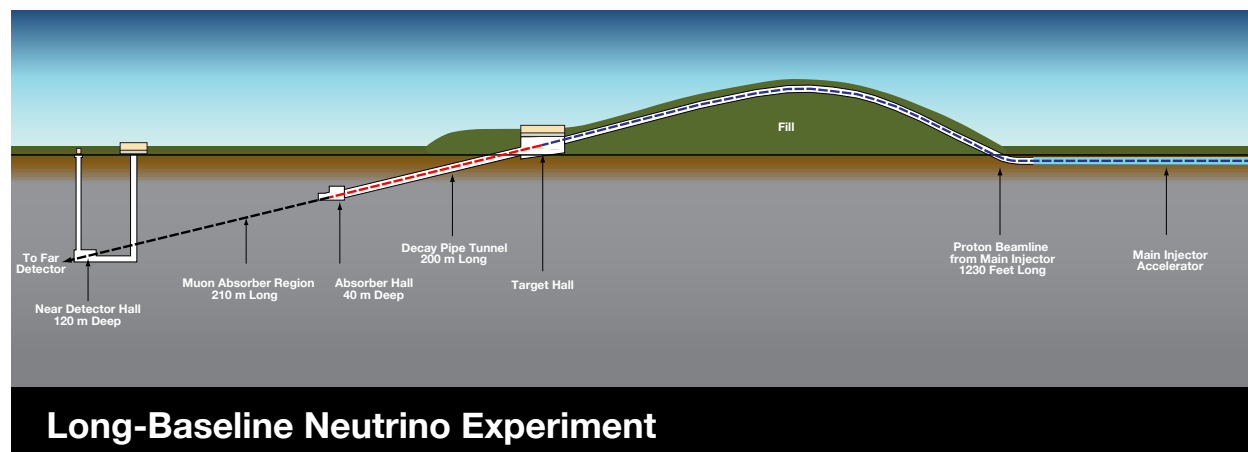
Figure 1–1: Schematic of the systems included in the LBNE Beamline subproject. The top of the engineered hill is 22 m above grade, less than half the height of Wilson Hall.

The target marks the transition from the intense, narrowly directed proton beam to the more diffuse, secondary beam of particles that in turn decay to produce the neutrino beam. The secondary particles are short-lived and each decay generates a muon (in addition to a neutrino), which penetrates deep into the surrounding rock and a neutrino that continues on toward the near and far detectors.

After collection and focusing, the pions and kaons that did not initially decay – the residual particles mentioned above – need a long, unobstructed volume in which to decay. This decay volume in the LBNE reference design is a pipe of circular cross section with its diameter and length optimized such that decays of the pions and kaons result in neutrinos in the energy range useful for the experiment. The decay volume is followed immediately by the absorber, which removes the remaining beam hadrons.

The LBNE Beamline subproject is broken into three principal systems for organizational purposes: the Primary Beam (referring to the components required for the initial, high-intensity proton beam), the Neutrino Beam (for the components used to create a high-intensity neutrino beam from the initial proton beam) and System Integration.

It is important to note that the design and construction of high-intensity neutrino beams has been an integral aspect of Fermilab's program for decades. The experience gained from the various neutrino projects has been employed extensively in the LBNE Beamline conceptual design. In particular, the NuMI beamline serves as the prototype design. Most of the subsystem designs and their integration follow, to a large degree, from previous projects.

Radiological protection is integrated into the LBNE beamline reference design in two important ways. First, shielding is optimized to reduce exposure of personnel to radiation dose and to minimize radioisotope production in ground water within the surrounding rock. Secondly, the handling and control of tritiated water produced in or near the beamline drives many aspects of the design. Production of tritium is unavoidable, and it is necessary to minimize its accumulation underground in the form of tritiated water (HTO).

The reference design for the primary beam and the neutrino beam is suitable for the initial beam power of 708 kW in all respects. Some aspects of the reference design are also appropriate for a beam power of 2.3 MW. These include the radiological shielding and the size of the underground enclosures as well as systems such as the beam absorber and the remote handling, which cannot be upgraded after exposure to a high-intensity beam.

Some aspects of the reference design are planned for a beam power upgrade to 2.3 MW. The underground enclosures will have the appropriate steel and concrete shielding required for future beam upgrades.

1.2.2   Primary Beam

1.2.2.1   Extraction from Fermilab's Main Injector

The primary proton beam for LBNE will be extracted from the Main Injector (MI) using a method called "single-turn" extraction, in which all the protons stored in the MI synchrotron ring will be diverted to the dedicated LBNE beamline within one circuit. Although the NuMI (and NOvA) beam operates at 120 GeV, further studies on optimizing the LBNE signal-to-detector backgrounds may indicate desirability of a lower energy. The design proton energy thus ranges from 60 to 120 GeV. Approximately 4.9×10^{13} protons are extracted every 1.33 seconds at 120 GeV, resulting in a beam power of 708 kW.

The extraction point, located near the MI-10 surface building and called simply *MI-10*, will be a new installation, different from the one used for NuMI and NOvA. The distance from the absorber to the Near Detectors must include enough rock to fully range-out (eliminate) muons in the Near Detectors, and extraction at MI-10 allows for a sufficient distance.

1.2.2.2   Beam Transport

The design of the primary proton beam transport is driven by both the goals of the LBNE physics program and radiological safety concerns. The beam must first of all be intense enough to create a flux of neutrinos at the Far Detectors sufficient to meet the physics objectives of the experiment. Secondly, the beam energy must be set to optimize the energy

Table 1–3: Summary of principal beam design parameters.

Parameter	Value
Protons per cycle (120 GeV)	4.9×10^{13}
Cycle time (120 GeV)	1.33 sec
Duration	1.0×10^{-5} sec
Energy	60 to 120 GeV
Protons on target per year	6.5×10^{20}
Beam size at target $\sigma(x,y)$	1.5 mm
Beam divergence (x,y)	17 μrad

spectrum of the neutrinos, yet not produce excess background signals that could compromise the measurements. And the system must be safe. Together these requirements imply that the beam must reach the target with very low losses to ensure both efficient production of neutrinos as well as minimal radiological activation of components in the beamline. Due to accelerator duty-cycles, we know that some reduction of total beam power at lower energies is likely. And of course sufficient shielding must be in place in case of any accidental mis-steering of the beam.

The primary beamline elements necessary for transport include dipole (bending) magnets, quadrupole (focusing) magnets, corrector magnets, monitoring instrumentation and vacuum equipment. LBNE will use conventional dipole and quadrupole magnets to guide the beam in the right direction and focus it on the target, respectively. Their optics will closely follow the design of the Main Injector elements. The magnets and their power supplies will be optimized for performance and cost, and will include both new and refurbished elements. The LBNE beam optics will be simulated and analyzed for optimum transport properties.

The general primary-beam specifications derived from the requirements are listed in Table 1–3. The accelerator complex and the LBNE Beamline are planned to deliver 6.5×10^{20} primary protons to the neutrino target per year. This number includes allowances for scheduled shutdowns for maintenance and upgrades as well as unscheduled failures estimated from past experience. The fast, "single-turn" extraction technique delivers all the protons in one machine cycle (1.33 seconds) to the LBNE target in 10 microseconds. When synchronized to the detector electronics, this short spill helps ensure a high rejection of background events at the Far Detector that do not originate from the accelerator beam.

1.2.2.3   Beam Stability

The primary beam needs to be stable in position and direction at the neutrino production target. Deviations in the beam position, for example, affect not only the spatial distribution of the distant neutrino flux, but can also affect the energy spectrum. These systematic effects must be minimized to the extent that they become negligible in the physics analyses.

Table 1–4: Beam stability requirements.

Parameter	Value
Position at target	± 0.45 mm
Angle at target	± 70 μrad
Size at target, rms	10% of $\sigma(x, y)$

Although the full physics analysis procedures will not be available for some time, guidelines from simple analyses and experience from previous experiments provide a basis for estimating the effects of a poorly positioned beam. Table 1–4 lists the maximum allowable deviations from the design goals of beam position, angle and size. A set of beam-position monitors with control feedback will be installed at points along the primary beamline to ensure stability.

1.2.3   Neutrino Beam

The neutrino beam must be optimized for direction and energy to enable the neutrino-oscillation physics at the Far Detector. The neutrino beam will be created from the primary (proton) beam in a three-step process.

1. The primary beam strikes the neutrino production target in the Target Hall.

2. The charged products of these interactions, mostly pions and kaons, are collected in the Target Hall and focused in the direction of the Far Detector.

3. Those pions and kaons that are aimed correctly enter the long pipe of the decay volume, where they decay into neutrinos forming the neutrino beam.

The beamline elements involved in these three steps must be designed to work together to maximize the neutrino flux in the useful energy range for the experiment.

The target, the first element of the neutrino beam system, will be designed to interact with approximately 85% of the primary protons and to minimally absorb the charged pions and kaons created in those interactions. To accomplish this, the target needs to be relatively small in cross section. This requires a tight focus of the primary beam, resulting in a very dense energy deposition in the target material. The challenge is to design a long and narrow piece of material that can be adequately cooled and can survive these demanding conditions for as long as possible before being degraded by radiation and requiring replacement.

The neutrino-beam energy spectrum must be tailored to maximize the signal in the ν_e appearance oscillation experiment, in which muon neutrinos oscillate to electron neutrinos. There are, in effect, two predicted energy intervals of interest in this experiment, referred to as the *first* and *second* oscillation maxima. The beam must provide a concentrated neutrino

flux at the energies bounded by these oscillation peaks, shown in Figure 1–2. The higher-energy regime, 1.5- to 5-GeV neutrino energy ("1" in Figure 1–2), corresponds to focused pions of approximately 3.5 to 12 GeV, and is relatively straightforward to reach with toroidal, or horn, magnetic focusing elements. The lower-energy part of the neutrino spectrum ("2" in Figure 1–2) is more challenging to produce with high efficiency; it corresponds to pions and kaons of less than a few GeV which are scattered more and emerge at large angles making a sharp focus difficult. LBNE's on-axis design, with the beam pointing directly to the detectors, optimizes the neutrino flux over the broad energy range needed to cover both oscillation maxima.
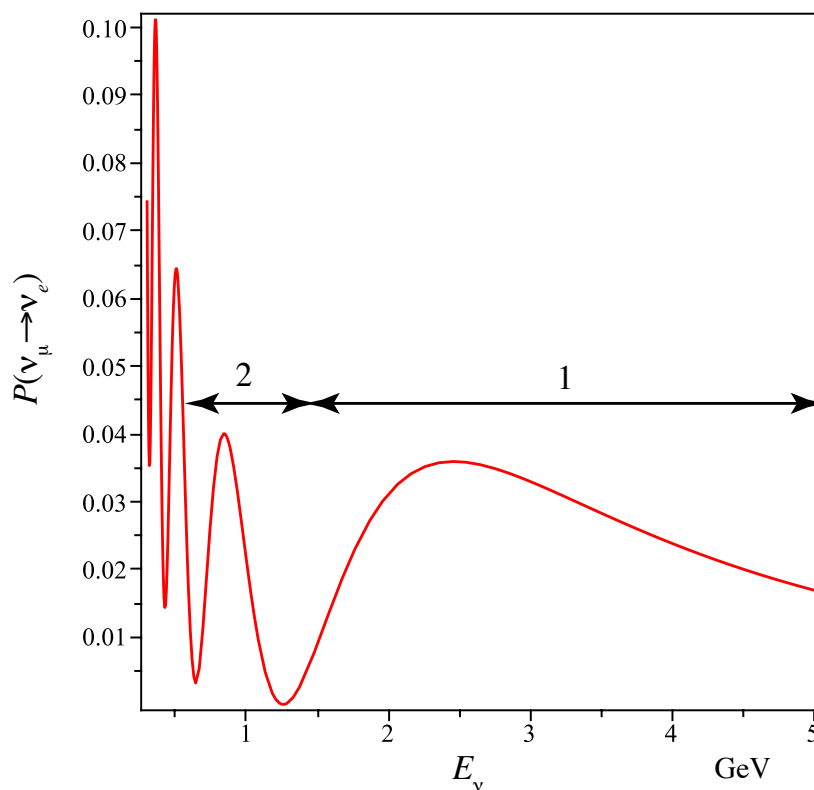
Figure 1–2: The energy range of the first and second oscillation peaks are denoted by the respective numerals. The beam design is optimized to produce neutrinos within this range. The true probability depends on a parameter, θ_{13}, yet to be measured.

The focusing of pions and kaons within the broad energy range of 2 to 12 GeV requires at least two horn magnets. The target and horns will be mounted inside a heavily shielded vault (called the "chase") that is open to the decay pipe at the downstream end. Low-energy pions and kaons usually pass through a large section of the magnetic field in the first horn and are focused to a point between the horns. A schematic of the first horn is shown in Figure 1–3. The second horn acts to redirect these particles toward the decay pipe. Most of the higher-energy pions and kaons are collected with the second horn, due to the small angles

at which they are produced. The reference design for the target and horns has been simulated, and the parameters have been tuned to deliver a neutrino-beam spectrum adequate for the physics goals. The parameters may be further optimized for the physics of LBNE, subject to material and engineering constraints. The neutrino flux at the Far Detector site is shown in Figures 1–4 and 1–5.
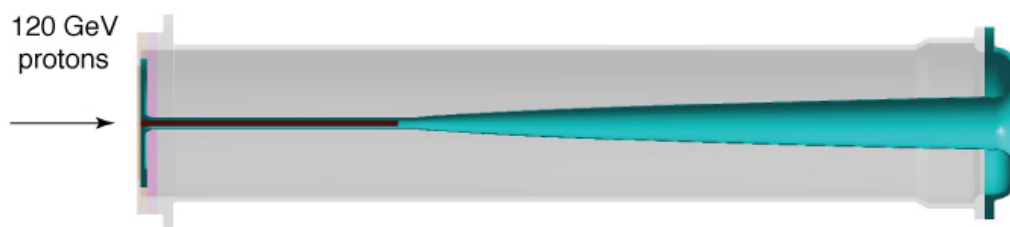
Figure 1–3: The first horn magnet. The conductor of the horn is shaded blue, and the graphite target (red) is inserted into the horn. The beam is incident from the left and the magnetic field region is between the shaped inner conductor and the cylindrical outer conductor (gray). Horn 1 is 336 cm long.

Over the lifetime of the experiment, the target and focusing horns will need to replaced. Accommodating the safe routine replacement of parts in a radioactive environment is an essential part of the Target Hall design, and remote-handling procedures involving activated targets and horns are being developed.

After collection and focusing, the pions and kaons that did not initially decay – the residual particles mentioned above – need a long, unobstructed volume in which to do so. This decay volume in the LBNE reference design is an air-filled pipe of circular cross-section, oriented toward the Far Detector. Its diameter and length are optimized to allow decays of pions and kaons such that they produce neutrinos in the useful energy range. In general, a longer pipe allows for the decays of higher-energy particles. These occur naturally at smaller production angles and are thus distributed close to the beam axis. Therefore longer pipes with smaller diameters are desirable for higher-energy beams. Lower-energy pions and kaons are not as well collimated and hence require a larger-diameter pipe. The two extrema in energy, as required by the physics measurements, provide the basis for optimization of the decay pipe geometry. The reference design calls for a 200 m long decay pipe (leaving open the option of increasing the design length to as much as 250 m) of diameter 4 m; this represents an acceptable balance between obtaining the desired neutrino energies and cost. See Figure 1–6.
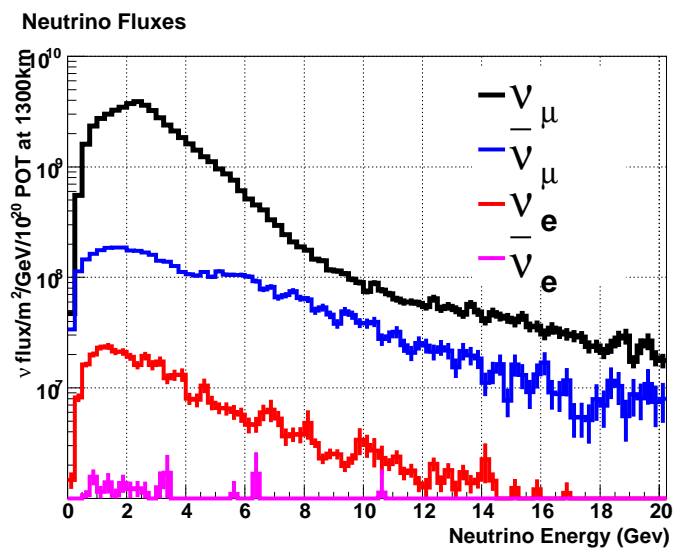
Figure 1–4: Neutrino fluxes at the Far Detector as a function of energy in the absence of oscillations with the horns focusing positive particles. Modeled using a 250-m decay pipe although the reference design is for 200 m. In addition to the dominant ν_μ ($\bar{\nu}_\mu$) flux, the minor components are also shown. Note the logarithmic scale.
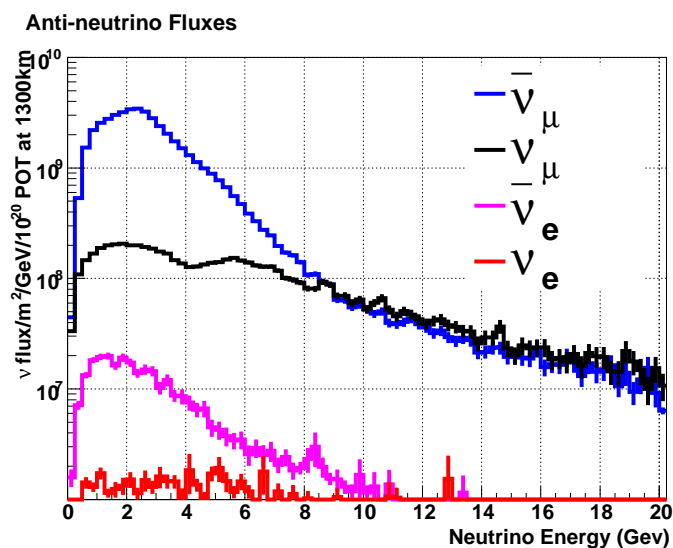
Figure 1–5: Neutrino fluxes at the Far Detector as a function of energy in the absence of oscillations with the horns focusing negative particles. Modeled using a 250-m decay pipe although the reference design is for 200 m. In addition to the dominant ν_μ ($\bar{\nu}_\mu$) flux, the minor components are also shown. Note the logarithmic scale.
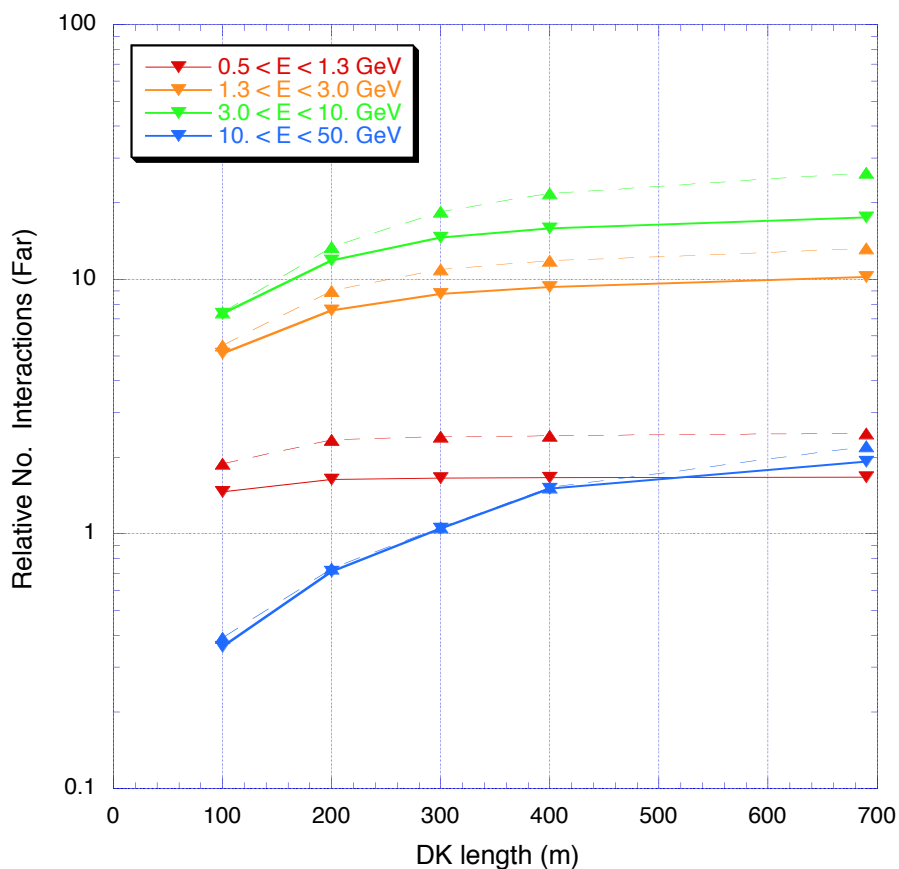
Figure 1–6: The number of neutrino interactions in the Far Detector depends on the length and diameter of the decay pipe. Here, the number of events is plotted as a function of length, with two curves for each colored energy range: solid is for a diameter of 2 m and dashed is for a diameter of 4 m. The reference design is a pipe 4 m in diameter and 200 m long.

A considerable fraction of beam power, 23%, is deposited within the decay tunnel. This heat energy will be removed by air convection with a system of blowers and heat exchangers. An alternative design under study would fill the main volume of the decay pipe with helium. The beam power in the decay tunnel implies creation of radioisotopes within the walls surrounding the pipe, requiring shielding and sealing from the surrounding water. The reference design uses a minimum of 5.5 m of concrete between the pipe and the native rock.

The roughly 15% of protons that do not interact with the target, along with the residual pions and kaons, must be absorbed to prevent them from inducing radioactivity in the surrounding rock. This is accomplished with a specially designed aluminum and steel pile, called the *absorber*, that transforms the beam's kinetic energy into heat, thus protecting the rock from beam-activated nuclides. The absorber occupies an excavated enclosure at the end of the decay pipe.

Table 1–5: This table presents partial set of the relevant parameters for the elements of the reference design. Other important details such horn shapes are found in the subsystem sections herein. The third column lists the range of a parameter that has been studied for both physics or engineering considerations.

Element	Parameter	Range	Reference design value
Target	material	graphite, Be	graphite
	diameter	5 to 16 mm	15.3 mm
	length	2 interaction lengths	966 mm
Focusing Horn 1	length	2500 to 3500 mm	3000 mm
	current	180 to 300 kA	300 kA
Focusing Horn 2	length	3000 to 4000 mm	3530 mm
	current	180 to 300 kA	300 kA
	dist. from Horn 1 (front)	6000 to 8000 mm	6600 mm
Decay Pipe	length	200 to 250 m	200 m
	radius	1.0 to 3.0 m	2 m
	atmosphere	Air, He, vacuum	air STP
Near Detector Hall	distance from target	Max., within site	459 m

1.2.4   System Integration

Integration of installation plans and procedures across the Beamline sub-project is an essential task given the complexity and interconnectedness of the beam systems. The System Integration group is responsible for a variety of control, monitoring, alignment and other elements that must ensure safe and proper operation of the beam. Control systems, in particular, will be built specifically for the LBNE Beamline, but will be based on and must integrate into Fermilab's present accelerator-controls system. Chapter 4 is dedicated to System Integration.

1.2.5   Near Site Conventional Facilities

The Near Site Conventional Facilities not only provide the support buildings for the underground facilities, but also provide the infrastructure to direct the beamline from the below-grade extraction point to the above-grade target. The layout is shown in Figure 1–7. Following the beam from east to west, or from right to left in this figure, is the underground Primary Beamline Extraction Enclosure, the in-the-berm Primary Beamline Enclosure/Pretarget Tunnel and its accompanying surface based Service Building (LBNE 5), the in-the-berm Target Complex (LBNE 20), the Decay Pipe, the underground Absorber Hall and its surface Service Building (LBNE 30), and the underground Near Detector Hall and its surface Service Building (LBNE 40). The Project limits are bounded by Giese Road to the north, Kautz Road to the east, Main Injector Road to the south, and Kirk Road to the west.

Figure 1–7: LBNE Overall Project Layout at Fermilab

These facilities are described in detail in Volume 5 of this CDR.

Following is a list of references to text in the current volume that justifies the various conventional-facilities design choices.

- Primary beam tunnel: Sections 2.1 and 2.5

- Service buildings LBNE 5, LBNE 20: Sections 2.7, 2.8, and 2.9

- Target Hall target chase: Sections 3.2, 3.3, 3.4 and 3.8

- Target Hall support rooms: Sections 3.5 and 3.9

- Near-surface storage and morgue: Section 3.11

- Decay pipe: Sections 1.2.3, 3.6

- Absorber Hall: Section 3.7

1.3   Participants

The conceptual design for the LBNE Beamline has been carried out by an LBNE subproject team, managed at Fermilab and to date made up entirely of physicists, engineers, designers and technicians from Fermilab. In addition, several contracts with other institutions and consultants have been completed for conceptual design work on particular beamline systems or components:

- Argonne National Laboratory (MOU, target)

- Brookhaven National Laboratory (MOU, target)

- Institute of High Energy Physics, Protvino, Russia (Accord, target)

- Oakridge National Laboratory (SOW, remote handling)

- Rutherford Appleton Laboratory (Accord, target)

- Bartoszek Engineering (SOW, Horn support structures)

The Beamline management coordinates the design activities of the consultants to assure that the efforts remain on track. The beamline is planned for construction at the Fermilab site, which is managed by the Fermi Research Alliance (FRA).

The LBNE Beamline effort is managed by the Work Breakdown Structure (WBS) Level 2 Manager for the Beamline subproject. The supporting team includes a WBS Level 3 Manager for the Beamline's two principal systems, Primary Beam and Neutrino Beam, as well as for System Integration. WBS Level 4 Managers manage the design of the components in these beamline systems and the interfaces between them. Figure 1–8 shows an organization chart down to Level 3 (L3).
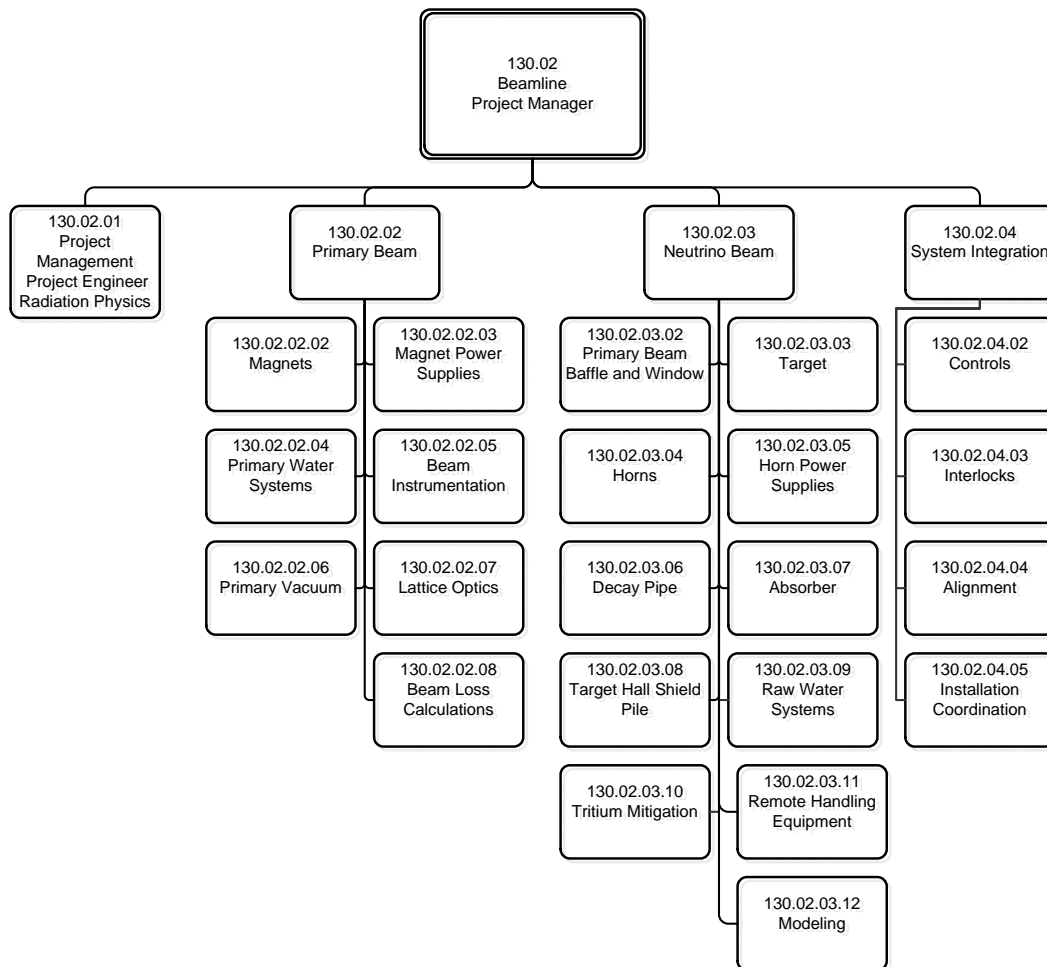
Figure 1–8: Organization chart for the Beamline subproject

Assisting and advising the Beamline subproject are an ES&H Coordinator, two Radiation Physicists and a Project Controls specialist.

Interaction amongst the Beamline team, and between this team and the design consultants as well as the LBNE Near Site design team, has been done via weekly meetings, periodic design interface workshops, and electronic mail.

2   Primary Beam (WBS 130.02.02)

2.1   Introduction

This chapter describes the reference design for the LBNE primary (proton) beamline. This system will extract protons from Fermilab's Main Injector (MI) synchrotron, using a fast-extraction method, and transport them to the target in the LBNE Target Hall. The nominal range of operation will be restricted to 60 to 120 GeV.

The principal components of the primary beamline include specialized magnets at the MI-10 extraction point to capture the entire store of protons in the synchrotron and redirect them to the LBNE beamline: a series of dipole and quadrupole magnets to transport the proton beam to the target, power supplies for all the magnets, a cooling system, beamline instrumentation and a beam-vacuum system for the beam tube.

All of the LBNE primary-beam technical systems are being designed to support sustained, robust and precision beam operation. Careful lattice optics design (described in Section 2.5) and detailed beam-loss calculations (described in Section 2.11) are essential for the proper operation of the primary-beam system, as are a detailed understanding and monitoring of component alignment and development of the comprehensive beam-permit and control systems, described in Chapter 4.

2.2   Reference Design Overview

The LBNE primary beamline is extracted using single-turn, or "fast" extraction, in which all the protons accelerated in the MI synchrotron ring will be diverted to the LBNE beamline within one circuit after each acceleration cycle. The train of bunches of protons in the MI extends most of the way around the ring. After extraction, the beam is controlled by a series of dipole (bending) and quadrupole (focusing) magnets collectively called the "lattice optics." This term refers to the overall design of the system, i.e., the magnet types, strengths, order, relative placement and other characteristics. The LBNE primary-beamline lattice optics is

designed to direct the beam toward the target and the downstream Near and Far Detectors, with a spot size appropriate for maximizing the physics potential of LBNE.

LBNE will implement a modular optics design comprised of three distinct lattice configurations in series: the specialized MI-to-LBNE matching section, the transport section and the final focus of the beam on the production target.

After kicker magnets extract the beam from the MI, the beam first passes through a set of three specialized magnets, called Lambertsons. The Lambertsons sit in the path of the beam, both when it circulates and when it is extracted, so they must accommodate both paths. The circulating beam passes through a field-free hole in the magnet yoke, and the extracted beam instead passes through the (separate) magnet aperture and is thus bent away (upward) from the MI trajectory. Each Lambertson in the line bends the beam more, such that after passing through all three (and one focusing quadrupole, a component of the MI lattice that sits between the first and second Lambertsons), the extracted beam is sufficiently separated from the MI orbit to pass through the first bending magnet external to the MI, a C-magnet. The C magnet barely clears the MI beam tube downstream of the third Lambertson and provides an additional upward bend, enough so that the extracted beam can pass above the outside of the next quadrupole in the MI lattice. The C-magnet is the last element of the specialized extraction channel.

The transport section includes a series of rolled dipole magnets (tilted about the beam axis to vary the direction of bend) interspersed with focusing quadrupole magnets placed at the same regular spacing as in the MI to maintain the same beam size as in the MI. The first dipole bends the beam horizontally further from the MI and reduces the rate of vertical rise. Several quadrupoles maintain the beam size as the beam tube passes through the wall between the MI tunnel and the LBNE primary-beam enclosure. The beam is then bent to the right and up, and back down from the apex at an angle of 101 milliradians (5.79°) toward the target, thus establishing the needed trajectory for the neutrino beam.

In the last section of the primary beamline, the beam size and its angular spread are tailored to the desired distribution for hitting the production target. This is accomplished by a set of five quadrupoles in the final-focus section, which can be tuned to produce a wide range of beam spot sizes while maintaining a narrow angular spread.

Some magnets will be grouped and powered by a single "magnet loop" and others will be powered individually, according to the lattice optics design. In order to maintain the lowest possible power consumption, all of the larger magnet loops will be ramped. A primary water system will feed cooling water to the magnets and power supplies. Beam instrumentation will characterize and monitor important beam parameters, for example, beam positions, stability, losses, intensity and transverse emittance. A vacuum system will maintain a vacuum of better than 1×10^{-7} torr residual gas pressure in the beam tube in order to reduce the beam loss due to proton-gas interaction.

2.3 Design Considerations

2.3.1 Length and Elevation

As discussed in the Alternatives Analysis document [5], primary-beam extraction at both MI-10 and MI-60 were considered, both for shallow and deep configurations, and the "MI-10 Shallow" design was selected after a thorough value-engineering process. It offers several advantages over the other designs, in particular over the "MI-60 Deep" design, its nearest competitor.

The shallow beam design offers a significant cost savings for the neutrino beam and Near Detector facilities, plus significant advantages with tritium mitigation for the near-grade Target Hall. Also, given the limited available site footprint, a deep Target Hall, as exists for NuMI/ NOvA, would require the primary-beam transport to be considerably longer to reach the depth at which sufficient structural rock cover exists above the hall. This added distance is neither necessary nor available with MI-10 extraction for a 120-GeV beam.

The target elevation of 750 feet, a few feet above natural grade level, is chosen to optimize overall facility-construction technical and resource requirements. Additional constraints include limiting the maximum primary-beam enclosure elevation angles to 150 milliradians, and achieving the required trajectory for transport of the neutrino beam to the Far-Detector site. A profile-view schematic of the target lineup for the primary-beam transport with Target Hall and decay region is shown in Figure 2–1. Colors in the figure illustrate the height of earth fill needed, including shielding for the primary-beam enclosure, along with the location of the Target Hall and decay region with respect to the underlying glacial till and rock strata.

The design requires support for the beam-enclosure regions above natural grade level. The addition of deep foundations to the underlying rock has been included in the facility design to ensure position stability of the technical components.

2.3.2 Existing Infrastructure and Shielding

The choice of a shallow beam extracted at MI-10 avoids beam crossings, which extraction at MI-60 would not, and it allows for a simpler extraction enclosure, enabling a cost-effective facility design of the entire extraction region. It interferes minimally with existing beam systems in this region, eliminates the need for small-aperture dipoles of the existing MI-60 extraction for the NuMI beam, and also provides some shielding separation from accelerator-tunnel beam losses at the beginning of the LBNE primary-beam transport enclosure. The MI-10 primary-beam layout on the Fermilab site is shown in Figure 2–1.
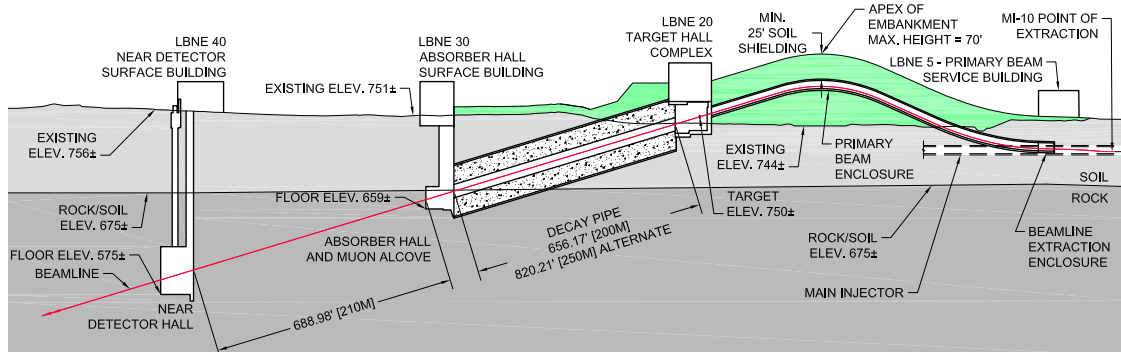
Figure 2–1: Elevation view showing the concept of elevating the beamline, thereby minimizing the amount of deep excavation and tunnels. The beam comes from the left through the primary beam enclosure and interacts at target within the Target Hall Complex. The green shaded part indicates fill used to elevate the beam.

2.3.3 Beam Energy and Intensity

The primary-beam energy that optimizes the physics of LBNE is an important aspect still under study. An energy lower than 120 GeV is preferable as long as the beam power is not compromised. The MI accelerates protons within a range of energies from injection energy (8 GeV) to 120 GeV and thus can transport protons anywhere in this range. However at lower energies, particularly under 60 GeV, acceleration-cycle times limit the number of protons per hour, and hence average power. Therefore energy less than 60 GeV is not currently being considered.

The expected beam intensity for a proton energy of 120 GeV (60 GeV) is 4.9×10^{13} (4.5×10^{13}) protons per pulse. At 120 GeV (60 GeV), the cycle time between pulses is 1.33 s (0.80 s), giving a proton-beam power of 708 kW (545 kW).

The calculated beam power as a function of beam energy [6] is shown in Figure 2–2 using assumptions outlined in the discussion of efficiency, above.

At this very high beam intensity, primary-beam control requirements must be stringent since only a few pulses of mis-steered beam will severely damage technical components. Residual activation of components must also be rigorously limited since, for example, replacing a multi-ton magnet on the steep enclosure slopes would require many hours of close-in work around the components. Severe limits on proton-beam transport loss will be imposed, keeping normal fractional beam loss at less than a few parts per million on a per-pulse basis.
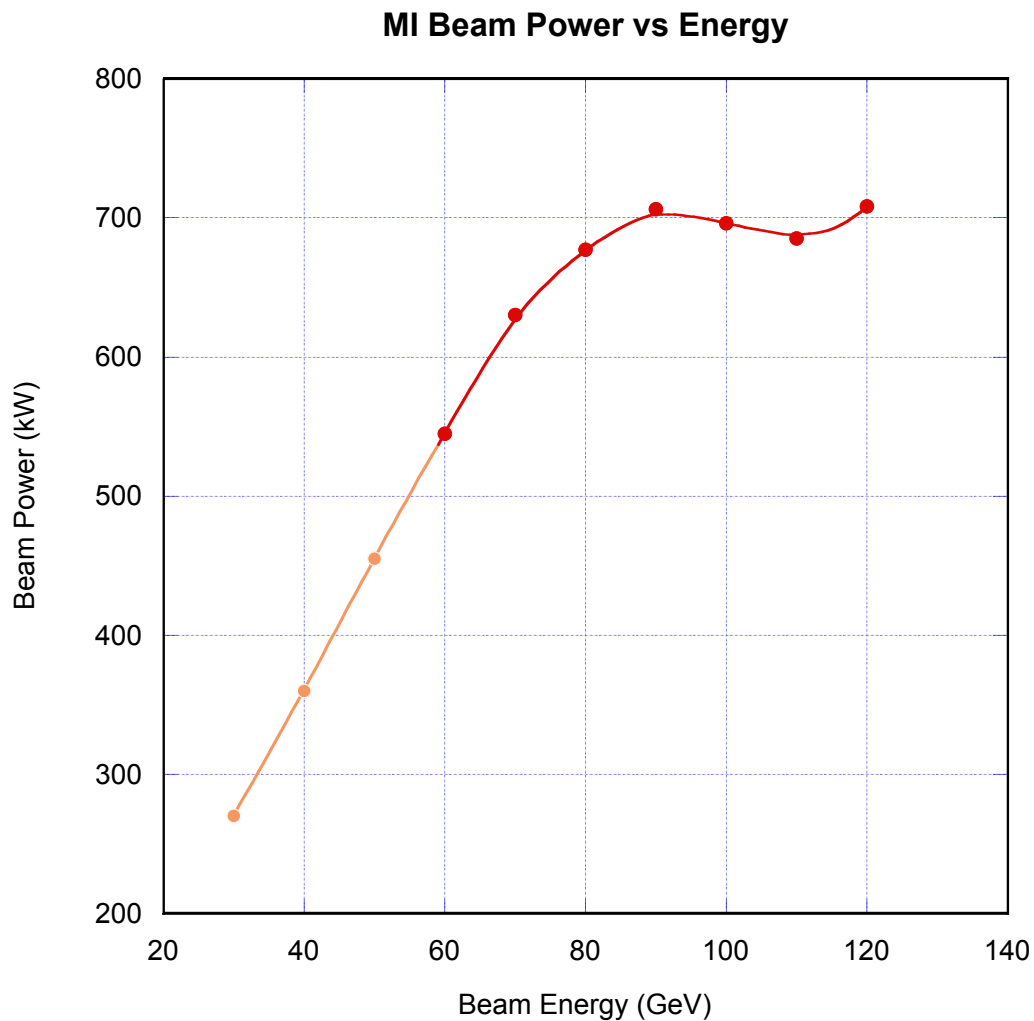
Figure 2–2: The Main Injector beam power as a function of beam energy. The decline of power at lower energies is typical of synchrotrons: all beam is injected into the machine at once at low energy and the acceleration time per GeV is fixed. The cycle rate in the Booster can be increased to 15Hz to compensate down to 90 GeV, but below ∼70 GeV the recycler ring limits the cycle time. The energy region of interest for LBNE is shown by the red line.

2.3.4   Beam Control

Techniques, hardware and control applications for accomplishing primary-beam control at the required level were developed for the NuMI 400-kW proton beam. These features have been demonstrated to perform very well during the six years of NuMI beam operation and are therefore being used in the design for the LBNE primary beam. Included are:

- A comprehensive beam-permit system (described in Section 4.2) with more than 250 parameters that are to be verified prior to each beam extraction

- Open-extraction channel and primary-transport magnet apertures capable of accepting a range of extracted beam energies

- Primary-extraction channel and LBNE beam-transport component apertures sized to accept a beam envelope larger than the MI dynamic aperture of 500 π mm-mrad, without beam loss

- Excellent magnetic-field uniformity to match the beam-envelope apertures

- Major power-supply regulation to a few parts per million to achieve good beam-transport stability

- A strong focusing-beam optics design, with excellent control of beam size and dispersion

- Fully automated beam-position control, with no manual adjustment of beam positions required during operation

- Robust beam instrumentation to enable maintenance of beam-targeting accuracy to approximately 100 μm

2.3.5   Estimation of Protons on Target

The goal for accumulating 120-GeV protons at the neutrino target with beam power of 708 kW is 6.5×10^{20} protons-on-target (POT) per year. This assumes 12 Booster batches with a per-batch intensity of 4.3×10^{12}. Given an MI throughput of 0.95, this results in 4.9×10^{13} protons per MI cycle (1.333 sec). The up-time includes the total expected efficiency of the accelerator complex as well as scheduled maintenance.

The total accelerator operational efficiency is the product of efficiencies of the Proton Source, Linac, Booster and MI. The product of the first three stages (Source, Linac and Booster) has historical average efficiency of 0.87 [7]. The number of protons delivered from the MI to NuMI has been limited by delivery to other programs (anti-protons source for collider operations and test beams). The up-time of the MI is very high, with efficiency of approximately 0.97.

The annual scheduled maintenance, a facility shutdown, has averaged 2.4 months (72 days) over the past four years (annual fraction of 0.8).

The estimated unscheduled down time, using data from the operation of NuMI, including power failures and downtime for chillers, dehumidifiers and tritium mitigation systems, is small; the efficiency is 0.97. Assuming that LBNE target and horn replacements take 30 days per year in addition to the facility shutdown,the LBNE "efficiency" due to component replacement is estimated to be 0.90. This efficiency takes into account two target replacements per year and one horn replacement where the target/horn replacement takes 2.5/3.5 weeks respectively including the cooldown period. It is assumed that one of the two target replacements will take place within the scheduled annual shutdown and that the horn replacement has 50% probability to take place within the scheduled shutdown. An additional 0.95 efficiency is assumed due to programmatic issues and very short downtimes (less than a few minutes). Thus, the total efficiency for LBNE is estimated to be approximately $0.87 \times 0.97 \times 0.80 \times 0.97 \times 0.90 \times 0.95 = 0.56$. It is also assumed this overall efficiency can be maintained over a ten-year period, from beam startup to completion of the oscillation physics goals. This is not a trivial statement: for example, the booster will be a 50-year-old machine in the year 2020.

The total expected POT per year, given above, is thus the product of the total efficiency (0.56), the number of protons per second (3.68×10^{13}) and the number seconds in a (perfect) year (3.15×10^7) [7].

The reliable delivery of a 708-kW beam to the target should be aided greatly by the startup and operation of NOvA, which will use the same accelerator sequence as LBNE, except for the final beam transport to the target. Therefore, the primary risk in beam delivery to the target can be isolated to the final primary-beam section built for LBNE. The reliability of very low-loss transport through the LBNE section will be enhanced by state-of-the-art beam monitors and an active control-feedback system. With deliberate beam commissioning and start-up, the efficiency in the LBNE primary beam should be very high. The corresponding operating efficiency for the NuMI primary beam over a six-year period has been greater than 0.99.

2.4 Principal Design Elements and Parameters

The principal design elements and parameters of the Primary Beamline reference design include:

- Single-turn extraction of primary beam at MI-10 and an extraction rate of 4.9×10^{13} protons per MI cycle (120 GeV)

- A primary-beamline design that allows a sufficient distance between the absorber and

Near Detectors so that there is a negligible flux of muons from pion decays at the Near Detectors

- Beam transport to target in the Target Hall exiting the MI-10 enclosure via an evacuated pipe heading west-northwest toward the Far Detector at the Sanford Laboratory in Lead, S.D., followed by a vertical bend upward, to a final downward pitch of 5.79°

- Construction of earthen embankment approximately 1,100 ft long and of peak height 70 ft acting as support and shielding

- Shielding for radiological protection, for all possible accidental beam losses and for long-term residual beam exposure

The general primary-beam specifications derived from the requirements [8] are listed in Table 2–1.

Table 2–1: Summary of principal beam design parameters.

Parameter	Value
Protons per cycle	4.9×10^{13}
Cycle time (120 GeV)	1.33 sec
Spill duration	1.0×10^{-5} sec
Energy	60 to 120 GeV
Protons on target per year	6.5×10^{20}
Beam size at focus (x,y)	1.5 mm RMS
Beam divergence (x,y)	17 μrad

2.5 Lattice Optics (WBS 130.02.02.07)

2.5.1 Introduction

LBNE will implement a modular optics design comprised of three sections in series: MI extraction with a specialized MI-to-LBNE matching section, the transport section and the final focus of the beam near the production target.

A series of five fast-pulsed magnets in the MI ring, called kickers (Section 2.6.3.6), extract the beam. The kicker magnets have a fast ramp-up to the required current followed by a ramp-down; the ramps occur during gaps in the circulating MI beam. The kickers are followed by the set of three Lambertson magnets that bend the extracted beam away further (upward) from the MI trajectory. To match the MI optics to the optics of the transport section, a string of individually controlled quadrupole and dipole magnets is used.

The transport section steers the beam from extraction/matching section up to and over the hill toward the Target Hall. The majority of the optical lattice consists of a series of six periodic focusing units, "FODO" cells, which terminates 70 m upstream of the target. A set of independently tunable quadrupoles form the final-focus (FF) optics to obtain the desired beam size on the target. This final focus is tunable to produce a spot-size (σ) from 1.00 to 3.00 mm over the entire momentum range 60 to 120 GeV/c.

2.5.2 Design Considerations

The design of the lattice for LBNE, as detailed in the next section, is constrained by the experimental needs, civil construction requirements and operational factors in transporting an intense beam over long periods of time. These include:

- large changes in elevation in order to keep the Target Hall above grade

- extraction and transport over a range of beam momenta (60 to 120 GeV/c)

- beam position and focus at target which is finely adjustable

- transport of beam with very low average losses

These constraints drive most of the fundamental aspects of the technical design. The optics presented here was computed using Methodical Accelerator Design (MAD) [9] and the design reflects the large amount of experience of the designers.

2.5.3   Reference Design

Protons are extracted from the MI-10 straight section. The extraction magnets are of the standard MI design with five kicker modules at the upstream end of the MI-10 straight section to kick the beam horizontally into three vertically-bending Lambertsons, plus a C-magnet straddling the MI quad Q102 located 90° in betatron phase downstream. A single, rolled, long (6 m) MI-style IDA/IDB dipole (Section 2.6.3.1) steers the beam horizontally towards the MI enclosure wall between MI quads Q105 and Q106, while leveling the beam off somewhat to a gentle vertical slope of +0.60°, thereby bisecting the space separating the MI and Recycler Ring magnets. A 15.6-m-long carrier pipe transports the beam through the MI tunnel wall into the new primary beam extraction enclosure that houses the main body of the line.

From that point the protons are transported a further 305.4 m to the target, located 10 ft above grade (750 ft above sea level) and aimed towards the Far Detector. In the main body of the beamline, 12 IDA/IDB dipoles plus 12 short (4-m) MI-style IDC/IDD dipoles together bend the beam −7.180° horizontally and −5.789° net vertically. Bends are grouped into twelve 4 + 6 meter pairs. The first three cells accomplish the horizontal alignment to the Far Detector while generating a +150-mrad vertical trajectory. This upwards trajectory continues through the three subsequent empty FODO half-cells, reaching maximum beam elevation 40 ft above grade. This is followed by three full cells that create the 251 mrad of downward bend necessary to obtain the final −101 mrad trajectory to the Far Detector.

Optical properties are defined by 24 quadrupoles (grouped as 23 focusing centers) of the proven MI-beamline-style 3Q60/3Q120 series (Sections 2.6.3.4 and 2.6.3.5). All focusing centers are equipped with redesigned MI-style IDS orbit correctors (Section 2.6.3.5) and dual-plane beam-position monitors (BPMs) (Section 2.9). Ample space is available in each cell to accommodate ion pumps and diagnostic instrumentation. Parameters for the main magnets are listed in Table 2–3.

2.5.3.1   Optics

This 60-120 GeV/c transfer line design is comprised of distinct optical modules, as illustrated in Figure 2–4: extraction/matching section, transport section and a widely tunable quadrupole triplet module to control beam size on target.

The first six quadrupoles in the beamline are powered individually to perform the optical match between lattice functions of the MI and those of the LBNE transfer line (the roll angles of dipoles in the first three half-cells are selected specifically to contribute to the dispersion matching of (η_x, η'_x) and (η_y, η'_y)). This matching section is followed by six 120° FODO cells characterized by quadrupoles Q207 through Q218. Cell length and phase advance are chosen such that beam size does not exceed that of the MI 90° lattice cell structure, while

DIPOLE TYPE	L (m)	B (T)	TILT (deg)		QUAD NAME	TYPE	L (m)	G (T/m)
					MI-10 EXTRACTION → LBNE			
MI_LAM	2.8000	0.5324	-90.000					
					MI-Q102	**3Q84**	**2.1336**	**+16.16016**
MI_LAM	2.8000	1.0000	-90.000					
MI_LAM	2.8000	1.0000	-90.000					
C-MAG	3.3528	1.0028						
					MATCH FROM MI → LBNE FODO LATTICE + 150 mrad UP BEND			
					Q201A → Q201B	3Q60	1.524	−11.13509
IDA	6.09981	1.2234	+62.847					
					Q202	3Q120	3.048	+12.48756
					Q203	3Q120	3.048	-9.18907
					Q204	3Q120	3.048	+13.06221
IDC	4.06654	1.4142	-45.398					
IDB	6.09981	1.4142	-45.398					
					Q205	3Q120	3.048	-13.06221
IDA	6.09981	1.4142	-45.398					
IDD	4.06654	1.4142	-45.398					
					Q206	3Q120	3.048	+16.16931
IDC	4.06654	1.1362	-49.440					
IDB	6.09981	1.1362	-49.440					
					120° FODO CELLS			
					Q207	3Q120	3.048	-15.83240
IDA	6.09981	1.1362	-49.440					
IDD	4.06654	1.1362	-49.440					
					Q208	3Q120	3.048	+15.83240
IDC	4.06654	1.0343	-57.288					
IDB	6.09981	1.0343	-57.288					
					Q209	3Q120	3.048	-15.83240
IDA	6.09981	1.0343	-57.288					
IDD	4.06654	1.0343	-57.288					
					Q210 → Q213	3Q120	3.048	±15.83240
					251 mrad ACHROMATIC DOWN BEND			
IDC	4.06654	1.6439	+90.000					
IDB	6.09981	1.6439	+90.000					
					Q214	3Q120	3.048	+15.83240
IDA	6.09981	1.6439	+90.000					
IDD	4.06654	1.6439	+90.000					
					Q215			-15.83240
IDC	4.06654	1.6439	+90.000					
IDB	6.09981	1.6439	+90.000					
					Q216	3Q120	3.048	+15.83240
IDA	6.09981	1.6439	+90.000					
IDD	4.06654	1.6439	+90.000					
					Q217			-15.83240
IDC	4.06654	1.6439	+90.000					
IDB	6.09981	1.6439	+90.000					
					Q218	3Q120	3.048	+15.83240
IDA	6.09981	1.6439	+90.000					
IDD	4.06654	1.6439	+90.000					
					FINAL FOCUS β* = 86.3 m [σ = 1.50 mm @ 120 GeV/c]			
					Q219	3Q120	3.048	-10.88170
					Q220	3Q60	1.524	+6.88602
					Q221	3Q120	3.048	+12.35390
					Q222	3Q120	3.048	-16.81837
					Q223	3Q120	3.048	+13.98115

Figure 2–3: Magnet parameters of the LBNE proton beamline at 120 GeV/c and β^*=86.328 m.
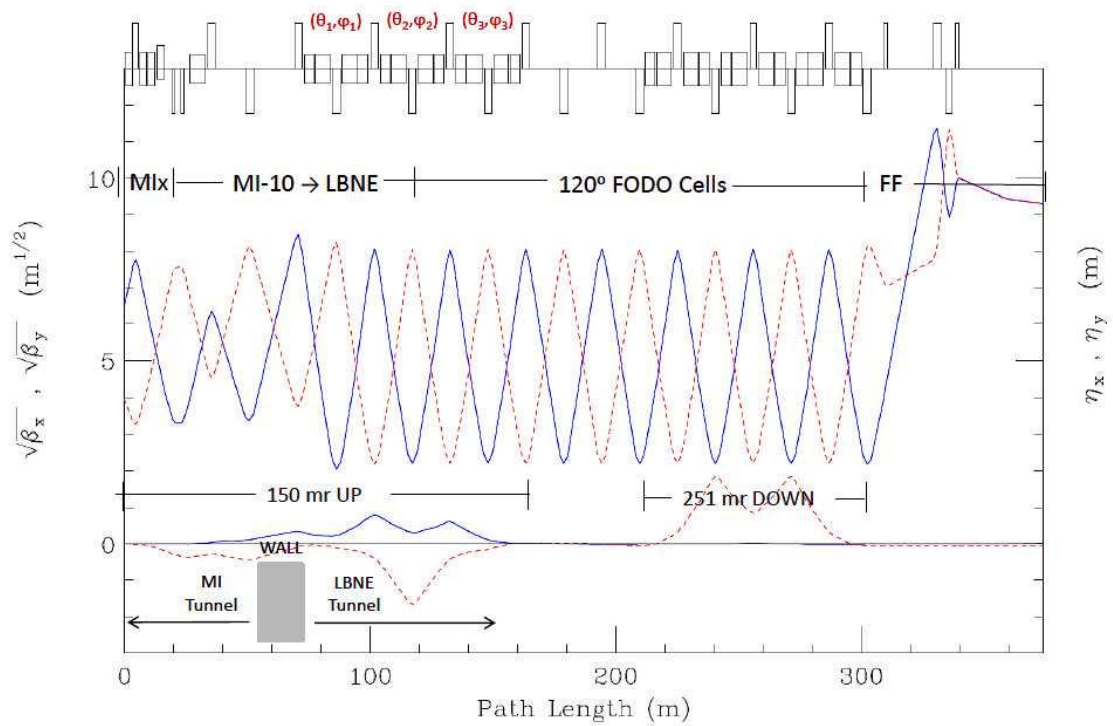
Figure 2–4: Horizontal (solid) and vertical (dashed) lattice functions of the LBNE transfer line. The final focus is tuned to produce a spot size of $\sigma_x = \sigma_y = 1.50$ mm at 120 GeV/c and $\epsilon = 26\pi$ μm (98%, normalized).
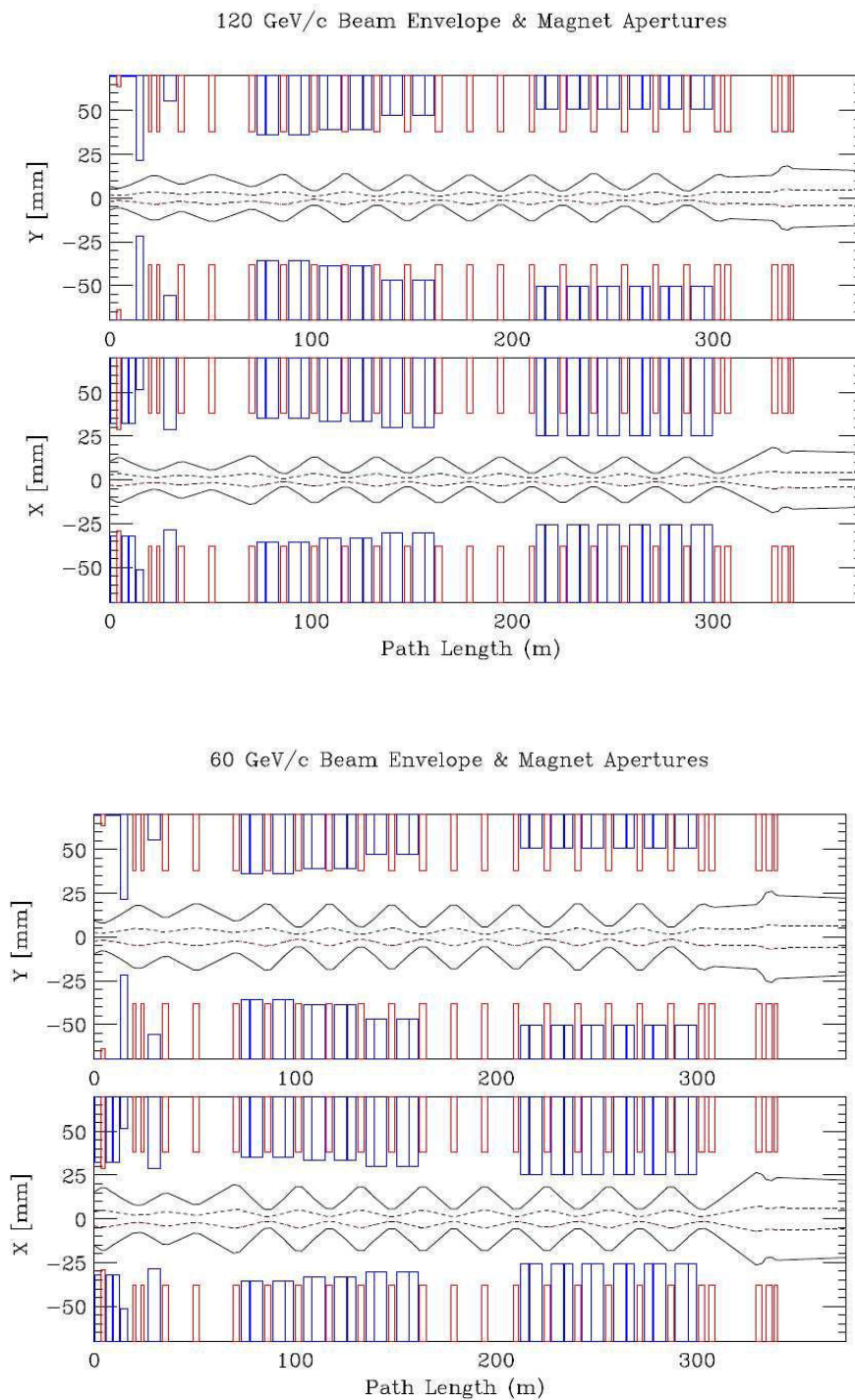
Figure 2–5: Magnet apertures and beam envelopes: The 98% contour (dashed) with nominal MI beam parameters, and the 100% envelope (solid) corresponding to the MI admittance at transition ($\gamma t = 21.600$).

also optimizing efficient use of space for the achromatic insertions. Dispersion generated by variations in the beam trajectory are corrected locally and can not bleed out to corrupt the optics elsewhere in the line. Quadrupoles Q219 through Q223 form the tunable final-focus optics to produce a spot-size of $\sigma = 1.00$ to 3.00 mm over the entire momentum range 60 to 120 GeV/c.

Magnet apertures (including the impact of rolls) and beam envelopes are shown in Figure 2–5. One contour corresponds to nominal MI beam parameters of $\epsilon = 26\pi$ μm (98%, normalized) and $\Delta p_{98}/p = 9. \times 10^{-4}$. The larger envelope shown is calculated for $\epsilon = 360\pi$ μm (100%, normalized) and $\Delta p_{100}/p = 28. \times 10^{-4}$. The latter values reflect the admittance of the MI at transition (γt = 21.600), and the transfer of such a beam to LBNE could only result from a catastrophic failure of the MI and LBNE safety and regulatory systems. The maximum transverse emittance of 360π μm is determined by the restricted horizontal aperture in the Lambertson magnets seen by the circulating MI beam. The momentum spread is the maximum value that can be contained in a radio frequency bucket through acceleration. The $\epsilon = 360\pi$ μm and $\Delta p_{100}/p = 28. \times 10^{-4}$ envelopes, therefore, demonstrate that the LBNE primary beamline should be able to transport without losses the worst quality beam that the MI could transmit.

2.5.3.2   Sensitivity to Gradient Errors

It is assumed that the optical integrity of the primary beamline will not be compromised by magnet-to-magnet variations in the integrated quadrupole fields. Experience with the MI-style 3Q120 magnets has shown that these magnets are very high quality, with a spread in gradient errors on the order of $\sigma(\Delta G/G) \sim 0.08\%$ or less [10]. Such a narrow error distribution cannot appreciably impact the beam characteristics or transport capabilities. Implementing even the most rudimentary strategy for sorting production quadrupoles, such as selecting those from the middle of the distribution for installation in the FODO cells, will reduce the spread even further. For nominal beam parameters at 120 GeV/c, a simple thin-lens calculation predicts that the largest error-wave expected in the 98% beam envelope (± 3.62 mm nominal at $\beta = 64.5$ m) would be less than 68 microns.

2.5.3.3   Beam Size at Target

An essential design requirement of the final focusing section is the ability to tune the spot size σ over a wide range. The optimum spot size is thought to fall in the range $\sigma \sim$1.5-2.0 mm, which would grow to $\sim$2.5-3.0 mm for a 2.3-MW upgrade. Spot size is still an evolving parameter. Ultimately, the choice will be driven to a large extent by details of the final target design, but other factors must also be considered. In addition to the 40% difference in beam size between 60 and 120 GeV/c, under real operational conditions the beam parameters ($\epsilon, \Delta p/p$) will certainly be different from the ideal nominal values assumed here. Currently,

the MI emittance at 120 GeV/c is $\sim 20\pi$ μm, but it is not clear how this value might change in the future. It is essential that the FF design be sufficiently robust and versatile to anticipate these possibilities.
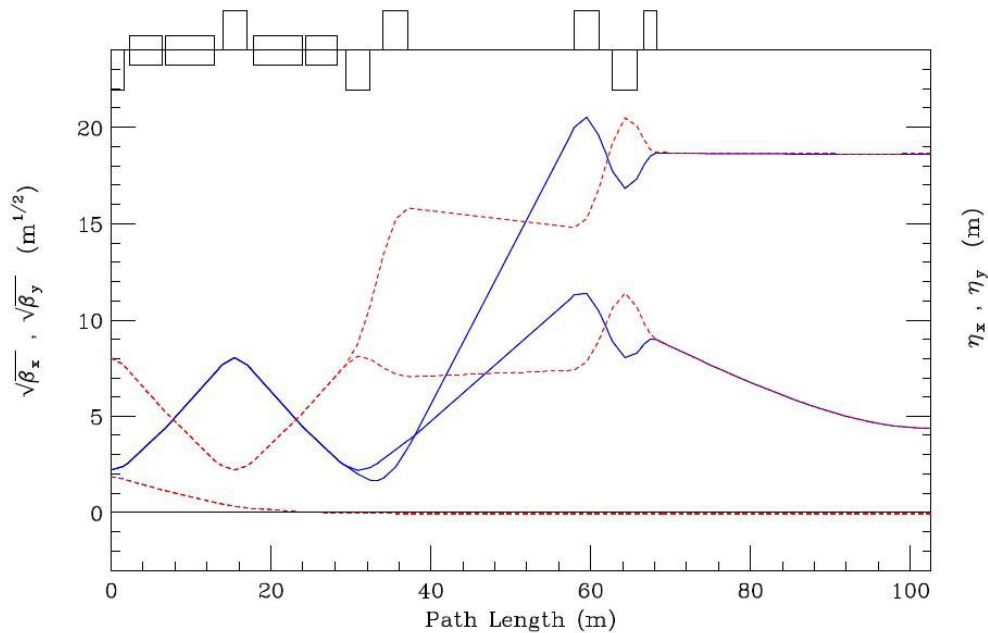
Figure 2–6: Tuning range of the Final Focus: These examples assume nominal MI beam parameters. At 60 GeV/c and $\sigma = 1.0$mm; $\beta^* = 19.184$m and $\beta_{max} = 104$m. At 120 GeV/c and $\sigma = 3.00$mm; $\beta^* = 345$ m and $\beta_{max} = 460$m.

Figure 2–6 illustrates the wide tuning range of the FF. Results are shown for the two extremes of operational requirements. Calculations were performed assuming nominal beam parameters but the plot demonstrates that the FF is clearly adaptable to any reasonable set of beam parameters. To meet the two extremes of spot-size criteria considered here β^* at the target must be continuously tunable over a range of 18. The corresponding quadrupole gradients are listed in Figure 2–7. The advantages of a modular optics design are evident - variations in the extracted MI beam parameters can be accommodated solely within the FF and do not involve tuning adjustments elsewhere in the line.

2.5.3.4   Trajectory Correction

Trajectory correction is an issue which, of course, must be addressed in the design of any transfer line, but for the ultra-clean transport requirements of LBNE it is critical that precise position control be available throughout the primary beamline.

QUAD	TYPE	L (m)	σ = 1.00mm @ 60 GeV/c β* = 19.184 m G (T/m)	σ = 3.00mm @ 120 GeV/c β* = 345.31 m G (T/m)
Q219	3Q120	3.048	-6.21424	+16.33683
Q220	3Q60	1.524	+2.31123	-14.33993
Q221	3Q120	3.048	+10.46613	+12.13973
Q222	3Q120	3.048	-11.31659	-14.41450
Q223	3Q60	1.524	+7.62203	+11.53926

Figure 2–7: Final Focus gradients for the examples in Figure 2–6

Correction of central trajectory errors have been simulated for dipole field errors and random misalignments assigned to all beamline elements (including BPMs). Realistic error values are on the order of $\sigma(\Delta x, \Delta y) = 0.25$ mm, and $\sigma(\psi_{roll}) = 0.50$ mrad [11]. Figure 2–8 shows the trajectory deviations resulting from randomly generated Gaussian error distributions (dashed). After correction using the LBNE trim dipoles the new orbits are also shown (solid), emphasizing the dramatic reduction in offset errors. Results of the tracking are summarized in Figure 2–9. All corrector strengths are well within the 250 μrad (60% of peak) design specification for the new IDS trims.

The (relatively) large residual value of x_{max} is an unrealistic artifact of the simulation model. For one random generator seed, badly misaligned quadrupoles ($\Delta x_1 > 3\sigma\Delta x_0$) at the beginning of the line produced the spike at Q202, and the Q201 vertical correctors could have no impact. In reality, a horizontal trim (corrector) magnet would probably be added to Q201's complement, or the errant quadrupole would simply be realigned. Beam position on the target is accurate to a few microns – far below the 150-μm tolerance set by horn focusing. The worst angular error found is $\sim$1.4 μrad which, 1,300 km away at the Far Detector, translates into $\sim$6 ft of position error, which is clearly negligible.

The fact that the orbit deviations are virtually the same in both planes indicates that quadrupole misalignments are the dominant source of errors. A 15-T/m quadrupole displaced transversely by 0.25 mm produces a kick $\sim 30\mu$rad which is larger than the error angle resulting from $\Delta B/B = 10^{-3}$ in any of the beamline's dipoles.
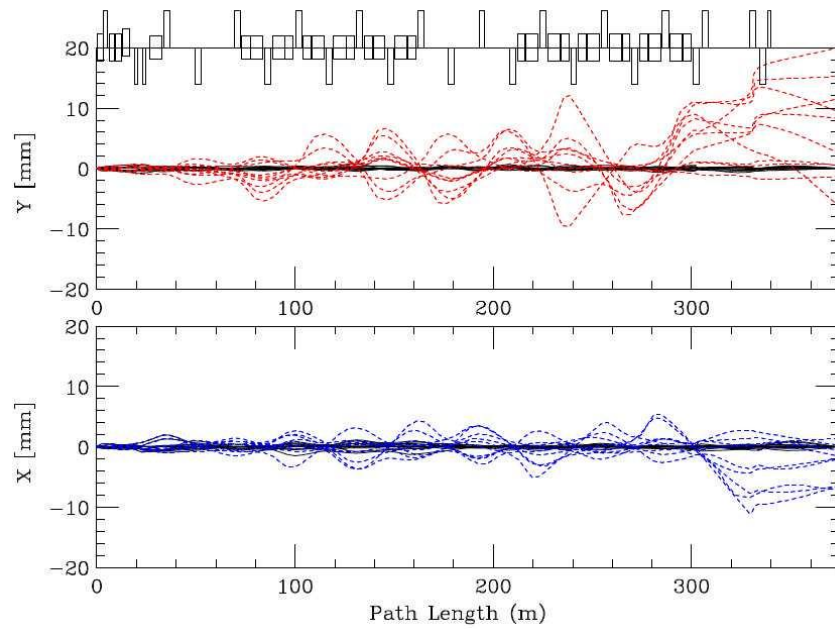
Figure 2–8: Uncorrected/corrected trajectories with random misalignments and dipole field errors; the plot begins at the upstream end of the first extraction Lambertson at MI-Q102

	ORBIT (mm)		CORRECTORS (µr)		ORBIT (mm)		CORRECTORS (µr)	
	X_{max}	X_{RMS}	θ_{max}	θ_{RMS}	Y_{max}	Y_{RMS}	max	RMS
UNCORRECTED	11.012	2.179			19.991	4.444		
CORRECTED	1.885	0.376	85.382	27.955	0.806	0.255	82.467	31.511
BEAM JITTER ON TARGET								
	X (µm)		X′ (µr)		Y (µm)		Y′ (µr)	
	X_{max}	X_{RMS}	X'_{max}	X'_{RMS}	Y_{max}	Y_{RMS}	Y'_{max}	Y'_{RMS}
CORRECTED	2.656	1.586	1.265	0.751	1.955	0.942	0.625	0.306

Figure 2–9: Orbit offsets and corrector kicks for the trajectories in Figure 2–8

2.6 Magnets (WBS 130.02.02.02)

2.6.1 Introduction

This section discusses the magnets that will be used in the primary beamline to steer and focus the beam. The set of magnets includes three extraction kickers, three Lambertson magnets, one current septum C-magnet (the first magnet that is external to the MI ring), 25 main dipole magnets, 24 quadrupole magnets and 24 dipole corrector magnets for fine-tuning. From the extraction point, the lattice optics have to transport the primary beam to the target with the highest possible intensity. The magnet counts are summarized in Table 2–2.

2.6.2 Design Considerations

There are two technical considerations for the beamline magnets beyond providing the integrated dipole field and quadrupole gradient to establish the design lattice. First, the magnet apertures must be large enough to allow for an upgrade of beam power to 2.3 MW and alignment of the magnets should be sufficiently precise so as to not require any further enlargement due to the relative placement of the apertures. Secondly, the magnets must support rapid ramping of excitation. Beam only passes through the magnets for 10 μs of spill time out of

Table 2–2: Summary of primary-beam magnet specifications

Magnet	Common Name	Steel Length	Nom. Strength at 120 GeV	Count
Kickers	NOvA extraction type	~1.720 m	0.0237 T	5
ILA	MI Lambertson	2.800 m	0.532 / 1.000 T	3
ICA	MI C Magnet	3.353 m	1.003 T	1
IDA/IDB	MI Dipole 6 m	6.100 m	1.034 - 1.644 T	13
IDC/IDD	MI Dipole 4 m	4.067 m	1.034 - 1.644 T	12
QQB	MI 3Q120 quadrupole	3.048 m	9.189 - 16.169 T/m	20
QQC	LBNE 3Q60 quadrupole	1.524 m	13.606 - 15.854 T/m	4
IDS	LBNE trim dipoles	0.305 m	0.548 T	24

each 1.33 s beam acceleration cycle, so we can turn down the current between spills to save power. This reduces the cost of the magnets (by reducing the amount of conductor needed), the cost of the power supplies, and the cost of the cooling systems, though the ramping does impose additional requirements. The rates at which the magnets can be ramped affect the average power consumption, which, in turn, affects the heat load and operating cost of the beamline.

The intention is to make use of existing magnets and designs as much as possible for both cost containment and a general commitment to recycling. For each magnet function, we reviewed the existing uncommitted magnets available at Fermilab and elsewhere. Suitable candidates have been identified for the Lambertsons and C-magnet; they will be refurbished or rebuilt as needed for use in the primary beamline. Existing designs to which additional magnets can be built will be used with no design changes except to the mechanical-support system. The main dipoles and quadrupoles fall into this category. The trim dipole magnets will be constructed according to a new design based heavily on current magnets. The kickers may be exact copies of or minor modifications to existing designs. We plan to use the existing tooling to the extent possible for all magnets.

2.6.3   Reference Design

2.6.3.1   Main Dipole Magnets

The dipole magnets are responsible for directing the primary beam to the target. As the biggest magnets in the beamline, they must be reliable and energy-efficient. They must also provide sufficient strength and aperture to cleanly transport the beam at any energy in the range of 60–120 GeV.

The same type of magnets as used for the MI dipoles are the logical choice for this function, in particular a combination of the 6-m IDA magnet and the 4-m IDD magnet designs. They

Table 2–3: Properties of IDA Dipoles [b].

Property	Value
Steel length	6.100 m
Magnetic field (nominal at 120 GeV)	1.296 to 1.733 T
Integrated field (nominal at 120 GeV)	7.91 to 10.57 T-m
Gap	50.80 mm
Number of turns	8
Aperture height (with beam tube)	47 mm
Aperture width (with beam tube)	120 mm
Current (nominal at 120 GeV)	6635 to 9403 A
Resistance (at 20°C)	0.8 mΩ
Inductance (at 100 Hz)	2.0 mH
Power dissipation (max, Irms = 0.5 Imax)	19 kW
Water flow (at 100 psid)	0.93 l/s
Temperature rise (max at 100 psid)	4.9°C
Weight	18,180 kg
Fermilab drawing numbers	5520-ME-274896, 5520-ME-274897
Color	Light blue

have performed successfully since the MI's commissioning in 1998. The LBNE magnets will be newly constructed to the existing designs, as mentioned above. The basic properties of these magnets are listed in Table 2–3 and 2–4. The magnet cross section is shown in Figure 2–10 and the layout of an IDA/IBD pair of dipoles, as used in the MI, is shown in Figure 2–11. An IDA/IDD pair has the same interconnection.

The MI dipoles are slightly curved to match the path of the bending particles. The sagitta (the distance between that curve and a straight line) in the 6-m dipoles is about 16 mm.

The beam-tube cross section used in the MI dipoles is shown in Figure 2–12 for reference. The beam-tube cross section is oval, wider in the magnet's horizontal dimension, to accommodate the width of the beam due to protons of (slightly) different momenta bending differently in the magnetic field. (Note that the magnets may be oriented at different angles depending on their locations in the beamline, so "magnet's horizontal" may not necessarily mean horizontal in an absolute sense. We use "width" to refer to the bending direction, perpendicular to the gap dimention between the poles.) Under vacuum, the beam tube's smaller dimension decreases to enough under 2.000 inches to allow its insertion into a magnet aperture and then to allow bending to match the beam sagitta. The MI tubes were cold-drawn through successive dies to produce the required shape. LBNE plans to take the less costly approach, employed in the Fermilab Recycler, of squashing round tubes to a roughly oval shape. The initial tube size will be selected based on aperture requirements. For example, a squashed 3-in (76 mm) outside diameter (OD) tube would yield an aperture width of about ±47 mm and a 3.5-in OD tube would yield a width of about ±58 mm.
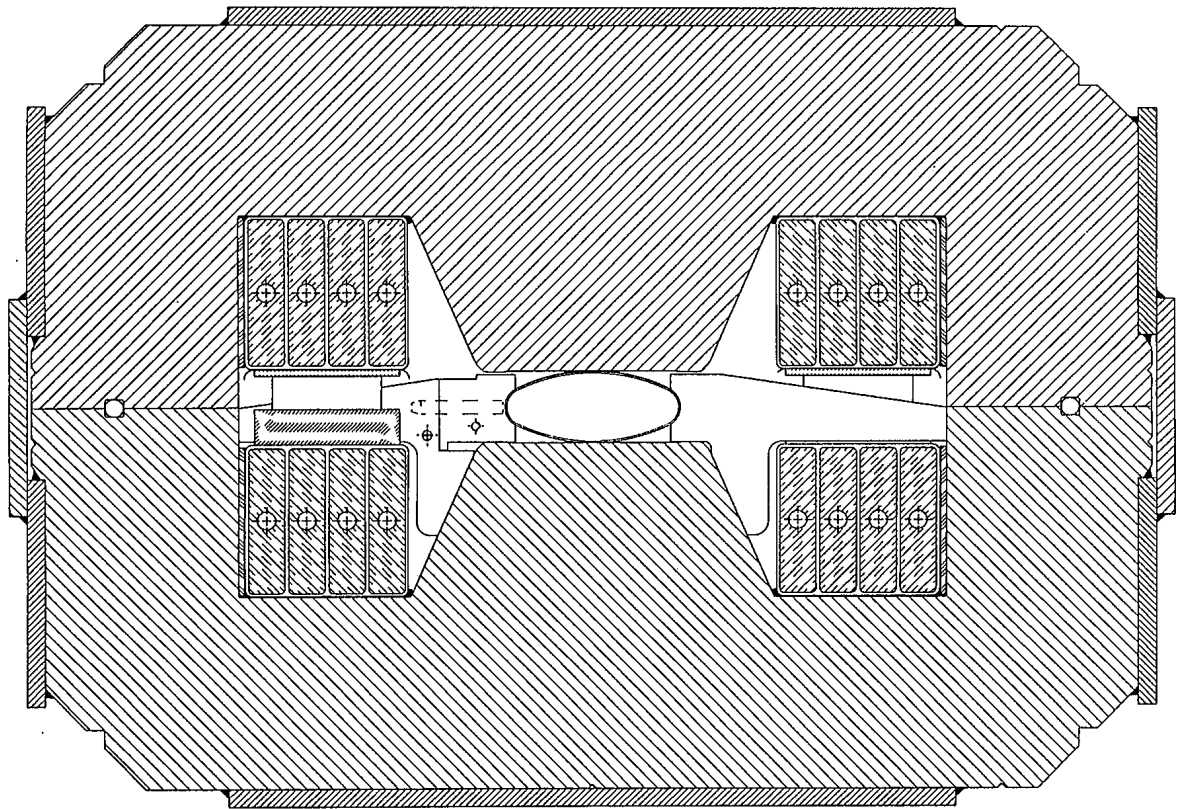
FMI DIPOLE
TYPICAL CROSS SECTION

Figure 2–10: MI Dipole cross section.
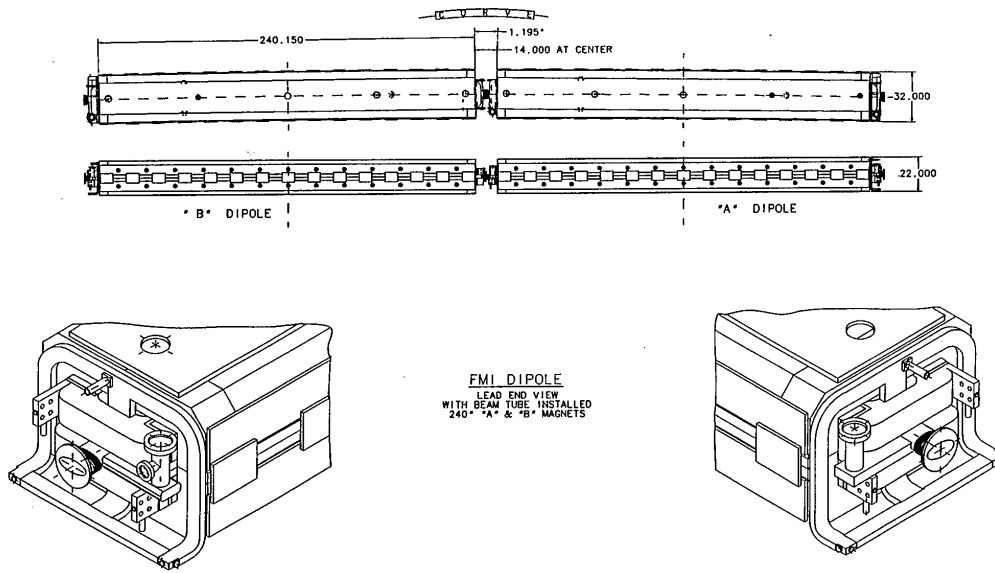
Figure 2–11: Layout of one IDA and one IDB dipole in a half cell .

Table 2–4: Properties of IDD Dipoles [b].

Property	Value
Steel length	4.065 m
Magnetic field (nominal at 120 GeV)	1.034 to 1.644 T
Integrated field (nominal at 120 GeV)	4.21 to 6.68 T-m
Gap	50.80 mm
Number of turns	8
Aperture height (with beam tube)	47 mm
Aperture width (with beam tube)	120 mm
Current (nominal at 120 GeV)	5268 to 8748 A
Resistance (at 20°C)	0.52 mΩ
Inductance (at 100 Hz)	1.3 mH
Power dissipation (max, Irms = 0.5 Imax)	10.6 kW
Water flow (at 100 psid)	1.10 l/s
Temperature rise (max at 100 psid)	2.3°C
Weight	12,300 kg
Fermilab drawing numbers	5520-ME-274910
Color	Light blue

The excitation curve of a typical IDA magnet, in Tesla-meters versus Amperes, measured during production is shown in Figure 2–13. The integrated strength of IDD dipoles was measured to be 2/3 the strength of IDA dipoles to better than 0.1%.

The dipole magnets have four terminals, significantly reducing the length of inter-magnet bus work in the main arc; see the center portion of the top image in Figure 2–11. Each length of magnet (6 m and 4 m) comes in two variants that differ only in the placement of the through-bus in the magnet and in the end of the magnet that has the more complicated bus and manifolding. The 6-m magnet variants are designated IDA and IDB; the 4-m magnet variants are designated IDC and IDD. In the MI, one IDA and one IDB (or one IDC and one IDD) magnet are compactly placed back-to-back, with their yokes approximately 0.35 m apart, leaving just enough room for the electrical jumpers between magnets and an ion vacuum pump where the beam tubes are welded together. An IDA can be just as well mated with an IDD. This pairing of a 6-m magnet with a 4-m magnet prevails in the LBNE primary beamline. The water connections and the power connections for the bus around the quadrupoles are made at the outside ends of the pair of magnets.

LBNE plans to follow the procurement strategy used during construction of the MI, developed to minimize the cost and maximize the magnet quality while making extensive use of outside vendors. The major components and subassemblies were fabricated in industry, with all contracts build-to-print (except the steel, which was based on performance) and awarded through a mix of straight bids and a source evaluation board. The cores, coils and beam tubes were assembled into complete magnets at Fermilab. This approach allows Fermilab
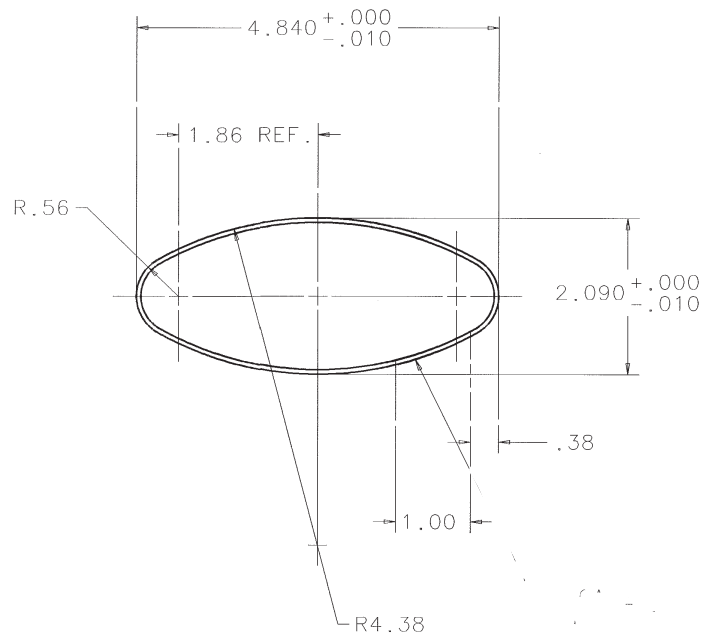
Figure 2–12: Beam tube cross section
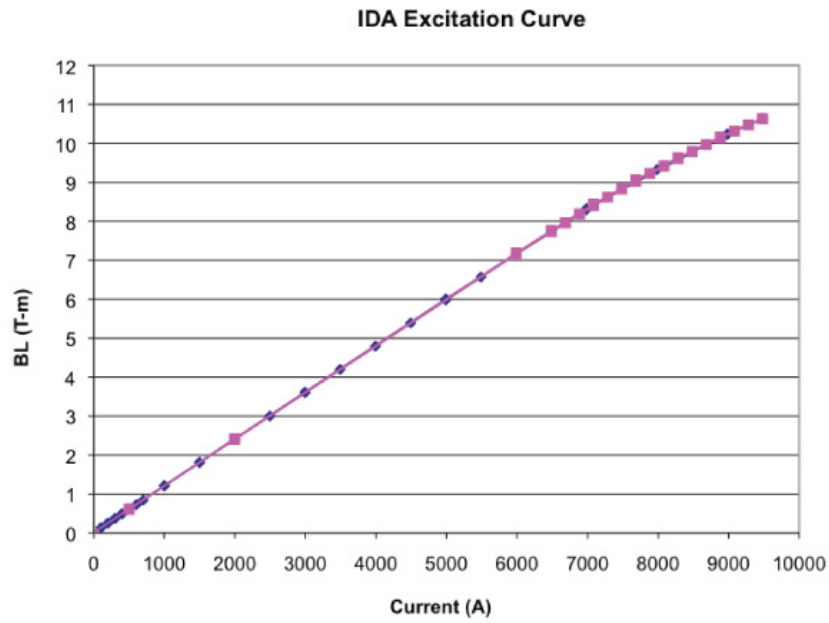
Figure 2–13: Typical IDA excitation curve.

to control the critical steps in the magnet fabrication and to assume the responsibility for the final performance with confidence, rather than trusting the vendors and paying for the vendors' potential liabilities. By taking ownership of the LBNE components, Fermilab will readily be able to make thorough inspections of the components before assembly and ensure that the final magnets meet the needs of the project.

For the MI, Fermilab purchased the coils of coated sheet steel, as that is a critical component whose magnetic properties need close control. Fermilab contracted for the stamping of the steel into laminations for the core and exercised tight oversight and monitoring of the critical lamination dimensions. Fermilab contracted with a fabrication shop to build the magnet half cores using Fermilab-provided stacking equipment, with Fermilab specifying which boxes of laminations were used in each half core based on steel and lamination data. Fermilab contracted with two specialized vendors to produce the coils, one to fabricate the bare coils and another to insulate them, though for LBNE the coil procurements may be combined. As in the Fermilab Recycler, it is expected that the beam tube will be formed from stock dimension tubes, and Fermilab welders will attach the various bellows, flanges, pump-out ports and other features.

For quality control purposes, all magnets will be subjected to magnetic tests.

During operation, the circuits must be ramped between beam pulses to maintain a conservative temperature rise in the magnets and avoid overheating. It is assumed that an RMS current of half the peak current can be achieved.

2.6.3.2   Main Injector Lambertson Magnets

LBNE will use three existing MI Lambertson magnets (ILA) for extraction from the MI and injection into the LBNE primary beamline. The magnets were built by Fermilab staff for the MI and NuMI projects. Due to the decommissioning of the Tevatron, a suitable pool of spares will become available, including the four ILA magnets in the Tevatron injection system. They will be inspected, with particular attention to the high-voltage insulation and the water circuits, and refurbished as necessary in preparation for long-term service in the LBNE primary beamline. The basic properties of the Lambertson magnets are listed in Table 2–5, and a sketch of the magnet is shown in Figure 2–14. A typical ILA excitation curve is shown in Figure 2–15.

To minimize the thickness of the septum between the hole for the circulating beam and the aperture for the extracted beam, no beam tube is used. Rather, vacuum in the aperture is maintained by a stainless-steel skin that encases the inner core. The large surface area of the laminations inside the evacuable volume necessitates an in situ bake after installation, using the attached electrical heating elements.

Table 2–5: Properties of the MI Lambertson magnets.

Property	Value
Steel length	2.800 m
Magnetic field (nominal at 120 GeV)	0.532 / 1.000 T
Integrated field (nominal at 120 GeV)	1.49 / 2.80 T-m
Gap	50.80 mm
Number of turns	24
Aperture height (with beam tube)	50.80 mm
Aperture width (with beam tube)	406 mm
Current (nominal at 120 GeV)	922 - 1815 A
Resistance (at 20°C)	12.9 mΩ
Inductance (at 100 Hz)	3.9 mH
Power dissipation (Irms = 0.5 Imax)	11.3 kW
Water flow (at 100 psid)	0.96 l/s
Temperature rise (at 100 psid)	2.8°C
Weight	23,500 lb
Fermilab drawing number	5520-ME-331492
Color	Siver

To maintain a conservative temperature rise in the magnet and to minimize the impact of any leakage field on the low-energy injected beam, we plan to ramp the magnets. It is assumed that an RMS current of half the peak current can be achieved.

2.6.3.3   Main Injector C-Magnets

As at the other high-energy extraction points in the MI, the Lambertson magnets are followed by a current septum C-magnet. The MI C-Magnet, the ICA, was based on the F17 C-Magnet design for the Tevatron I project. Several C-magnets were used in the A150 anti-proton beamline from the MI to the Tevatron and will be available for use in the LBNE beamline. The basic properties of these magnets are listed in Table 2–6, and a sketch of the magnet is shown in Figure 2–16. The beam tube cross section is shown in Figure 2–17. The excitation curve of a typical ICA magnet is shown in Figure 2–18.

In preparation for use in LBNE, the C-magnets will be inspected, and refurbished as necessary, with particular attention to the high-voltage insulation and the water circuits.

To maintain a viable temperature rise and avoid overheating, the magnets must be ramped between beam pulses. It is assumed that an RMS current of half the peak current can be achieved.
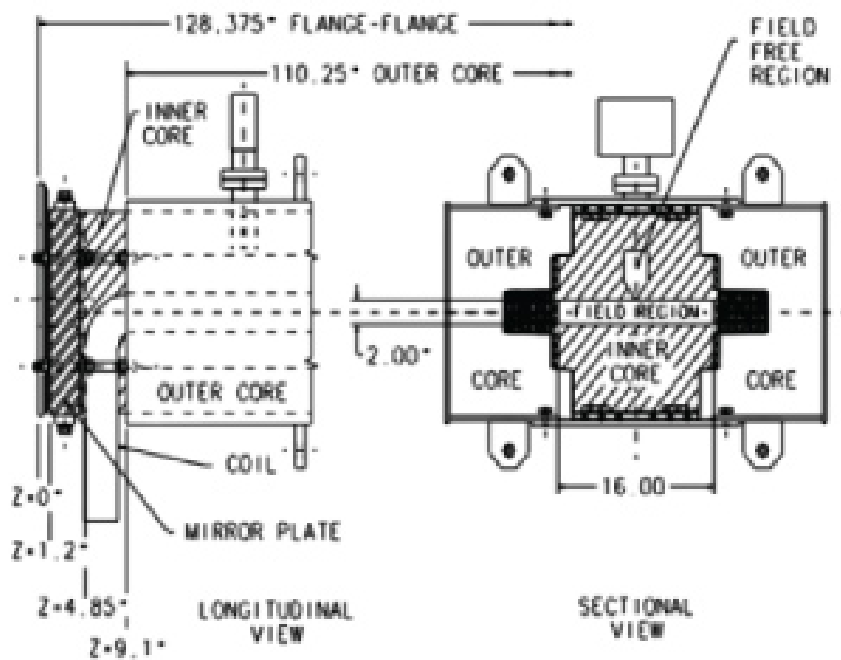
Figure 2–14: MI Lambertson magnet end and cross section.
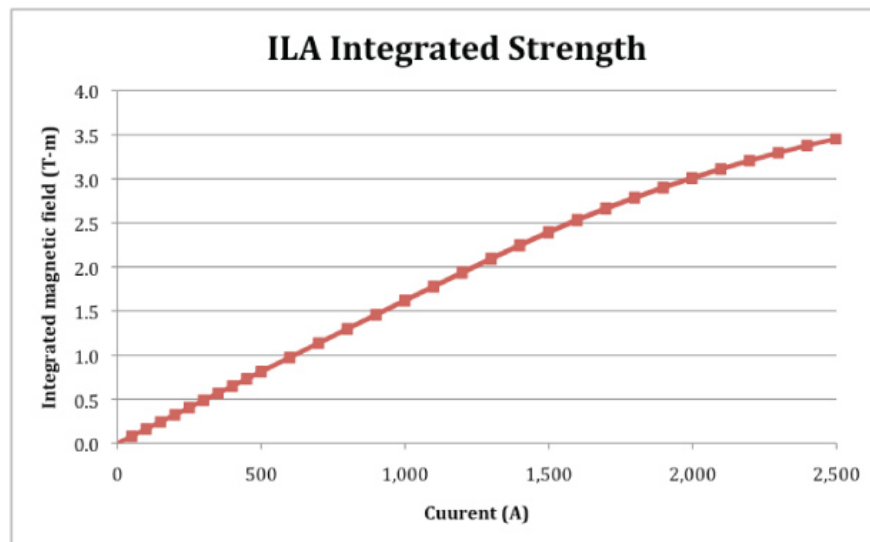
Figure 2–15: Excitation curve of a MI Lambertson magnet.

Table 2–6: ICA Main Injector C-Magnet Properties.

Property	Value
Steel length	3.353 m
Magnetic field (nominal at 120 GeV)	1.003 T
Integrated field (nominal at 120 GeV)	3.36 T-m
Gap	40.61 mm
Number of turns	12
Aperture height (with beam tube)	37.5 mm
Aperture width (with beam tube)	98.3 mm
Current (nominal at 120 GeV)	2679 A
Resistance (at 20°C)	2.11 mΩ
Inductance (at 100 Hz)	14 mH
Power dissipation (Irms = 0.5 Imax)	12.6 kW
Water flow (at 100 psid)	0.57 l/s
Temperature rise (at 100 psid)	5.3°C
Weight	8,500 lbs
Color	Light blue
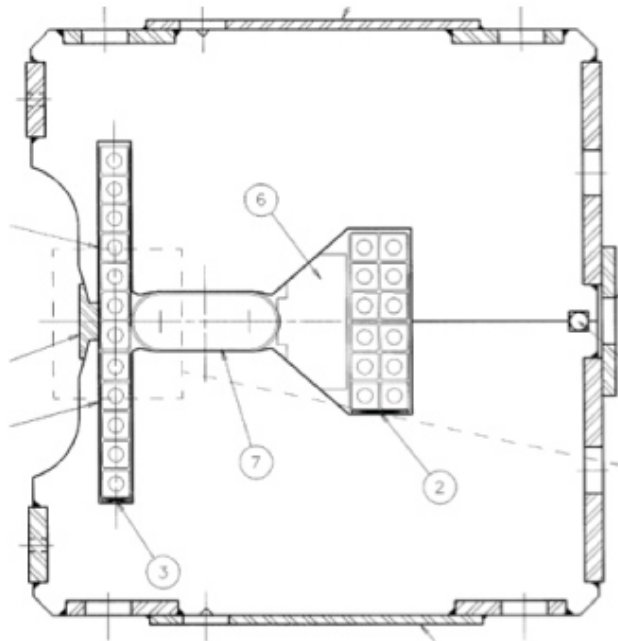
Figure 2–16: ICA MI C Magnet.
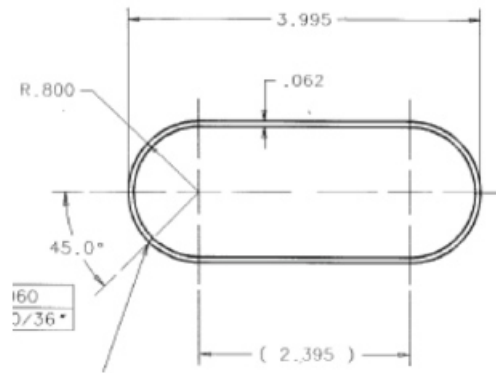
Figure 2–17: ICA beam tube shown in horizontal bending orientation.
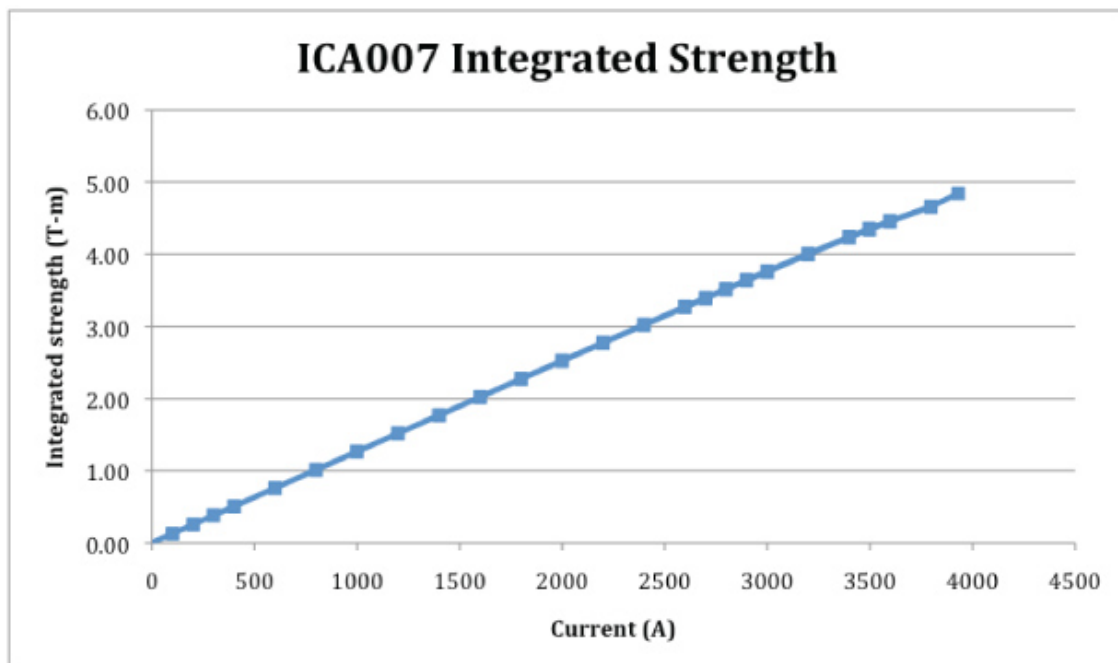
Figure 2–18: ICA integrated strength as a function of current.

Table 2–7: QQB: Hollow conductor 3Q120 Properties.

Property	Value
Steel length	3.048 m
Magnetic gradient (nominal at 120 GeV)	9.19 to 16.8 T/m
Integrated gradient (nominal at 120 GeV)	28.0 to 51.24 T-m/m
Pole diameter	76.02 mm
Number of turns	28 per pole
Aperture (with round beam tube)	72 mm
Current (nominal at 120 GeV)	192 to 360 A
Resistance (at 20°C)	156 mΩ
Inductance (at 100 Hz)	82 mH
Power dissipation (Irms = 0.533 Imax)	6.2 kW
Water flow (at 100 psid)	0.35 l/s
Temperature rise (at 100 psid)	4.2°C
Weight	7,400 lbs
Color	Orange

2.6.3.4   Quadrupole Magnets

The LBNE primary beam will be focused with 3Q120 and 3Q60 quadrupole magnets of the specific styles QQB and QQC. These styles of quadrupoles are reliable, compact, energy-efficient and suitably strong. The basic properties of the magnets are listed in Tables 2–7 and 2–8. The magnet cross section is shown in Figure 2–19 and the excitation curves are shown is Figures 2–20 and 2–21. The beam tube is round, with a 71.9-mm (2.82-in) minimum inner diameter.
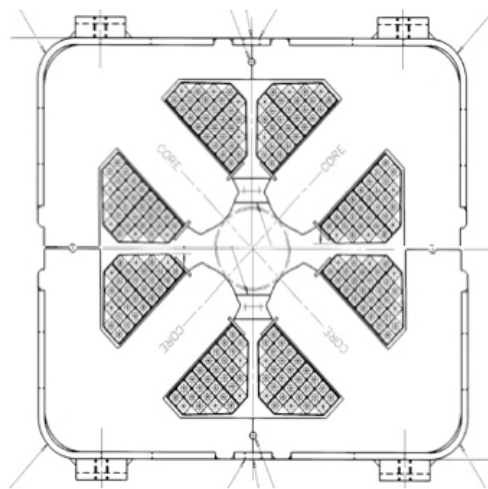
Figure 2–19: Cross-section of QQB and QQC quadrupoles.

The 3-m QQB magnets are the main focusing quadrupoles of the primary beamline. Shorter

Table 2–8: QQC: Quadrupole magnet properties.

Property	Value
Steel length	3.048 m
Magnetic gradient (nominal at 120 GeV)	9.19 to 16.8 T/m
Integrated gradient (nominal at 120 GeV)	28.0 to 51.24 T-m/m
Pole diameter	76.02 mm
Number of turns	28 per pole
Aperture (with round beam tube)	72 mm
Current (nominal at 120 GeV)	192 to 360 A
Resistance (at 20°C)	156 mΩ
Inductance (at 100 Hz)	82 mH
Power dissipation (Irms = 0.533 Imax)	6.2 kW
Water flow (at 100 psid)	0.35 l/s
Temperature rise (at 100 psid)	4.2°C
Weight	7,400 lbs
Color	Orange

Figure 2–20: Typical QQB excitation curve.
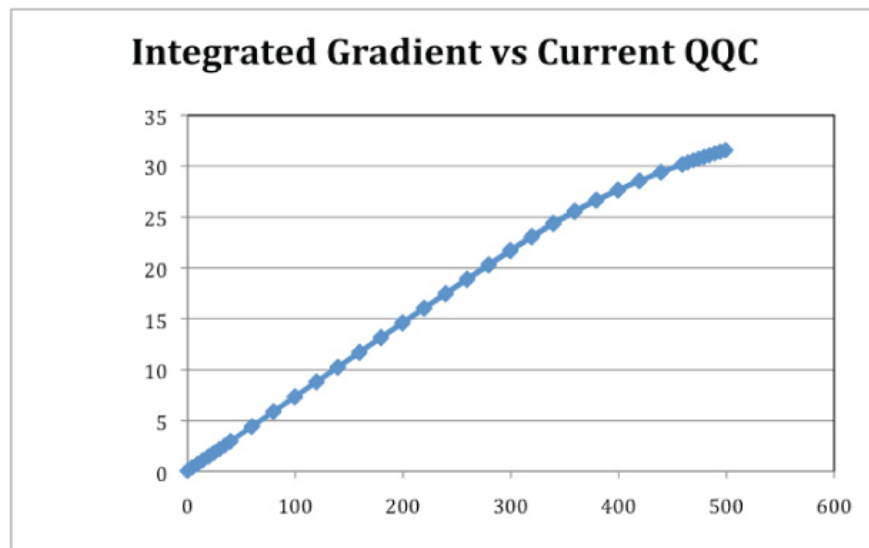
Figure 2–21: Typical QQB excitation curve.

QQC quadrupoles are used at four locations because of spacing. At the upstream end of the beamline, just following the C-magnet, the functionality of a single 3-m quadrupole is implemented with two 1.5-m quadrupoles; this avoids interference with a quadrupole in the MI ring. At the other end of the line, two of the five quadrupoles in the final focus are sufficiently weak to suggest a shorter magnet. The second of them is the last magnet in the line and has a direct impact on the available space, reinforcing the choice of a short magnet.

The basic design of the 3Q120 and 3Q60 dates from the 1970s, when they were first used extensively in the external beamlines of the Fermilab fixed-target program. They are still commonly used, although the yoke and coil configuration have evolved over the years. The QQB and QQC magnets have a slightly larger yoke than the earliest versions (15 in × 17 in rather than 13 in × 17 in), providing more mechanical stability. They also use hollow, water-cooled coils, which allow a higher current density than the original indirectly cooled, solid-conductor models. The water manifolds will be of the same style as designed for the MI. The coil will be vacuum-impregnated in the core.

For quality-control purposes all magnets will be subjected to magnetic measurements.

Once operational, the stronger circuits must be ramped between beam pulses to maintain a conservative temperature rise in the magnets. It is assumed that an RMS current of 53% of the peak current can be achieved.

2.6.3.5   Corrector Magnets

A trim dipole (fine-tuning) magnet, called an IDS, is located at every focusing location. One of these locations has two quadrupoles functioning as one element and two locations are sufficiently sensitive to require steering in both planes, so the trim magnet count may not exactly match the quadrupole count.

This is a new design based on the IDH horizontal trim dipole correctors built for the MI and subsequently used, with modifications, in the NuMI beamline. The gap, pole shape, length and number of conductor turns will remain the same. To allow operation over a wider range of excitations without overheating, the conductor size will be increased from 10-gauge square copper to 8-gauge square copper. To maintain better linearity over the extended operating range, the back leg thickness will be increased.

These magnets are designed to operate in the same plane as the main bends (vertical for LBNE), but a variant of this magnet with a spacer in the back leg to increase the gap is expected to be suitable for corrections in the orthogonal (horizontal) plane. In the NuMI beamline, the power limitation was addressed by adding indirect water-cooling through the core. In the MI, the linear range of the exictation curve has been successfully extended by strapping extra steel plates onto a few magnets to increase the flux return path. Because the water-cooling and added steel plates are cumbersome and labor-intensive to install, it was decided to address both of these issues with a new design. Depending on location, the beam tube will either be round, to match the adjacent quadrupole, or the same shape as the tube in the nearby main bending magnets. The basic properties of the magnets are listed in Table 2–9, and a conceptual drawing of a trim dipole is shown in Figure 2–22.

The measured excitation curve of a MI trim dipole magnet with an enhanced back leg is shown in Figure 2–23. Since the pole shape, length, and number of turns in the coil are the same, and the yoke is comparable, this closely matches the expected performance of the LBNE IDS.

To maintain a conservative temperature rise in the magnets during operation, the stronger circuits must be ramped between beam pulses. It is assumed that an RMS current of half the peak current can be achieved. Because heat dissipation is a primary motivation of the new design, the thermal performance has been modeled. To validate the modeling, a prototype magnet will be subjected to extensive thermal tests. The prototype will also be thoroughly measured magnetically to ensure conformance with the design requirements, as will at least a quarter of the production magnets, for quality assurance purposes.

Table 2–9: LBNE Trim Dipole Properties

Property	Value
Steel length	0.305 m
Magnetic field (maximum peak)	0.548 T
Integrated gradient (maximum peak)	0.195 T-m
Pole gap	50.8 mm
Number of turns	812
Aperture height (with beam tube)	47 mm
Aperture width (with beam tube)	120 mm
Current (maximum peak)	30 A
Resistance (at 20°C)	1.4 Ω
Inductance (at 100 Hz)	980 mH
Power dissipation (maximum)	315 W
Cooling	Air cooled
Temperature rise (internal)	32°C
Weight	295 kg
Color	Yellow
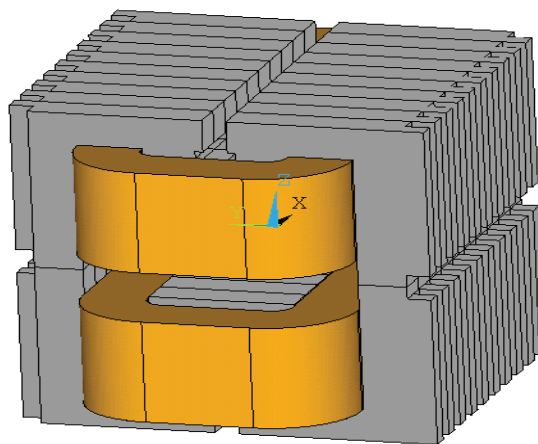
Figure 2–22: Schematic of LBNE trim dipole.
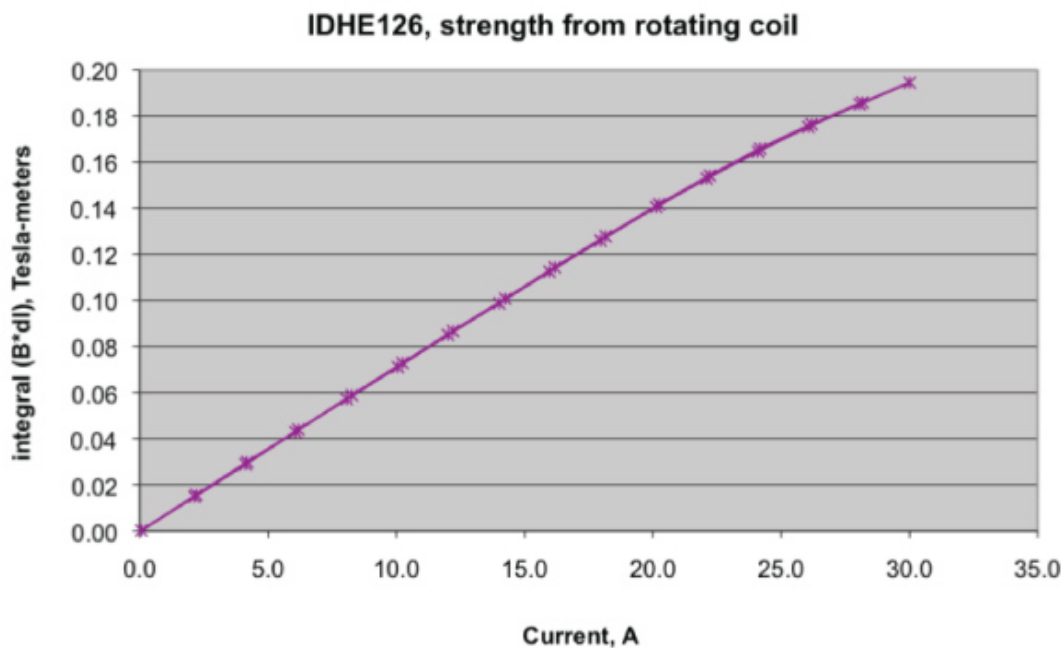
Figure 2–23: Excitation curve for a modified MI horizontal trim dipole.

2.6.3.6 Kicker Magnets

To extract the beam at the MI-10 straight section, a five-kicker-magnet system is needed. These magnets will be similar to the recently built RTV-potted NOvA extraction kickers ("RKB" type). Table 2–10 summarizes the parameters of these kickers. The cross-section of the kicker is shown in Figure 2–24.

A temperature-regulation system is required for the loads of the kicker magnets to meet the stability requirement on kicker amplitude and to remove heat from the loads. A regulation of $\pm0.5\circ$C is needed on the fluid to meet the stability requirement. Fluorinert is used because it is a good high-voltage insulator and thermal conductor, and it has low viscosity.

The LBNE Fluorinert recirculation system will be very similar to the one currently located in MI-10 which is used for the 8-GeV Injection Kickers. It will run parallel to it, terminating at the LBNE kicker loads. It will be cooled by LCW as if it were simply another power supply load. The skid will also have a heater, along with a temperature-control valve and circuit, for fine-tuning of the operational temperature.
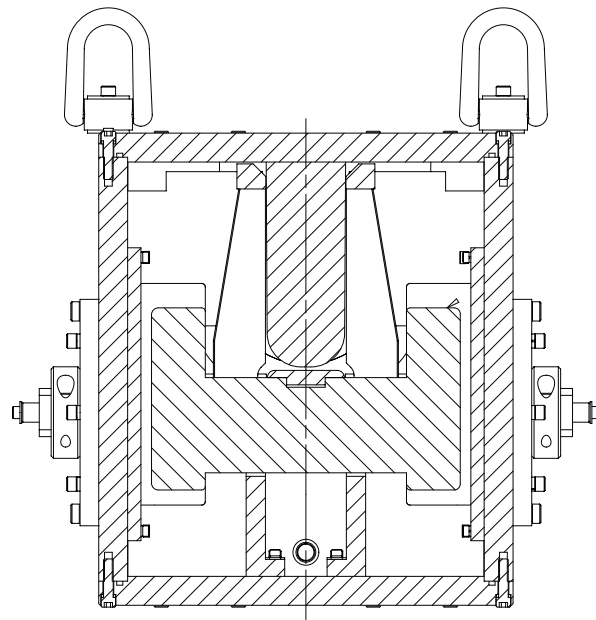
Figure 2–24: Cross section of a NOvA extraction kicker, "RKB" type

Table 2–10: Properties of the NOvA extraction kicker magnets

Property	Value
Length	1.7 m
Magnetic field (maximum peak)	0.0237 T
Integrated gradient (maximum peak)	0.0281 T-m
Number of turns	1
Aperture height	38 mm
Aperture width	86 mm
Current (maximum peak)	1000 A
Kick Angle (@120 GeV)	815 μrad
Field rise time (1% to 99%)	1.6 μs
Field flattop time	9.8 μs
Power dissipation (maximum)	250 W
Flattop stability	$\pm$1%
Cooling	Air cooled
Drawing number	5520.000-ME-460906
Color	Silver

2.6.3.7   Magnet Installation

LBNE magnet installation covers installing about 80 magnets, listed in Table 2–2, in the primary beamline enclosure. For the purposes of this discussion, the roughly 1,200-ft primary beamline consists of three sections: the MI/extraction, the vertical up-bend section and the vertical down-bend section. Based on experience with NuMI and other MI projects, LBNE beamline installation will use a combination of methods. The methods for transportation and positioning will vary for different sections, however the scheme of supporting and adjusting will be the same. Each magnet will have a stand that provides three-point support and six degrees of freedom for precise adjustment; the characteristics of magnet installation are shown in Table 2–11.

This section focuses on the technical aspects of installation. Chapter 4, on system integration, explains how to best sequence the installation steps relative to each other and other tasks. Because magnet installation is a very significant part of the beamline installation, it must be integrated into the overall plan to ensure that it is done safely and efficiently.

Magnets will be transported to the Magnet Installation Tunnel near LBNE 5 and the Target Complex (LBNE 20) by flatbed trucks, where they will then be lowered into the underground enclosure with a crane. A tugger and dolly will move each magnet to its designated tunnel location in the MI. For magnets in the sections of vertical bend, the tugger is not suitable because of the large declination in the floor (150 mrad at maximum), so each magnet and its loading dollies will be moved by a winch system.

Table 2–11: Characteristics of magnet installation.

	Extraction Stub	Vertical Up-Bend	Vertical Down-Bend
Section Length	150 ft	600 ft	450 ft
Enclosure Notes	Co-existing with other beam lines in existing enclosure, location high in enclosure	Various slopes up to 150 mrad.	Various slopes up to 101 mrad
# of Major Magnets	9	35	12
Support/Adjustment	Stand/hanger of new design	MI stands with modification	MI stands with modification
Transportation Method	Tugger, dolly via MI-10	Tugger, dollies and winch via LBNE Ent.	Tugger, dollies and Winch, via Target Hall
Positioning Method	Lift table + track	MI hydraulic carriage with modification	MI hydraulic carriage with modification

The winch system has a similar line speed (35 feet per minute) as the one used in NuMI for a similar installation, but with larger capacity (up to 40,000 lbs), a longer range (1,200 ft) and new features such as variable speed control, self-guidance and dual-directionality. After installation is finished, the winch system will be removed from the tunnel and will be reinstalled only as necessary for future use.

The dollies will require redesign so they are able to work in two different situations: together with a tugger to transport magnets across non-sloping floors and together with the winch system to transport magnets across sloping floors.

Before positioning a magnet in its final position, the locations of the beamline and magnets will be marked on the floor with the help of a survey crew. Each stand or hanger will be installed within ± 0.25 in of its ideal position; a mounting template may be necessary to achieve this. The stands will be set to the proper position to receive the magnets. The magnets will then be transported and secured at their aisle location, and the hydraulic carrier can be set and secured in its designated position. The carrier can then extend its carriage underneath each magnet and transfer the magnet transversely to its beamline location. The stands can then be adjusted to engage with the magnet and take the load from the carrier. At that point, the magnet dollies and the carrier can be removed. The stands are then adjusted to their neutral positions, and the final precise adjustment will be performed by a survey crew. For the magnets in the MI, a lift table and transverse tracks will be used to position each magnet.

In general, MI magnet stands will be used. Their features include: thrust bearing for heavy
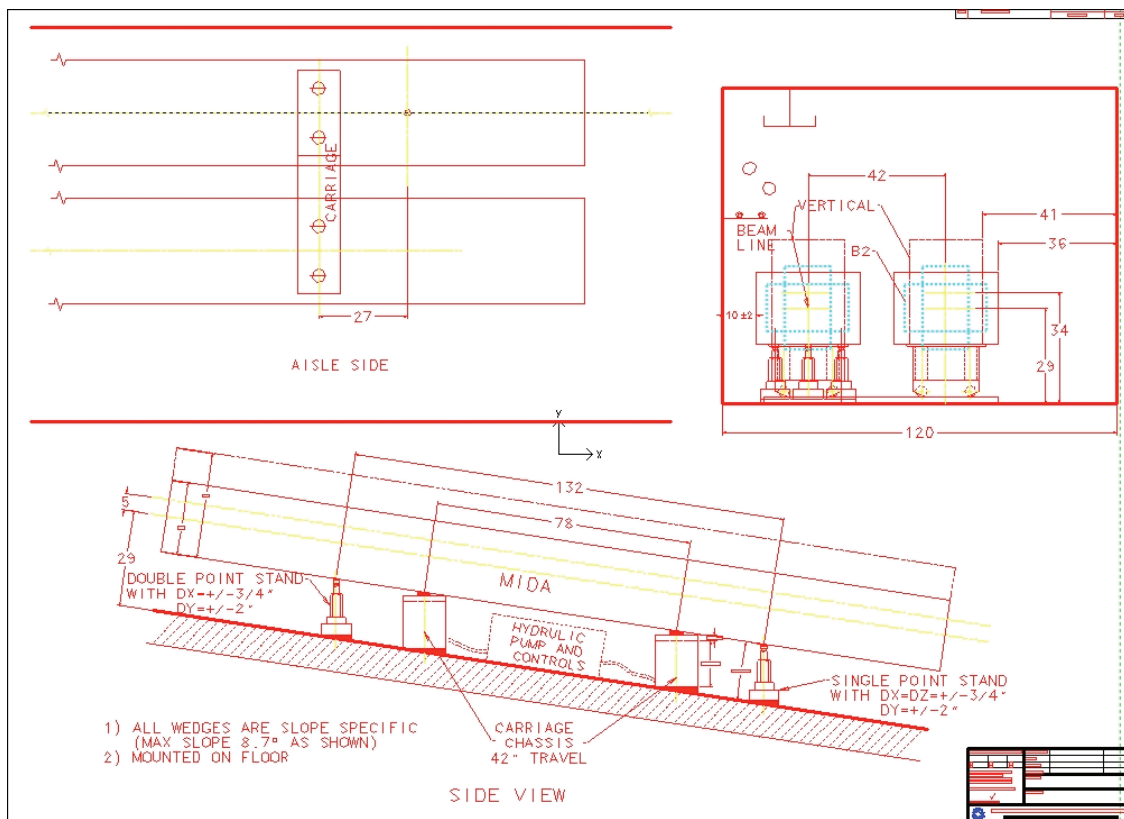
Figure 2–25: Magnet installation on sloping surfaces.

magnets (up to 40,000 lbs), a low-friction-coefficient insert for easy sliding and a bronze bearing for easy adjustment. The stands have a transverse axial adjustment of ± 0.75 in and a longitudinal axial adjustment of ± 2 in because of a deviation of the tunnel floor from its nominal elevation due to construction tolerance and settlement. Cradles will be designed to accommodate magnets in their rotated positions.

Wedging will be used to modify the bottom part of stands located on slopes based on the degree of slope, so that each stand sits upright. Shimming may be needed to level wedges due to imperfections in the floor. With the wedges at the bottom of the magnet stand, these stands provide vertical support against gravity, so there are no lateral forces even though a magnet may be located on a slope (see Figure 2–25). However, the addition of wedges at the bottom of the magnet and at the bottom of stands requires five more inches to be added to the distance between the beamline and the floor.

2.7 Magnet Power Supplies (WBS 130.02.02.03)

2.7.1 Introduction

This section describes the power supply system for the magnets that comprise the lattice optics for the primary beamline. Fermilab has a long history of developing and procuring power supplies for large magnet systems and this experience will guide the design of the LBNE magnet power systems. Some magnets will be grouped and powered by a single "magnet loop" and others will be powered individually, according to the lattice optics design. The power-supply system design seeks to minimize power consumption, reuse existing supplies from the Tevatron when possible.

2.7.2 Design Considerations

Power consumption is a cost driver during operation, and thus a design driver. In order to maintain the low power consumption, all of the magnet currents will be ramped. Each power supply will be constructed to use the maximum voltage necessary to reach the peak current and settle into regulation before the beam is extracted from the MI Each power-supply design will be selected to provide the best balance between the voltage stresses on the magnet and average power consumption.

A cycle time of 1.3 seconds is defined by the maximum MI radio frequency (RF) system, with a 0.02-second fill time and a 0.02-second flattop time. The power supplies will need to provide the ramp current in less time than the MI cycle in order to avoid crossover in the time-line generator. The ramp cycle defines the power-supply output voltage needed to supply current to a given magnet type. The efficiency of the magnet defines the total power

consumption and cooling requirements. The average power defines the 13.8-kVAC system for the main transformer usage, feeder sizing and harmonic-filter design.

Power-supply spacing for minimum voltage-to-ground requires equal impedance between power supplies. All supplies with a large output-filter-capacitor bank require a non-zero rest-current level; this makes very low current difficult. Changing this has little effect on the RMS current in the magnet string. This rest level can be adjusted on each power supply loop as needed to maintain a ramp shorter than the 1.33-second MI cycle.
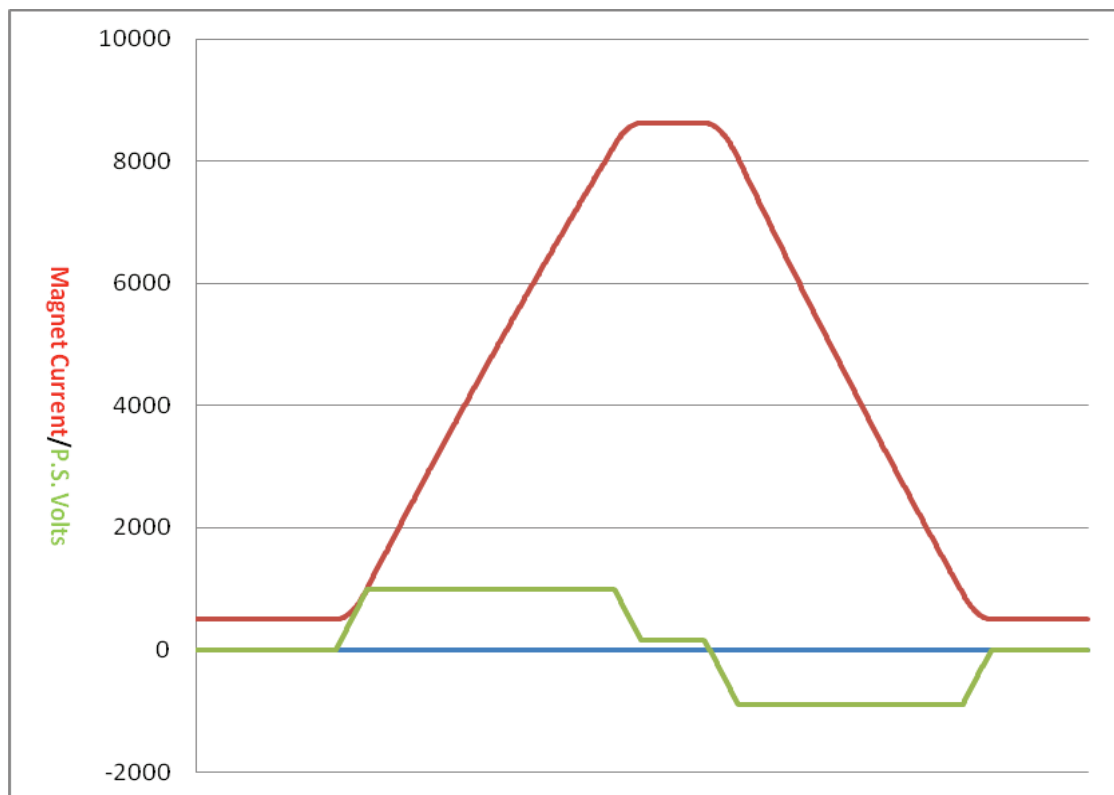
Figure 2–26: Magnet current and power supply voltage. The horizontal axis is time, the actual values would depend on the final energy of the extracted beam (1.33 s cycle time at 120 GeV).

2.7.3   Reference Design

A typical power supply ramp cycle is shown in Figure 2–26, with a ramp-up during the acceleration of the beam, a flattop for extraction, followed by the ramp-down before the next acceleration cycle. Although the cycle time depends on the energy of the beam at extraction, the shape is approximately invariant. A generic magnet power supply block circuit diagram is shown in Figure 2–27.
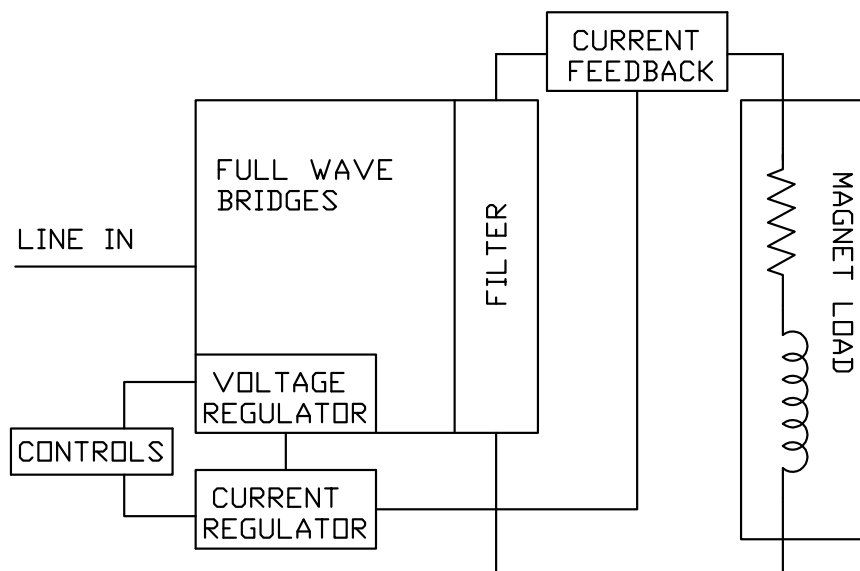
Figure 2–27: Magnet power-supply block diagram

2.7.3.1   Power-supply Loops

The primary beamline will contain five major bending-magnet power-supply loops, one large quadrupole loop, twelve minor quadrupole loops and a series of corrector-magnet power supplies. Table 2–12 shows a complete listing of the dipole magnet loops, and Table 2–13 lists the quadrupole-magnet loops and the assumed location of the equipment. Table 2–14 shows the corrector-magnet system, which will use MI corrector supplies.

Two extraction loops, LAM1 and LAM12, will be placed at the beginning of the beamline for the Lambertsons that are part of the MI enclosure system. New equipment will be procured to match the power requirement as well as possible, plus a new supply for the C-magnet loop, V1001. These supplies will be located in the MI-10 power-supply building and will use MI pulse power from an existing transformer.

Two Tevatron low-beta quad supplies will relocated and assembled in series to provide the needed power for the H204, H207 and H208 loops. Reuse of these supplies will require some work to allow them to invert and draw power out of the magnet during ramp-down. Work on similar supplies was done in the MI and NuMI beamlines. In addition there will be two Tevatron/MI "Quad" (2.8 MW) power supplies for the H214 magnet loop. Tevatron supplies have not been paralleled in any in installation to date, but the MI dipole power-supply design will be used to implement this with two paralleled 1000-V supplies.

Table 2–12: Dipole magnet loops.

Magnet Loop Name	Number of Magnets	Power Supply Location	Power Supply Type	Power Supply Voltage	Peak Magnet Current	RMS Current	RMS Power
E:LAM1	1	MI-10	150 kW	75	922	432	36 kW
E:LAM12	2	MI-10	400 kW	200	1,815	882	65 kW
E:V001	1	MI-10	375 kW	80	2,679	1,212	194 kW
E:H202	1	LBNE 5	375 kW	50	6,251	3,479	191 kW
E:H204	2/2	LBNE 5	two 375 kW	100	7,289	3,852	847 kW
E:H206	2/2	LBNE 5	two 375 kW	100	5,795	2,907	640 kW
E:H208	2/2	LBNE 5	two 375 kW	100	5,268	2,598	571 kW
E:H214	6/6	LBNE 5	two 2,800 kW	840	8,746	4,288	4,717 kW

One power supply will be placed on each dipole magnet loop, and two on the large quadrupole loop. The H202 dipole loop will have one power supply and one IDA/IDB magnet. The H204, H206 and H208 magnet loops will have two IDA/IDB and two IDC/IDD magnets each. The large magnet loop H214 will have six IDA/IDB and six IDD/IDC magnets. The quadrupole loop, Q209 will have two 625-Volt power supplies connected in series and will require that the magnet string be divided into two equal sections to reduce the voltage stress. Figure 2–26 shows the ramp current and voltage for the IDA string H214.

2.7.3.2   Power Supply Topology

The ramped power supplies will be constructed using 12-pulse rectifiers with a passive filter connected to the output. Only supplies using 12-pulse rectifiers will be connected to the pulse power feeder because a tuned harmonic filter is installed on the feeder to reduce the voltage stress on the 13.8-kVAC components. The feeder will be extended to connect to the MI beamline feeder system which has a harmonic filter with the capacity to power the LBNE beamline. The feeder will need to be extended from MI-10 to the new LBNE service buildings, LBNE 5 and LBNE 20. The details of the feeder and filter construction are in Volume 5 of this CDR. The on/off switch for the 13.8-kVAC feeder system will be controlled locally at each LBNE service building using a motor-driven disconnect to make access to the MI and LBNE easier for the operation crews. This will allow for access into the LBNE enclosure without turning off the MI.

2.7.3.3   Dipole Power Supplies

The first power supply (LAM1) powers the extraction Lambertson ILA-type magnet in conjuction with the LAM12 power supply that powers two ILA Lambertsons just as the

NuMI extraction is done from the present MI-60 location. New equipment will be procured to get the best power match for these supplies. The AC input power for this supply will be 480 VAC 3-phase, which will be derived from a dedicated 1.5 MVA pulse power transformer on the 13.8-kVAC pulsed power feeder system in the MI-10 service building. In addition, new equipment for the C magnet V1001will be procured and then installed in the MI-10 service building. Lambertson device will act as the Critical Device Controller connect to the 480-VAC line input. This device, in combination with H202, will prevent beam from being sent down the LBNE beamline when it is available for access. The magnets for this loop are in the MI tunnel enclosure and are part of the MI safety system.

The first LBNE power supply (H202) powers one IDA/IDB style dipole. The H202 magnet will be powered from single upgrated Low-Beta Quad power supply reused from the TeV. The AC input power for this supply will be 480 VAC 3-phase, which will be derived from a dedicated relocated 1.5-MVA pulse power transformer on the 13.8-kVAC pulsed power feeder system.

The next group of supplies power two IDA/IDB and two IDC/IDD magnets in series. It is planned to relocate two Low-Beta Quad supplies from the Tevatron and connect them in series to provide the ramping voltage and current for each magnet loop. These supplies were new but upgraded by Fermilab when installed in the Tevatron. These supplies will require an additional upgrade to allow them to invert (draw power from the magnets); this has been done on many other supplies of this type currently in operation in the MI and NuMI beamlines. The AC input power for this supply will be 480 VAC 3-phase, which will be derived from a dedicated, relocated 1.5-MVA pulse power transformer on the 13.8-kVAC pulsed power-feeder system.

2.7.3.4   Reuse of Tevatron Power Supplies

The Tevatron power supplies consist of two 1.4-MW, 15-Deg extended delta transformers in a single oil-filled tank. Each of these transformers is connected to three paralleled, 3-phase fullwave bridges with bypass SCRs. These bridges are then connected in series. In the LBNE installation we will use two of these supplies for the large magnet loop connected in parallel. The series bridges will be paralleled using the output filter chokes that are part of the supply. This arrangement is very similar to the MI dipole power supply that parallels two 1000-V supplies through two chokes. These supplies will be disconnected then relocated and reconfigured in the LBNE-5 service building. This plan calls for relocating all of the equipment for the two Tevatron supplies we need: 13.8k-VAC switch gear, transformers, rectifier cabinets, filter cabinets, filter choke and four output switches. In addition we will take all the regulation equipment including: eight each of Low-Beta Quad DC-current transformers (DCCT), LBQ current regulator and TeV/Low-Beta Quad voltage regulators.

The fifth power supply (H214) will be powered using two Tevatron-style dipole supplies

Table 2–13: Quadrupole magnet loops.

Magnet Loop Name	Number of Magnets	Power Supply Location	Power Supply Type	Power Supply Voltage	Peak Magnet Current	RMS Current	RMS Power
E:Q201	1	LBNE 5	75 kW	150	233	111	4.0 kW
E:Q203	1	LBNE 5	75 kW	150	262	132	4.1 kW
E:Q204	1	LBNE 5	75 kW	150	192	91	1.9 kW
E:Q205	1	LBNE 5	75 kW	150	275	134	4.3 kW
E:Q206	1	LBNE 5	75 kW	150	285	141	4.7 kW
E:Q207	1	LBNE 5	75 kW	150	344	178	7.5 kW
E:Q208	1	LBNE 5	75 kW	150	337	173	7.2 kW
E:Q209	11	LBNE-20	625 kW	625	336	184	61 kW
E:Q220	1	LBNE-20	75 kW	300	228	111	2.9 kW
E:Q221	1	LBNE-20	75 kW	150	144	71	1.4 kW
E:Q222	1	LBNE-20	75 kW	150	260	131	4.1 kW
E:Q223	1	LBNE-20	75 kW	150	360	189	8.5 kW
E:Q224	1	LBNE-20	75 kW	150	295	153	4.7 kW

connected in parallel to a string of six IDA/IDB and six IDC/IDD MI dipoles. This IDA/IDB magnet string is proposed to run at 8,748 A and will operate using a power supply designed for 840 V, 10,000 A, 5.6 MW, similar to the MI dipole supply. The AC input power for these supplies will be a 13.8-kVAC 3-phase feeder, which will be derived directly from the pulsed power-feeder system. Due to high harmonic content on the line caused by the switching of these large supplies, a harmonic filter that is present on the MI beam line feeder will be needed at the 13.8-kVAC level.

2.7.3.5   Quadrupole Power Supplies

None of the quadrupole power-supply equipment has an equivalent component in the Tevatron, so it will all need to be new for LBNE.

A large quadrupole-magnet loop (Q209) consisting of 11 3Q120 magnets will be powered from two new power supplies, each 625 V at 320 A. The remaining 11 magnet loops will use a custom-designed supply constructed for the 3Q120 magnets in the MI beam lines. These supplies will all be procured as voltage sources and each will use a Fermilab voltage/current regulator, which is the same method used in the present 75-kW supplies for the other quadrupole loops in the MI. A single current-regulator card will be installed in the voltage regulator, just as in the present system for the single-magnet loops. These supplies have proven to be reliable and will continue to be used. The Q209 magnet loop will require two supplies at 625 V each and will need to be spaced equally on the magnet string to control the voltage-to-ground on the magnets for best reliablity. Even though this is a large magnet

Table 2–14: Corrector magnet power supplies.

Magnet Loop Name	Number of Magnets	Power Supply Location	Power Supply Type	Power Supply Voltage	Power Supply Current
E:VT209 thru E:HT271	24	LBNE 5	FNAL Booster 40A Trim	180	40

string, it will only run at 336 A (peak) and 184 A RMS so it will be powered using cable for the connections to the magnets. This will make it simple to balance the voltage on the load, necessary for limiting the voltage stress in order to improve the lifetime of the magnets.

2.7.3.6 Corrector-Magnet Power Supplies

The LBNE primary beamline will utilize 24 MI-type correction-element magnets. These magnets will all be IDH style, oriented horizontally or vertically, and placed at each of the quadrupoles in the beamline. The power supplies will be the newly designed Booster-correction elements. These are individual switch-mode units that utilize a common bulk supply similar to those used in the present MI installations. A single installation is capable of driving all of the proposed 24 individual magnets. The installation will need 3-ft to 8-ft relay racks in the control room dedicated to the correction-element system. Two different cable styles have traditionally been used for correction element loads. For short cable runs, two-conductor #10 AWG shielded cable is used. This cable has a DC resistance of 2.48 Ω per thousand feet (two-way resistance of #10 wire). For longer runs, two-conductor #8 AWG shielded cable is used. This cable has a resistance of 1.56 Ω/kilofoot (two-way resistance of #8 wire). Assuming a single service building at LBNE 5, the longest run is about 1,700 ft. This gives a maximum load resistance (longest cable plus magnet) equal to 5.0 Ω, which limits the current in the magnets to 36 A on the very long runs. We will need to either adjust the system layout to reduce the length or increase the wire size to #6 AWG. The power supply is intended to be used as a ramping supply. We plan to ramp the magnets to the 40-A peak as needed to achieve the longest life in the magnets.

2.7.3.7 Kicker Power Supplies

To extract the beam from the MI we will require new kicker magnets and kicker-magnet power supplies. The present extraction kicker magnets at MI-60 for the NuMI line use three long magnets, whereas at MI-10 extraction five short magnets will be used (see Section 2.6.3.6). This change has little effect on the power supply, mostly in the number of cable terminations on/at the loads. This power supply system will be copied from the NuMI extraction kicker with little changes. The NuMI extraction kicker design is proven and reliable.

The power-supply design consists of a pulse-forming network (PFN), charging supply, resonant charger, switch tube in an oil tank and terminated transmission-line loads. To maintain regulation, high-resistance cooling liquid is circulated through the loads, requiring a heat exchanger to maintain load temperature. All of the controls for this system will be identical to the latest design installed during the NoVA upgrade to the MI.

2.7.3.8   Power-Supply Control

The power-supply control system will use the latest design of the controls interface from the Electrical Engineering Support department of Fermilab's Accelerator Division (AD E/E Support). This controller includes a built-in transient recorder and a single E-Net connection that provides the status and control back to the front-end computers. Our current reference design is similar to the ramp generator series commonly used today and referred to as a C46x card. However in the future LBNE will be moving to a VME-based control system that will provide a ramp generator that emulates the present system. The actual regulation will be provided using our Basic Micro Learning Box (BuLB-v3), highly temperature-stable DCCTs and an 18-bit DAC reference.

2.7.3.8.1   Voltage Regulator

In order to improve maintenance and operation of power supplies used in the accelerator complex, a standard voltage-regulator chassis was developed. This Fermilab voltage regulator is specified when procuring 12-pulse supplies. This has reduced the maintenance load on our engineering staff because we have many copies, >150, and are not subject to unique designs supplied by different vendors. The primary beamline will continue to use this chassis design in all of the 12-pulse high-current supplies in the line as well as in the Fermilab high-stability current-regulation system. All of the regulators will come from the Tevatron.

2.7.3.8.2   Current Regulator

The ramps for the beamline magnets move very fast, so for the magnet loops with two supplies both must be programmed to operate at the same voltage. This is in contrast to the MI where instead a controller MECAR (the Main Injector Excitation Controller and Regulator) removes supplies from the loop to reduce feeder-loading during the ramp. This type of regulation and controller is installed in the NuMI beamline now for HV101 (two supplies) and V118 (three supplies).

The current-regulation system for the large supplies will use the latest version of the BuLB v2.0 current regulator which is a subset of the MECAR regulator and will have a response in current regulation comparable to the MI. These regulators have been installed in the

present NuMI beamline high-current supplies to improve the accuracy from pulse to pulse. This regulator is used to provide the highest pulse-to-pulse stability in the current-regulation system in any we have designed. It is constructed with a built-in learning system that is used to correct the systematic errors in the current. If a known and repeatable error is found, it adds a correction to the following ramp to remove it. This has the effect of increasing the analog gain in the system and improving the real-time regulation loop response.

The operation of this system includes a temperature-regulated DCCT, stable to better than 0.25 ppm/°C, subtracted from an 18-bit DAC that is in a temperature-regulated module. This provides a <0.25-ppm stable signal with a conversion time of 2μs. This subtracted (error) signal with a gain of 100 is sent to the BuLB regulator that learns the systematic errors reducing them to zero. Using the subtracted signal with gain on the analog signals has the effect of increasing the A-to-D resolution limit and is used to generate the voltage-loop drive. The BuLB regulator has real-time fast feedback correction to correct for small random changes in the current error. This regulator also provides feed-forward drive to the power-supply voltage regulator to supply the first-order voltage needed to create the ramp current.

This signal provides an $L(i)di/dt+iR$ signal that is tailored to the parameters of each magnet load. The $L(i)$ term allows correction for the saturation level of the magnet and better tailoring of the power-supply feed-forward voltage. Correcting for the magnet saturation results in lower inductance and enables reduction of the feed-forward voltage drive to the correct level without having to use up-feedback gain. We expect to need the $L(i)$ correction term on all the bend loops in the beamline because most of the dipole-magnet loops will be used in the saturation level of the magnets. The actual current-regulation loop will still have a response time on the order of 30 Hz so the length of time the magnets are at flattop will affect the flatness of the current.

The pulse-to-pulse stability of this type of regulation is very high; the absolute resolution of the current reference is limited by the 18-bit DAC (0.76 amps/bit of FS). The power supplies will have filters that will ring during the step-down into flattop. It will be impossible to "learn out" the effect of the ring, so the shorter the flattop is, the more structure will be seen in the current. The learning system will make this repeatable ramp-to-ramp and should not affect beam transfer any more than the changes in MI bend-magnet current do. This regulation limit is not unique to LBNE but is fundamental to ramped-power systems, including that of the MI.

In addition to providing the current regulation, this system has a built-in transient recorder to capture single-event trips, allowing for faster analysis of random events. We use this to capture infrequently occurring events. In the MI beamline we use a system, commonly called the C204 module, that captures errors in the settings and operation of the large supplies. The BuLB system has a built-in limiting system that prevents the supply from operating outside of a set of limits. The first limit, on the current setting, makes sure that the requested current is in a nominal range. If that's fine, then the real-time current error and current are

checked against a set limit just before extraction of beam from the MI. The current reference and limit windows are set through an independent path to avoid mistakes in the settings that would permit an incorrect extraction. The window on the current reference is needed to allow operations to tune the beamline during normal operation. The window on the amplified current error allows for a much closer evaluation to ensure that the supply is providing the requested current. The regulator will remove the permit to the beam-extraction system (the permit system is described in Section 4.2.2.2) if any of the measured values are out of the limit window thus preventing extraction. There is also a hardware beam-abort window detector to back up the regulator which will look for large current error and remove the beam-abort permit. This abort signal looks for large errors, e.g., the power supply set to off, and prevents the beam from circulating in the MI through an independent abort loop path.

2.7.3.8.3 Series Power Supply Controller

Connection of multiple power supplies in series or parallel increases the risk of back-feed from the other devices. A system of knife switches and disconnect switches will be used to isolate the supplies from the load and beamline for maintenance. The knife switches, removed from the Tevatron, will be installed in all the large dipole-magnet systems to improve the maintainability of the supplies. In the case of the Quad loop Q209, which will require new construction, these types of switches will be included in the design.

In the MI, many supplies are spaced (in series) over a two-mile ring, each able to supply 1000 V to ground – higher than the magnets are designed to support. This requires a special controller to ensure that the supplies all go off at the same time, when we need them to go into bypass (zero volts) and prevent higher voltage to ground than the magnets are designed for. In the above-mentioned case of the Q209 loop, these supplies should be in close proximity to each other making the bypass control much simpler than for the MI system, and DC cable routing will balance the load voltage to ground. This new, custom controller will provide the voltage drive to both supplies and manage turn ON and OFF of the supplies as if they were a single supply. Controllers of this type are used on three magnet loops in which up to three 500-kW supplies in series use a commercial controller (based on a Programmable Logic Controller, PLC) in operation in the NuMI beamline. This controller also manages the magnet-loop monitors, temperature, voltage-to-ground, bus-water differential pressure and ground current.

The magnet system will need a distributed grounding system to help keep the voltage-to-ground balance during operation and a close-to-equal spacing between magnets. All of the high-current power supplies will use a distributed ground system to check for excessive ground current (ground fault) in the power supplies and magnet and, if detected, trip off the supplies. The ground-fault system is built into the smaller supplies but will be part of a separate controller in the series-connected supplies.

2.7.3.9 Power Feeder Loading

The feeder system that provides power to the primary beamline supplies will be routed from the Kautz Road substation, via an extension of the MI beamline feeder 96/97 to both of the LBNE service buildings. This feeder system already incorporates a harmonic filter to reduce the voltage stress on the 13.8-kVAC devices. The peak loading on the feeder is expected to be 13.8 MVAC and the harmonic filter will add 5 MVAC of correction to the beamline-feeder system. Beam will not be sent through the NuMI or F-sector beamlines during LBNE pulses, so the supplies in the MI beamline will be at idle and not drawing high power. This will allow the needed pulse power to be drawn from the existing capacity of the MI, and continued running with a mix of beamline choices on a time-line generator mix, as is done now, without changes to the feeder system.

To access the LBNE primary beam enclosure, a local lockout point needs to be installed. This system needs to be implemented in a way that reduces the switching-related exposure to the operations crew when locking out the system. One switch will be installed at LBNE 10 that will allow for remote operation of the 13.8-kVAC with voltage monitors and windows to inspect the switches. This switch will lock off the two large supplies, and will lock out the 1,500-kva transformer used to power all the 480-VAC supplies. A single switch will also be installed in the LBNE-20 service building on the 1,500-kva transformer to lock out the rest of the 480-VAC supplies. This type of system is installed in the NuMI beamline at MI-65 to make the lock-out/tag-out (LOTO) of the power system as simple and safe as possible. The controller that operates this switch first turns off all the supplies connected to it, then opens the switch using a motor drive. The operations crew then locks out the control power to the motor, and a key is returned to the Main Control Room which can then be locked over. The last thing the operations crew does before leaving MI-65 is to verify that the switches are open by looking through the viewing window.

2.7.3.10 Power Supply Large Equipment Installation

The large power supplies consist of multiple sub-assemblies that will need final assembly in-place in the service buildings. The outdoor equipment is large and will be put in place by a local rigging company. As equipment is taken from the Tevatron it will be disassembled using a combination of Fermilab labor and local contractors. All electrical work will be performed by local contractors. Fermilab will locate and assemble the large subsystems and perform all testing and integration into the controls system.

Fermilab will act as the general contractor to have the large sub-assemblies constructed and complete the final assembly work on site for only the large supplies, new and MR/Tevatron-size equipment. The smaller, high-current supplies will be constructed off-site and come in fully operational. They will be installed by Fermilab personnel and the power connections will be made by local contractors. The final testing and integration to the controls will be

done by Fermilab.

2.8 Primary Water System (WBS 130.02.02.04)

2.8.1 Introduction

The primary water system will feed cooling water to the magnets, power supplies and other equipment of the primary beamline, both in the enclosure and in service buildings LBNE 5 and LBNE 20. The system will include a heat exchanger, filtration systems, pumps, expansion tank, instrumentation, buswork, and piping, valves, fittings and other hardware.

This system will supply low-conductivity water (LCW) of a resistivity in the range of 16 to 18 MΩ/cm, at a supply temperature of 95°F. The majority of the system's components will be located in the pump room at ground-level in LBNE 5. From there, LCW will be fed to components upstairs in LBNE 5, as well as into and throughout the beamline enclosure, and finally to LBNE 20 Service Building and Target Hall horn power supplies. This system may be used to supply the make-up water to the Target Hall radioactive water (RAW) systems. Beamline components at the extraction point in the Q-100 area of the MI will be fed from the MI Global LCW System.

2.8.2 Design Considerations

Full system modeling needs to be accomplished once all component requirements are well understood and all configuration options are decided. System schematics will be created in parallel and should include a piping and instrumentation diagram (P&ID). Piping-installation drawings and specifications will be created from this, with sufficient documentation to provide for outside bidding practices.

Piping will be designed and installed in accordance with ASME B31.3 Code for Process Piping. Pressure vessels shall be designed in accordance with ASME Boiler and Pressure Vessel Code Section VIII Division 1. Both will adhere to FESHM [12] Chapter 5031, as well as the Fermilab Engineering Manual [13].

2.8.3   Reference Design

2.8.3.1   Heat Loads and Heat Exchanger

Total heat loads for the system will be in the range of 0.8 to 1.0 MW, depending upon the final choice of dipoles and power supplies used and the final configuration of all other equipment. Final removal of this heat will be through transference in pond water to an LCW heat exchanger, to be located at LBNE 5. This will be a tube-and-shell style exchanger, with pond water on the tube side and LCW on the shell side to facilitate the cleaning of the pond-water side.

A three-way valve setup will be used to control the LCW temperature, by directing LCW flow either to the heat exchanger or to bypass the heat exchanger. This will regulate the temperature of the LCW supply leaving the pump room. Flow on the pond water side will remain at full throughput.

2.8.3.2   Pumps

LCW will be supplied to the magnets in the enclosure with a pressure differential of 100 psid or greater. This will require pump output at 150 psid to compensate for losses along the route and equates to a dynamic head of 350 ft. Flow will be determined by the final system configuration, but is estimated at this time to be in the range of 900 to 1,200 gpm. LCW pumps will be located in LBNE 5. The arrangement will be for three 100-hp pumps to be piped in parallel, with normal configuration as two pumps in operation and one offline in standby mode.

2.8.3.3   Piping, Valves, Fittings and Hardware

Piping for LCW will be schedule 10 304/304L stainless steel, with full penetration welds. Because the total run length in the direction of the beamline will be about 800 ft, as well as runs to and from the service buildings of roughly 100 ft otherwise, thermal stresses and the need for expansion should be addressed in the design. At this time, it appears that 6-in IPS will be adequate for enclosure flows, requiring 10 in from the LBNE 5 pump room to the tunnel connection.

Piping for the pond water lines to and from the heat exchanger within the LBNE 5 pump room are to be schedule 40 carbon steel. These will have a strainer upstream of the heat exchanger (Hx) and a bypass around the strainer. In addition, building isolation valves will be necessary.

Individual magnet and power-supply component connections will have ball valves on both supply and return taps wherever possible. Where standard FODO cells provide magnets in a dipole-quad-dipole string, secondary manifolds such as used in the MI would be a very good consideration. When this is not possible, such as for the bus lines feeding the dipoles, suitable valving to ensure local isolation will be implemented. At this time, all LCW connections to all magnets are planned to be hosed connections, and will be separate from the electrical connections of the bus.

Hangers and brackets will be stock, such as Unistrut or B-Line, where possible. All nut-bolt-washer hardware is to be 304 stainless steel. All brackets not stainless steel will have a rust-preventing finish such as paint or plating.

2.8.3.4   De-ionizer / Filter Loop

Cooling water will require filtration and deionization polishing to maintain the "low-conductivity" status. This filtration will be located in LBNE 5 and will include pre- and post-filters, as well as several 7-ft^3 bottles of mixed-bed de-ionizing (DI) resins in parallel between the filters. DI-polishing options include: re-use of the MI-Tevatron columns in place at the Central Utilities Building (CUB), installation of a new column at LBNE 5, or use of many smaller individual DI bottles in parallel at LBNE 5. Using smaller individual bottles located at LBNE 5 appears to be the easiest and most cost-effective method.

This system will require a fill loop to make up water using LCW supplied from the MI. This water will come into the system through the filtration loop. This system will also require a storage and expansion tank, of around 1,000 gal, that will be an ASME U-stamped coded vessel, supplied with a level indicator and a pressure-relief device. LCW is cycled by passing a small part of the pump discharge stream through the filtration loop and into the expansion tank. This flow then exits the tank as a mix and returns to the main system on the suction side of the pumps. This ensures that the LCW in the tank remains as polished as it is in the remainder of the system.

2.8.3.5   Instrumentation and Control

The pumps will require Motor Control Centers (MCCs) in the LBNE 5 pump room. Variable-frequency drives (VFDs) will be investigated for this purpose. These, and the Temperature Control Valve (TCV) power, are high-voltage devices, requiring panels similar to what is used in the MI pump rooms.

Both LCW and pond-water systems should have suitable pressure, temperature and flow-measuring instruments, and LCW will require at least two inputs for DI status. All readings should feed to ACNET (described in Section 4.2) for remote reading and data-logging.

2.8.3.6 Buswork

Since buswork must hold water and be leak-tight, and is similar to piping, its installation is within the scope of the LCW systems. This will include the purchase and installation of the bus that runs from the power supplies into the enclosure and to the magnets, as necessary.

Where standard FODO cells provide magnets in a dipole-quad-dipole string, 1-in $\times$ 4-in rectangular bypass bus lengths such as used in the MI will be required. Existing MI designs may be sufficient. Bus discard from the magnet-building process could be used as material. Also, a location for a bus jumper run of 650 ft in length (500 ft along the enclosure, plus 150 ft from the enclosure to the power supplies in LBNE 5) will need to be determined. This bus should be water-cooled as well, and of 2-5/8-in OD bus. In addition, all exposed bus between the power supplies in LBNE 5 and the enclosure must be contained in aluminum shielding panels such as those used in the MI Service Buildings.

2.8.3.7 Other Options

The location of the power supplies is not fully mapped out, but they may be located in LBNE 20. The LCW cooling load for them is expected to be quite low. Also, there is a possibility that beamline corrector elements will require cooling water, although these needs will be minimal compared with the entire LCW system. These decisions will have an impact on the final LCW system design.

Because of the large vertical hump in the beamline trajectory, significant fluid-dynamics modeling of the entire system will need to be done, representing all the components as completely as possible, before committing to a final design.

2.9 Beam Instrumentation (WBS 130.02.02.05)

2.9.1 Introduction

The LBNE primary beamline includes instrumentation and diagnostics to characterize important beam parameters, for example, beam positions, stability, losses, intensity and transverse emittance, and to continuously monitor the operation of all the beamline elements under operating conditions, i.e., with a high-power beam. During the first commissioning and machine studies, the diagnostics systems also have to operate with a low-intensity beam (approximately 3×10^{11} protons per batch).

The four core instrumentation systems for the primary beamline are:

1. Beam-Position Monitors (BPM): 24 dual-plane BPMs for beam-trajectory measurement, based on button-style pickups and digital-receiver read-out electronics

2. Beam-Loss Monitors (BLM): 30 ion-chamber BLMs for local beam-loss monitoring, and four long (approx. 250-ft) total-loss monitors

3. Beam-Intensity Monitors: one or two toroidal transformer-based beam-intensity monitors

4. Tranverse-Beam Profile Monitors: six dual-plane secondary emission monitors (SEM) to measure the transverse beam profile (effectivley a 2D intensity plot of the beam at a given location), from which the beam emittance can be derived.

BPMs and BLMs are part of an integrated machine-protection system (MPS), where a beam-based technical interlock is used to prevent damage from a mis-steered or out-of-control, high-power beam.

Possible additions to this set of beam instruments include, for example:

- A broadband wall-current monitor for beam-timing measurements

- An imaging system to monitor the 2D beam profile at the exit window

- Non-invasive transverse beam-profile monitors, for example, IPMs or e-beam scanners, as required

2.9.2   Reference Design

Table 2–15 summarizes important beam parameters, to which all installed beam diagnostics must be sensitive. All read-out hardware (signal processing, data acquisition, timing, triggers, power supplies, and so on) will be located outside the enclosure and wired using low-insertion-loss, high-shielding cables for the detection elements in the tunnel. Housing these electronics systems in service buildings MI-10 and LBNE 5 along with the Target Complex will minimize the cable length.

2.9.2.1   Beam-Position Monitors

The BPM system will be based on simple electrostatic "button-style" pickup detectors. The measurement of integration time will be a few 100 nsec, which allows for observation of beam displacements within the batch. The anticipated resolution is 25 to 30 μm in a beam pipe with a 3-in circular cross section. The read-out system is based on digital downconverter and

Table 2–15: Beam parameters relevant for instrumentation issues.

Beam energy	60 - 120 GeV
Number of protons per pulse (6 batches each 84 bunches)	4.9×10^{13}
Repetition rate	1.3 sec (@ 120 GeV) 0.7 sec (@ 60 GeV)
Nominal beam power	708 kW
Beam intensity / batch (84 bunches)	8×10^{12} (nominal) 3×10^{11} (minimum, commissioning)
Beam size (RMS, transverse)	1.3 mm

Table 2–16: Specifications for the ion chamber loss monitor.

Materials	Glass, Nickel
Volume	110 cm^3 Argon gas at 1 Atm
Calibration	70 nC / rad
Response time	1-2 μsec
Leakage current	< 10 pA
Operating range	1 mrad -100 rad

signal-processing technologies very similar to the existing installations at other Fermilab accelerators, for example, the Tevatron, MI, Recycler, transport beamlines and experimental beamlines (e.g., NuMI, BNB). An automatic gain-correction system will continuously monitor and calibrate the electronics and correct slow drifts due to temperature and aging effects of electronics components.

2.9.2.2 Beam-Loss Monitors

The BLM system will be very similar to the installation in the NuMI beamline. Figure 2–28 shows an ion-chamber beam-loss detector, the basic element for the 30 BLMs in the primary beamline for detecting local beam losses. These sensors will be placed near the dipole and quadrupole magnets. They offer a 10^6 dynamic range, and will be operated in a window between 10^{-8} fractional beam loss (lower limit) and 10^{-2} fractional beam loss (saturation). A digital FPGA-based read-out system may also be considered, similar to the one in the Large Hadron Collider (LHC) at CERN.

A set of four total-loss monitors (TLM), based on argon-filled Heliax cables, will complement the BLMs and monitor the integrated beam loss along the beamline.
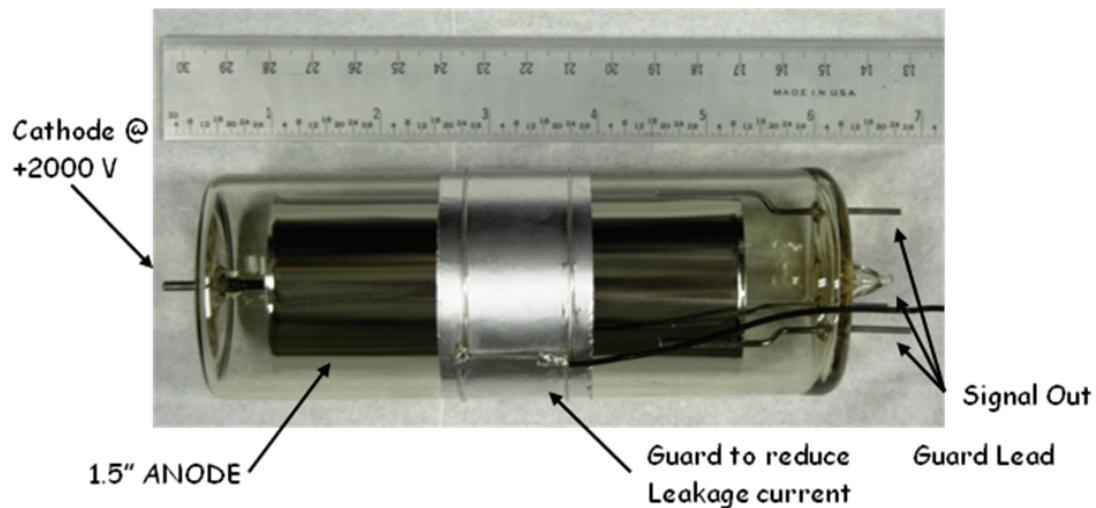
Figure 2–28: Ion chamber loss monitor.

2.9.2.3   Beam-Intensity Monitors

Only one or two beam-intensity monitors are needed for the primary beamline and will be based on 3.5-in Pearson toroidal transformers. The analog gain and filter stages may need to be located in the enclosure and the digital signal-processing and calibration systems will be located in the service building.

2.9.2.4   Beam-Profile Monitors

The beam-profile monitors are based on the secondary-emission principle. Two orthogonal arrangements of 48 thin titanium wires or foils are used, spaced 0.5-1 mm aprart, mounted on a fork-like ceramic carrier substrate, as shown in Figure 2–29 (left). A rotary-motion system sweeps the SEM wire or foil frame into the beam and performs a pulse-by-pulse measurement of the transverse beam profile. Figure 2–29(right) shows an estimation of the heating using thin, 5-μm by 150-μm titanium foils with 1-mm pitch as target for a 708-kW beam. With the inserted SEM foil, the maximum tolerable fractional beam loss is limited to 2.5×10^6. For operation of a higher beam power, for example, 2 MW, carbon filaments may need to be used as the SEM target or non-invasive monitoring techniques (IPM or e-beam deflection) may be necessary.
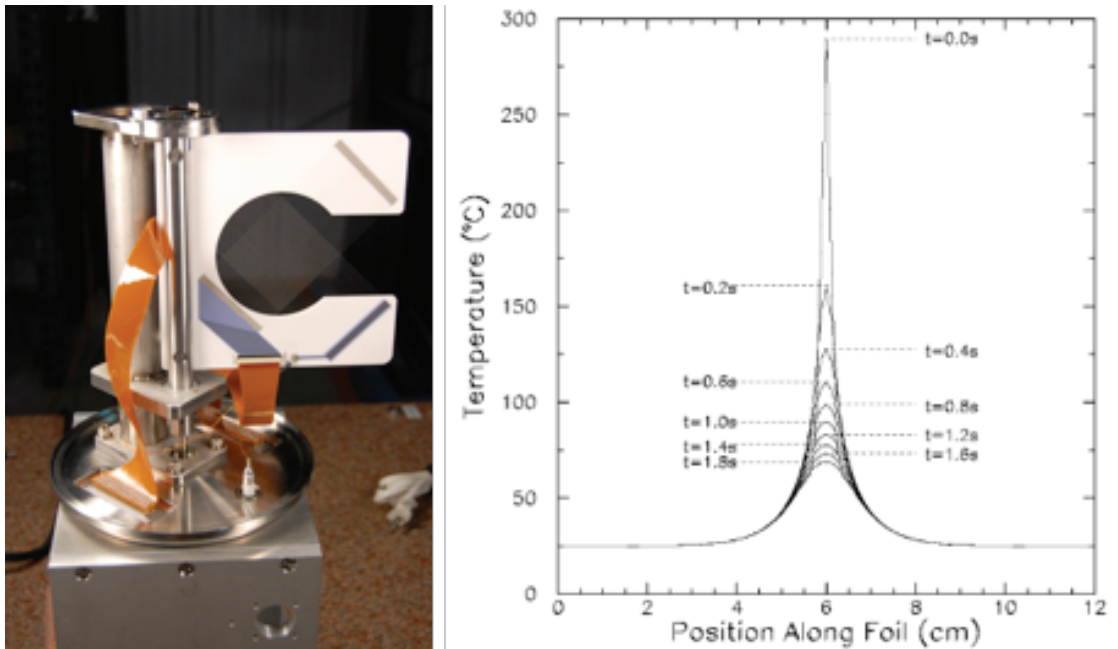
Figure 2–29: SEM beam profile monitor. Left: rotary mechanics with Ti multiwire frame; Right: Ti foil heating estimation for 708 kW beam power.

2.10   Primary Vacuum (WBS 130.02.02.06)

2.10.1   Introduction

The primary vacuum system is intended to maintain a vacuum of better than 1×10^{-7} torr residual gas pressure in the beam tube in order to reduce the beam loss due to proton-gas interaction. The entire primary beamline, about 1,200-ft long from extraction at MI-10 to the pre-target enclosure, will be divided into several independently evacuated sections according to the physics requirements, installation and pump scheme. Each section of approximately 300 to 400-ft will have about 20 ion pumps to achieve and maintain this pressure level.

2.10.2   Design Considerations

LBNE's design is of a typical single-pass beamline. The requirement on residual gas pressure in the beam tube is not difficult to meet, however, NuMI's experience shows that a highly reliable, low-maintenance vacuum system is critical for minimizing outgassing and the potential for leaks, and thus for improving the overall operational efficiency of the beamline.

Table 2–17: List of major vacuum components

Ion Pumps	Section Valves	Instrumentation cross	Bellows	Tubes
70	4	8	50	4" dia, 700 feet
Distributed pumping, distance should be not larger than 20'	Interlocked gate valve, Section length is less than 400 feet.	For pumping/venting port, Pirani gauges, CC gauges, and diagnosis.	Oval, and 3", 4" round	SS 304

2.10.3   Reference Design

The system will consist of 70 45-l/s ion pumps, four sector valves and eight gauges for separation and interlocking. All beamline devices exposed to vacuum will have to comply with UHV practice regarding material choices, cleaning and handling, in order to minimize outgassing and contamination. Although there is no plan to bake the entire primary beamline, prebaking may still be required for some devices. The following pumping scheme will be applied at each section: (1) pump down to 10^{-6} torr solely by turbo stations at two pumping ports along the whole section, and perform a leak check with a minimum sensitivity of 2×10^{-10} torr l/s, (2) start all ion pumps, and (3) valve out turbo stations (i.e., close the valves and remove the temporary turbo pumps) when 10^{-7} torr of average pressure is achieved.

In making the beamline-vacuum connections, as many of them as possible will be welded, especially in areas where a low maintenance is required. In addition, all beam instrumentation, such as BPM, toroids, and multi-wire will use conflate flanges, as well vacuum gauges and pumps.

2.10.3.1   Pumps

The roughly 70 ion pumps will be distributed along the beamline with spacing of 20 feet or less. Once a given section is evacuated to 10^{-6} torr by two portable turbo carts and the section is thoroughly leak-checked, the ion pumps in that section will be turned on.

2.10.3.2   Beam Tubes

The shape and size of beam tubes will vary along the beamline. The vacuum interface between dipoles, dipole-quadruples and beam-tube sections will be welded. The interfaces related to beam-diagnosis instrumentation are a type of Conflat-copper gasket. The beam

tubes that reside inside the magnets will be part of the magnet. Dipole beam tubes have an elliptical cross-section of 2 in by 4.8 in, and quadrupole beam tubes have an outer diameter cross-section of 3 in. The beam tubes in other areas have an outer diameter cross-section of 4 in. Various quantities of bellows, flanges, tees, crosses, stands, vacuum-grade bolts, nuts and gaskets are also needed.

2.10.3.3   Valves and Gauges

Four 4-in, fast-action gate valves will be used for protection from failures, convenience of installation and maintenance. They will be interlocked with beam operation and trigged by Pirani gauges or cold cathode gauges in each segment. About 12 all-metal right-angle UHV valves will be used for pumping ports.

2.10.3.4   Instrumentation and Control

Three standard 8-ft racks for the controllers of ion pumps, gauges and valves, will be located in a designated service building, and their outputs will be logged via ACNET. All the ion pumps, gauges and valves will be remotely controlled. Also needed are leak detectors, residual gas analyzers, and local controllers of ion pumps, gauges and valves for diagnosis and maintenance.

2.10.3.5   Baking and Cleaning

In-situ vacuum baking for the whole beamline is not required, but pre-baking some components may be necessary, especially for invading beam-instrumentation components. All components must go through UHV cleaning procedures before installation. Equipment includes heat tapes, temperature controllers, thermal couples, VariAC transformers, thermal insulating blankets, sheets, foils, UHV gloves, lint-free wipers, cleaning fluids, etc.

2.11   Beam-Loss Calculations (WBS 130.02.02.08)

2.11.1   Introduction

This section provides an overview and important examples for simulations that give information about the mechanisms and results of an improperly controlled primary beam. The high-intensity beam needs to modeled and understood to a very high precision to ensure that beamline components are kept to low activation levels and to be confident that accidental

losses are rare and not damaging. The model is as complete as possible, from extraction through the Target Hall, where beam particles (protons) and their interactions are tracked individually and in full detail. Simulated magnets are controlled in groups appropriate to the designed power-supply bus configuration. Errors in magnetic fields for individual magnets can be inserted as random manufacturing errors and as simulated current fluctuations from power-supply errors. Beam loss studies provide one key input in the requirements for the magnet power-supply stabilities.

In addition to providing validation of operational beam-loss control for environmental and component protection, the simulations can provide a level of confirmation for the design of the beam-interlock systems (Section 4.3).

Additional studies are needed to determine criteria appropriate for LBNE enclosure and building construction, as well as equipment installation during the MI operation.

Calculations that provide distributions of losses along the primary beamline are obtained with STRUCT codes [14]. The STRUCT output goes into calculations, done by MARS [15], of energy deposition and groundwater and component activation.

2.11.2   Design Considerations

The main design criteria for the primary beamline are (1) the transmission of high-intensity beam with minimum losses, (2) precision of targeting and (3) minimization of component activation. Mitigation of groundwater activation is relatively straightforward for the above-grade beam, however protection from prompt radiation, such as muon plumes, requires mitigation.

Serious consideration must also be given to accidental beam losses that, within just a few beam pulses, can cause beamline-component damage. Significant sources of beam-position instability on the target as well as increased beam loss along the beam line include the power supplies for the extraction kicker, and the quadrupoles and dipole magnets. Variations in the element strength that occur over a period of minutes or hours can be corrected. However, for variations on shorter time scales, such as pulse-to-pulse jitter, the specification on beam instability would have to be met directly at the power supply.

2.11.3   Reference Design

The proton beam extracted from the MI-10 straight section is transported 375 m to the LBNE target located 11.4 m above the MI elevation. The design is based on a 708 kW beam with intensity of 4.9×10^{13} for a 1.33-second MI cycle. The design must be compatible with an upgraded capability of 2.3 MW beam power with intensity of 1.6×10^{14} per cycle.

Table 2–18: Aperture half-size of primary beam line elements used in simulations

Element	L (m)	Hor. (mm)	Vert. (mm)	Aperture
LAM10	2.80	32.0	25.4	rectangular
Q102 quadrupole	2.1336	63.0	29.0	special
beam line quads (3Q120)	3.048	36.6	36.6	round
beam line quads (3Q60)	1.524	36.6	36.6	round
V100 (vertical dipole)	3.3528	51.6	21.7	rectangular
MI dipole (IDA/IDB)	6.09981	60.0	23.5	elliptical
MI dipole (IDC/IDD)	4.06654	60.0	23.5	elliptical
H-corrector	0.3048	60.0	23.5	elliptical
V-corrector	0.3048	36.6	36.6	round
Long drift sections	-	36.6	36.6	round
Baffle	2.50	7.5	7.5	round
Horn 1 entrance	-	12.0	12.0	round
Target (round target)	0.966	7.5	7.5	round
Horn 1 exit (conical, 10mr, round)	2.00	23.0	23.0	10mr,conical
drift Horn 1 to Horn 2	3.20	50.0	50.0	round
Horn 2	3.00	39.0	39.0	round

The worst-case conditions are simulated using a 3σ emittance of 30π mm-mrad for the beam core, with halo cut-off at 360π mm-mrad or 10.4σ, and momentum spread of $dp/p = 0.0004$ with cut-off at $dp/p = 0.0028$. The simulations show that 1% of the beam in halo is distributed with horizontal and vertical amplitudes in a range from $A_{min} = 3\sigma$ to $A_{max} = 10.4\sigma$ as $F=1/A_{x,y}$. The beam intensity is assumed to be 1.6×10^{14} per 1.33-s MI cycle (2.3 MW case), that is a factor of six higher compared to the NuMI design. The effects of magnet power-supply instabilities to beam distributions at the target and baffle, discussed in Chapter 3 are calculated for nominal emittance of 30π mm-mrad.

The beamline aperture half-sizes used in simulations are presented in Table 2–18.

2.11.3.1   Primary-Beam Loss

We have produced beam distributions that represent a sum of 100 distributions for independent random values of magnet strengths in the beamline. The calculations are done assuming a common power supply for several magnets, with instabilities as follows: LBNE quadrupole, dG/G=±0.001; extraction kicker, dB/B=±0.005; Lambertson magnet, dB/B=±0.002; MI quadrupoles, dG/G=±0.001; and MI closed orbit, dA=±$1\sigma_{x,y}$ or ±1.3mm. Figure 2–30 shows the calculated horizontal and vertical 3σ beam distributions at the baffle entrance as a function of dipole and quadrupole power-supply instability. The effect of quadrupole strength instability to the resulting beam size is much less significant than that for the dipole magnets.

The halo particle-loss distributions along the beamline as a function of dipole and quadrupole strength instability with (1) an individual power supply for each magnet and with (2) a common power supply for several magnets are shown in Figure 2–31. The resulting distribution is a sum of 100 distributions for independent random values of magnet strengths in the line. The 360π mm-mrad amplitude corresponds to 10.4σ=13.2 mm at the baffle. For an aperture radius of 7.5 mm, the baffle intercepts ∼15 kW of power from beam halo.
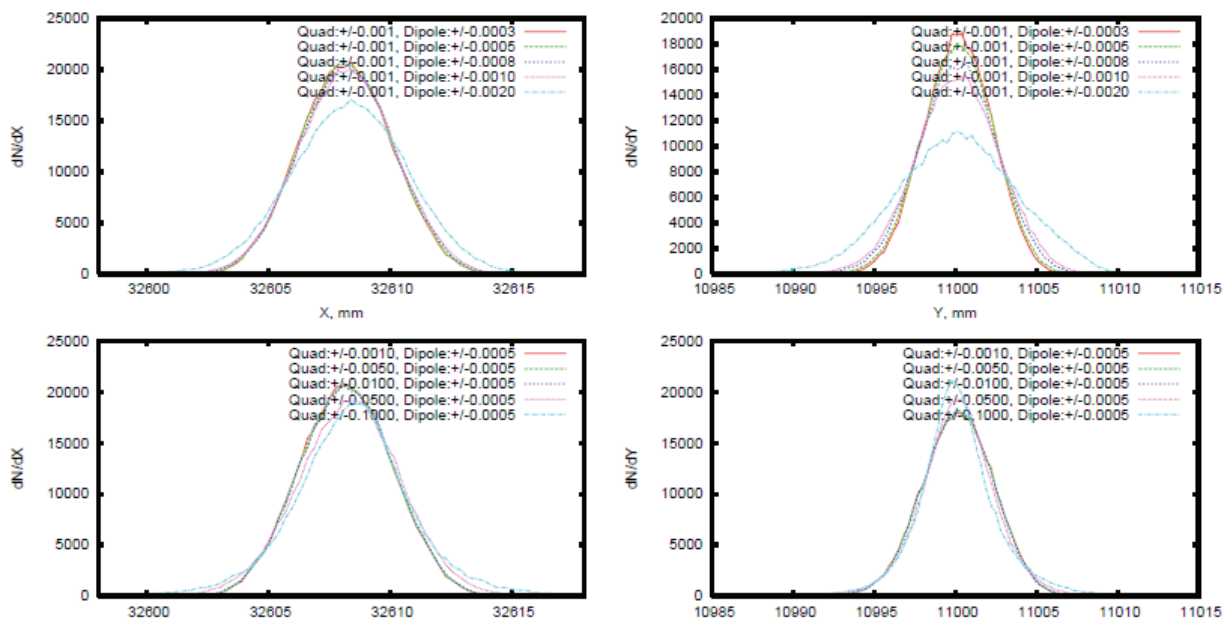
Figure 2–30: Horizontal (left) and vertical (right) beam distributions at baffle entrance as a function of dipole (top) and quadrupole (bottom) power supply instability.

Figure 2–32 shows a 3σ beam population and distributions at the baffle (left), and at the Far Detector located 1,300 km distant from the target (right) for a dipole power-supply instability of dB/B=±0.0001, ±0.0003, ±0.001 and ±0.002. Calculations are done for assuming a common power supply for several magnets with instabilities as follows: LBNE quadrupole, dG/G=±0.001; extraction kicker, dB/B=±0.005; Lambertson magnet, dB/B=±0.002; MI quadrupoles, dG/G=±0.001; and MI closed-orbit, $dA=±1\sigma_{x,y}$ or dA_m=±1.3 mm. It is assumed in these calculations that there is no proton-beam interaction with matter in the target and in the ground downstream of it. Beam distributions are shown for 100 independent, random distributions of magnet strength deviations. The beam spot size is $\sigma_{x,y} > 30$m in the far detector at dB/B=±0.0004.

The halo and core beam losses along the primary beamline and at the baffle as a function of dipole magnet power-supply instability with a common power supply for several magnets are presented in Figure 2–31. NuMI operates now at 0.4 MW with maximum allowed fractional beam loss of 10^{-5} from the total intensity. For LBNE's 0.7 MW, the safety level will be 5×10^{-6}, and for 2.3 MW it will be 1.5×10^{-6}. To have a viable operational margin, one has to keep normal beam loss an order of magnitude better than this, or 5×10^{-7} for 0.7 MW
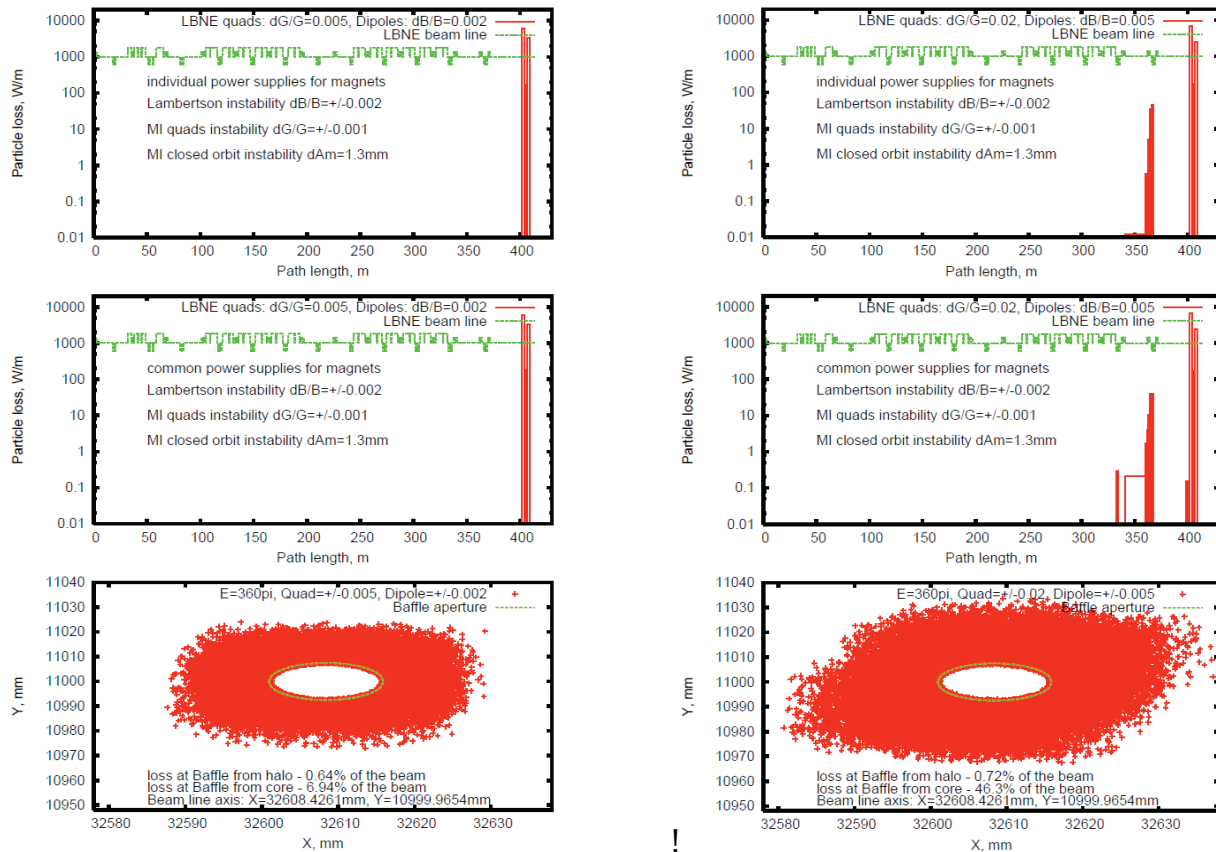
Figure 2–31: The halo particle loss distribution along the LBNE beamline at dipole strength instability of dB/B=±0.002 (left), dB/B=±0.005 (right) and quadrupole strength of dG/G=±0.005 with individual power supply for each magnet (top) and with common power supply for several magnets (second line). Beam loss population at the baffle is shown on the bottom.

and 1.5×10^{-7} for 2.3 MW, that is $\sim$0.4W. From this point of view, the dipole instability should be less than dB/B<$\pm$0.0025, which keeps losses below 1 W/m.
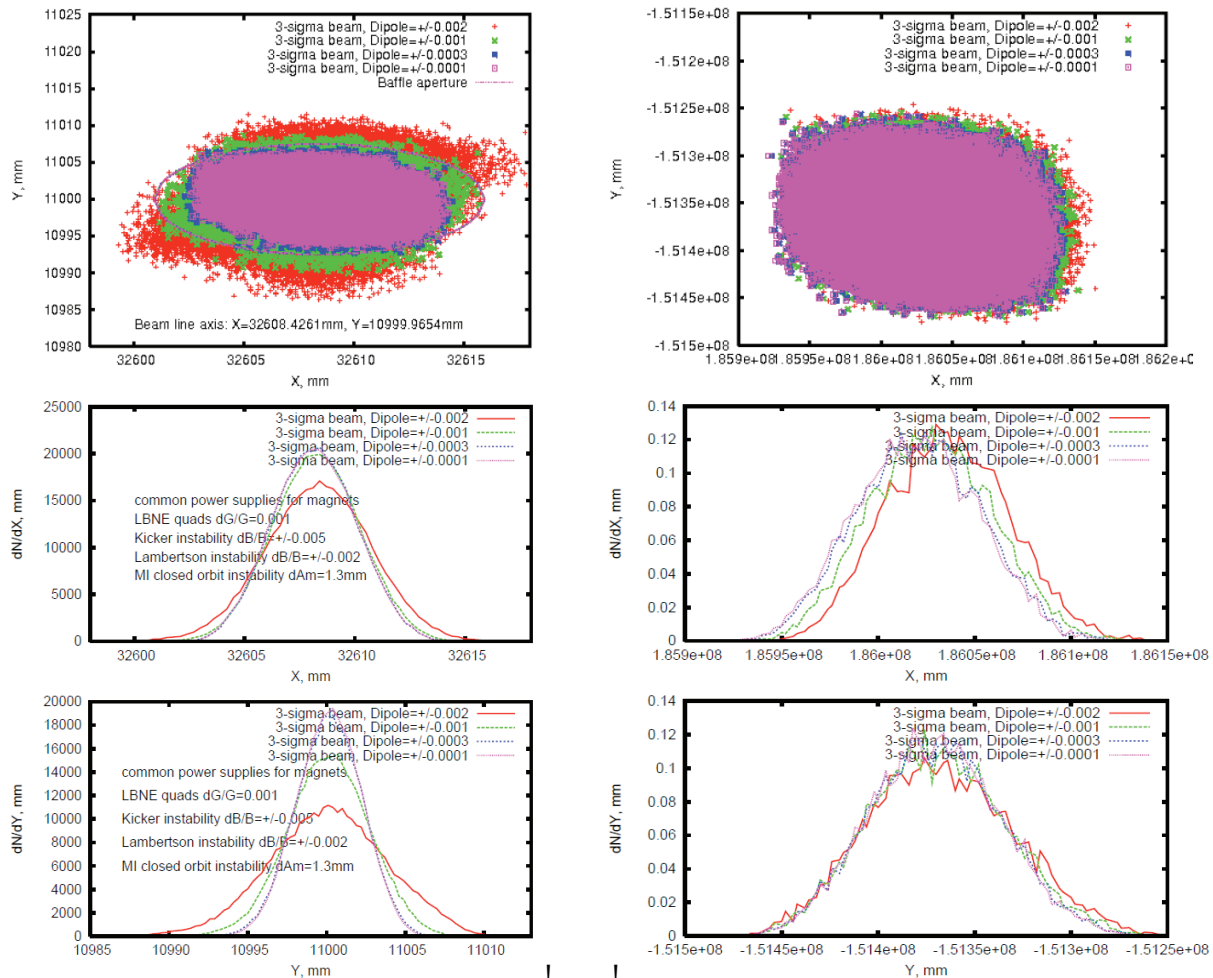
Figure 2–32: The 3σ core beam population (top) and distributions (middle and bottom) at the Baffle (left), and at the far detector (right).

2.11.3.2 Accidental Total Beam Loss

An accidental total beam loss will likely cause component heating and damage, may induce groundwater activation and cause radiation concerns outside the tunnel. The lost-beam trajectories along the beamline due to an accidental degradation of bending-magnet strength have been calculated and are shown in figure 2–33.

The instantaneous temperature rise in a dipole-magnet beam pipe following the loss of the entire beam (2.3 MW) is $\sim$ 2500 K, which is a factor of two higher than the melting point

of stainless steel. The beam vacuum pipe or a magnet would be effectively destroyed in one beam pulse (or a few pulses at 708 kW). This possibility must be eliminated by analyzing all parameters of the system just before extraction, and then abort the beam to the MI beam dump if any critical parameter is out of the safety region (for details of the LBNE beam-permit system see Section 4.2).

2.11.3.3   Activation of Components

Beamline-component activation is a critical issue in a high-intensity beamline whose operational life is measured in decades. A sample case is presented here, where 0.3% of a 2.3 MW beam is lost continuously, as the outer-most part of the beam envelope interacts with the vacuum pipe, magnets and other installed components. The magnitude of this loss is chosen to be typical of what one might have anticipated in lower-intensity beamlines of the past. Of course for LBNE, this value is unacceptably high, but results from this study can be scaled to estimate tolerable losses. Residual dose rates for losses of 0.003 of total intensity for 30 days, followed by one day cool-down, is shown in Figure 2–34. Residual dose rates on the surfaces of bending and quadrupole magnets reach 50 rem/hr, which is three orders of magnitude higher than the goal of less than 50 mrem/hr. Scaling these results to acceptable limits implies that losses need to be no greater than order 10^{-6}. The methods proposed to achieve this are listed in Section 2.3.4.
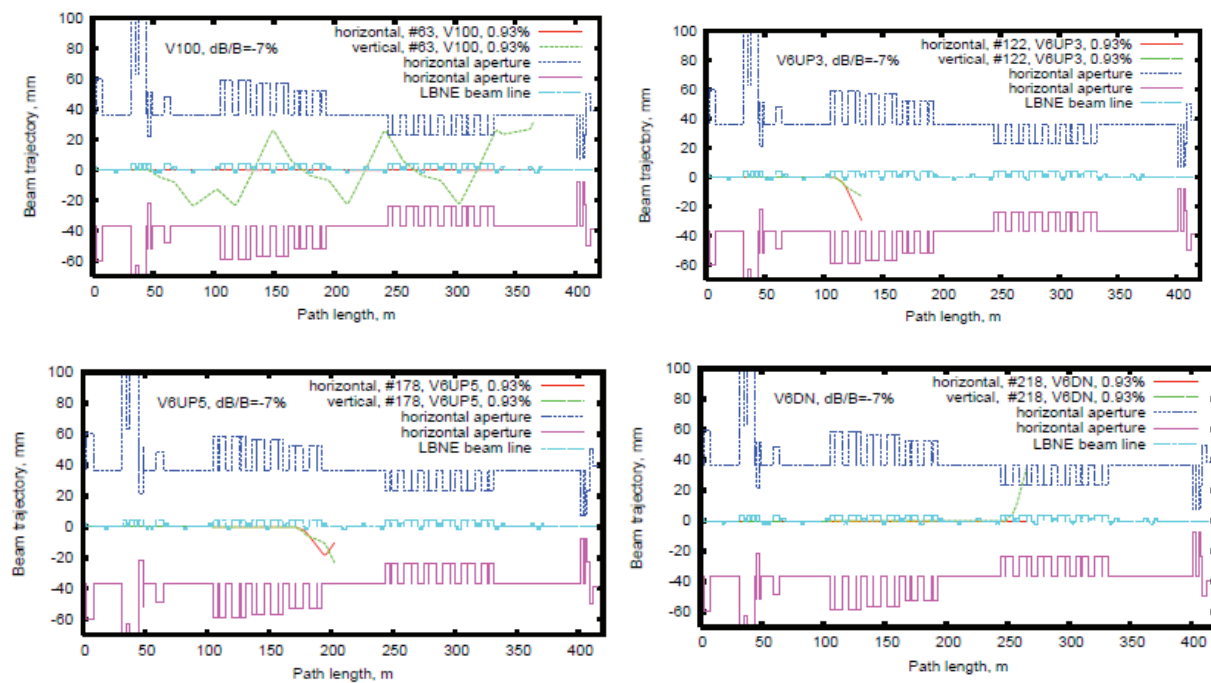
Figure 2–33: An example of beam trajectories along the beamline for a beam lost due to accidental degradation of bending magnet strength
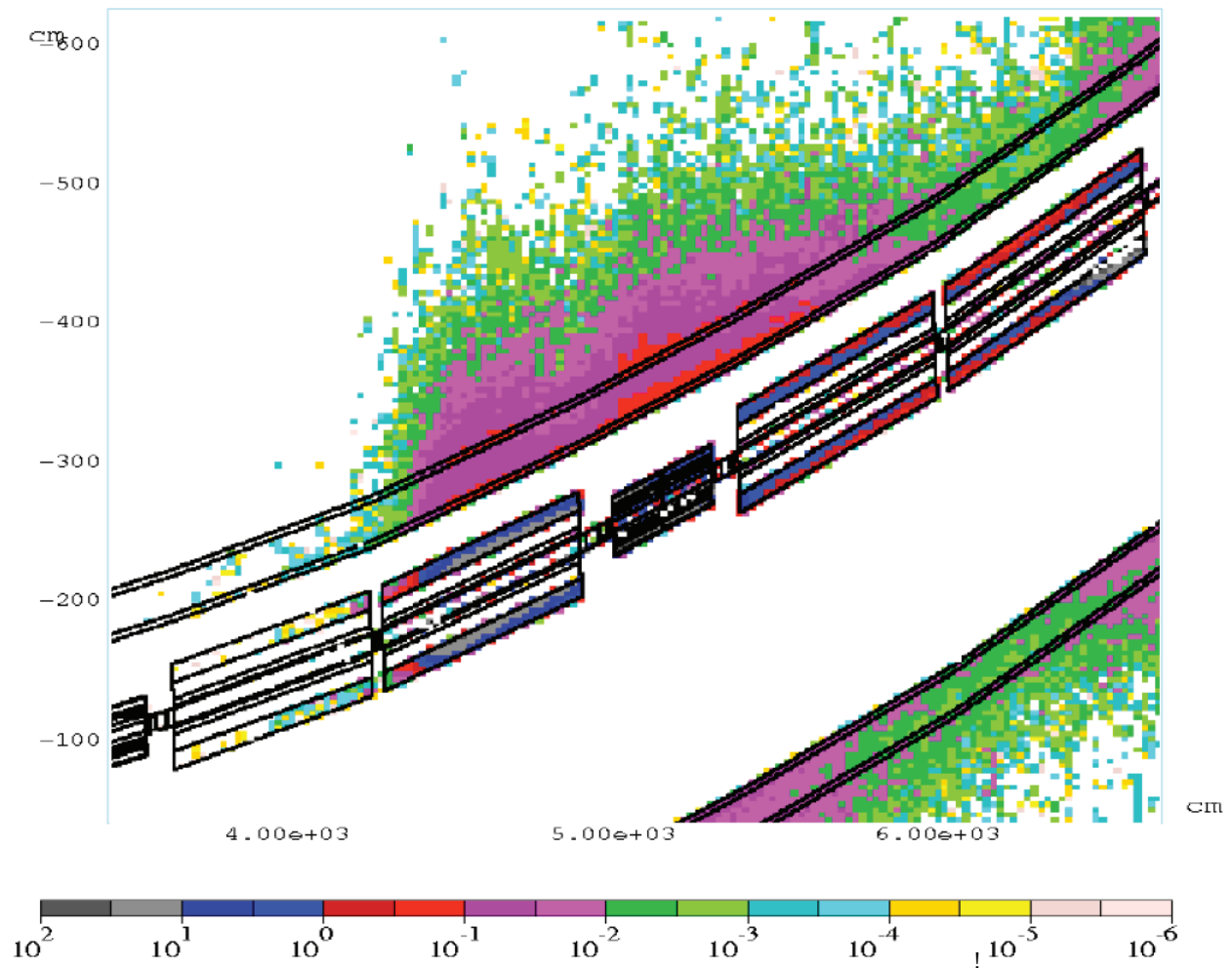
Figure 2–34: Residual dose rates along the beam line and magnets following a loss of 0.3% of the beam for 30 days followed by one day cool-down. The color-coded logarithmic scale has units of m-Sv/h (1 m-Sv/h is equivalent to 100 mrem/h)

3   Neutrino Beam (WBS 130.02.03)

3.1   Introduction

This chapter discusses the conceptual design of the second main system within the LBNE Beamline, the Neutrino Beamline, which refers to the set of components and enclosures designed to efficiently convert the initial proton beam into a high-intensity neutrino beam aimed at the far detector, 1,300 km away.

The LBNE neutrino beam would be the fourth large neutrino beam facility designed and built at Fermilab. Its design is very similar to the NuMI beam constructed in 2004 [16]. All major elements of the LBNE design have their analogs in the NuMI beamline. Thus, the experience gained in constructing and operating the current facility can be incorporated into LBNE design as improvements. The LBNE neutrino beam must necessarily be of even more robust design since the initial beam power is expected to be increased threefold after some years of operation at 708kW. For most elements, the increased capacity will be met by incremental improvements and replacement strategies.

A proton-beam pulse from the primary-beam system enters the neutrino beamline system (from the left in Figure 3–1) through a beryllium "window." This window seals off the evacuated beam pipe of the primary beamline, and the protons enter the air-filled target chase (the volume surrounding the target and focusing mechanisms). Initially they travel through a narrow, 4-m-long cylindrical volume. It is surrounded by shielding material, called a baffle, which is intended to shield the downstream equipment in case of a mis-steered beam pulse. A meter and a half past the end of the baffle, they reach the target, a long, thin graphite cylinder in which about 85% of the protons interact and produce secondary particles. The target is surrounded by the first horn, a magnetized structure which provides initial focusing for the secondary particles, predominantly pions and kaons. A second horn, a few feet downstream, provides additional focusing for the secondary particles before they enter the decay pipe, where a large fraction of the pions will decay to neutrinos, forming the neutrino beam. The final portion of the neutrino beamline is the absorber, downstream of the decay pipe. The absorber is intended to stop the protons that failed to interact in the target and the secondary particles that failed to decay to neutrinos; it must be designed to
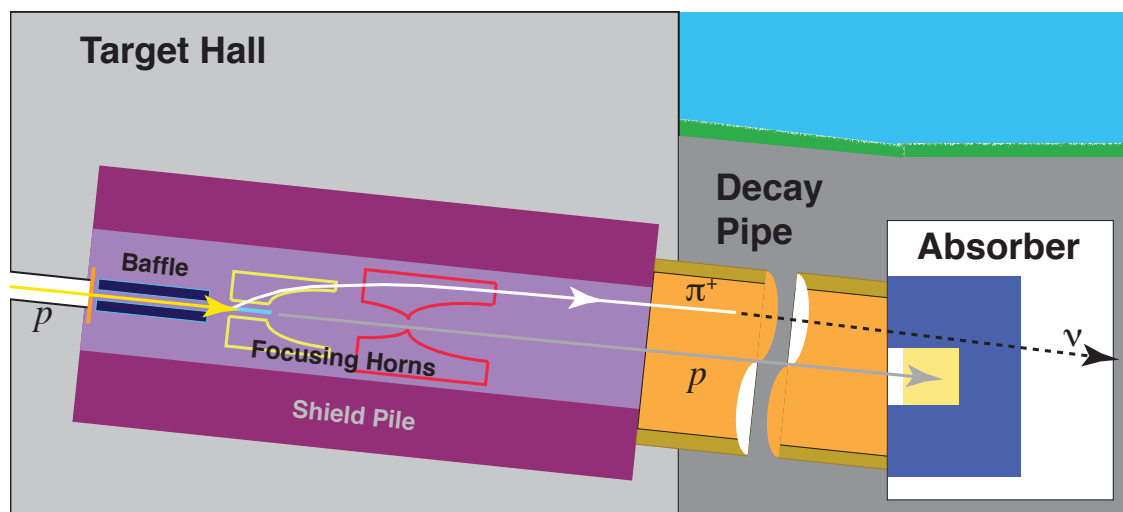
Figure 3–1: A cartoon of the neutrino beamline showing the major components of the neutrino beam. From left to right, the beam window, horn-protection baffle, target, the two toroidal focusing horns, decay pipe and absorber. The air volume surrounding the components between the window and the decay pipe is called the target "chase". The target chase and rooms for ancillary equipment (power supplies, cooling, air recirculation and so on) is included in the area called the target complex (not pictured).

sustain the beam energy deposition under expected normal operational conditions as well as under accident situations.

Section 1.2.3 presents a more thorough introduction to the Neutrino Beamline.

3.1.1   Design Considerations

Primary design considerations include the need to provide a wide-band beam to cover the first and second neutrino-oscillation maxima and the need to plan for an eventual upgrade in incident primary beam power from 708 kW to 2.3 MW without retrofitting.

To avoid both technical and cost/schedule problems in the future, the potential beam-power upgrade has design implications for several subsystems, including: the baffle and window-replacement infrastructure, the two-horn system, the dimensions of the target pile, decay pipe and absorber as well as the cooling systems for the target chase, decay tunnel and absorber.

Radiological concerns, such as prompt dose, residual dose, air activation and tritium pro-duction are also important considerations. They have been extensively modeled, and these issues have been addressed in the system design.
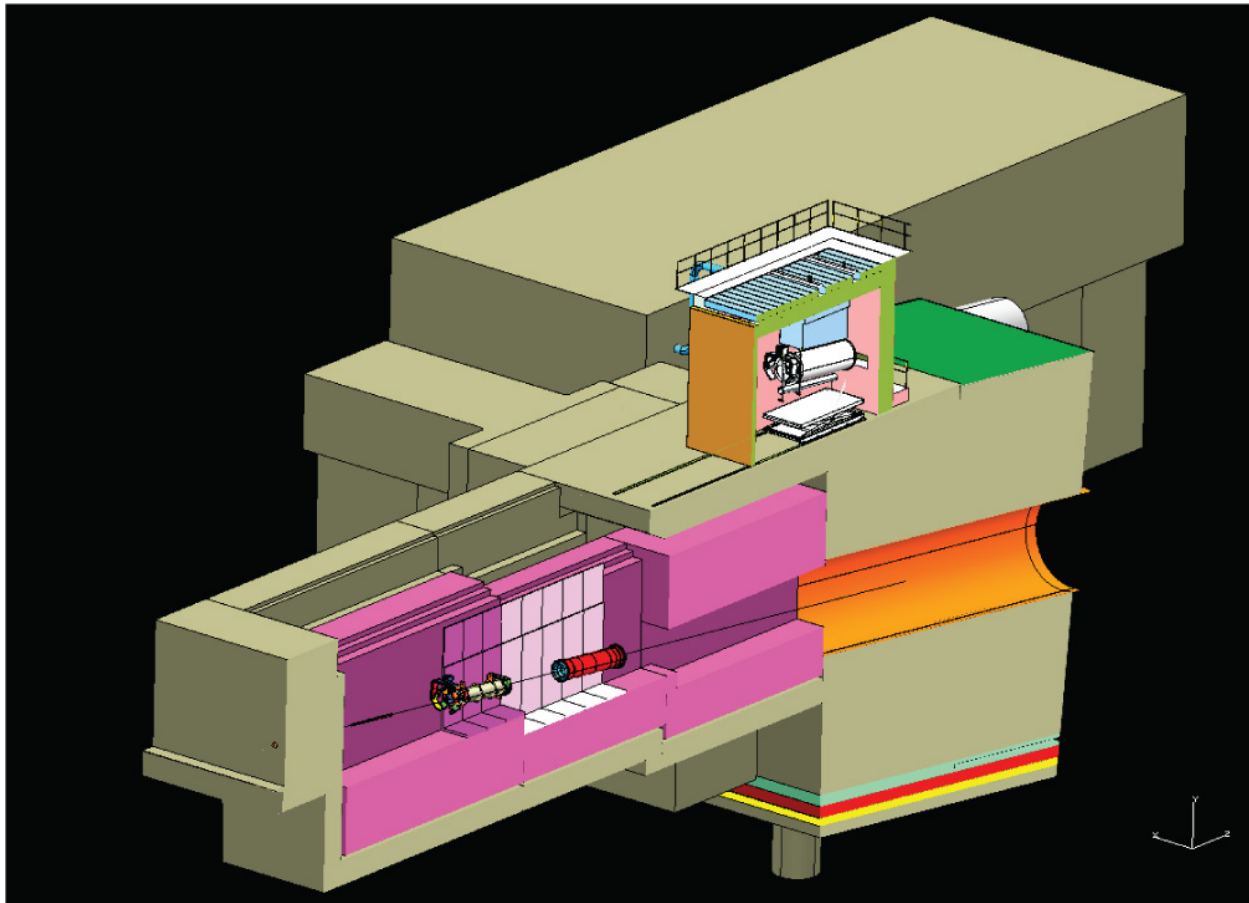
Figure 3–2: A cut view of an engineering model of part of the target complex, showing the relationship of the components depicted in Figure 3–1 to scale (the target chase, purple zones, is 23m long). The upstream end of the decay pipe is shown (orange), the absorber is not represented here. Above the target pile the Target Hall work cell (Section 3.11) is shown. The air handling room is largest rectangular structure beyond the start of the decay pipe. Other rooms not shown include the power supply room and support equipment rooms, located to the left on an upper level.

3.2   Primary Beam Window and Baffle (WBS 130.02.03.2)

3.2.1   Introduction

The upstream beamline enclosures are separated from the target chase by a 3.9-m-thick concrete shielding wall to isolate the upstream (evacuated) beamline from high radiation dose rates. The primary protons enter the target chase through a window in the wall; it is a beryllium hemisphere that seals the evacuated primary beampipe.

The baffle, just downstream from the window, is a passive device that works essentially as a collimator. It is a graphite structure intended to prevent any mis-steered beam pulse from from causing damage. In particular, it protects the inner conductors of the horns from the primary beam directly striking the aluminum. The baffle design depends on the geometry of the parts it protects as well as beam size, so the reference baffle design follows from the beam, horn and target specifications.

3.2.2   Design Considerations

An important consideration is allowing for replacement of the primary beam pipe and the mating flange to the window in the event of damage to the latter. A primary beampipe cartridge design with an embedded liner within the concrete shielding wall will allow this, with a primary beampipe pressure of 1×10^{-8} Torr.

A second important consideration is the potential beam-energy upgrade from the initial 708 kW to 2.3 MW. First, this affects the window design since the spot size for the 708 kW beam energy design, 1.5 mm (*rms*), similar to the NOvA design [17], may increase by a factor of two for a 2.3 MW beam. The aperture will be scaled by a factor of two, as a conservative estimate. The window housing and mating primary-beampipe aperture also require a larger size. Secondly, the window itself will need to be interchangeable. The 708-kW primary-beam window design validated by NOvA considers an air cooled, 0.25-mm-thick, 25.4-mm-diameter beryllium grade PF-60 membrane.

Thirdly, the window itself (also referred to as the beryllium membrane) may require active cooling at the 2.3-MW value.

In either beam energy case, the construction tolerance is 0.2 mm (*rms*); the goal for overall baffle position accuracy is 0.5 mm, including thermal effects, survey tolerance, and carrier instability. The construction and alignment tolerance of the hole through the baffle must be 0.5 mm or better [18].

In general, each baffle design must withstand two thermal conditions induced by the proton

beam: normal operation under ∼2% continuous beam loss (DC) and a one-pulse accidental event. To accommodate both these conditions, the 708-kW baffle design relies on heat transfer to the existing airflow through 18-pin radiator sections clamped along the baffle's length. In addition, conductive filler will be used to bridge the thermal-resistance gap between each radiator pin section surface and the 61-mm-diameter aluminum tube outer surface. These thermal conditions increase for both normal operation and one-pulse accidental event going from 708 kW to 2.3 MW, as well, and the conductive filler may require further investigation.

Early detection of a beam mis-steering event and beam termination through the upstream Beam Position Monitor (BPM), described in Section 2.9.2.1, and baffle thermocouple instrumentation, described in Section 3.2.3, limit the amount of errant pulses received.

3.2.3   Reference Design

The embedded 273 mm O.D., 6.4 mm thick stainless-steel stepped liner pipe implemented during the civil construction is shown in Figure 3–3(a). The primary beam pipe cartridge consists of an internal 76 mm O.D., 1.5-mm-thick beam pipe suspended within an outer 260 mm O.D. stepped pipe housing, both constructed from stainless steel as shown in Figure 3–3(b). Spider collars at each end provide adjustment between the cartridge housing and internal beam pipe. These collars will lock following pre-alignment and the annular void between cartridge inner housing and outer beam pipe surfaces is filled with epoxy to prevent US radiation back-scatter. Silver plating the exterior cartridge surface and implementing a 550 mm O.D., 25 mm thick stainless steel cartridge extraction flange eases removal. This extraction flange also provides indexing of the cartridge to establish longitudinal position and fixed rotation.
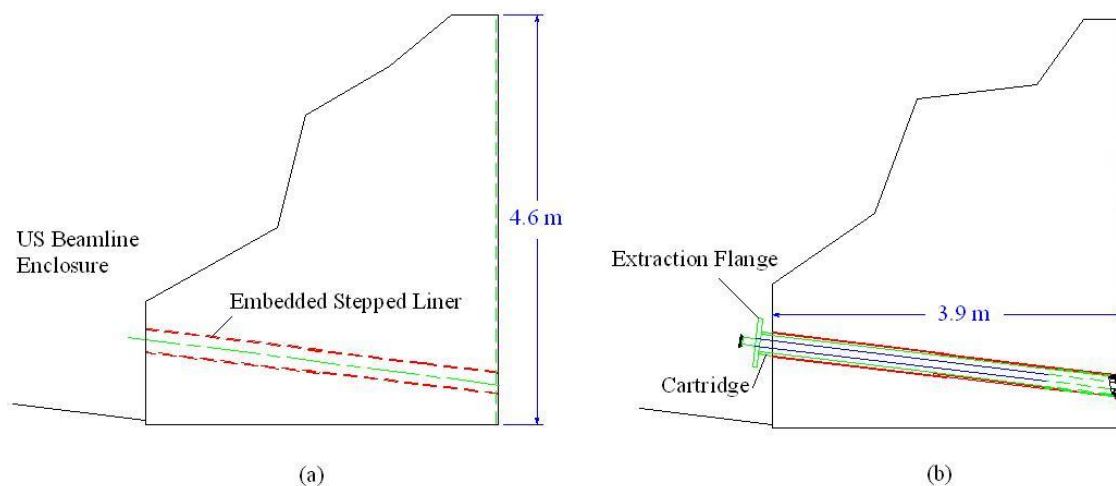
Figure 3–3: Shielding wall with embedded stepped liner. (b): After cartridge insertion.

Alignment of the primary beam pipe is multi-stepped process. First, the embedded liner is fudicialized and mapped from the US beamline enclosure prior to beamline commissioning.

Remote pre-alignment of the cartridge is necessary relative to the mapped liner. Then, after securing the primary beam pipe position within the cartridge (locking end collars and filling void with epoxy), a cart and cable system transports the assembly to the US beamline enclosure for installation. Insertion of the cartridge involves a combination of support from the cart and overhead rigging operation while moving axially.

Initial alignment of the beam pipe cartridge and attached window is obtained by using a DS docking feature shown in Figure 3–4 and attachment at the US extraction flange. This support-alignment system provides repeatable positional alignment within a final alignment resolution of ±0.5 mm. There is a provision for the insertion of an US and DS aperture shielding plug used for protection during primary beam pipe cartridge replacement. These aperture shielding plugs would be constructed from steel and moved into the US beamline and target chase only during periods of cartridge replacement. DS remote handling of the aperture shielding plug within the target chase is possible through a rail/cable system, which attaches to an embedded stainless steel plate within the concrete wall at the target chase US face.

(a)   (b)
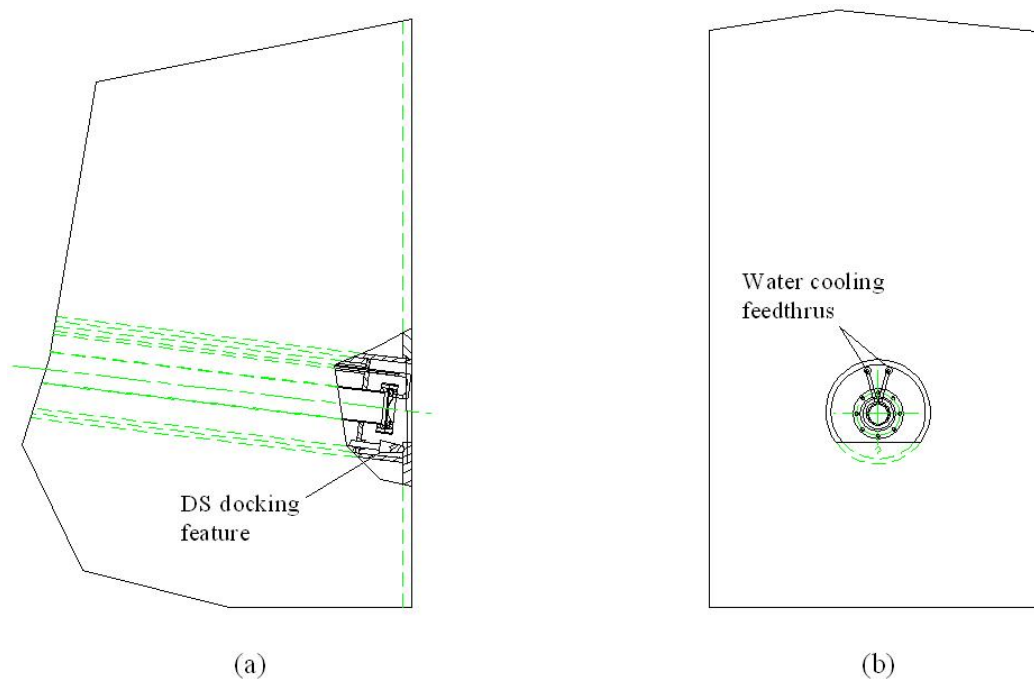
Figure 3–4: Section view of replacement window assembly. (b): End view of window assembly.

The 708-kW primary beam beryllium thin window design is able to withstand the stress waves and also pressure and thermal loading given a 1.5-mm spot size while periphery air-cooled. At 2.3-MW beam energy, a 50-mm diameter partial hemispherical beryllium window with a 3.5-mm spot size and natural convective cooling also is sufficient. A 1.5 mm spot size at 2.3 MW is not acceptable since the combined maximum shock stress, transient stress and transient temperature induced within the window are above the ultimate tensile stress for

beryllium. Optimization of a periphery air-cooled, hemispherical tapered beryllium window shape with a thin center and gradually thicker outer crown which allows greater conduction could be applied with further investigation [19].

A conceptual section view of a 50-mm diameter, 0.2-mm-thick partial-hemispherical beryllium window shape periphery water-cooled given the 2.3 MW (1.5 mm spot size) case is shown in Figure 3–5. The primary beam window design constructed from a 117.5 mm O.D., 19.1 mm thick 316 stainless-steel Conflat flange. This flange is a bolted connection which attaches to the primary beam pipe mating Conflat flange with a knife edge seal. The window construction and knife edge seal must maintain a leak rate of 10^{-9} Pa-m^3/s or less required to achieve primary beam pipe design pressure.
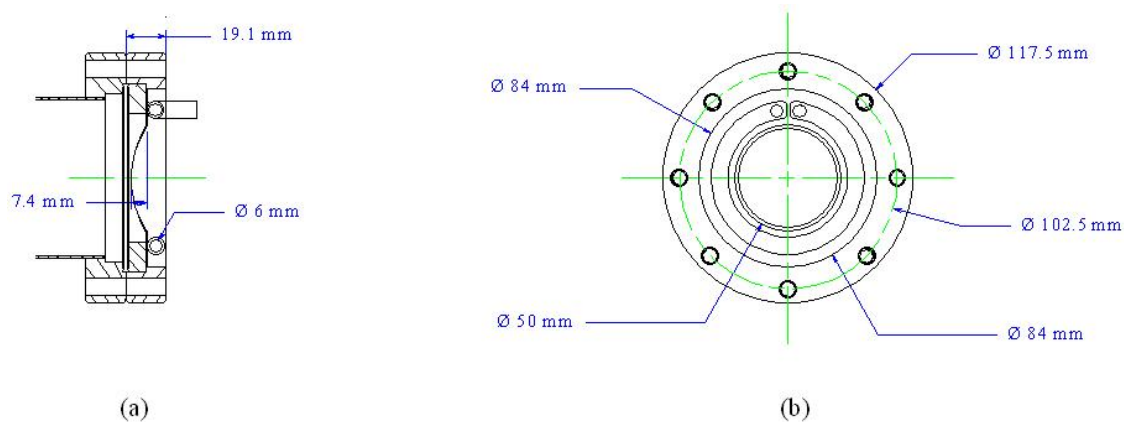
Figure 3–5: Section view of 2.3-MW-capable beryllium window. (b): End view of window assembly.

The baffle is a passive device, essentially a collimator, which protects the inner conductors of the horns from the primary beam directly striking the aluminum. A critical aspect is determining the size and position of the aperture with respect to the target and horns. The baffle design depends on the geometry of the parts it protects, so the reference baffle design follows from the horn and target specifications.

The 708 kW baffle baseline design consists of ten 57 mm O.D. × 13 mm I.D. × 150 mm long graphite R7650 grade cores which are enclosed by a 61 mm × 3 mm thick × 150 cm long aluminum tube after annealing. Eighteen 66-mm long radiator pin sections are evenly placed along its length at 11.5 mm intervals with a provision for two 33.4 mm openings supporting the baffle ∼22% of the length from each end as shown in Figure 3–6. The target and baffle are supported independently from a separate carrier and module. A greater distance between baffle and target is planned as compared to the medium energy NOvA design.

Performing horizontal and vertical beam scans across the baffle and using the hadron monitor for primary instrumentation will provide an accurate check on the baffle centroid position
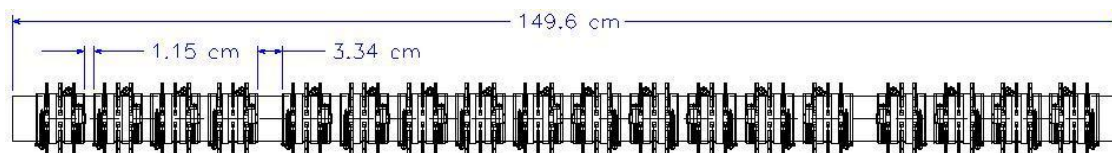
Figure 3–6: 708 kW (NOvA) baffle baseline design for LBNE

with respect to the beam axis. However, this technique has limited sensitivity to the baffle angle. A fairly simple way to derive the angle is to have a position sensitive device rigidly mounted to the baffle, positioned one meter US of the baffle (shown as a cylinder US of the baffle in Figure 3-5). A set of nickel tabs positioned one cm above, below, and left/right of the beam axis, instrumented with thermocouples, would suffice. (Such a scheme was used for the NuMI target tests in AP0). The beam should be able to scan to at least ±12 mm at low intensity. At NuMI, these scans are done with 8×10^{11} protons per pulse, which is 2% of full intensity; a similar intensity should also work for LBNE beam scans.

The baffle support module is shown in Figure 3–7 as a solid steel structure with dimensions; 0.66 m width $\times$ 1.02 m height (upper section) and 0.44 m width $\times$ 1.02 m height (lower section), and 2.5 m along the beamline. This structure's weight is within the crane capacity of 40-tons. Motorized vertical drives will independently adjust the vertical rods on each end block of baffle support module. The module is fixed in station (longitudinally) by location of the spherical socket mechanisms. This is established through the design of the longitudinal beam and slightly adjustable mating plates where the setup is performed once and secured. Transverse (horizontal) and yaw are controlled by motorized sliding kinematic mount points. Pitch and vertical position are controlled by the rods down the centers of the end walls of the module. The primary window shielding structure found US of the Support rails for LBNE are planned to be horizontal and level with respect to gravity.

3.3   Targetry (WBS 130.02.03.3)

3.3.1   Introduction

This section details the neutrino-production target, its support module and the accompanying instrumentation for commissioning, alignment and monitoring of the target and focusing system in the beam. The target is the source for the pions and kaons which later decay to produce neutrinos. Although the production of these particles can obviously be increased with more beam power, engineering and material properties place a limit on beam power for a practical target. These practical concerns include removing beam heating, understanding thermal shock and coping radiation damage to solid materials. Target replacement strategies also play a major role in design. For LBNE, a conceptual design for a target operating at 708 kW is given, which appears to have appropriate margins for reliability in this regime.
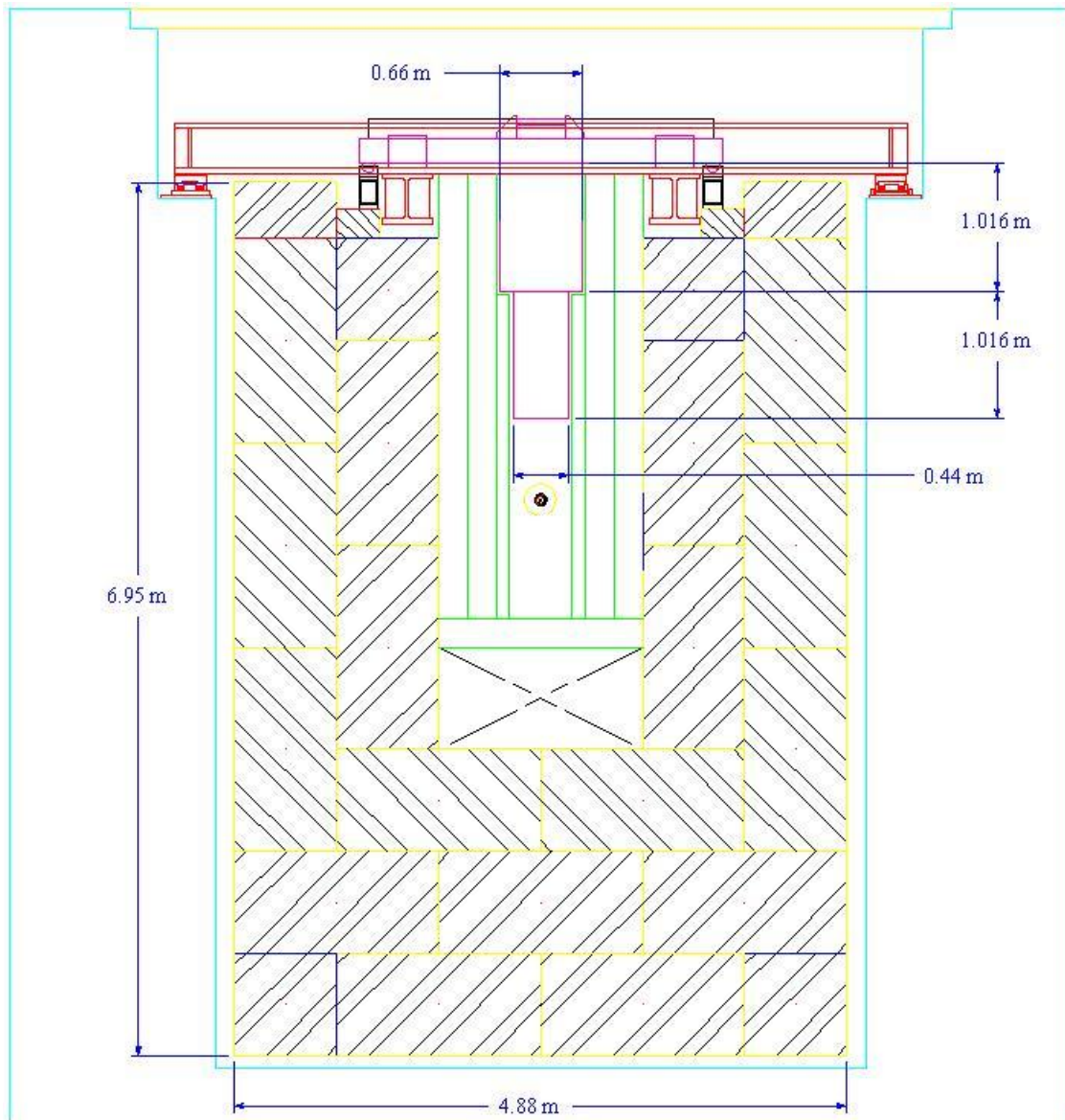
Figure 3–7: Section-view of baffle support module design

Research and development of solid target designs that operate at a significantly higher beam power are also being actively pursued.

The LBNE Beamline target, based on both the NuMI experience and other studies for a higher-power beam, is a graphite core segmented into short cylinders that are shrink-fitted inside a stainless-steel tube. The encapsulated core is surrounded by a double-annulus cooling tube, through which water flows to remove the heat. The segments are 15.3 mm in diameter and 25 mm in length. A total of 38 cylinders, spaced 0.2 mm apart, result in a total graphite length of 95 cm, corresponding to two radiation lengths. Drawings of the target are shown in Figure 3–8 and Figure 3–9. The target will be cantilevered into the horn and supported by alignment features that are rigidly attached to the face of the horn.

The shielding above the target, part of the thick steel target chase barrier, is called the target support module (Section 3.3.5). It provides access to the target utilities (e.g., cooling water, gas, instrumentation) and is removable to allow replacement of the target. During the initial commissioning of the beam, the Target Hall Instrumentation, discussed in Section 3.3.6, will be used to establish that the components and systems are working and will allow a beam-based alignment of their positions. Later, the instrumentation will be used to re-commission the beam whenever major components (e.g., targets, horns) are replaced. The instrumentation will also perform long-term monitoring of the beam properties to provide signs of degradation or failure.

3.3.2 Design Considerations

The neutrino-production target design is determined by balancing the ideal production of mesons for neutrino production and the survivability of the device for tens of millions of beam pulses. The target must have the following features:

- Adequate material to convert the protons, while not absorbing too many secondaries

- The ability to withstand the instantaneous thermal and mechanical shocks of the beam

- The ability to withstand the sustained thermo-mechanical stresses and temperatures

- A cooling system to remove the heat deposited by the beam interaction (approximately 20 kW, or 3% of the beam energy)

- Resistance to the effects of radiation damage so as not to encounter substantial change in mechanical properties during the run

Target longevity is a major issue for the performance of the LBNE facility. Graphite, the material used in the NuMI target, has been adopted as the LBNE reference-design target

Table 3–1: Properties of graphite and beryllium at 20°C, from manufacturers (POCO Graphite and Brush Wellman).

	Graphite (POCO ZXF-5Q)	Beryllium (S-65C)
Apparent density (g cm^{-3})	1.81	1.82
Compressive Strength (MPa)	195	260
Tensile Strength (MPa)	90	370
Modulus of Elasticity (GPa)	12.5	310
Thermal Conductivity (W m^{-1} K^{-1})	70	200
Coeff. of Thermal Expansion (μm m^{-1} K-1)	8.1	10.7
Specific Heat (J kg^{-1} K^{-1})	710	1770

material, but alternatives are under study. Whereas the NuMI target performance has been largely successful, a total of six targets have failed or shown deterioration in the neutrino-production rate over a span of months. Each of these incidents caused operational and experimental complications, required beam downtime for repairs or replacements or led to a slow decrease in production efficiency. The LBNE target is being designed to reduce the failure and degradation rate.

Regarding the target's mechanical properties, deviations in size, shape or density of a few percent will impact the experiments' using the neutrino beam. The source of these changes can be structural damage (change in material strength leading to disintegration), direct decomposition of the material (radiolysis), oxidation of the material, swelling or contraction and other changes.

Thes considerations lead to a long, thin target design, for which the exact length must be determined by optimization of the entire beamline, but is approximately two nuclear-interaction lengths (1 m for materials with density $\sim$2 g/cm^{-3}). The target width must be sufficient to cover the beam spot but otherwise minimized, except for the practical concerns of heat removal and mechanical integrity. The primary target material must have high mechanical strength, high specific heat, high thermal conductivity, a low coefficient of thermal expansion, and good radiation properties. Although a number of single-element materials generally fit the above requirements, the two best materials for neutrino beams are beryllium and graphite. Their properties are listed in Table 3–1.

The primary target material must be integrated into a structure that provides cooling, structural integrity and environmental isolation. For NuMI, other neutrino beams, and thus LBNE, the target is positioned within the upstream portion of the horn to preferentially focus low-energy pions. A position within the horn adds two complications: 1) the horn focuses some secondaries back into the target, increasing the heat load; and 2) the target requires support either through cantilevering or contact with the horn conductor. The outer target structure would provide either the stiffness for the cantilever or the interface with the horn inner conductor. Typically, the simplest solution is cantilevering the target.

3.3.3   Reference Design

The reference target design is being jointly developed at the Institute for High Energy Physics (IHEP) in Protvino, Russia and Fermilab. The target, based on both the NuMI design and studies for higher-power beams , is a graphite core segmented into short cylinders that are shrink-fitted inside a stainless-steel tube. The tube encapsulates the target, separating it from the cooling fluid while still allowing good thermal contact. The encapsulation prevents movement of pieces of the cylinders as they age, and the small distance between cylinders reduces the possibility of material detaching from the core segments.

The encapsulated core is surrounded by a double-annulus cooling tube, through which water flows to remove the heat. This concept has been adapted to a 708-kW configuration, where the instantaneous shock and heating load are not as large as for 2.3-MW capability [20]. The 708-kW design allows a smaller core size, smaller cooling volume and a correspondingly smaller beam spot size. The segments are 15.3 mm in diameter and 25 mm in length. A total of 38 cylinders, spaced 0.2 mm apart, result in a total graphite length of 95 cm (*sim* two interaction lengths). Drawings of the target are shown in Figure 3–8 and Figure 3–9, the heat load in Figure 3–10 and the core temperature in Figure 3–11. The complete design can be found in the 708-kW target design study [20].

The target will be inserted into the horn by the remote-handling system, described in Section 3.11. It will be cantilevered into the horn and supported by alignment features , that are rigidly attached to the face of the horn. In this design, the horn itself is the operating support structure, and the mechanical alignment features are relied upon to provide alignment. The alignment features on the target could be modified to change the relative target position with respect to the horn. This option may be desirable to produce a higher-energy neutrino beam. However, the alignment features will likely be permanently attached to any particular target, so each target will have a single position with respect to the horn.

Beryllium windows provide entry and exit ports for the beam into the target. The windows are not designed to hold a vacuum; the atmosphere within the target volume (around the graphite) will be an inert or specialized gas to minimize the effects of radiolytic oxidation.

The cooling water flows along the inner annular cylindrical region and returns along the outside. The separation between the cylinders is maintained by ribs. The water flow is relatively modest, resulting in a 1-atm head and a temperature rise of 12.7°C. The core temperature of the graphite does not increase beyond 280°C.

One issue of concern has been the instantaneous heating of the water. Water, being relatively incompressible, can produce large pressures when heated in a confined area. This is known as the "water hammer" effect. A straightforward calculation at 30°C suggests the pressure increase could be as much as 50 atm, although further study has indicated that the flexibility of the steel walls will reduce this by a factor of three. While the pressure
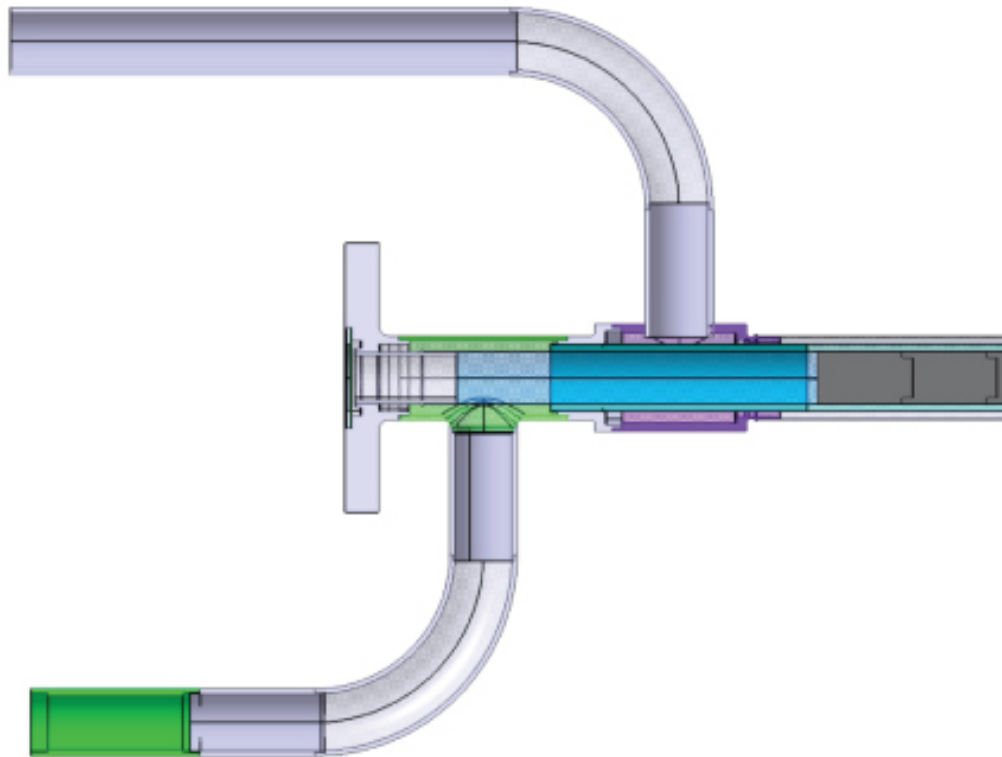
Figure 3–8: Upstream portion of the conceptual 708-kW target. The beam passes from left-to-right, entering through a beryllium window and passing into the core of the target. Cooling water enters from the pipe above, flows down the target, returns to the front and exits below.
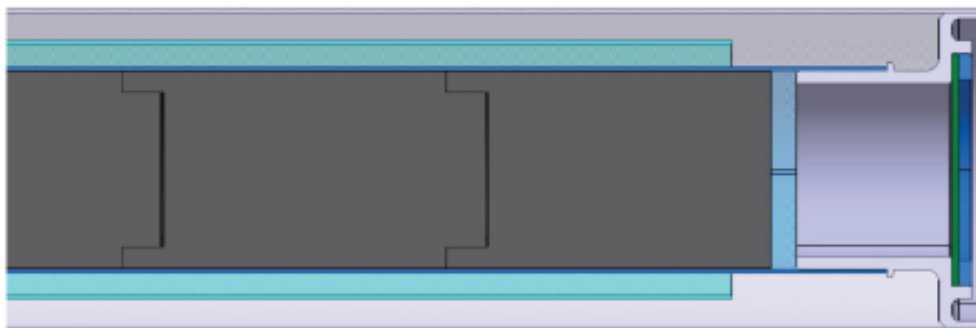
Figure 3–9: Downstream portion of the conceptual target. The beam exits the core of the target through a beryllium window. The cylindrical graphite segments (gray) are surrounded by the water-cooled stainless jackets (light blue).
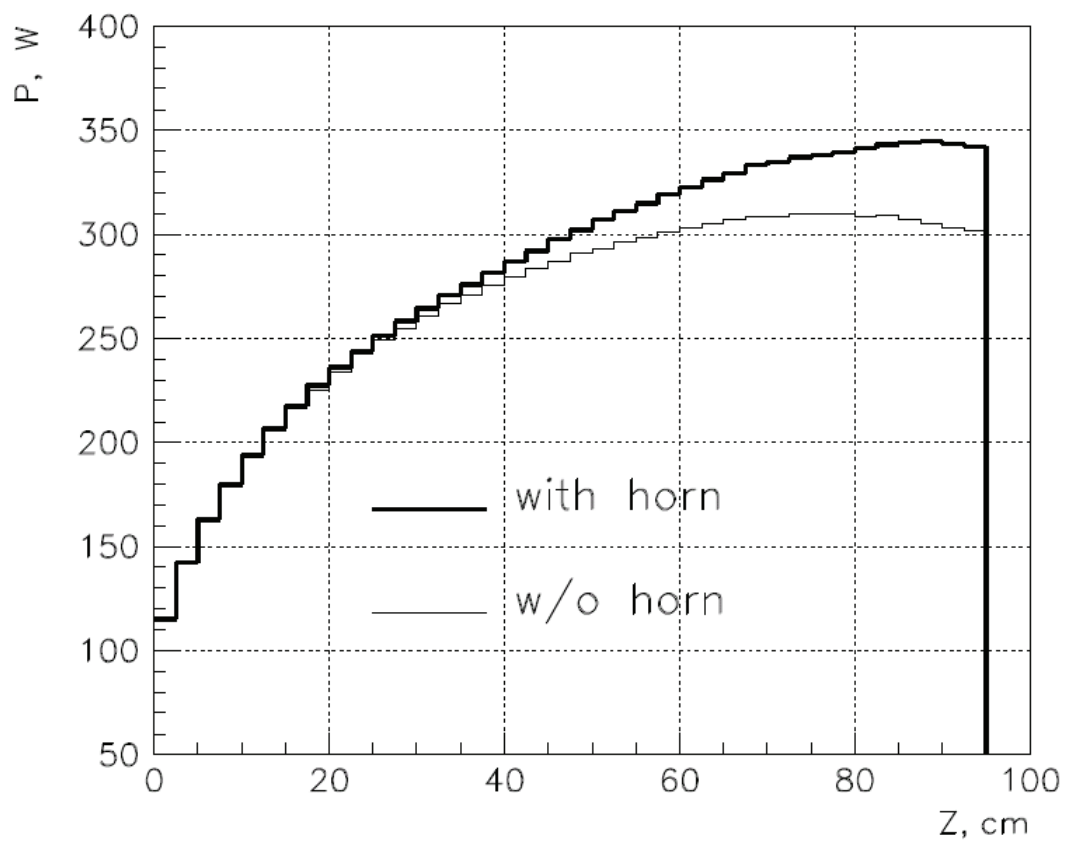
Figure 3–10: Longitudinal energy deposition in the 708-kW target. Horn focusing helps in increasing the heating in the downstream portion of the target.
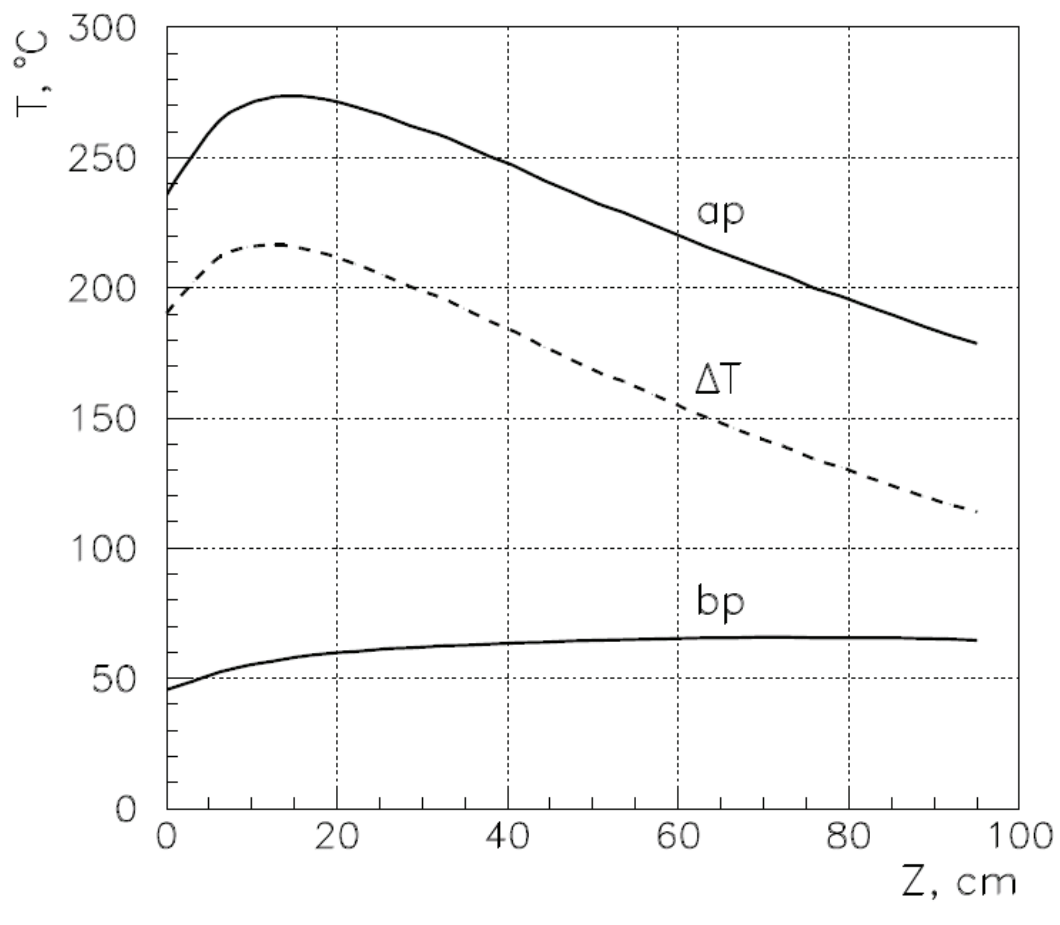
Figure 3–11: Temperatures in the center of the target while running. This plot shows the temperature immediately before a pulse (bp), the temperature after the pulse (ap) and the change of temperature (ΔT).

level itself is not of concern, the cyclic loading is. To ameliorate this problem, the plan is to introduce bubbles of a gas (probably helium) to absorb the shock. Additionally, lowering the temperature of the water can reduce the water hammer effect, as water's coefficient of thermal expansion decreases at lower temperatures (zero at 4°C). Conversely, cooling water of higher temperatures will have a correspondingly larger instantaneous pressure rise.

The LBNE target can be compared to the targets used or planned for the NuMI beamline. The MINOS target was inserted into the NuMI horn, but designed for a beam power of 400 kW. The target consisted of fins instead of cylindrical slugs. A finned design results in slightly enhanced neutrino production, but includes weak points at the sides of the fins and must conduct its heat out to relatively small water-cooling lines. The cooling lines must be far enough from the beam spot to be in the baffle protection area, so as not to be damaged by errant beam pulses. Six MINOS targets have failed. The actual causes of failure are not well understood because the target cannot be easily inspected due to residual radiation. Once the radiation levels decrease, autopsies are planned to further investigate the failures. At least five failures seem to result from weak points in the device itself: in the cooling lines or the exterior capsule. The most relevant failure is in the second MINOS target (NT-02). NT-02 had the greatest run period and showed a gradual degradation of neutrino production during its 6×10^{20} proton run. The degradation was not uniform in neutrino energy (consistent with various models) but amounted to 15% at the peak. NOvA has indicated that a 10% degradation would be an upper bound, and that 5% would be preferable. As such, target lifetimes of 4×10^{20} protons or less must be considered, if the degradation mode cannot be addressed. For LBNE, this implies up to two targets per year will need to be replaced and these failures must be considered as part of the normal operation of the beam.

The NOvA target was developed from a design for the MINOS medium-energy target. It is designed for 708 kW, but does not have to be inside the horn, thus improving the construction options. The NOvA 708-kW target makes use of long (70 mm) segments that connect to a cooling plate that is well outside the baffle aperture. This longer cooling path simplifies construction and improves the thermal characteristics of the target, thus allowing target segments to handle much higher temperatures (up to as much as 800°C). The mechanical and radiation resistance of graphite is known to improve at higher temperatures (with the exception of oxidation). Additionally, the temperature gradients within the graphite are reduced.

The LBNE target cannot make use of all the improvements that the NOvA target includes, as it must fit inside the LBNE horn. The most straightforward approach, which is taken by IHEP, is to encapsulate the target. The IHEP approach is more mechanically robust in order to accommodate the 708-kW beam in close quarters and has the potential to improve the longevity of the targets.

3.3.4   Target Options: R&D

Target longevity is a major issue for the performance of the LBNE facility. A target R&D program will explore options of target material, geometry, cooling, and other design issues.

As mentioned in the previous section, a target replacement rate of two per year is likely, based on experience with the NuMI target. The logistics of target replacement in NuMI cost 2-3 weeks of runtime; the LBNE duration may be similar. Two target replacements per year compromises the facility performance by 10-15%. Additionally, there is substantial additional cost in the storage facilities and radioactive handling required for that volume of targets. Reducing the frequency of target replacement could reduce the cost of the project, reduce the cost of operations and produce a more capable facility.

The goal of the target R&D program is to be able to produce targets of greater longevity through design choices that negligibly impact neutrino production, however, the choices are somewhat limited. The previous section described some innovations in the IHEP 708-kW reference design that have the potential to improve target lifetime. These innovations do come at a cost of neutrino flux in that the numbers depend on realistic comparison and the actual beamline optimization, but the degradation is in the range of 5-15%. The R&D program of work has two major components:

- Radiation testing of potential target materials

- Design studies of beryllium as an alternative to graphite

A first round of radiation testing has been performed at the Brookhaven Linac Isotope Producer (BLIP). A series of materials were tested, including different grades of graphite, a carbon-carbon composite and hexagonal boron nitride (hBN): a graphitic form of Boron Nitride that theoretically has superior mechanical properties. These materials have been irradiated to a fraction of the NuMI irradiation of NT-02, well into the range that mechanical properties should be affected. Material studies have begun in which the samples will be gauged for integrity, tensile strength, thermal conductivity, density and other mechanical properties. Figure 3–12 is a picture of the sample holder for the BLIP test.

Initial results from the irradiated samples give support to the historical use of a small grain size, anisotropic grade of graphite from POCO (ZXF-5Q). Additionally the results invalidated previous tests that had shown quite severe radiation damage. Those sample had been irradiated directly in water. The present BLIP test [21] demonstrated that identical samples experienced much greater degradation when irradiated in water instead of an inert environment (argon). The alternative material hBN fared poorly, seemingly to ablate in the radiation. Among graphites, POCO was among the best in terms of its retained strength

Figure 3–12: BLIP test sample holder. This figure shows cassettes of material samples irradiated in the BLIP facility. The beam enters from the right.

and ductility. Further investigations will study temperature-dependent effects, particularly annealing.

Additional radiation testing may be warranted, though few facilities can provide comparable irradiation. Reactor irradiation is easily available, but the effects of neutron irradiation can depart widely from that of high-energy protons. The BLIP facility was a good compromise, except for its limited exposure.

The second approach is to consider beryllium as an alternative target material to graphite. Beryllium has some history as a target material, notably as the Fermilab MiniBooNE target, which has been exposed to in excess of 1.5×10^{21} protons at 8 GeV. A naive examination of beryllium's basic materials properties suggests that its single-pulse resistance to damage will be somewhat less than graphite. However, the precise modeling of beryllium damage is somewhat more involved. Particularly, beryllium as a metal has substantially greater tensile strength than graphite and thus may be more immune to fracture. Also, the radiation damage threshold of metals such as beryllium is substantially higher than the crystalline forms of graphite (the data are imprecise, but the difference is about an order of magnitude).

Rutherford Appleton Laboratory (RAL, Oxfordshire, UK) has been analyzing the issues associated with a potential 708-kW LBNE beryllium target and has produced several conceptual designs that appear promising [19]. The two most appealing possibilities are that of a target integrated into the horn and an air-cooled cantilevered beryllium rod. More analysis is underway as to determine the feasibility of these approaches.

An integrated target would have the target comprise the upstream portion of the horn's inner conductor. In this case, the target carries the horn current. The skin depth is relatively large (4.3 mm) so that the current and magnetic field penetrate deep into the target volume. The design current of 300 kA would deposit a large amount of energy into the target, so a small diameter is not possible. The exact limit is not yet understood, but 15-20 mm is an approximate range.

An air-cooled target would have a rod structure cantilevered into the horn. It would then be cooled by an airflow travelling between the target and the horn's inner conductor, exhausting into the chase. This option is attractive for its lack of a water system and its simplicity. Additionally, the target in this case can be small (9 mm in diameter) for 708-kW beam power, so it may have advantages for neutrino production because less pions are absorbed within the target.

Among the many issues analyzed, two stand out as fundamental in design: the large axial stresses produced by differential expansion of the inner and outer portions of the target; and the extreme lateral displacements (3 cm) possible in the case of off-center beam producing differential expansion between sides of the target. These two issues generally preclude solid targets or require substantial bracing to reduce the possibility of motion. For a cantilevered target, the challenge will be to segment the target to prevent the growth of all these modes,
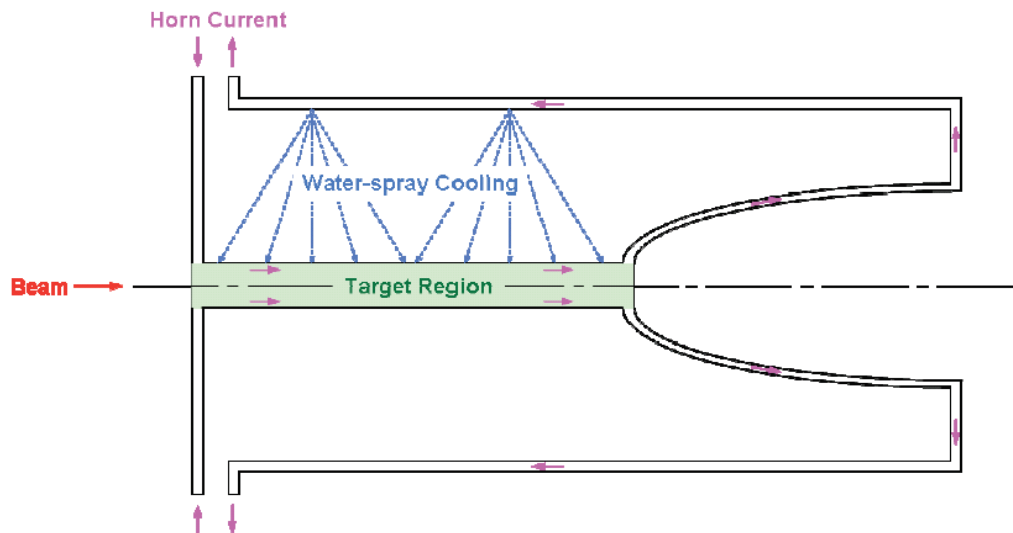
Figure 3–13: Diagram of an integrated target/horn. Current travels along the target as the upstream inner conductor of the target. The target and horn are cooled by the water spray of the horn.

while still providing sufficient rigidity to support that target.

While beryllium has several known advantages over graphite, it has the overwhelming disadvantage of not being the material that has operated in the NuMI beam or other high-power neutrino beams (CNGS, T2K). An invaluable test will be to include beryllium as an operational neutrino production target in NuMI and verify its performance over an appreciable run period. Options are under consideration to modify a NOvA target to test beryllium as a target material. If successful, this material would have all the listed advantages to the LBNE Project and facility, as well as potentially being implemented for the NOvA experiment.

3.3.5   Target Support Module

The target support module is a portion of the shielding that sits directly above the area just upstream of the horn. In contrast to the NuMI target module, the LBNE module does not physically support the target. Instead, the target is rigidly mounted to the horn. The LBNE module provides the required feedthroughs for target support utilities and is removable for target replacement.
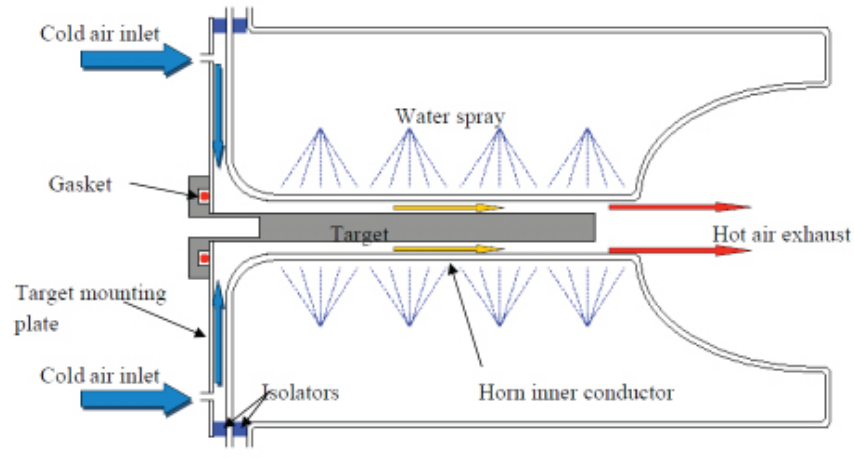
Figure 3–14: Diagram of an air-cooled beryllium target. Air travels between the solid target and the inner conductor of the horn. It is then exhausted into the target pile.

3.3.5.1 Design Considerations

The requirements of the module will be matched to the utilities required by the target. At minimum, it is expected to have a cooling system of air, water or helium. Additionally, there may be drains, inert gas lines and electrical connections for instrumentation. The details will not be set until a final target concept is chosen for LBNE.

3.3.5.2 Reference Design

The reference design is matched to the IHEP 708-kW target concept. Feedthroughs are provided for water, a drain, an inert gas line and instrumentation. Design features, as in the NuMI modules, will allow remote connection and disconnection of the utilities. Alignment is not expected to be necessary other than that already in place for the horn. No moving parts are expected. The shielding block itself will be fabricated out of steel and support additional T-Block shielding, as in the NuMI modules.

3.3.6 Target Hall Instrumentation

The Target Hall Instrumentation (THI) is a set of detectors that provide measurements of the secondary beam for commissioning, alignment and monitoring purposes. It supplements the primary beam instrumentation and the neutrino detectors. The THI's role is to provide experimental and operational information to aid in the maximization of neutrino production and to limit the experiment's systematic uncertainties due to beam mis-modeling and variation. The major roles can be broken down as follows:

- Commissioning: on initial operation of the beam, the commissioning team will go through a series of tasks to demonstrate that the beam can be delivered to the absorber, target, horn and baffle. The THI will be able to provide live verification of these tasks. For example, the primary beam will be delivered to the beam absorber before installation of the target, and the THI will measure the beam distribution at the absorber. Additionally, recommissioning will be needed whenever major components are replaced.

- Alignment: many of the neutrino beam components will have tight tolerance on their alignment at the start of and during the run. The THI measures the locations of the devices through beam-based alignment, which entails determination of the positions of the devices with respect to the primary proton beam. This alignment is most relevant for evaluating the uncertainties on neutrino production without propagating the uncertainties of several optical surveys.

- Monitoring: long-term monitoring of the beam characteristics will give indications or measurements of slow variations in the beam. The most significant variation will likely be target degradation. The NuMI NT-02 target was known to degrade up to the point where 15% of the peak flux had been depleted. Monitoring this depletion is necessary for modeling the neutrino beam. Additionally, THI can give indications of shifting alignment and events in which components are damaged.

3.3.6.1   Design Considerations

The detailed tolerances for components, and thus the measurement requirements, must be derived from a physics-based analysis of the effects of misalignments, target degradation and other deviations. The treatment of systematic errors in the MINOS experiment provides guidance, but the nature of the measurements is not precisely the same (MINOS was primarily a muon-neutrino disappearance experiment, while LBNE is an electron-neutrino appearance experiment; additionally, the detectors are substantially different in composition and modality). Another requirement for the Target Hall instrumentation is that results must be readily apparent and available. A package of software integrating the instrumentation must be available to personnel performing the above analyses online. This software must also be able to interface to primary beam instrumentation and (ideally) the neutrino beam detectors. Correlation of the various data is necessary for the THI measurements.

3.3.6.2   Reference Design

The model for LBNE Target Hall instrumentation is based on the NuMI systems. Primary-beam loss monitors measure the spray of secondary particles produced through interaction of the primary beam together with crosshair-alignment features on the horns and a hadron monitor at the end of the decay pipe to measure the remaining secondary particles. The

muon monitors are separate, an isolated into a set of monitors in the Absorber Hall that assist in target diagnostics and absolute beam flux estimates. The muon monitors are part of the Near Detectors beamline-measurements system and not considered further here.

A Budal monitor tests the beam on-target by electrically isolating the target, and measuring the charge ejected or deposited into an amplifier. This device worked well in NuMI for commissioning and alignment, but may not be appropriate with the large-diameter IHEP target since the target occludes the entire baffle aperture. This issue is under design study.

The horn loss monitors, the primary tools for horn alignment, are similar to primary-beamline loss monitors. They will be integrated into the horn modules or Target Hall shielding. During horn alignment, the target will be removed, allowing the primary beam to pass through the horn apertures. The beam is scanned across crosshair features fixed to the horn's upstream and downstream ends, producing a modest spray of particles that is detected by these loss monitors.

The hadron monitor is an additional tool for alignment and commissioning. It measures the intensity, location and shape of the hadron beam just upstream of the absorber. In NuMI, the hadron monitor was used extensively for alignment by analyzing the change in the remnant beam as the primary beam was scanned transversely. It was used for commissioning, alignment, monitoring and for diagnosing failures. The NuMI hadron monitor was a 7×7 m^2 array of parallel-plate ionization chambers. The ionization medium uses helium at atmospheric pressure. The NuMI hadron monitor design cannot simply be redone for LBNE, however, because LBNE will have a shorter decay pipe and will thus produce a smaller and more intense beam spot at the hadron monitor. The hadron monitor must withstand the heating and irradiation of this more intense beam. Additionally, it must be able to produce measurements at the higher particle fluxes. The NuMI hadron monitor was known to show saturation effects at high intensity; it also was known to show variability with temperature, pressure and impurity level in the helium supply. An evolved concept for the LBNE hadron monitor is to use argon at low pressure (~ 1 torr) to reduce the ionization intensities, and to reduce the variation with gas supply quality. A higher channel count is necessary as the pixel size will need to be at least a factor of three smaller, probably a factor of five.

For LBNE, the target-degradation monitor will consist of small arrays of loss monitors, or other sealed ionization chambers, at muon-monitor locations. Having sealed devices reduces the effects of temperature, pressure and gas quality. These devices will be configured in such a way as to produce a live measurement of target degradation through the ratio technique, wherein the ratios of muon-monitor signals provide an immediate indication of target degradation, after compensating for other detector effects. The whole system of the above devices will be integrated with data from primary-beam devices and neutrino devices, if available. The software to integrate these devices will be readily available as a live accelerator-controls application, as well as recording all these data into the appropriate accelerator and experimental databases.

3.4 Horns (WBS 130.02.03.04)

3.4.1 Introduction

The horns are the focusing devices for the secondary particles; they act as magnetic lenses that focus and direct charged pions and kaons toward the decay pipe. The focusing is produced by the pulsed toroidal magnetic field present in the air volume between the co-axial inner and outer conductors that form the horn. LBNE will position two horns in series; the first surrounds the target and extends about 2 m further downstream in a parabolic shape, as shown in Figure 3–15, and the second is a double paraboloid, shown in Figure 3–16 a few meters downstream of the first. The shapes of the horns' inner conductors were designed to produce the neutrino event rate in the far detectors in the energy range appropriate for the primary physics goals of LBNE [22], subject to engineering and material constraints. Horns will be supported and positioned by support modules, described in Section 3.4.4. Current to the horns is supplied via a stripline.
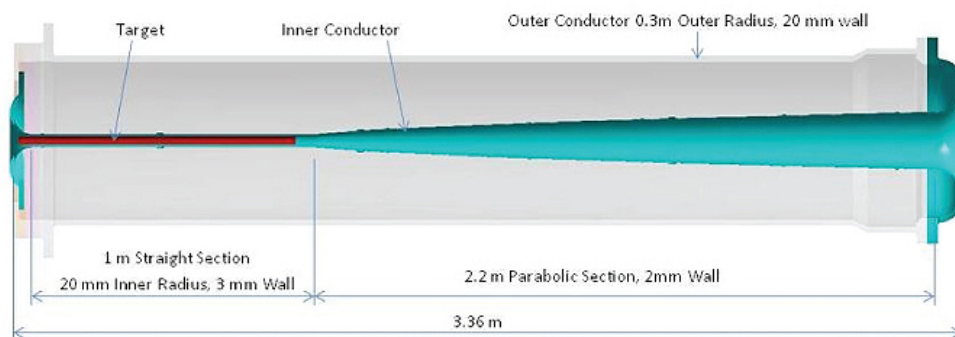
Figure 3–15: Horn 1 section
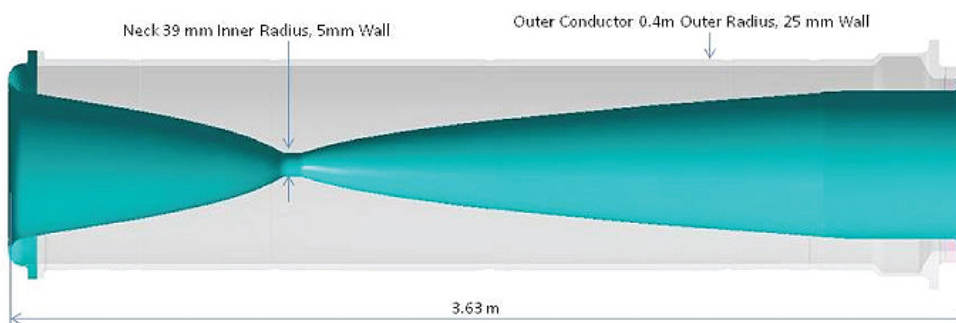
Figure 3–16: Horn 2 section

Table 3–2: Horn parameters. The inner and outer conductor parameters are abbreviated by IC and OC, respectively.

	Horn 1	Horn 2
Material	Al 6061-T6	
Peak Current	300 kA	
Min. aperture "neck" radius	20 mm	39 mm
IC Thickness	2 mm	3 mm
Length	3.36 m	3.63 m
OC radius (outer)	300 mm	400 mm
OC Thickness	20 mm	25 mm

3.4.2   Design Considerations

The horns (i.e., the conductors) must be able to endure the combined heat load from the secondary particle interactions in the horn material and resistive heating by the current flowing through them. To address the former, the thickness of the inner conductor should be minimized to reduce absorption and scattering of secondary particles in the conductor material. To minimize resistive heating, the conductors and the power-supply stripline must be cooled to an acceptable temperature. Meanwhile, the inner conductor must withstand repetitive thermal and magnetic stresses over millions of current pulses.

Another design criterion is that a horn, its support module and stripline block together not exceed 50 tons, the Target Hall crane capacity.

3.4.3   Reference Design

The focusing system will be a two-horn design, with the upstream end of the second horn (Horn 2) located 6.6 m from the front face of the first horn (Horn 1). The horn consists mainly of an inner conductor, an outer conductor, a current-supply stripline, a cooling system and a support structure. The inner conductor of Horn 1 has a straight cylindrical section (the neck) upstream surrounding the target, followed by a parabolic section downstream [22]. Horn 2 is a double-paraboloid [23]. The conductors are made of aluminum 6061-T6.

The outer surfaces of the inner conductor will be cooled by water spray nozzles distributed along the beam axis and 120° azimuthally. Nozzles at the top of the outer-conductor cylinder will spray water to form a film running down from both sides. The radioactive cooling water will be collected at the bottom of the horn and will return to an external heat exchanger through a closed circuit. The external surfaces of the horn will be exposed to the target chase airflow. To resist water corrosion and possibly electrical breakdown, the surface of inner conductors will be coated with electroless nickel.
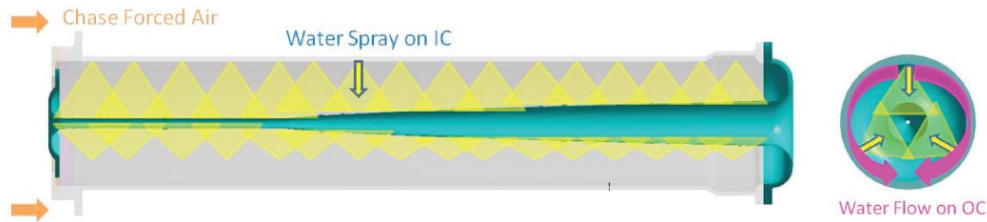
Figure 3–17: Horn cooling system
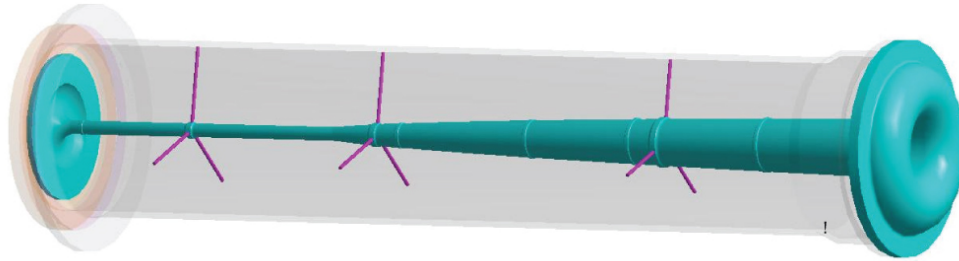
Figure 3–18: Additional support and stability for the thin inner conductor are provided by welded struts or "spider" (web) supports (thin purple pieces).

The inner conductor will consist of seven segments welded together with in-house CNC TIG welding machine. Welds will be designed with a thicker wall at the joints, located away from the high-stress areas to compensate for the reduced strength in the heat-affected zone. Single pass, full-penetration welding will minimize the conductor distortion. Cosmetic passes will be applied if needed to achieve an overall straightness of ± 0.020 in. A few sets of spider supports, illustrated in Figure 3–18 will provide the position adjustment of the inner-conductor center line and meanwhile allow free thermal expansion of the conductors. Vibration analysis will be performed to determine the appropriate number and locations of the spider supports, to make sure the first vibration mode frequency is significantly above excitation pulse frequency.

The electrical connection between the power supply and the horn is provided by a planar-design stripline, which has minimal inductance and resistance to allow thermal expansion/contraction of the horns and transmission lines. The stripline consists of nine layers of aluminum 6101-T61 bus bars that are spaced by zirconia ceramic insulators, as shown in Figure 3–19. The stripline is flared out to connect to the horn inner and outer conductors at the upstream end and is insulated by an alumina (ceramic) ceramic ring. The upper portion is connected to the transmission line via a remotely controlled stainless-steel clamp assembly. The horn current pulse is a half-sine wave with a peak current of 300 kA, pulse width of 1 ms and a repetition rate of 1.33 s.

The heating sources on the horn conductors include electrical-resistive heating by current and instantaneous beam heating due to secondary particle interactions in the material. The beam energy deposition rates in materials are calculated with MARS, a Monte Carlo code [24]. Because of its smaller radius, the heating loads on Horn 1's inner conductor are much higher
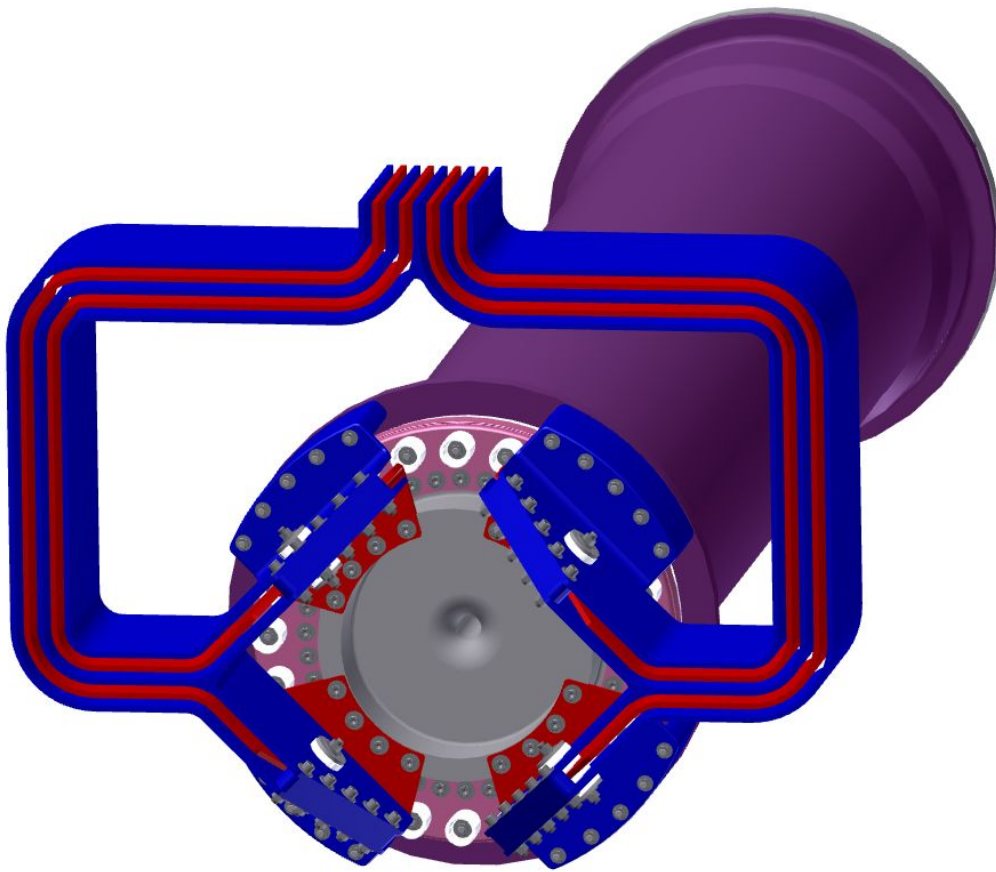
Figure 3–19: Horn 1 stripline connection at the upstream end

Table 3–3: Summary of heating loads on the horns. The results are separate for the inner conductor (IC) and the outer conductor (OC).

LBNE	Horn1		Horn2	
	IC	OC	IC	OC
Beam Heating Loads	15 kW	13.5 kW	4 kW	14 kW
Resistive Heating Loads	7.6 kW		1.5 kW	

than those on Horn 2's inner conductor. Horn 1's maximum heating-load density occurs on the neck immediately upstream of the transition to parabola. See Figures 3–20 and 3–21 and Table 3–3. The steady-state temperature of Horn 1 is shown in Figure 3–22.
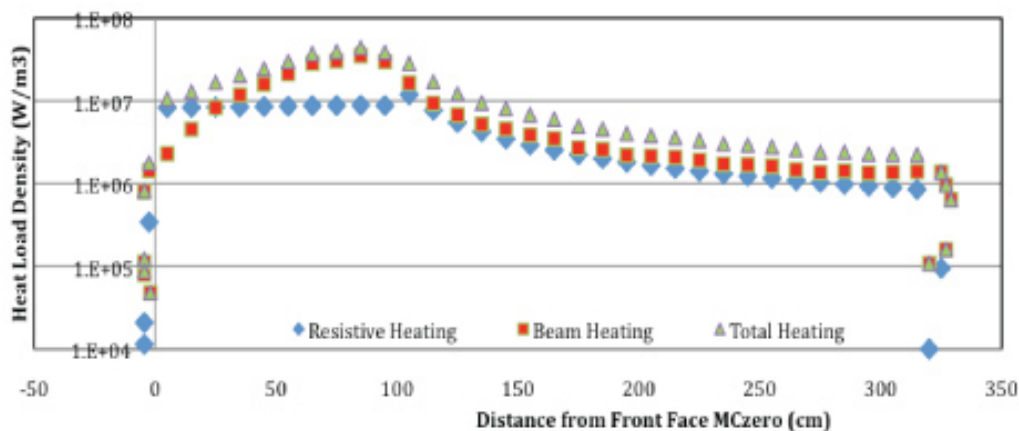
Figure 3–20: Heating loads on the inner conductor of Horn 1

Heating of the inner conductors produces thermal stresses, and electromagnetic forces generate magnetic stresses on the inner conductor during current pulsing. Thermal and structural finite element analysis (FEA) will be carried out to guide the design and study the fatigue strength of the inner conductors, the alignment stability of the horns, and the temperature profile of the striplines. Modal and buckling analysis will be performed to study the vibration and buckling characteristics of the horns.

Preliminary FEA calculations indicated that with the current design and a convective heat transfer coefficient of 7,000 W-°C/m^2, the neck would reach an equilibrium temperature of 40°C after five beam pulses as seen in Figure 3–23. After reaching equilibrium, during each pulse at full beam power the neck's maximum temperature would rise to 63°C halfway into the current pulse after the instantaneous beam spill (mid-pulse) and would reach 65°C at the end of current pulse (end-pulse) as shown in Figure 3–24. Figure 3–25 shows the temperature profile during a single pulse.

While the neck gets hot during current/beam pulsing, both end caps of the inner conductor remain cool. Thermal gradients produce compressive stress on the inner conductor, and electromagnetic forces generate compressive circumferential/radial stresses and tensile axial
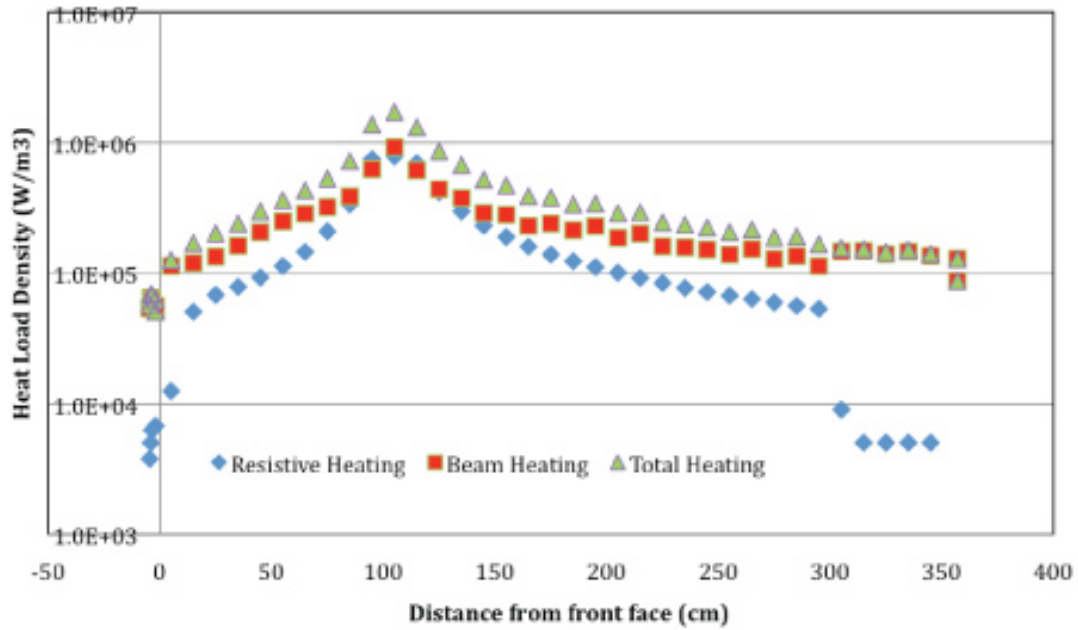
Figure 3–21: Heating loads on the inner conductor of Horn 2
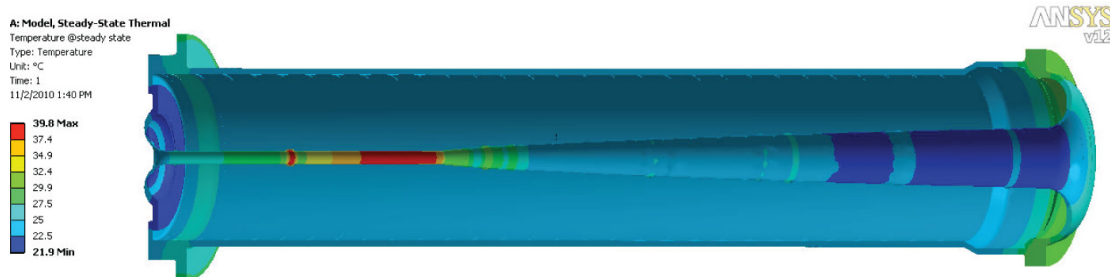
Figure 3–22: Temperature of Horn 1 at steady state
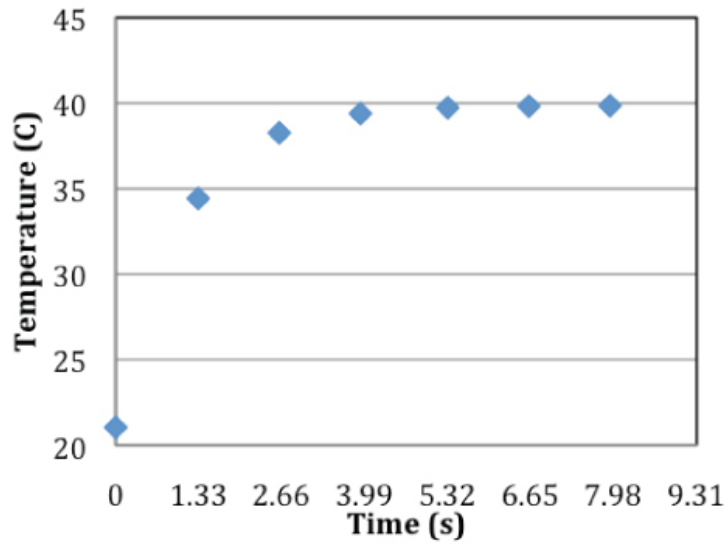
Figure 3–23: Temperature trends in the Horn 1 neck at beam cold start-up
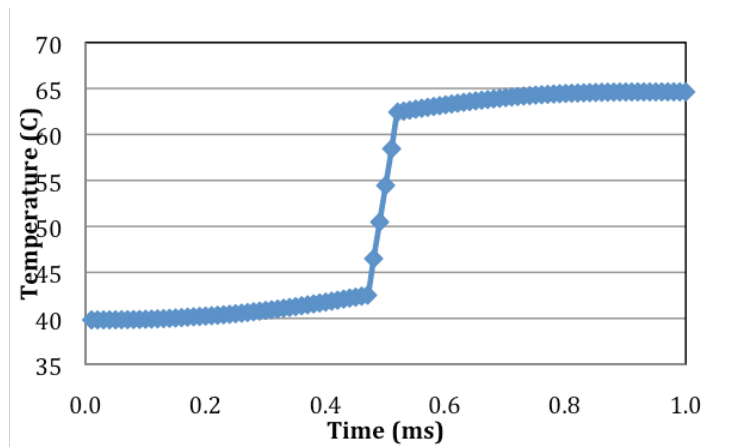
Figure 3–24: Temperature trends in the Horn 1 neck during a single pulse after equilibrium
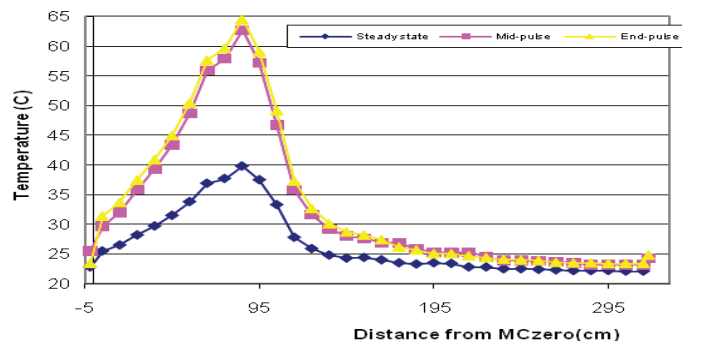
Figure 3–25: Temperature profiles of the Horn 1 inner conductor during a single pulse

stress. The combination of thermal and magnetic loading results in a range of stress magnitudes and types of stress at different locations and times on the inner conductor. Stress calculations were performed to study the scenarios of steady state, mid-pulse and end-pulse for the normal beam operation at full power of 708 kW.

The following figures 3–26 and 3–27 show calculations of stress on Horn 1.
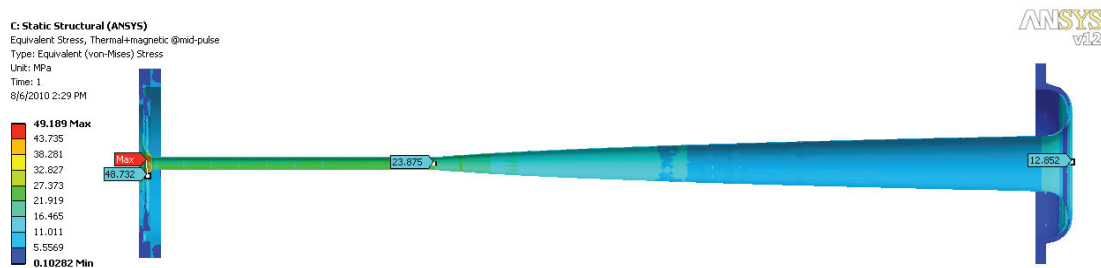
Figure 3–26: Calculated equivalent stress of the Horn 1 inner conductor at mid-pulse
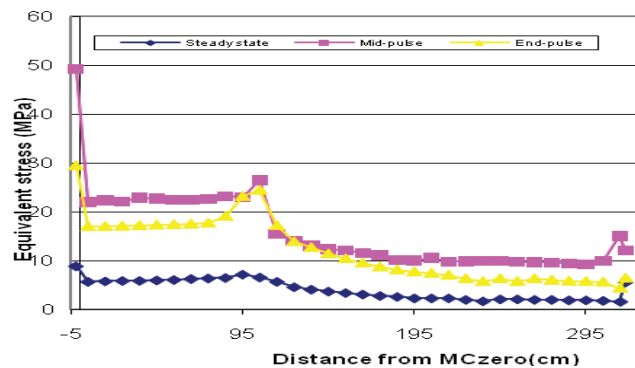
Figure 3–27: Profiles of equivalent stress on the Horn 1 inner conductor during a single pulse

The cyclic thermal and magnetic loading over millions of beam/current pulses may lead to microscopic physical damage to the inner conductor material, even at stresses well below the ultimate strength. Thus it is critical to evaluate the fatigue strength of the inner conductor of Horn 1 and optimize the design. Preliminary finite element analysis static stress calculations indicated that the transition section of the upstream part (US transition) and the neck upstream of the parabola section of the inner conductor would experience high stress fluctuations during each pulse, shown in Figure 3–28 and Figure 3–29. The compressive instantaneous thermal stress on the neck due to the beam spill is calculated to be 32.5 MPa.

A stress-based approach is used to analyze the fatigue strength (the stress level a material can endure for ten million cycles) at these two locations. With the maximum and minimum stresses, the alternating stress, the mean stress and the stress ratio are obtained. The stresses at the upstream transition and the neck are such that the fatigue lifetime of the inner conductor is estimated to be beyond ten million cycles. Using a standard relation (modified

Goodman relation [25]) a fatigue-safety factor can be estimated, which needs be well above unity. This safety factor is approximately 5.8 at the neck, 5.6 at the US transition and 3.4 at the weld taking into account of a welding correction factor of 0.5.
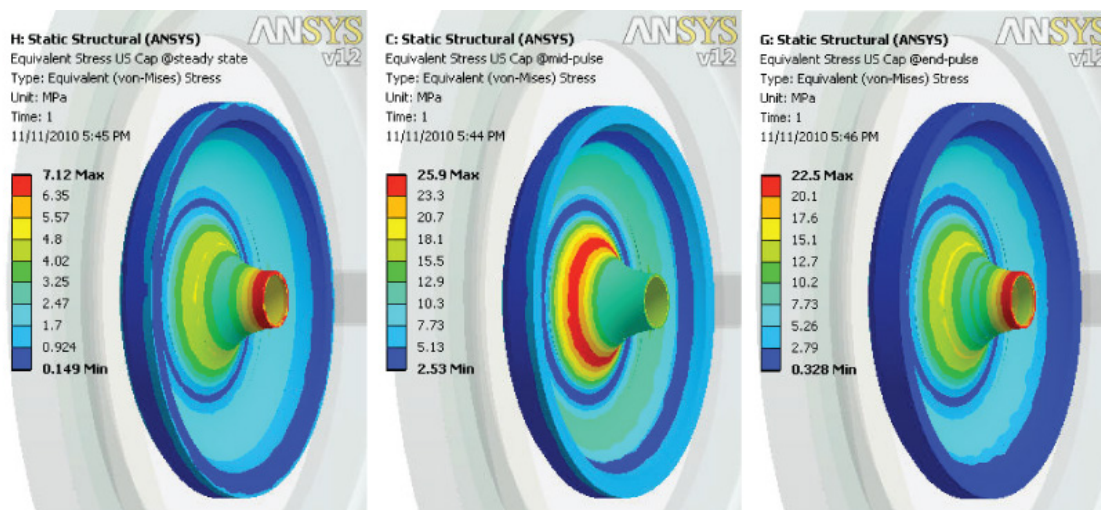
Figure 3–28: Calculated equivalent stress of Horn 1 US cap/US transition during a single pulse
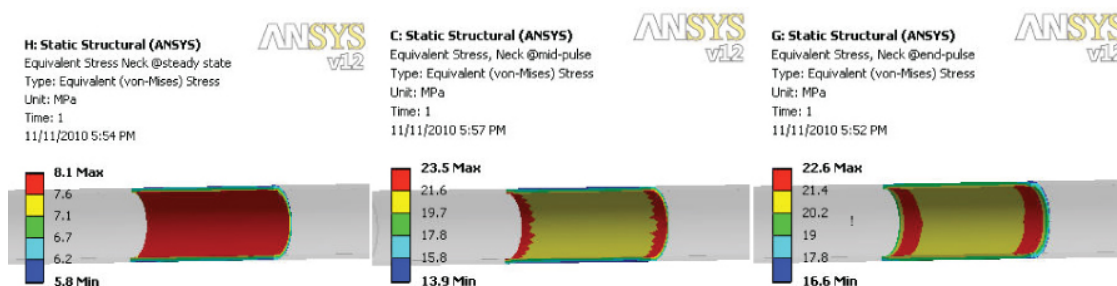
Figure 3–29: Calculated equivalent stress of Horn 1 neck to parabola transition during a single pulse

Other studies of stress components were carried out not only for the normal operating conditions but also for scenarios of thermal stress only at mid-pulse and magnetic stress at room temperature, to understand the stress conditions of the inner conductor. Table 3–4 gives a wide range of stresses at different locations in the neck, with positive numbers indicating tensile stresses and negative numbers indicating compressive stresses. It shows that a maximum compressive hoop stress of 27.4 MPa would occur at mid-pulse, while a maximum compressive axial stress of 23.9 MPa would occur at end-pulse.

The stress components in Table 3–5 show that magnetic stress is the major component of the hoop stress and the tensile axial magnetic stress would compensate the compressive axial thermal stress at mid-pulse to lower the overall axial stresses.

Table 3–4: Stress components at the Horn 1 neck under different scenarios (MPa).

	Cold start (pulse+beam)		At equilibrium			Pulsed without beam		
σ_{axial}	-5.5 to 8.5	-15. to -4.5	-7.6 to -3.7	-4.0 to 3.1	-21. to -14.	-3.7 to -1.1	-2.3 to 14.4	-9.7 to -2.5
σ_{hoop}	-28. to -8.9	-7.1 to 5.3	-1.9 to 1.6	-27. to -17.	-4.6 to 2.1	-0.9 to 0.7	-25. to -13	-3.4 to -2.7
σ_{radial}	-6.4. to 5.8	-4.2 to 3.3	-0.1 to 0.1	-4.8 to 0.6	-2.4 to 0.3	-0.1 to 0.0	-3.1 to 1.8	-1.5 to 1.5
σ_{equiv}	15. to 29.	5.0 to 18.	4.6 to 6.9	17. to 26.	14. to 19.	1.6 to 3.6	18. to 30.	3.6 to 11.

Table 3–5: Stress components at the Horn 1 neck under different scenarios at mid-pulse (MPa).

	Combined Stress	Magnetic Stress	Thermal Stress
σ_{axial}	-4.0 $\sim$ 3.1	14.8 $\sim$ 15.6	-19.1 $\sim$ -12.1
σ_{hoop}	-27.4 $\sim$ 3.1	-22.6 $\sim$ -19.3	-5.2 $\sim$ 2.0
σ_{radial}	-4.8 $\sim$ 0.6	-2.9 $\sim$ 0.2	-3.1 $\sim$ 0.4
σ_{equiv}	10.5 $\sim$ 26.5	29.9 $\sim$ 32.9	11.8 $\sim$ 17.9

3.4.4   Horn Support Modules

Horns will be supported and positioned by support modules. The intensely radioactive environment of the target chase requires that the horn-support module be adjustable and serviceable by remote control. The horn-support modules provide radiation shielding, and allow the mounting and dismounting of feed-through connections for the stripline, cooling water and instrumentation cabling from the top of the module mainframe, away from the most highly activated areas.

The horn module support concept is shown in Figure 3–30.

Horn-support modules are rectangular boxes open at the top and bottom, and made from different thicknesses of plate steel. The walls perpendicular to the beam at the upstream and downstream ends of the box will be up to 10-in thick. The side walls oriented parallel to the beam line will be up to 2-in thick with two plates welded together to form overhangs that create a labyrinth to shield radiation.

The modules fix the horn with respect to the module in the horizontal degrees of freedom, but not in the vertical. The module is adjusted with respect to the beam for transverse horizontal position and yaw. The horn is adjusted with respect to the module for vertical and pitch alignment. This is accomplished by two separate motorized systems shown schematically in Figure 3–31.
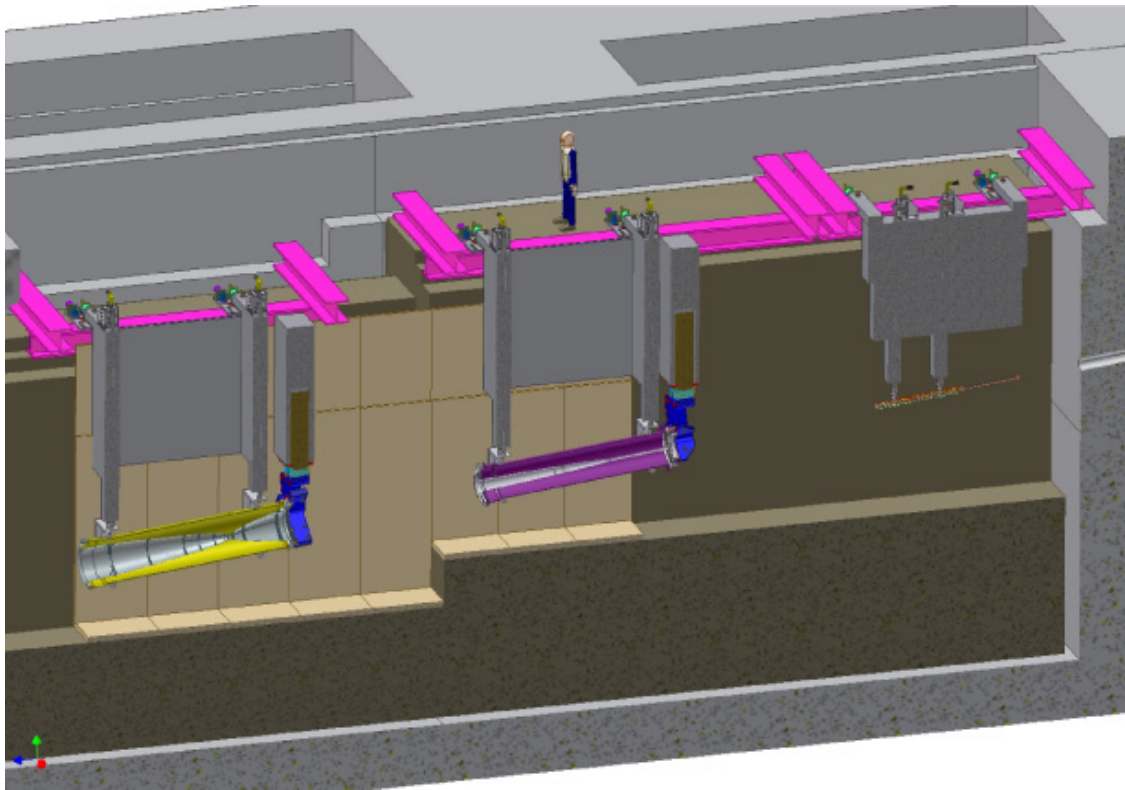
Figure 3–30: Horn support module concept. The beam comes from the right, through the baffle, supported by a similar module.
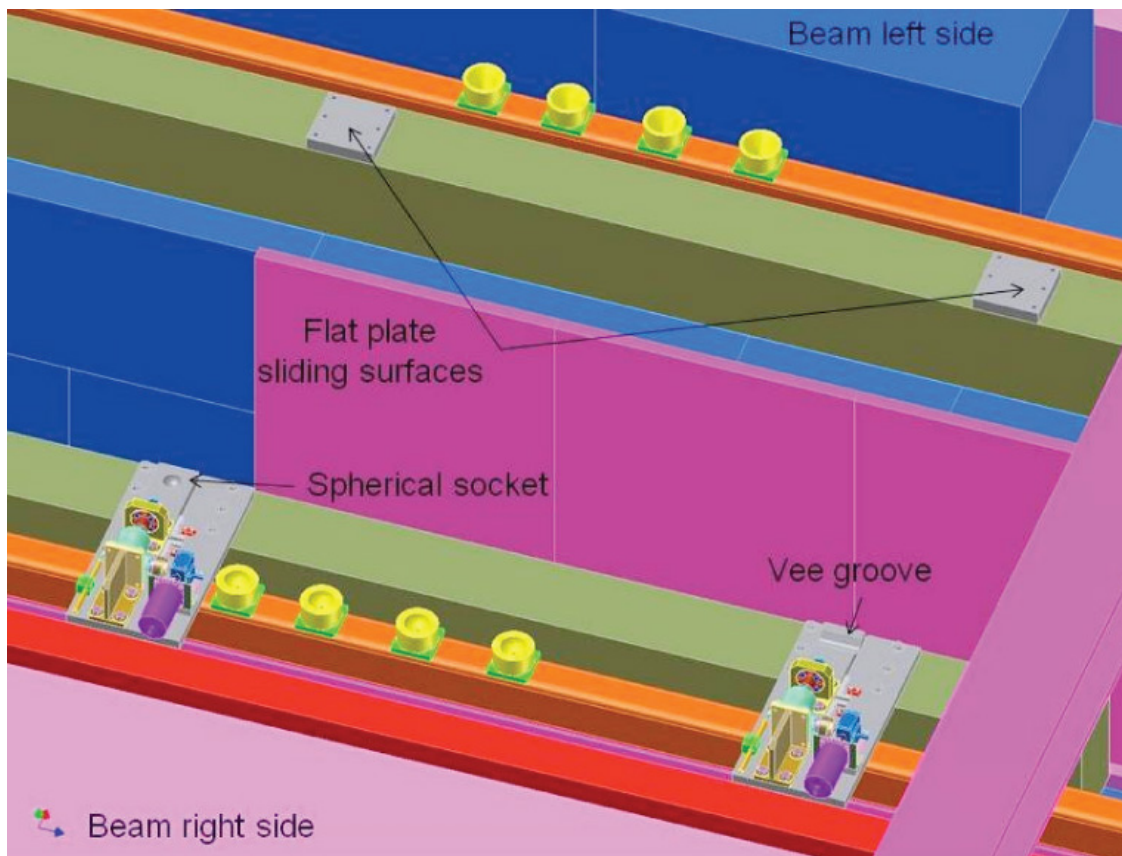
Figure 3–31: Adjustment fixtures for the horn-support module concept. The modules are fixed only horizontally along the beam direction.

Table 3–6: Estimated circuit parameters for the horn power supply; based upon NuMI system.

	Inductance (μH)	Resistance ($\mu\Omega$)	Power (kW)
Horn 1	1.191	243	14.4
Horn 2	0.51	71	4.2
Capacitor bank and connects*	0.1	68	4.0
Transmission Line			
Supply to beamline (30m)	0.24	210	12.5
Between horns (18m)	0.144	126	7.5
Totals	2.185	718	42.6

The horizontal system is mounted to the carriage rails to allow the module to be pushed or pulled horizontally perpendicular to the beam with two independent five-ton screw jacks. The screw jack is powered by a radiation-hard stepper motor. The design is based on the existing hardware for the Booster Collimators. By differentially driving the horizontal motors at each end of the module, yaw is controlled. The vertical adjustment system is a simple screw-jack-gear-box-motor configuration conceptually similar to the horizontal mechanism. To allow the horn to be crane-lifted out of the beamline for repairs and then replaced without changing its position in the beam line, the module adjustment mechanism includes a kinematic mount. A standard kinematic mount is a three-point support with the third support point sitting on a flat plate to allow free horizontal motion. The modules are on four point supports, so both of the beam left support points are simple flat plates. Once the modules have been surveyed into place the first time, the motorized adjustment mechanisms can be used to scan the horn across the beam for final alignment. High-strength steels – alloys whose yield strength is above 87 ksi – have been found to be a problem in high-radiation areas because of "stress corrosion cracking". This class of materials will not be used on any component of the modules or their adjustment systems.

3.5 Horn Power Supplies (WBS 130.02.03.05)

3.5.1 Design Considerations

This section discusses the horn power supplies, which will be designed to supply the horns with a minimum of a 300-kA sine-wave peak, within tolerances set for a minimum beam pulse of 10 microseconds. They will include the ability to switch polarity remotely and quickly. One supply will power both horns.

A damped LC discharge circuit (as shown in Figure 3–32) will achieve the peak current when the silicon controlled rectifier (SCR) switch releases stored energy from the capacitor bank to the horns via a planar transmission line ("stripline"). The estimated circuit parameters are as listed in Table 3–6.
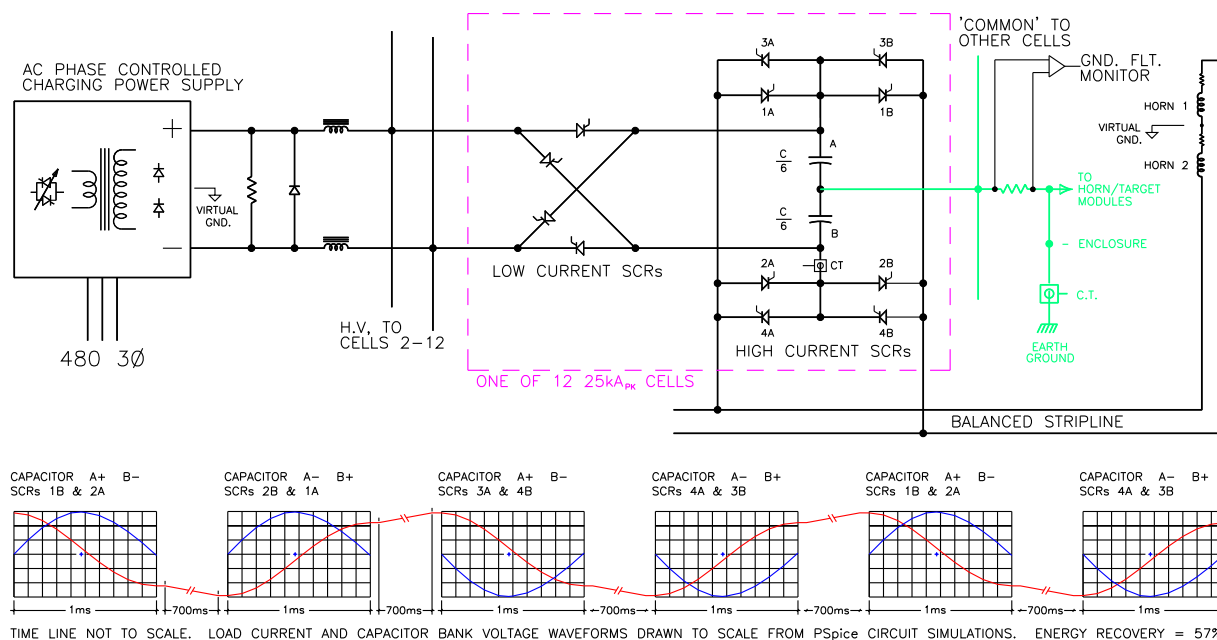
Figure 3–32: Design of horn power supply with energy recovery and output polarity reversal.

3.5.2   Reference Design

3.5.2.1   Charging Source

The capacitor bank will be charged during the quiescent period between discharge cycles by a 120-kW rated AC phase controlled, unfiltered, made-to-order unit specified to an outside vendor via bids. Operating voltage for the capacitor bank will be nominally 2.8 kV. Calculated AC-power consumption during operation of the focusing horns is 80 kW.

To avoid transients on the AC power line, a 10-mH inductance will be installed between the DC charging source and the capacitor bank. One unit of 5 mH will be in each leg of the DC output. These will be made-to-order components specified to a commercial vendor via bids.

3.5.2.2   Capacitor Bank

Based on the inductance and resistance value estimates, the capacitance required for the bank is 48 mF. This will be made up of an array of individual center-tapped energy storage capacitors connected in parallel, but electrically separated into 12 separate cells. The number of capacitors in each cell will be chosen to limit the amount of energy per cell to a value that can be safely contained within an individual capacitor case in the event of an internal fault. The center-tap grounded capacitor configuration allows a virtual ground to be created between the two horns, reducing the voltage-to-ground at the horns to half the system voltage.

3.5.2.3   Discharge Resistors and Safety System

A safety system will be included to continuously monitor operating parameters during the charge and discharge portions of the cycle, safely shutting down the system if out-of-tolerance conditions are detected. Parameters to be monitored include personnel entry, charging source over- current, over-voltage, over-current on any one cell, total load over current, out of balance conditions between cells, ground fault currents, and excessive temperatures. The loss of cooling to the charging source power supply capacitor bank, transmission line and the horns will also be monitored. When fault conditions are detected, the charging source will be shut down and the capacitor bank immediately discharged via a redundant array of dump resistors and electronic and mechanical switching devices to dissipate all stored energy.

A slow-start controller, regulating output current from zero to full over a time period of 30 s, will be included to allow the system to trip at low-level conditions during initial turn-on in the event the load has been compromised by any form of fault.

3.5.2.4 Switching Elements

An SCR-reversing switch between the charging source and each respective capacitor bank cell allows recharge of that cell in either chosen polarity and simultaneously isolates the cell from all other cells. A high-current reversing switch SCR configuration at the end of each capacitor cell allows the load current to be selected from either cell voltage polarity to provide load current in either direction. This allows all cells to operate in harmony. These switches also provide safety related cell-to-cell isolation on the discharge side.

3.5.2.5 Current Transducers

Passive current transformers installed within each capacitor bank cell monitor the cell performance to 0.4% accuracy. These 12 signals are also summed to provide individual stripline currents plus total load current for over-current monitoring and readout display.

3.5.2.6 Transmission Line

A stripline consisting of a nine-layer assembly of parallel aluminum electrical bus conductors will connect the capacitor bank to the two series connected horns. The aluminum alloy of choice is 6101-T61, having nearly the conductivity of pure Al but with enhanced mechanical properties. Of the successful designs presently in service for the NuMI and MiniBooNE horn systems, the MiniBooNE design is best scaled to the higher LBNE peak current. Its balanced configuration offers much reduced electromagnetic, vibration and mechanical stress. Its cross section is shown in figure 3–33.

Additionally, the stripline design must have minimal inductance and resistance, allow for thermal expansion and contraction at horn and capacitor bank connections, and allow rapid reliable connection and disconnection at each horn location. In high-radiation-field portions of stripline, the conductors are spaced with alumina ceramic insulators. In minimal radiation portions, lower-cost inorganic materials will be sought. Lengths between spacers are separated by an air gap. The assembly will be held in compression by overall steel bar-clamps at each spacer location. Vertical floor-mounted stanchions will support the completed structure. The connection is shown in figure 3–34.

Power loss in the transmission line is 890 W/m, 42 kW total, based on an estimated stripline length of 48 m. Overall ducting and filtered forced-air cooling will protect personnel and control temperatures. It will be sized to carry the normal 7,700 A$_{rms}$ operating current plus a 20% design margin in terms of current.
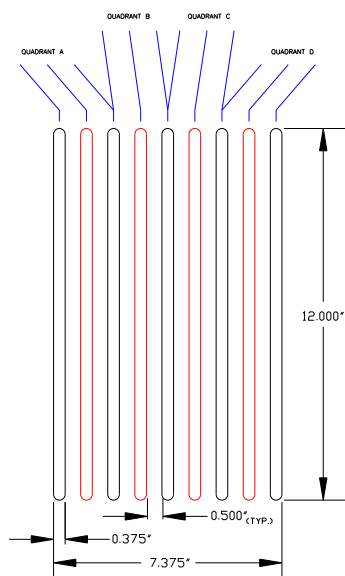
Figure 3–33: Stripline cross-section.

3.5.2.7   Ground-Fault Protection

To protect other beamline instrumentation equipment from the possibility of Horn Power Supply high current ground faults, its energy storage capacitor bank, D.C. charging source, stripline and horn loads are, by design, isolated from earth ground. To prevent these components from floating to potentials above ground, the common terminal of all capacitors within the system is connected via a suitably rated low value power resistor of $< 1000\ \Omega$ to Earth-ground depicted in Figure 3–32. The chosen resistance value shall limit any such fault currents to 20 Amperes or less. Additionally, the resistor serves as a shunt that is continuously monitored by the local controls for ground fault current detection. Detected faults initiate immediate termination of system operation and via electronic crowbar redirect of all remaining stored energy to an internal dump.

Most importantly, all high-voltage equipment enclosures will be connected directly to an Earth ground utilizing low-impedance techniques. This protects personnel making incidental contact with the exterior of any of the system enclosures from transient "ground bounce" should such faults occur during routine operation or maintenance activities.

3.5.2.8   Water Cooling

The SCRs and series charging source inductors will require low-conductivity water (LCW) cooling at a combined total flow rate of 4 gpm. Water flow rates for the charging source supplies will be determined and specified by the vendor. Dump resistors are sized to absorb the maximum stored energy of the capacitor bank by a safety margin of two and can be
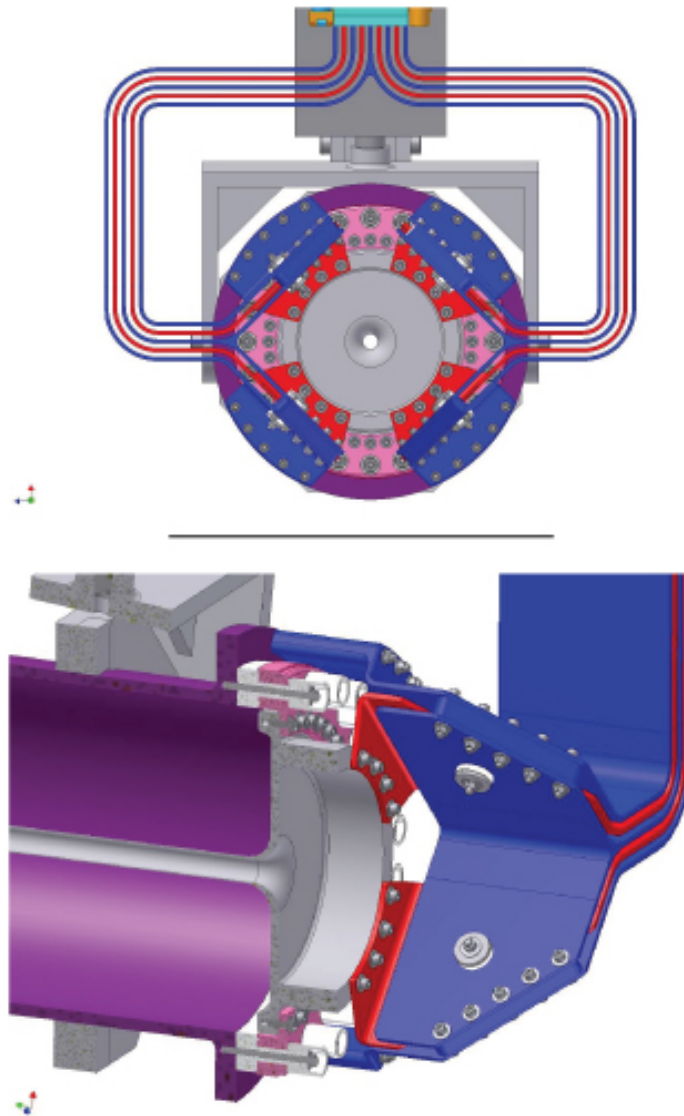
Figure 3–34: Upper: Connection to Horn-1, end view looking DS; Lower: Vertical section, Horn/stripline Interface.

convection cooled as a consequence of their infrequent operation.

3.5.2.9   Enclosure

The enclosure design, as used by both the NuMI and MiniBoone experiments, is well suited for LBNE. The heavy steel design provides additional safety for energy containment in the event of internal faults. Its pan-style base serves also for capacitor oil containment in the event of impregnant leakage and allows access to internal components on all four sides.

3.6   Decay Pipe (WBS 130.02.03.06)

3.6.1   Introduction

The decay pipe is the region where the pions and kaons generated from the target decay into neutrinos. The length is determined by the distance at which most of the pions decay, producing neutrinos near the maximum energy required by the physics goals of LBNE. The pipe must be of sufficient diameter to allow for decay of the lowest-energy pions required by the experiment. The decay-pipe reference-design length is 200 m, but an extension up to a length of 250 m is still under consideration. A decision on the length requires a full understanding of the optimization between cost and physics sensitivities. This is expected to be completed prior to CD-2.

Concrete radiation shielding surrounds the decay pipe to minimize activation of surrounding ground water. Heat generated in materials due to beam reactions will be removed by airflow through the decay pipe. Impermeable membranes surround the decay-pipe concrete to act as a barrier for minimizing ground-water inflow. Any ground water that penetrates the barrier system will be collected in pipes and conveyed to sumps located in the Absorber Hall, described in Section 3.7.

The scope of work described in this section includes specifying (1) the length, material, diameters and wall thicknesses for the concentric decay pipe, (2) the thickness for the shielding concrete, (3) cooling parameters, and providing the end closure. Conventional Facilities (see Volume 5 of this CDR) designs and provides the corrosion-protected concentric decay pipe, shielding concrete and the impermeable membrane ground-water barrier and drainage system.

3.6.2   Design Considerations

The decay pipe and its shielding are built underground and their size cannot be significantly modified or upgraded after completion. Therefore, this part of the neutrino beam has been designed for 2.3-MW beam-power operation, corresponding to the maximum anticipated power. The concentric decay pipe and shielding concrete are illustrated in Figure 3–35, which shows the system designed by the Conventional Facilities at the Near Site to satisfy the Beamline requirements [8]. The CF design is described in more detail in Volume 5 of this CDR.
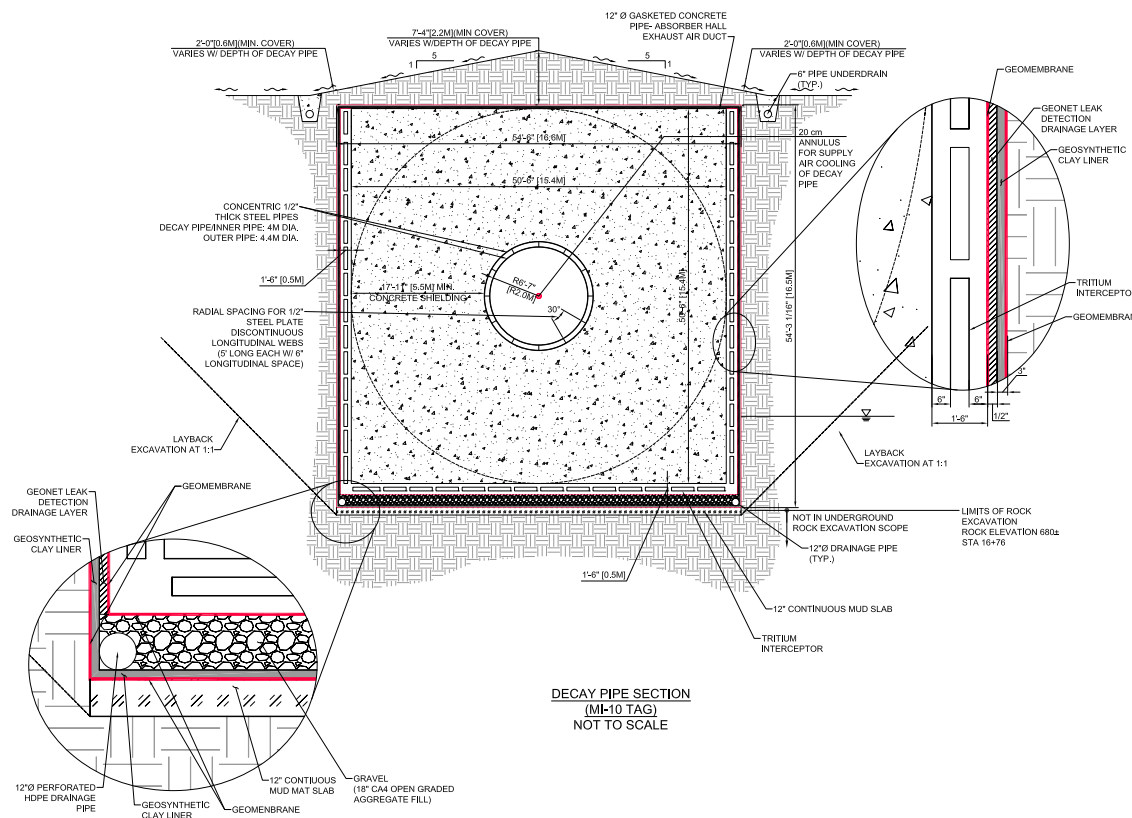
Figure 3–35: Typical cross section of concentric decay pipe and shielding concrete.

The decay pipe CF construction must be built to accommodate these requirements:

- 200-m length

- 4-m inside-diameter steel pipe installed concentrically in a 4.43-m inside diameter steel pipe; the radial annular gap between the tubes is 0.2 m

- commercial-grade pipe with thickness of 12.5 mm

- a ground-water barrier system to drain water away from the decay pipe as part of the overall tritium-mitigation strategy discussed in Section 3.10

- maintain alignment accuracy of 20 mm

- resist temperature rise of $50_\circ$C which generates compressive stress of 15,600 psi with fully constrained concrete end walls

- external and internal steel-corrosion protection for radiation resistance and corrosion lifetimes

- concrete radiation-shielding thickness of 5.5 m with upstream and downstream 6-m ends

The decay-pipe region begins 22.2 m downstream of the target. The upstream end of the decay pipe opens to the chase within the Target Hall (see Figure 3–36), accepting cooling-air return-flow from the target chase on its way to the combined air-return duct at the upstream end of the decay pipe, as discussed in Section 3.8. Heat generated by beam interaction has been calculated to be 511 kW, distributed non-uniformly down the length of the decay pipe. Approximately half of this heat is generated in the inner steel tube, with the remainder generated in the outer steel tube and first 0.5-m depth of concrete. A maximum temperature of $35_\circ$C is estimated in the steel tubes and a maximum temperature of $40_\circ$C is estimated at the geomembrane layers with the cooling airflow of 50,000 scfm discussed in Section 3.8 and air supply temperature of $15_\circ$C ($59_\circ$F). The downstream end of the decay pipe must be closed as part of the air cooling of the pipe.

It is anticipated that the CF design will include concrete at normal strength of 4,000 psi with appropriate flow characteristics for pouring. It is also expected that the stiffeners will be positioned between the inner and outer pipes to maintain concentricity.

3.6.3   Reference Design

The decay pipe ends in the upstream wall of the Absorber Hall, as shown in Figure 3–37. The Beamline subproject will provide the end closure at the downstream end of the decay pipe for the outer steel tube. This will be a steel, formed head with a central 1-m-diameter region of 6-mm-thick aluminum. The head will be sized to minimize deflections due to air pressure. The central aluminum window will be air-cooled as the air flows out of the annular radial gap and turns $180_\circ$, flowing against the end closure, to head upstream in the 4-m-diameter inside steel tube. This window will be welded in place and will not be replaceable.

Supply and return air ducts connected to the concentric decay pipe (Fig. 3âĂŞ36) for the cooling airflows are discussed in Section 3.8.

The decay pipe will be 200 m, with the option of going to 250 m. A decision on the length includes a full understanding of the optimization in progress between cost and physics sensitivities. It consists of a 4-m inside-diameter steel tube installed concentric in a 4.43-m inside diameter steel tube; the radial annular gap between the tubes is 0.2 m. Spacers are welded between the two tubes to maintain concentricity. The spacers are spaced around the circumference and do not interfere with the cooling airflow in the annular gap. A typical cross section of the decay pipe concrete is a square with 5.5-m thickness in the vertical and horizontal planes. A system of geomembranes, bentonite clay, gravel, and geo-net mesh material encase the decay pipe concrete to act as a ground-water barrier and to drain water away from it as part of the overall tritium-mitigation strategy discussed in Section 3.10.
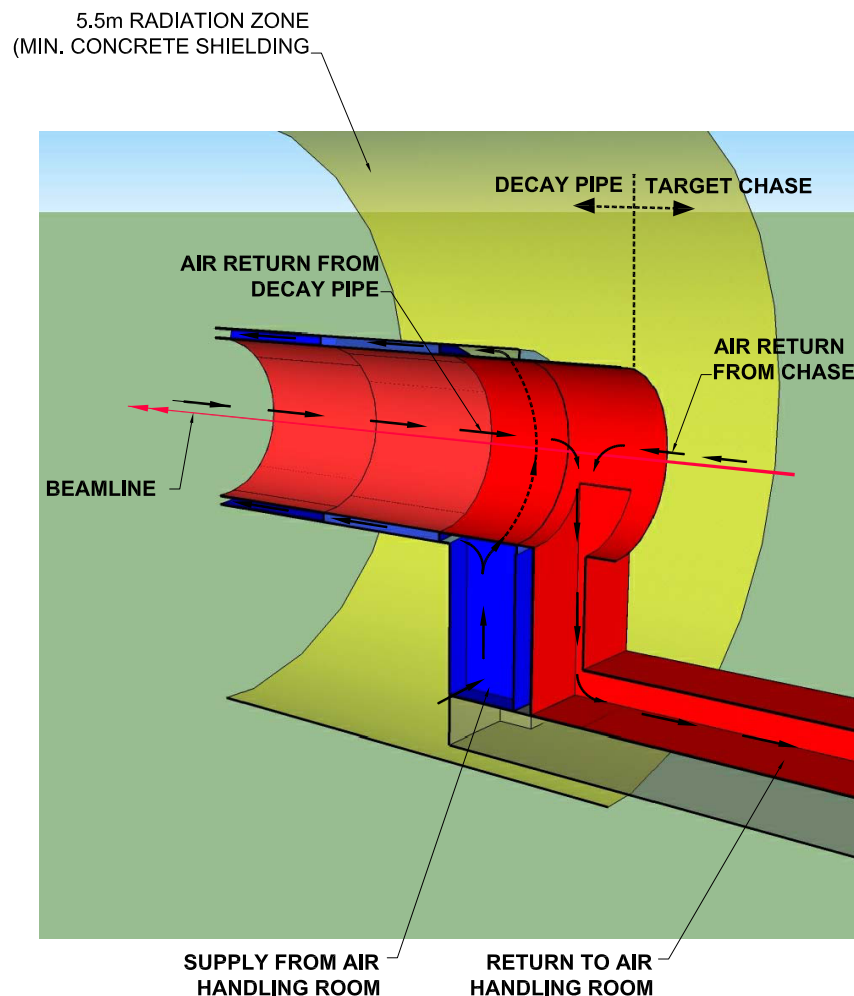
Figure 3–36: Section of the decay pipe at its upstream end. The airflow for cooling within the pipes is indicated.

3.7 Hadron Absorber (WBS 130.02.03.07)

3.7.1 Introduction

The hadron-absorber structure (also called simply the "absorber") is located directly downstream of the decay pipe. The absorber, a pile of aluminum (Al), steel and concrete, is intended to absorb the residual energy from uninteracted protons and the secondary particles (hadrons) which do not decay. The power absorbed is a large fraction of the total beam power and thus needs to be contained to prevent activation of subsurface soils and groundwater.

The absorber consists of the following components: the absorber core (including the aluminum and steel sections and the Al pre-absorber core mask), the absorber shielding (including steel blocks and concrete), and the temperature-monitoring and cooling infrastructure.

Figure 3–37 shows a simplified view of the absorber within the Absorber Hall. The yellow zone represents the absorber core where the vast majority of the non-interacted protons and secondary particles that reach the absorber will start hadronic and elecromagnetic showers.

3.7.2 Design Considerations

The LBNE absorber is designed to support a beam power up to 2.3 MW at an energy range from 60 to 120 GeV. The absorber should operate without maintenance during the lifetime of the experiment; extensive upgrades at a later time would be impractical.

The absorber must be designed to sustain the beam-energy deposition under expected normal operational conditions as well as under all accident situations that may occur with some reasonable probability. In the case of normal operation, the absorber should dissipate 560 kW of power per beam spill. In the case of an accident, the absorber should sustain at least 15 pulses at full 2.3-MW beam power for a total duration of 20 s. During this time, the thermal protection embedded in the core blocks should generate a signal to inhibit the beam permit. Such power requires special attention to the cooling of the absorber components, especially its central part - the aluminum core.

The interaction of the protons and residual secondary particles with the absorber media creates thermal neutrons that get mostly absorbed by the external concrete. The majority of muons pass through the absorber, depositing negligible amounts of energy before they stop in the rock downstream of the Absorber Hall. According to the simulation [26], 24% of the total beam power is deposited in the absorber, 60% of which comes from the primary protons.
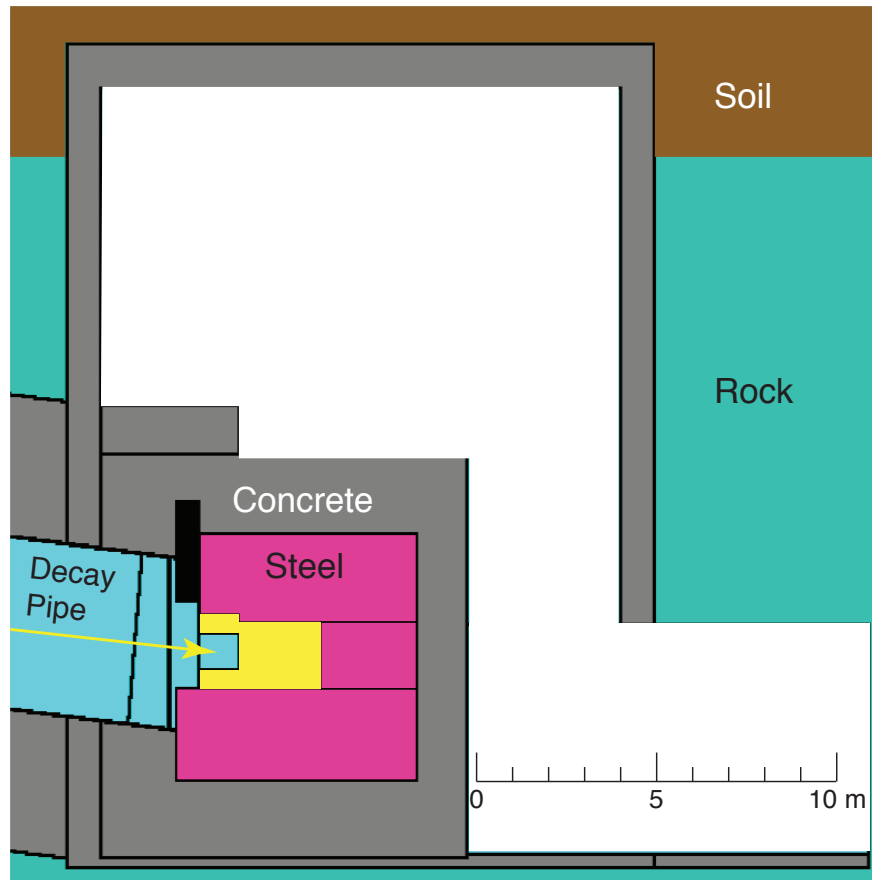
Figure 3–37: Simplified elevation view of the absorber within the Absorber Hall. The white zones are air. Most of the energy (from the uninteracted protons) is deposited into the aluminum absorber core (yellow). The excavation at the lower right is an alcove for beam muon monitors. The soil-rock interface is approximately 23m below the surface.

3.7.3   Absorber Modeling

3.7.3.1   Normal Operations

The longitudinal energy deposition in the Al core in the case of normal operation is shown in Figure 3–38. The maximum energy deposition is between the third and fourth blocks (hatched zone, Figure 3–38). Accordingly, the reference design places the center of the third block in the transverse center of the hadronic shower. For this block, the calculated energy deposition was transferred to finite element analysis software (FEA using ANSYS) to simulate the temperature distribution and the necessary cooling conditions. Figure 3–39 (left), shows the maximum temperature in the absorber-core block over 10,000 normal beam pulses. The temperature reaches a plateau at approximate 187.3° C. Figure 3–39 (right) shows the final temperature distribution in the block. For this simulation, the cooling lines were placed around the perimeter of the block and water temperature was assumed constant at 25° C. This analysis shows that maximum operational temperature is below any critical temperature of the Al material. This relieves a point of concern that exposure of Al material to high temperatures ($\sim$275° C) for long period of time could raise the issue of creep (time-dependent plastic deformation) and possible thermal distortion.

Similar simulations were performed for all other absorber blocks, and the results were taken into consideration in the overall design of the cooling scheme. To simplify the design, the steel blocks of the absorber core have the same cooling channel pattern as the aluminum ones.

The absorber core, like the target and decay pipe, needs to be adequately shielded to prevent a build-up of radionuclides in the water contained in the surrounding rock. To satisfy this requirement, the core, like the NuMI absorber [16], should be surrounded with steel and concrete blocks, which form the absorber shielding. Additional specification for the amount of shielding comes from a requirement that the residual radiation dose in the Absorber Hall, after decay of the short-lived radionuclides, should be on the level of 100 mrem/h. This requirement is imposed by the necessity of servicing the detectors placed in the Absorber Hall, e.g., the hadron and muon monitors. To satisfy the these requirements for the LBNE absorber, the MARS simulation indicated that at least seven feet of steel and three feet of concrete shielding are needed.

The hadron monitor, which is placed in the front of the absorber core, is expected to have an average lifetime of one year (see Volume 3, Section 3.2 of this CDR). To store both the highly activated monitors after their service life and any faulty absorber blocks, a specially designated radioactive material storage place is included in the absorber concrete wall. It has three slots to store the activated Monitors and/or absorber blocks before their removal to the surface.

It is unlikely, but possible, that the water-cooled absorber modules and steel shielding blocks
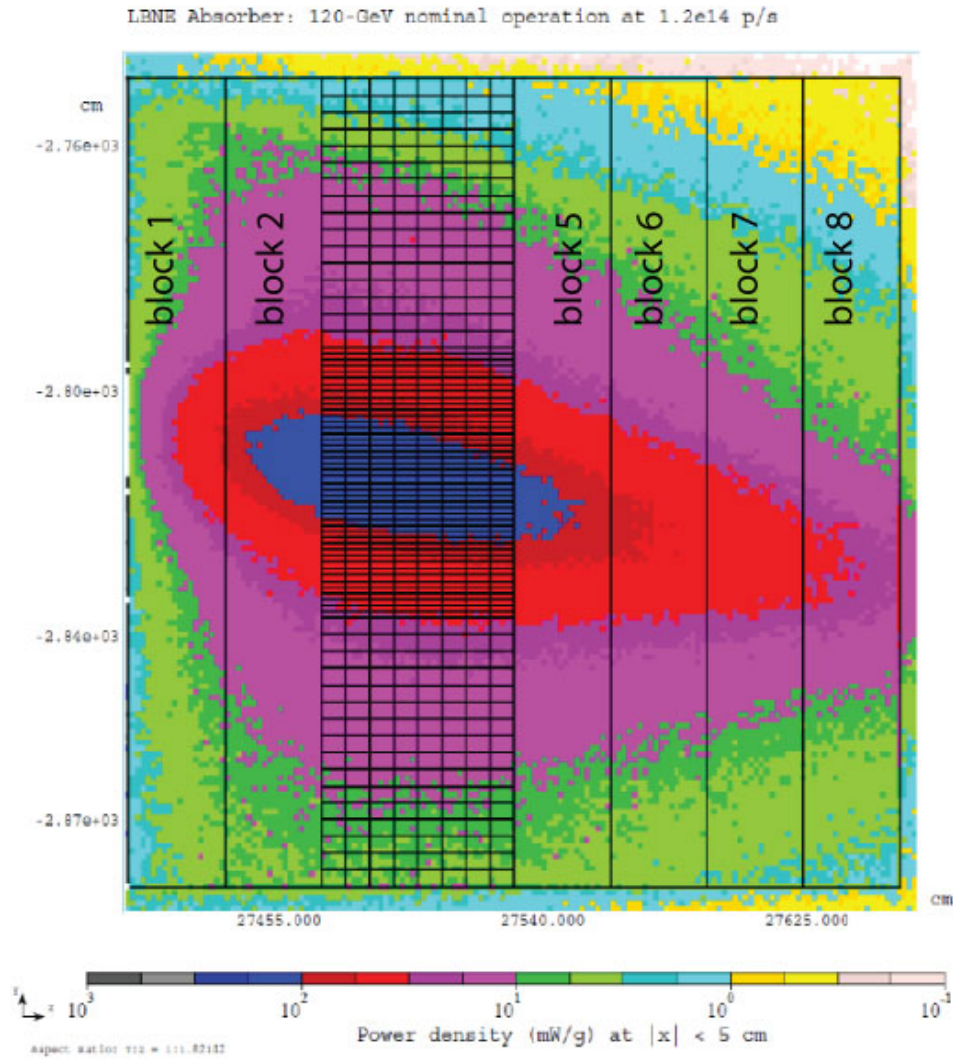
Figure 3–38: Result from MARS modeling showing the longitudinal energy deposition in the aluminum core of the absorber for normal operation.
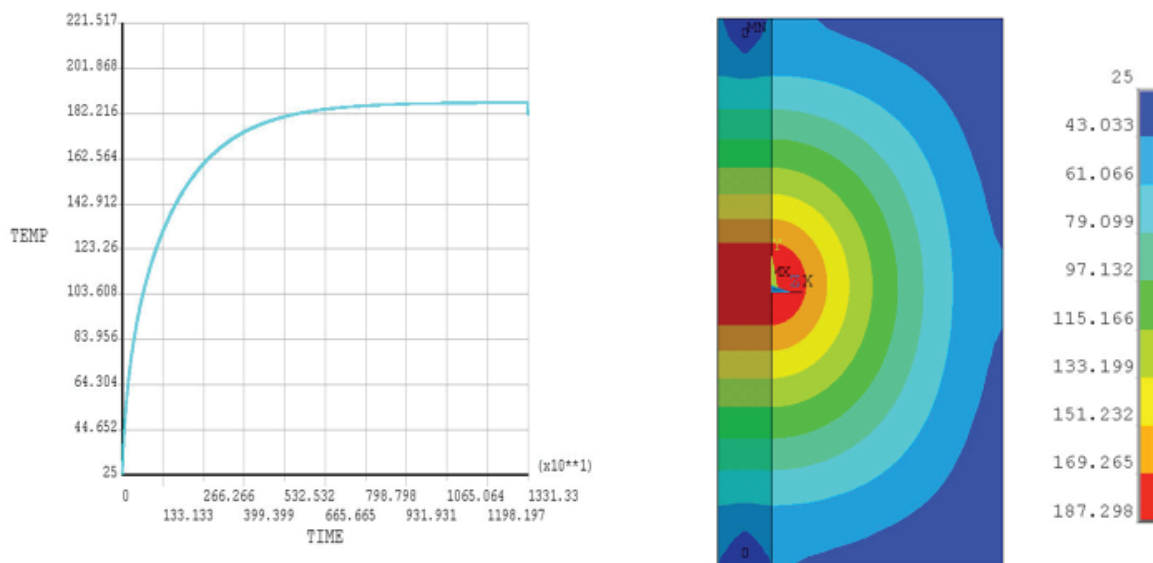
Figure 3–39: Results from ANSYS simulation. The maximum temperature (°C) versus time × 10 (s) for the third aluminum core block is shown (left) after 10,000 normal pulses. The temperature distribution in the same block is shown to the right.

will fail. Although the absorber components are designed to last the lifetime of the facility and will include at least three redundant water-cooling lines, the consequences of complete failure might be significant. Because of the low probability of complete failure, the design and construction of remote handling equipment for the absorber modules and water-cooled shielding will not be included in the current design. If complete failure of a water-cooled block occurs during operation, a long downtime (6 months to 1 year) would then be required to design, build, develop procedures and safely replace the failed component(s). Following repair, failed components could be stored in the slots provided to keep the activated hardon monitors in the Absorber Hall.

3.7.3.2   Modeling Accident Cases

Two accident conditions have been modeled.

The first accident case assumes that a mis-targeted primary proton pulse hits directly in the central part of the absorber. In this case the full beam power of 2.3 MW is deposited directly into the absorber structure. An analysis was performed to determine how many direct beam pulses the Al core can take before the maximum temperature reaches over 600° C (the melting temperature for pure Al is 660° C). Figure 3–40 shows the temperature distribution in the third block after ten direct beam pulses imposed over the operational regime with temperature of 187°C. The FEA shows the temperature increasing to 465°C, or

every beam spill increases the temperature in the center of the core by approximately 27.8°C. The requirement is that the absorber should sustain at least 15 accident pulses, for the total duration of 20 s. An extrapolation of this dependence showed that after approximately 15 faulty pulses the maximum temperature in the center of the third Al-core block will reach ~ 600°C which is below the melting temperature for the Al core. To prevent such a high temperature, every core block will be instrumented with a number of thermocouples (eight by current design) connected to a National Instrument (NI) data-acquisition system. It is worth mentioning that the first steel block in the absorber-core (block number 9) will reach operational temperature of 247°C and 387°C after 15 faulty pulses.
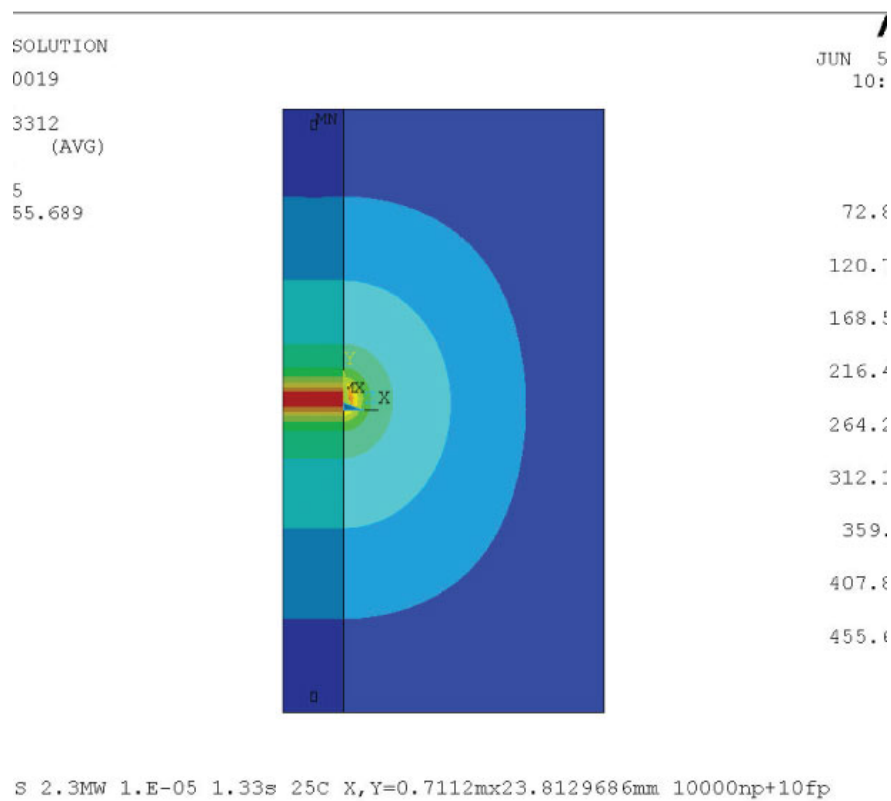
Figure 3–40: Temperature distribution in the aluminum absorber-core block. Ten beam pulses under the fault condition are superimposed on 10,000 normal ones. The maximum temperature in the center of the block is 456° C after ten faulty pulses.

Table 3–7: Operational and accident conditions for the absorber used in the design study with 2.3-MW beam power.

Beam Power in absorber normal operation	500kW
Beam Power in absorber accident condition	2.3MW
Primary beam size at absorber (target in)	20mm H × 12mm V (σ)
Primary beam size at absorber (target out)	15mm H × 12mm V (σ)
Accident condition - direct beam	15 pulses (20 s)
Accident condition - mis-steered beam	2 pulses (2.6 s)
Max. temp. in Al core - normal	187° C
Max. temp. in steel core - normal	247° C
Max. temp. in Al core - accident	606° C
Max. temp. in steel core - accident	387° C
Temperature rise per accident pulse Al (steel)	27 (9) ° C

The second accident case assumes the beam is mis-steered relative to its original direction, causing a beam-control failure. This is a single pulse accident condition and it is assumed that primary-beam instrumentation will trip the beam permit before a second or at most a third pulse. Using a simple target/baffle model (one baffle and one passive aperture restrictor, 10 m apart, with diameters 40 mm upstream and 20 mm in front of the target) a maximum "hittable" radius of 900 mm at the absorber is estimated. The primary concern for this accident case is hitting a water-cooling channel, possibly setting off a water hammer effect. MARS [24] energy-deposition modeling, followed by an ANSYS [27] Finite Element Analysis (FEA) simulation indicated that if the water-cooling channels are kept outside the 900-mm-radius, the absorber core will overheat (the water-cooling channels must remain at ~750 mm radius to prevent overheating). To prevent a direct beam hit on the core cooling channels placed inside this radius, a pre-absorber-core mask will be used to protect them (see Section 3.7.4.1).

Table 3–7 summarizes the operational and accident conditions for the absorber.

3.7.4   Reference Design

A 200-m-long decay pipe is assumed for the reference design; a longer pipe, up to 250 m, also remains under consideration as an alternate. No modification of the absorber is needed for the case of a 250-m-long decay pipe.

Figure 3–41 shows the top view of the absorber. The magenta represents the walls of the concrete shielding. The Al pre-mask and core is shown in blue, while the steel core blocks are represented with red. The green color around the core represents the steel shielding. On the right, three storage slots are reserved for the activated hadron monitors and faulty absorber-core blocks, in case they require replacing.
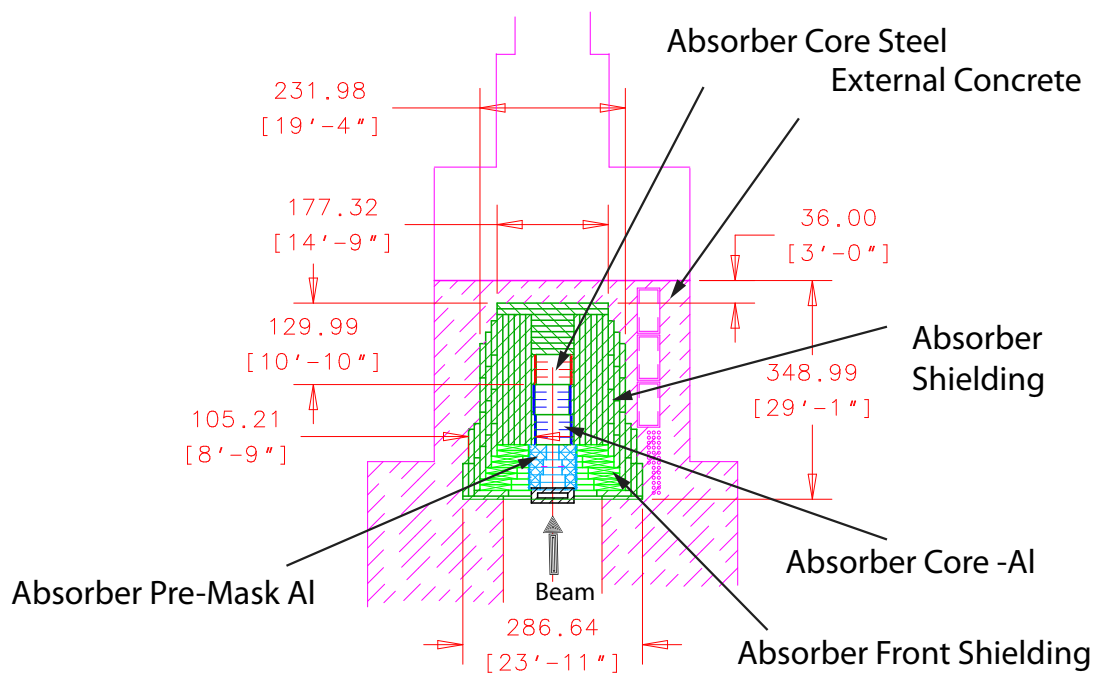
Figure 3–41: Model of the absorber conceptual design; top view. The core of water-cooled aluminum blocks is 96-in deep, followed by 130 in of steel (first 32 in are water-cooled) and 36 in of concrete at the rear. The routing of the cooling pipes has not been finalized.

3.7.4.1   Absorber Core

The absorber core consists of eight one-foot-thick aluminum blocks (each 60-in × 60-in × 12-in). The core receives approximately half of the total energy deposited within the absorber pile, and thus requires water-cooling. The design of the block is shown in Figure 3–42. At least three continuous aluminum water-cooling lines are welded to the four sides of the block. By design, one cooling line is enough to support the absorber operation. In case of an emergency water leak from one of them, the second or/and third cooling line will be used.

The core dimensions depend on the energy, size and intensity of the incident hadron beam. A MARS simulation, using a simple target and decay-pipe geometry, of the LBNE beam incident on the absorber was used to define the parameters of the core [26]. The parameters lead to an LBNE absorber core similar to the NuMI ones with an increase of the transverse cross section to 60-in × 60-in, including the water-cooling channels. The core is leveled horizontally and the beam hits it at an angle of 101 mrad, crossing the absorber horizontal middle plane between the third and fourth blocks at maximum energy deposition.

To absorb the longitudinal tails of the hadronic showers initiated in the core, the core is extended by an extra seven feet of steel; see Figure 3–42, red and green blocks behind the Al core. Four of these blocks (red blocks) form the steel part of the absorber core. By design, they are identical to the aluminum blocks except that their aluminum cooling tubes are clamped to the edges of the block. The other part of the steel shielding (green blocks) is made from continuous-casting salvage steel (CCSS), with a thickness of 9.11 in. The total number of steel blocks behind the Al core is chosen to maintain a safe amount of residual radiation in the Absorber Hall, since service work will need to be performed behind the absorber pile.

This entire structure must be encased in concrete of sufficient thickness to moderate or absorb thermal neutrons and to keep the flux at the absorber shaft entrance at acceptable radiation levels. This design may allow a core block change in case of a total failure of both cooling channels. To perform this operation a 30-ton crane that will be installed in the Absorber Hall.

During normal operation, the FEA [28] of the energy deposition in the first steel block (number 9) shows a maximum temperature of 247° C (see Table 3–7). To avoid such a high-temperature condition for this block (ninth block), an option to increase the thickness of the aluminum part of the core by adding one more block is being investigated. This block will further spread the hadronic shower, thus decreasing the amount of the deposited energy in the first steel block. Furthermore, some minor optimization to the geometry of the absorber core is in progress.

To avoid accidents in which beam directly hits a core cooling line, as described in Section 3.7.3.2, an aluminum pre-core mask has been introduced. The design of this module
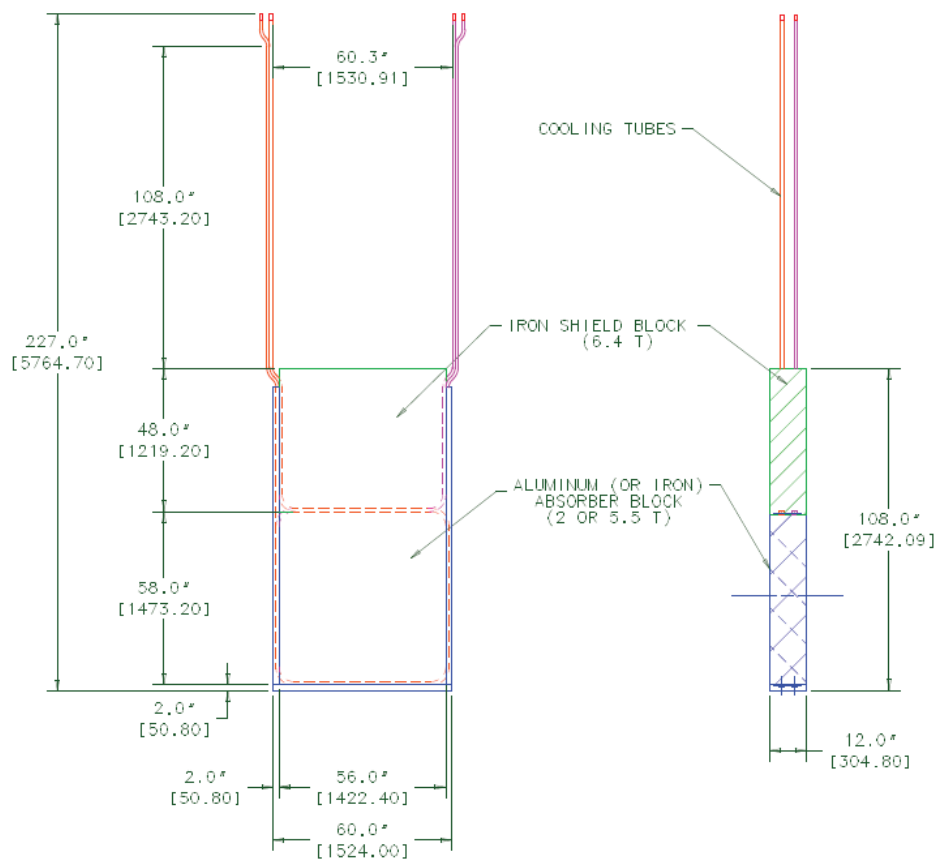
Figure 3–42: Design of the absorber core blocks. Note that the part of the top steel shielding (green box, left) is attached to it for easy replacement.

is shown in figure 3–43. Six of these pre-core blocks are installed in front of the aluminum core blocks. The masks are similar in design to the absorber-core blocks, but with larger cross-section. The diameter of the through-hole decreases from 40 in to 20 in over 6 foot distance and center of the hole is offset to follow the beamline slope. The cooling tubes of the pre-core mask blocks are outside of the possible accidental beam-hit area.

3.7.4.2 Absorber Shielding

To decrease the absorber cost, the external shielding around the core also uses CCSS slabs (shown in green, Figure 3–41). The other dimensions of the slabs can be custom ordered; the only limitation is the capacity of the Absorber Hall crane of 30 ton. The absorber core and these blocks are staggered horizontally by ±1 in to exclude the possibility of creating a longitudinal air gap where the hadron shower could propagate. There is no staggering in the vertical direction because the beam is tilted vertically. Some of the front shielding blocks should be water-cooled; the power dissipation in them is too large to rely on just the air convection cooling. The minimum thickness of the absorber core shielding is 87 inches.

In comparison with the NuMI absorber, where the external shielding is built mostly from standard concrete square blocks, for LBNE, the absorber will be surrounded by a cast-in-place concrete bed to provide external shielding of (minimum) thickness 36 in (shown in magenta in Figure 3–41). This concrete is provided by the Conventional Facilities at the Near Site, and is discussed in Volume 5 of this CDR. The only removable blocks will be in the area above the absorber core, which is covered with two overlapping layers of standard concrete blocks (3-ft × 3-ft × 6-ft), the area above the radioactive-material storage place, covered with two overlapping layers of concrete blocks (3-ft × 3-ft × 7.5-ft); and the area above the Hadron Monitor in front of the first block of pre-absorber core mask, covered with two overlapping layers of standard concrete blocks (3-ft × 3-ft × 6-ft).

3.7.4.3 Absorber Water-Cooling System

The water-cooling system is based on the detailed simulation of the power losses in different parts of the absorber. The total calculated loss in the core at normal operation is 347 kW (120 kW in the aluminum blocks and 227 kW in the steel blocks). To dissipate these losses with the cooling water, 165 gpm of water flow is needed through the absorber blocks. At this flow, the water temperature will rise approximately 10°C, varying from block to block. Some additional cooling is anticipated for the front steel shielding blocks.

A closed loop of distilled water with a nominal pressure of 100 psi is assumed. Depending on the cooling and heat-exchanger scheme, the pressure may be adjusted between 60 and 100 psi, and the water-cooling tube size will be selected accordingly. The water-cooling system must be equipped with pressure-relief valves to prevent any damage to the radioactive-water
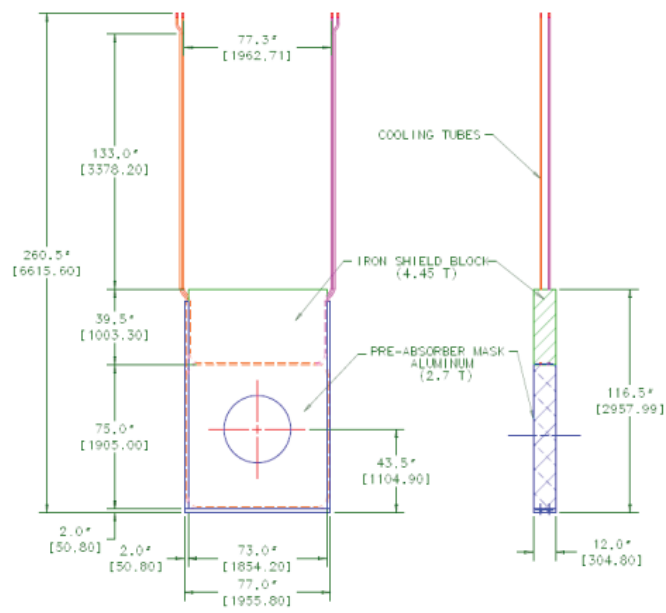
Figure 3–43: Design of the aluminum pre-core mask.

system; a loss of water flow could be serious during an accident condition, for example, while significant energy is stored in the absorber blocks.

For redundancy, the absorber-cooling infrastructure is divided into three or four independent loops. Each loop supplies water to one of the cooling lines for each absorber block. If a problem occurs in the one of the cooling lines of any absorber block, the supply cooling loop will be switched off until a shutdown time can be scheduled. Meanwhile, the absorber will continue to work using a spare cooling loop.

A metal containment pan will be installed underneath the absorber to collect cooling radioactive water in the event of a leak from a cooling line. This water will be routed to a holding tank placed in the Absorber Service Building (LBNE 30).

3.7.4.4   Absorber Temperature Monitoring

Absorber-core blocks will be instrumented with at least eight thermocouples, distributed radially every 45° at a radius of approximately 400 mm. The output voltages from the thermocouples will be read out by five precision temperature loggers (for example, NI PXI-4351 modules), which can each be used to measure the temperatures from 16 thermocouples. The digitized signals will be analyzed by the data acquisition computer, which will provide a beam-permit signal if the temperature is within the specified limits.

This is important in the case of a missing or destroyed target, where the primary beam would directly hit the absorber, depositing maximum power and causing a fast temperature rise.

3.8   Target Hall Shielding (WBS 130.02.03.08)

3.8.1   Introduction

The Target Hall shielding (also called the target pile) is designed to (1) keep the accumulated radionuclide concentration levels in the surrounding soil below standard detectable limits; (2) keep prompt radiation levels low enough for electronics in the Target Hall to have adequate lifetimes; and (3) keep residual radiation rates on top of the shield pile low enough to allow personnel to access the top of the steel shielding pile for maintenance with beam off. It consists of two portions, the Target Hall Shield Pile and the Target Hall Air-Cooling Flows.

3.8.2   Design Considerations

The target pile is built underground, and its size cannot be significantly modified or upgraded after completion. Therefore, this part of the neutrino beam has been designed for 2.3-MW beam-power operation, corresponding to the maximum anticipated power.

3.8.3   Reference Design

3.8.3.1   Target Hall Shield Pile

The Target Hall steel shield pile refers to the steel shielding surrounding the beamline components (baffle, target, Horn 1 and Horn 2) installed in the target chase. The chase runs the entire length of the steel shield pile, which extends from the primary-beam window down to the decay pipe. The chase is 54-in wide at the water-cooling panels in the region of the horns and 64-in wide elsewhere. Its height varies along the length of the shield pile; the chase floor has three horizontal steps. The beam center-line in the Target Hall region slopes downward at 101 mrad (5.79°) from upstream to downstream, as illustrated in Figure 3–44.
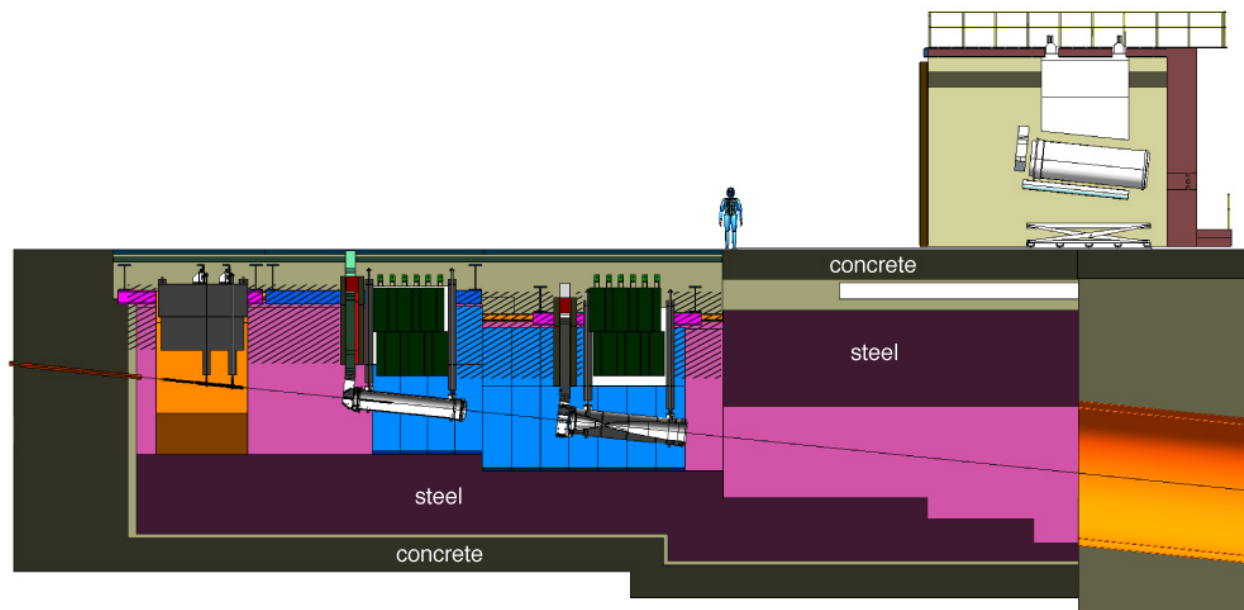
Figure 3–44: Beamline elevation view. The beam comes from left. The non-modular steel shielding is shown in purple shades. Special steel modules (left to right) are the baffle support module (gray) and the horn support modules (dark green). Other removable shielding is shown as cross-hatched areas. Removable marble and polyethylene shielding will be placed along the roof of the chase shield, where the figure is shown. The work cell is at the top right.

The chase acts as a collimator for pions from the target and horns that are not well-focused.

This collimation is intended to reduce the beam power deposited in the decay pipe.

The shield will consist of two main layers. An inner, steel layer will absorb all the stray particles from interactions of the primary beam, except neutrons below a few MeV energy. An outer concrete layer is used to moderate and absorb most of the neutrons that escape from the steel layer. Component carriages for the beamline components span and rest on the equipment ledge of the concrete target pit. Component modules are installed in their carriage and hang from the carriage into the shield pile chase as shown in the cross section, Figure 3–45.

The shielding is divided into two sections: (1) the bottom and side shielding which must appropriately shield the surrounding earth and ground water from tritium activation; and (2) the top shielding which must shield the upper Target Hall (see figure 3–45).

The LBNE steel, concrete, marble, and borated polyethylene shielding requirements are given in Tables 3–8 and 3–9. Additionally, there is a 120-in-thick concrete wall at the upstream end to separate the target pile and pre-target tunnel. For comparison, NuMI has 1 m of concrete and 52 in of steel shielding on the bottom and sides and 73-82 in of steel and 18 in of concrete on the top.

Table 3–8: Shielding requirements for the top of the target chase.

	Iron (in)	Marble+ Borated Poly (in)	Concrete (in)
Baffle	92	6	0
Horn 1	124	6	0
Between horns Sec. 1	116	6	0
Between horns Sec. 2	92	6	0
Horn 2	106	6	0
Downstream Horn 2	116	0	36
End of TH	36	0	158

The open space between the steel shielding and the floor and walls of the Target Hall concrete pit form air cooling channels for the exterior surface of the steel pile. The channels are named "bottom" for the floor and "side" for the walls. The space between the top of the steel shielding pile and the marble and poly layers is called the "top" channel. The marble and poly layers are part of the covers over the Target Hall pit. The cooling airflow, discussed below, flows through these channels to enter the chase. Shielding steel is stacked in a staggered and interlocking fashion so there are no line of-sight cracks through the steel shielding pile. Two methods are used to close the top of chase. Removable, specially cut steel blocks called "T-blocks" are used where beamline components are installed. Steel blocks and slabs are used in the other areas.
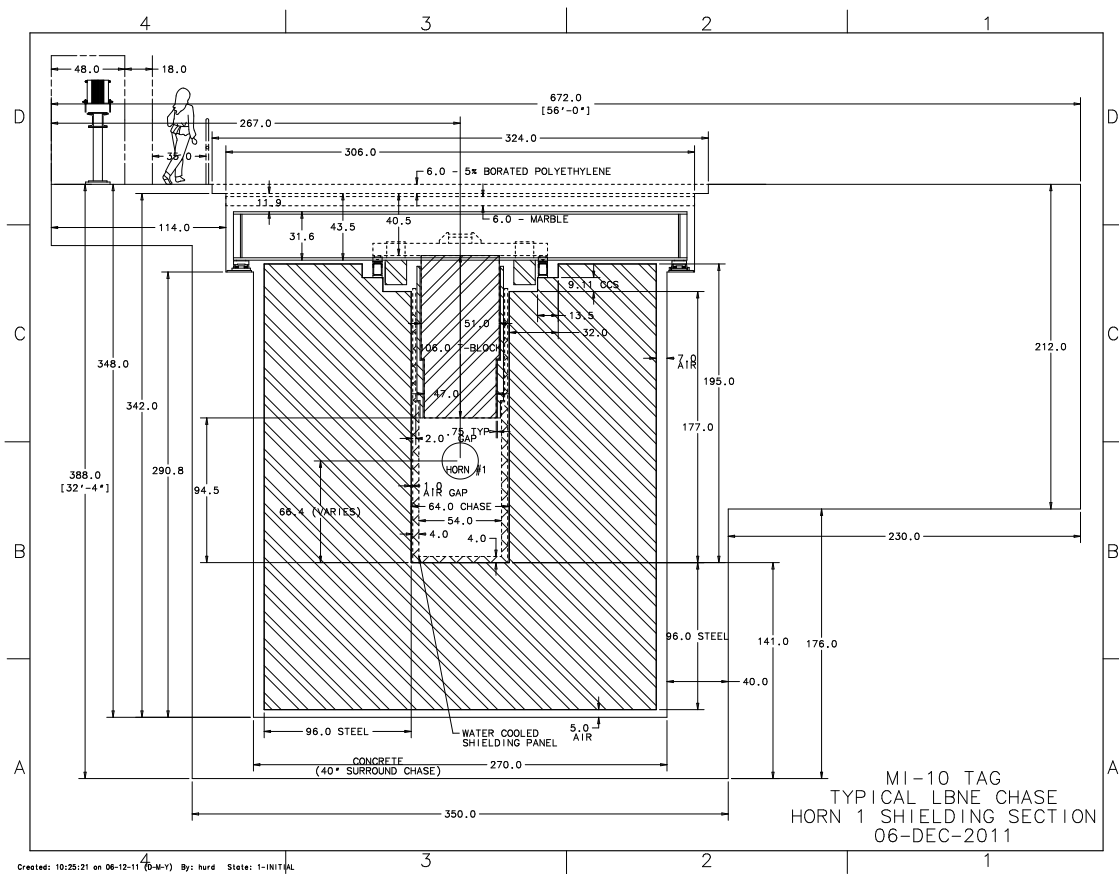
Figure 3–45: Cross section of target chase steel shielding (cross-hatched areas). The secondary beam is confined to the rectangular opening in the center (approx. 1.6 m × 2.4 m).

Table 3–9: Shielding requirements for the walls and the floor of the target chase.

	Iron (in)	Concrete (in)
Baffle floor	96	40
Baffle right wall	96	96
Baffle left wall	96	40
H1 floor	96	40
H1 right wall	96	85
H1 left wall	96	112
Btwn Horns floor Sec.1	96	40
Btwn Horns right wall Sec.1	76	112
Btwn Horns left wall Sec.1	76	112
Btwn Horns floor Sec. 2	96	40
Btwn Horns right wall Sec.2	76	112
Btwn Horns left wall Sec .2	76	112
H2 floor	76	40
H2 right wall	76	85
H2 left wall	76	40
DS of H2 floor	76	40
DS of H2 right wall	76	85
DS of H2 left wall	76	40
End of TH floor (decay-pipe region)	76	40
End of TH right wall (decay-pipe region)	76	85
End of TH left wall (decay-pipe region)	76	40

3.8.3.2   Target Hall Air-Cooling Flows

Energy deposited by the 708-kW beam in the shielding pile and the beamline components is removed by an air-cooling system and cooling systems on the beamline components; water-cooled shielding is not required for 708-kW operation. For the 2.3-MW beam, water-cooled shielding, i.e., panels, T-blocks and module bottoms, intercept most of the beam energy leaving the chase. This shielding will be installed for 708-kW operation but water cooling will be enabled only at 2.3 MW. The air-cooling system and cooling systems on the beamline components remove the balance of the deposited beam energy. Energy deposited by the 708-kW beam or the 2.3-MW beam in the decay pipe is removed by the air-cooling system, water cooling is not needed.

The discussion below outlines the air-flow requirements and the routing design to enable the Target Hall air cooling. The equipment needed for the air cooling is provided by Conventional Facilities at the Near Site, and discussed in Volume 5 of this CDR.

Table 3–10: Airflows in the target pile and the decay pipe.

	Flow (cfm)
Target pile chase supply duct	75,000
Top channel	69,000
Side channels (2)	2500 ea.
Bottom channel	1000
Chase return	75,000
Decay pipe side	50,000
Annular gap	50,000
4-m inner pipe	50,000
Combined return duct	125,000

A single air handler, located in the Air Handling Room, provides 125,000 scfm of dehumidified air to cool the shielding pile and the decay pipe. There are two supply ducts, one to the target pile and one to the decay pipe. Airflows to the shield pile and to the decay pipe are balanced with dampers in the air handler. The airflows mix after they traverse their cooling paths and return to the air handler in a single duct. The combined air return duct is connected to the upstream end of the 4-m-diameter decay pipe, just beyond the end of the steel shield pile. The supply and return ducts have labyrinths, i.e., multiple right angle turns, and steel shielding where the ducts enter or leave the shield pile or the decay pipe to attenuate radiation leakage out through the ducts.

Approximately 75,000 scfm cools the steel shielding. The cooling airflow enters the target pile at the downstream end above the steel shielding and flows upstream in the top, bottom and side channels. All of the air exits the bottom and side channels at the upstream end of the pile, turns 180°, and enters the chase. Chase cross sectional area at the baffle is restricted with steel blocks to increase air speed for baffle cooling. All of the air flowing in the top channel flows vertically downward through clearances between the T-blocks and into the chase. The 75,000 scfm cooling airflow exits the chase at the downstream end, mixes with the cooling airflow from the decay pipe, and enters the air return duct.

Approximately 50,000 scfm cools the decay pipe. The cooling airflow enters the annular gap of the concentric decay pipe at its upstream end and flows downstream. At the downstream end the air flows out of the annular gap into the 4-m-diameter decay pipe, turns 180°, and flows upstream. At the upstream end the 50,000 scfm mixes with the 75,000 scfm from the chase and enters the air return duct back to the air handler.

3.9   RAW Water Systems (WBS 130.02.03.09)

3.9.1   Introduction

Many components in Target Hall as well as the core of the absorber are water-cooled. Since these elements are operated in an environment with a high flux of energetic particles from the beam and target, the cooling water itself will be activated and cannot be allowed to mix with unactivated water. Therefore, these components are cooled using a closed-circuit water system; the heat being moved by conduction and convection to secondary water heat-exchanger/chiller system connected to the outside world. The closed Radioactive Water Systems (RAW systems) are used extensively at the laboratory in removing heat from high-flux particle environments. They are generally mounted on transportable skids with secondary containment systems.

3.9.2   Design Considerations

All the RAW systems will require radiologic inspection of welds, and all storage vessels will be designed to the requirements of ASME Boiler and Pressure Vessel code. All RAW equipment skids will have suitable containment for RAW leakage and tritium capture, and all should be designed with an intermediate loop between the RAW system and exposure to systems outside of the enclosures.

All RAW system volumes are expected to fall into the range of 100 to 200 gal each. RAW skids will have sufficient containment to capture these volumes. Also, Fermilab's guideline is to limit RAW activity to 670,000 pCi/ml [29]; LBNE will design the system to operate around an activity level of 500,000 pCi/ml. The activation limit is expected to be reached on a monthly basis for the horn systems and biannually or so for the remainder of the systems. Because of this, the addition of RAW capture and drainage systems are included. Their purpose is to help with the recapture of RAW waters from each of the skids in such a way as to limit manpower exposure and frequency of water change-out. Similarly, the Target Hall and Absorber Hall will have adequate space for the local storage of hot de-ionization (DI) bottles and components.

3.9.3   Reference Design

3.9.3.1   Target Hall Systems

Located outside the Target Hall will be a RAW equipment room, which will hold the majority of the equipment for RAW skids, for cooling of the baffle, target, horns 1 and 2, and shielding.

The estimated overall heat load is around 300 kW. The method to cool the Target Hall RAW systems is not yet determined. The options include cooling supplied by primary beamline low-conductivity water (LCW), industrial chilled water (ICW) supplied by the Central Utility Building (CUB) or via a local system with a chiller at ground loop. Due to the requirement for the horns to have 16°C supply water as opposed to the 35°C standard of LCW, the last two choices seem more appropriate. Due to the distance from CUB, a local system may prove advantageous. Local chillers were selected for the reference design and the load is included in the CF Target Complex design of 1,200 tons.

The reference-design Target Hall RAW systems are as follows:

- Target and Baffle RAW skid

- Horn 1 RAW skid (supply at 16-18°C)

- Horn 2 RAW skid (supply at 16-18°C)

- Shielding/cooling system skid (undecided)

- RAW Exchange and Fill System

- Groundwater tritium mitigation skid (see Section 3.10)

3.9.3.2 Absorber Hall Systems

Located outside the main Absorber Hall will be a RAW equipment room, which will hold the majority of the equipment for RAW skids, for cooling of the absorber.

The estimated total heat load for the Absorber Hall RAW systems is approximately 450 kW (at 708 kW beam power). The most likely source of outside cooling water would be for a chiller system at ground level and a recirculation and cooling system to supply the enclosure. While possible, a local pond water-cooling system would most likely prove too expensive for consideration.

The reference-design Absorber Hall RAW systems are as follows:

- Absorber RAW skid

- Intermediate cooling skid

- Deep tunnel cooling system

- RAW Exchange and Fill System

- Groundwater tritium mitigation skid (see Section 3.10)

3.10   Radiological Considerations

3.10.1   Introduction

In this section, radiological issues for operation of the LBNE beam line with 2.3 MW beam power are considered, since retrofitting the LBNE facility for 2.3 MW after years of operation at 708 kW is very costly and not practical. The scope of these issues includes the primary transport line, Target Hall, decay pipe and the Absorber Hall. The analyses contained in this section are based on current requirements of the Fermilab Radiological Controls Manual, FRCM [29]. Other measurements and verification data available are also used where applicable. The posting and entry control requirements for access to areas outside of beam enclosures where prompt radiation exposure may exist for normal and accident conditions are given in the Fermilab Radiological Controls Manual. All results presented in the following subsections are based on the MARS modeling of the LBNE facility (See Section 3.12).

In NuMI (400kW), fractional beam losses are controlled to better than 10^{-5}. Scaling to 2.3 MW this corresponds to controlling the losses at 1.6×10^{-6} for LBNE. Control of the LBNE beam average operational losses is assumed to be 10^{-5} for shielding purposes, which gives a sensitivity/safety factor of more than 5. Larger, accidental beam losses are difficult to estimate from first principles. Again, the NuMI beam can be used as the analog to LBNE for this estimation. During the six years of NuMI primary beam operation, more than 50 million beam pulses have been transported to the NuMI target with a total of more than 1.2×10^{21} protons on target at 120 GeV. A total of 6 beam pulses have experienced primary beam loss at the 1% level, all due to Main Injector RF problems. Therefore, it is assumed that control of LBNE primary beam losses to less than 2 pulses/week is possible by using a control system similar to that developed for the NuMI beam.

The radiological requirements outlined in this section are applied to the designs of the technical systems and equipment for the Beamline discussed in this volume, as well as to the conventional facilities discussed in Volume 5 of this CDR.

The radiological requirements outlined in this section are applied to the design of technical system and equipment for the Beamline in other sections of this CDR volume, as well as to the Conventional Facilities described in Volume 5.

3.10.2   Shielding

3.10.2.1   Primary Beamline

The Conceptual Design for the LBNE facility has been developed with external primary beam soil shielding of 25 feet (7.6 m), matching the shielding over the Main Injector beam tunnel. This provides an additional safety factor beyond the calculated LBNE required shielding for both the normal and accidental losses. The calculated soil shielding required for 2.3 MW beam, for unlimited occupancy classification, is 21 feet (6.4 m) for continuous fractional beam loss of 10^{-5} level and 23 feet (7.0 m) for 2 localized full beam pulses lost per hour.

To reduce the accidental dose from muons at the site boundary to less than 1 mrem, 326 feet (99 m) of soil in the path of the muons is required. However, because of the offsite annual dose limit, the shielding for the longitudinal muons either must be increased to 400 feet (122 m) or beam control should limit full beam losses to less than one pulse per day.

3.10.2.2   Target Hall/Target Chase

The Target Hall shielding is designed to contain prompt radiation, residual radiation, activated air and accidental spills of radioactivated water, to reduce a thirty-year buildup of the radionuclides in the soil outside the shielding to below the standard detection levels. The goal of the design is to have an average dose rate of less than 100 mrem/hr in the Target Hall during the normal beam operations. A combination of steel, marble and borated polyethylene is used for shielding on top of the target chase. Because of the skyshine considerations, the walls and the ceiling of the Target Hall are required to be 5 feet (1.5 m) and 7 feet (2.1 m) of concrete, respectively. For the sides and the bottom of the target chase, combinations of steel and concrete shielding are used. Details of the Target Hall and the target chase shielding are given in Section 3.8.

3.10.2.3   Decay Pipe

Given the geology in the region near the Main Injector, if the Decay Pipe was constructed horizontally at the elevation of the Main Injector with enough shielding such that the production of radionuclides in the soil are below the *surface* water concentration levels, no additional mitigation would have been required. However, the Decay Pipe will be partly underground with the downstream end close to the aquifer. Under these conditions, it is prudent (ALARA) to reduce the concentrations by two orders of magnitude; e.g. tritium concentration to be 0.3 pCi/ml, which is below the standard level of detection. Based on the requirement set by the project [30], the decay pipe will use 18 feet (5.5 m) of concrete shielding. Additionally, to protect against tritium leaking out of the shielding and being released to the environment,

protective outer layers of water impermeable material and a water drainage layer are added to the decay pipe shield (see Section 3.6).

3.10.2.4   Absorber Hall

The absorber (Section 3.7) and the Absorber Hall shielding is based on the ground water management requirement [30] set by the project using the latest MARS model [31]. The Absorber Hall shielding design is intended to reduce a thirty year buildup of the radionuclides in the soil outside the shielding to below the standard detection levels, to reduce the residual dose rates outside the absorber block to less than 100 mrem/hr. and not to cause any significant activation of the equipment in the absorber RAW room. The activated air will be combined with the Target Hall air and expelled at the NuMI exhaust shaft EAV2 (see Section 3.10.3.4).

3.10.2.5   Near Detector Hall

The distance between the Absorber Hall and the near Target Hall is chosen to allow the residual muons coming out of the Target Hall to range out in the intervening rock [32]. There are no radiological safety issues due to the muons or hadrons in the near detector hall.

3.10.3   Other Radiological Design Issues

3.10.3.1   Groundwater and Surface-water Protection

The production of potentially mobile isotopes such as tritium (^{3}H) and sodium-22 (^{22}Na) is an unavoidable consequence of high-energy particle collisions with nuclei. Since the primary transport line is located in the glacial till, with no direct connection to the aquifer, all radionuclides produced in the soil surrounding the enclosure will have to migrate down through the soil layers to reach the aquifer. These seepage velocities, for the layers in the glacial till, are very small and the concentrations of the radionuclides are reduced by 5 to 7 orders of magnitude.

For the rest of the beam line, from the primary Target Hall to the end of Absorber Hall, there will be sufficient shielding and water impermeable layers to render the concentration of the radionuclides of interest, accumulated in the soil over 30 years, to be less than the current standard detection limits. The current accepted detection limits are 1 pCi/ml for tritium and 0.04 pCi/ml for sodium-22.

3.10.3.2   Tritium Mitigation (WBS 130.02.03.10)

Tritiated water molecules (e.g. HTO) are highly mobile, especially in humid air, and can create significant concentrations in drain waters that are then collected in the pumping processes that keep the beam line areas dry. These basic processes, namely tritium production and migration, show that strategies to avoid unnecessary effluent will rely on isolating the materials in which the tritium is produced from water, and in the dehumidification of air in contact with these materials, together with subsequent collection and evaporation of the tritiated condensate. Additionally,

1. There will be barrier material installed between the decay pipe concrete and the soil that is largely impervious to water. In this way the decay pipe concrete (in which tritium is created during operations) will be held at a low saturation. Numerical studies using the NuMI system indicate that if shielding concrete is unsaturated, the mobility of created tritium is low [33].

2. The profile of the decay pipe shielding is such that water collection from the surrounding soil is facilitated. The lowest point of the system and its corresponding drain piping are easily accessed from Absorber Hall. This makes the operational design of a sampling and monitoring program straightforward, and allows for maintenance of the drainage system.

3.10.3.3   RAW Systems

The cooling water for the baffle, target, horns and the absorber will be highly activated after a short time of operation. The prompt dose rates from the RAW (RadioActive Water) skids belonging to these devices will be high and in addition to the short lived radionuclides, large concentrations of the tritium will build up in these systems. Shielding and cool-down times will be used to reduce the dose from these systems. Automated top off and top up with fresh water will be used to keep the tritium concentrations at manageable levels. Alarms and containment systems will be used to prevent spills and contamination of the soil and surface waters. Water from these systems will be disposed of as low level radioactive waste.

3.10.3.4   Activated Air

High levels of radioactive air will be produced in the target chase, decay pipe and Absorber Hall. The air to the chase and decay pipe is part of a closed, isolated loop. The two separate streams of air that feed the target chase and the decay pipe (Section 3.6) combine on return and then are routed to the air handling room. In the air handling room, this air is chilled and dehumidified before returning to the decay pipe and the target chase. The air handling

room structure and the doors are designed to be air-tight. A few percent of the target chase air leaks into the Target Hall, where it is combined with the Absorber Hall air, dehumidified and sent to the NuMI air exhaust stack EAV2. The transit time from LBNE Target Hall to EAV2 is several hours, which is sufficient time to allow the airborne radionuclides to decay by several orders of magnitude. The current laboratory radioactive air emissions permit allows the annual exposure of a member of public offsite to the radioactive air emissions, from all sources to be less than 0.1 mrem. It is the goal of the LBNE design is have the air emissions to contribute to less than 30%-50% of this limit which allows for the emissions from other accelerators and beam lines at the laboratory.

3.10.3.5   Outside Prompt Dose

There are two ways where the prompt dose rates may reach outside the facility: (1) direct attenuated radiation outside the shielding and (2) skyshine, which is radiation, primarily neutrons, due to back scattering from air. FRCM Article 1104 [29] describes the regulatory requirements/limits regarding the maximum annual allowable dose to the public. The LBNE primary beam transport line, Target Hall and the decay pipe can contribute to outdoor doses. Based on the latest MARS calculations [34,35] both the annual direct and skyshine doses are calculated for both offsite and onsite locations. Direct accidental muon dose at the apex of the transport line is also included in the offsite dose.

3.10.3.6   Offsite Dose

To allow operations of other experiments, beam-lines and accelerators, the offsite goal for LBNE is set at 1±1 mrem in a year, from all radiation sources generated by this beam-line. The total offsite dose, at the nearest site boundary, due to both direct and skyshine is estimated to be 1.03 mrem in a year.

3.10.3.7   Onsite Dose

Wilson Hall is the publicly occupied building closest to the LBNE beamline. Both the maximum direct and skyshine annual dose to the occupants of the Wilson Hall has been calculated.The total annual dose, at Wilson Hall, due to both direct and skyshine is estimated to be 0.06 mrem. Doses for other locations onsite, further away, will be less.

3.10.3.8 Residual Radiation

Based on the past experience and the difficulty of component replacement with the steep grades (∼10%) of the LBNE primary beam enclosures, the beam loss and beam control devices would be employed to keep the residual radiation inside the beam line to no more than 50 mrem/hr on contact. This allows for repair or replacement of the beam line elements with little programmatic impact and keeping the dose to the workers ALARA.

There are other beam line devices, such as targets, horns, cooling panels or modules that are exposed to high levels of beam sprays and are expected to become highly radioactive. These devices may need to be repaired or replaced. The shielding of the work/repair cell used for these devices is designed such that for a 1000 R/hr object, the dose rate outside the cell is less than 1 mrem/hr. The shielding of the containers used for the over the road transport of such devices will be such that the dose rate outside the containers is less than 100 mrem/hr at one foot.

3.11 Remote Handling Equipment (WBS 130.02.03.11)

3.11.1 Introduction

Technical components installed in the Target Hall areas are subjected to intense radiation from the primary or secondary beam. The level of irradiation in some LBNE environments will reach levels that are unprecedented at Fermilab. These radiation levels will be too high for workers near such components. The failure of some of the technical components (such as target or horns) is likely over the lifetime of the LBNE experiment. Therefore remotely operated removal and handling systems are an integral part of the Target Hall design. Because the remote handling systems are integrated into the infrastructure of the Target Hall and cannot be upgraded after irradiating the Target Hall areas, they must be designed to be sufficient for 2.3-MW beam power.

3.11.2 Design Considerations

Components to be handled, serviced and/or stored range in size (from 0.20 m^3 to 26 m^3), range in weight (from 10 kg to 30,000 kg) and range in estimated dose rate (from 5 R/hr to 8,000 R/hr on contact), as described in the Remote Handling Component Lists [36]. Shielding requirements for work cells and storage areas have been determined to be 3 ft of concrete or 11 in of steel to reduce dose rates to workers to below 5 mrem/hr at 1 ft. Storage and work cell areas must have redundant sump systems with emergency back-up power systems to mitigate contamination of in-flow water by radioactive particulate from serviced and/or

stored components. Steel casks used to transport radioactive components will be sized to reduce dose rates to workers to below 5 mrem/hr at 1 ft where possible (limited by the crane capacity of 50 tons). Where not possible, it is expected that casks should be of sufficient thickness (4-in wall thickness) to allow brief hands-on access by radiation workers (300-500 mrem/hr at 1 ft maximum).

The design is based upon a conceptual design study performed by the Remote Systems Group at Oak Ridge National Laboratory. The final report of this study is available [37]. The results of that study are reflected in the following sections.

3.11.3   Reference Design

The LBNE remote-systems reference design includes equipment and systems in three functional locations. These are the Target Hall, the Target Service Building at LBNE 20 and the underground Absorber Hall. Along with shielded, remote-capable work areas, each of these three locations will have the variety of equipment, lifting fixtures and vision systems (cameras, lead glass, etc.) required to carry out needed operations. In addition, due to the current prediction of target lifetime (Section 3.3), a specialized, efficient system to replace the target in situ is specifically addressed in the reference design.

3.11.3.1   Target Hall Remote-Handling Facilities

The Target Hall contains the components for generating neutrinos and focusing them toward the near and far detectors. The beamline component arrangement is shown in Figure 3–46. The remote handling of components in the Target Hall chase will be accomplished with long-reach tools, a bridge crane and a shielded work cell. The high levels of radioactivity within the Target Hall while running beam restricts access to facility shut downs after a short cool-down period. The conceptual design closely resembles the layout for the NuMI Target Hall. Since this layout eliminates the possibility for personnel to access any portion of the Target Hall during facility operation, it will require a separate maintenance cell located adjacent to the Target Hall at the morgue and laydown area as shown in Figure 3–47. The Target Hall work cell would be used primarily for horn maintenance, but provisions could be included for removal of targets from Horn 1 should the in-chase target-removal operation encounter problems. The target-replacement concept is treated separately.

The main hallway for transport of equipment shielding, and components is located at the downstream portion of the Target Hall and connects to the Target Service Building (floors of both Target Hall and Morgue/Maintenance areas of the Service Building are at the same elevation). It is through this hallway that radioactive components must pass to get from the Target Hall to the maintenance and morgue (short-term storage) areas. Since most of the Target Service Building is planned to be occupiable with beam on, a thick shield door/plug
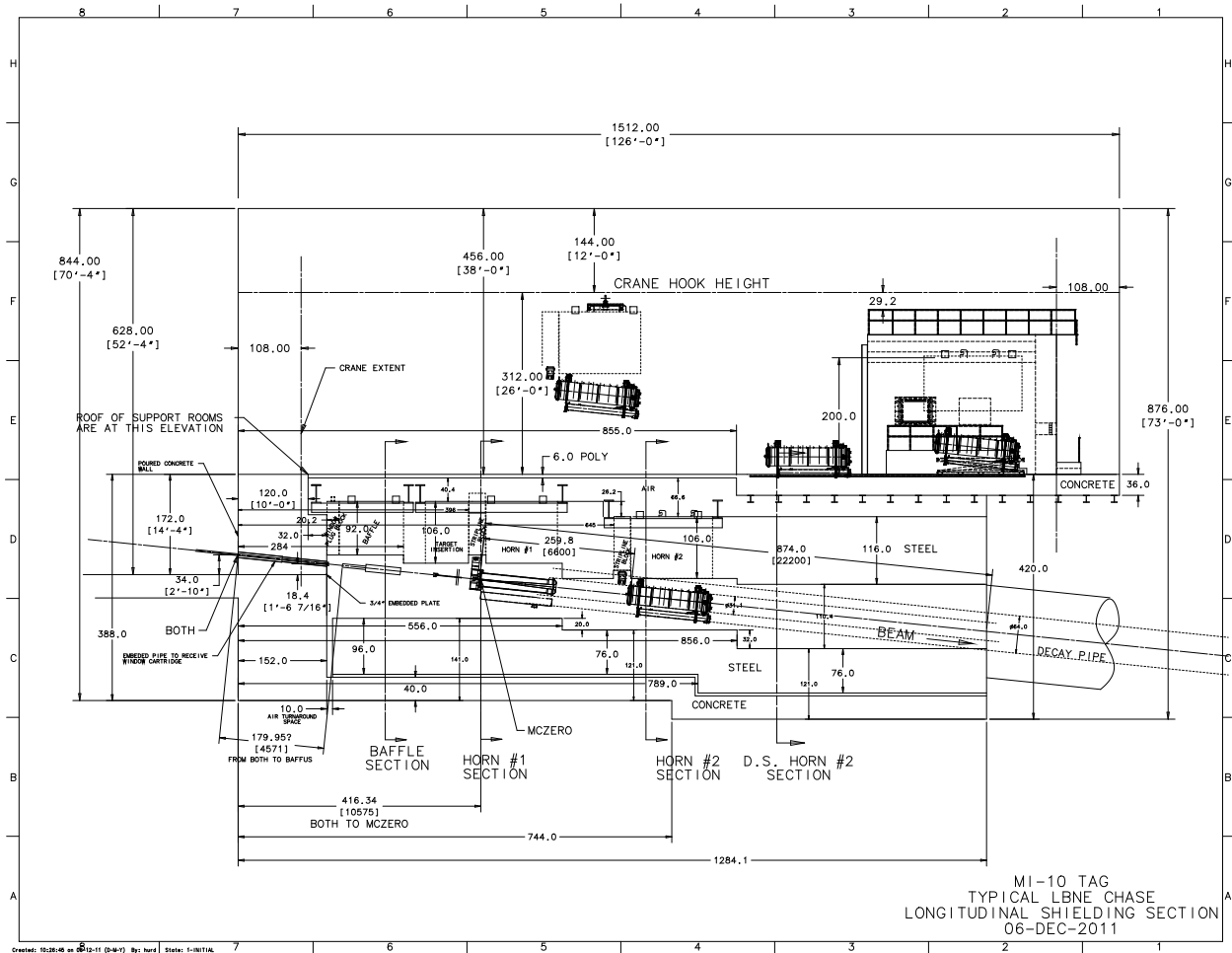
Figure 3–46: LBNE beamline elevation section
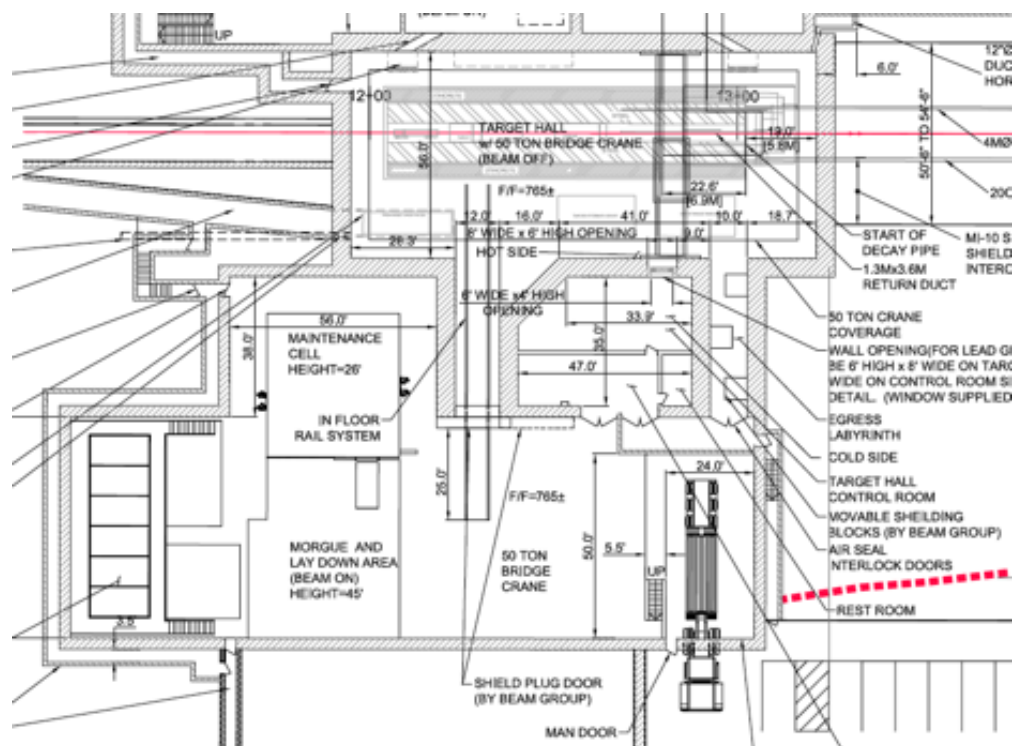
Figure 3–47: Target Service Building Plan View

must be provided to shield the Service side from the Target Hall side. In addition, the air volume of the Target Hall and the air volume of the Target Service Building must be separated to avoid radioactive-air contamination of the Target Service Building. The shield door/plug will incorporate an air seal to achieve this air-volume separation. This Target Hall shield door is included in the scope of the remote systems WBS and is discussed further in the Target Service Building design description.

The Target Hall remote operations plan incorporates two hot storage racks in the Target Hall, designed to provide short- or long-term storage for Horn Module "T-blocks" during component replacement activities and of a failed horn along with its attached module. The hot storage can also provide temporary storage of other components that the Target Service Building cannot accept at the time of removal from the chase. The hot-storage rack is configured as a pit with carriage mounts similar to the carriage mounts that exist in the chase. It is located in the Target Hall floor next to the decay pipe with a removable shielding cover. Space for two pits is recommended so that temporary storage is still available should one of the pits be filled with a failed horn module too large to be stored in the Target Service Building. The hot-storage rack pit depth will allow storage of the tallest module with component attached. One should note that without the hot storage, there is no place to store a failed module outside of the work cell.

It is assumed that Target Service Building storage cannot accommodate a failed horn module.
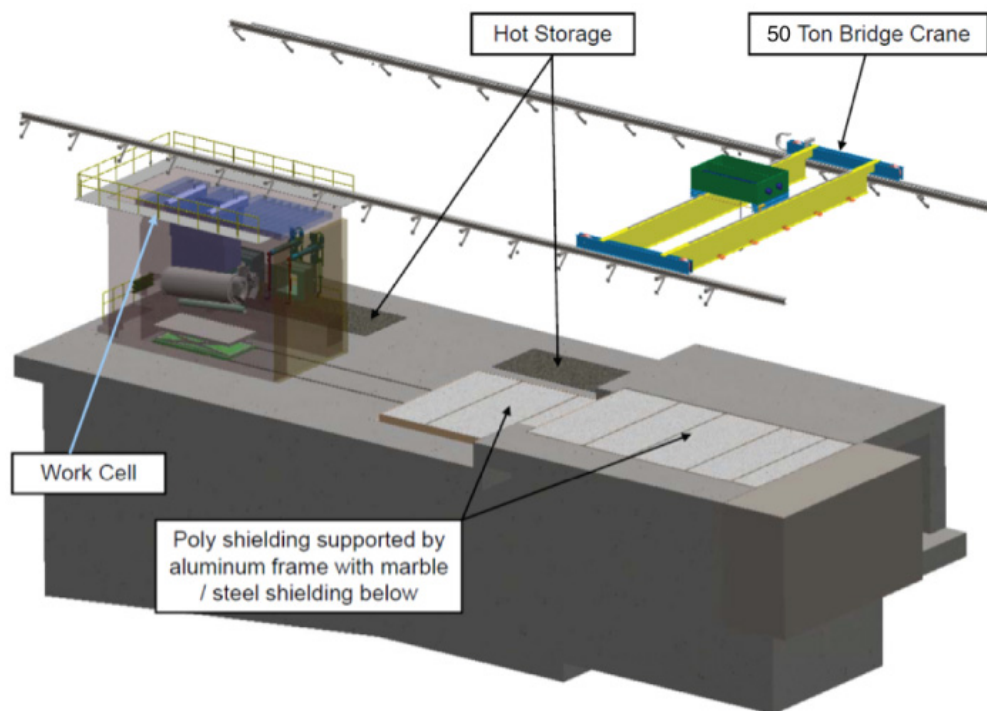
Figure 3–48: Target Hall with work cell using long-reach tools for remote handling

As these items are relatively simple and have no active pieces, they are assumed to be life-of-facility items. However, provisions should be made to provide long-term storage for at least one horn module, and a logical place for this storage is in the Target Hall. The storage could be used for a failed horn module or the temporary storage of a module with an attached horn.

The work cell and hot-storage rack are located at the downstream end of the Target Hall over the upstream end of the decay pipe. This maximizes the crane hook height available for handling tall components, such as the horns. The work cell is primarily used to remotely remove a failed horn from an activated module and attach a new horn. The rest of the remote handling is expected to be completed in the Target Service Building, with the exception of the target, which is intended to be replaced in the chase.

The chase is covered with shielding composed of steel, marble and borated polyethylene. The borated polyethylene functions as a neutron shield. The marble functions as a residual radiation shield to help reduce the dose to workers during beam-off access. The space between the chase and the work cell will be used as set-down space for equipment and shielding. This space is sized to hold all the shield blocks removed to access any component. The replacement of a horn or target is likely to require the greatest number of shield blocks to be removed. One should note that at this point in the conceptual design, Horn 1 with the module attached is the tallest item moved during operation. The shield blocks cannot be stacked so high as to block access of the horn to the work cell. In addition, this space also has recessed rails in

the floor for a translating cart that rolls out of the work cell. It is not expected that shield blocks from the chase will be occupying the set-down space while the cart needs to be rolled out of the work cell, but if this situation arises, additional set-down space is available over the hot storage pits.

Support systems for the Target Hall remote handling operations (video monitoring, bridge crane and remote handling control room) are well understood and should remain consistent as the preliminary design of the Target Hall develops. See Figure 3–49.
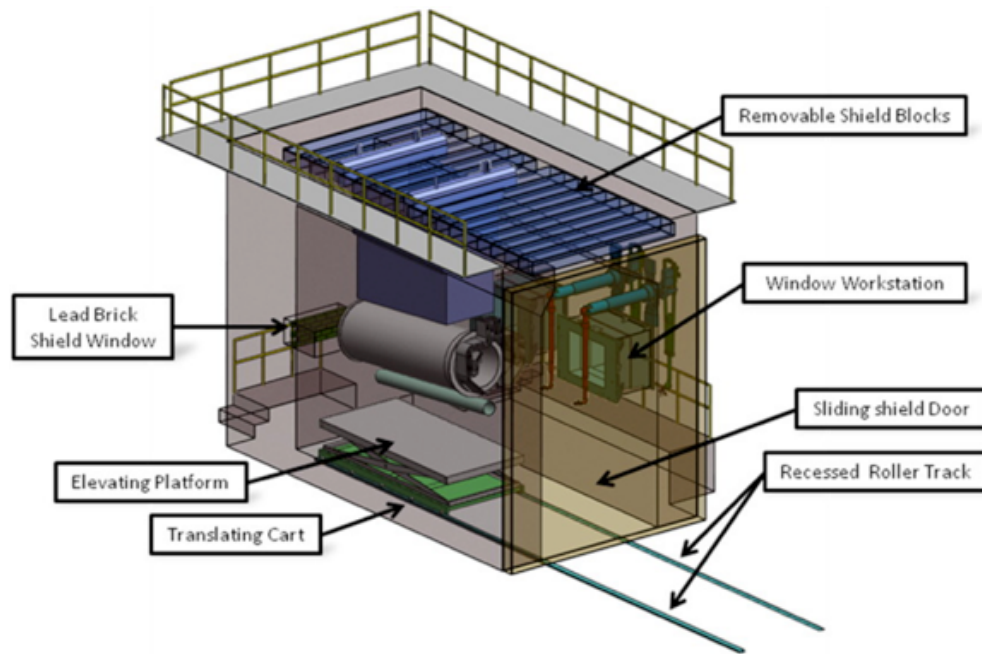
Figure 3–49: Target Hall work cell conceptual design

Similar to the NuMI work cell design, the Target Hall work cell conceptual design uses three shield walls fit together into a "U"-shape with a sliding shield door on the side facing the upstream end of the Target Hall. The door allows a horn module with horn attached to enter into the cell. The sliding shield door is fabricated from steel with a thickness of 11 in. The door translates using a v-groove track and multiple v-groove rollers along with an additional set of rollers at the top of the door to prevent door tipping. The shield door is moved by a power screw driven by an electric motor located outside the cell, which is similar to what has proven successful with NuMI. Proper controls must be added to allow the shield door to be remotely operated via the control room. The top of the work cell is covered with removable shield blocks that fit around the top of the module. The design of this cell minimizes construction cost while maintaining all required capability for completing a horn replacement operation as well as supplying a backup location for target replacements should the in-chase replacement fail. This cell is approximately 28-ft long, 15-ft wide and 20-ft tall (excluding the personnel safety railing). On the bottom of the cell is a translating cart. The cart rails extend out of the cell under the shield door, allowing the cart to roll out

from under the removable shield blocks where the bridge crane can access. Failed horns are removed from the cart and transported using the bridge crane to a shield cask, and a new horn is placed onto the translating cart to slide under the module for installation.

The work cell also features one lead glass window and telemanipulator station (2 manipulators). This station allows for repair of components and modules. It will be the only facility for repairing radioactive modules in the entire Fermilab site. The station is also envisioned to be necessary to exchange targets should there be problems with the in-chase replacement procedure. A lead glass block window, similar to that in the NuMI work cell, will be utilized in the downstream wall to allow alignment activities (also similar to NuMI) as needed.

Before the horn replacement operation begins, the new horn and top-loading shield cask must be placed in the Target Hall, and the floor in front of the cell is covered with vinyl-clad fabric or similar material to contain potential contamination. With the floor protected, the shield cask is placed on the vinyl to the side of the recessed tracks. The top loading shield cask is designed to provide maximum shielding while maintaining a total loaded weight under 50 tons, the capacity of the Target Service Building and Target Hall bridge cranes. The top loading shield cask comprises a shield container and shield lid. The shield lid is removed and placed next to the shield container.

With the cell prepared, the module with failed horn attached can be removed from the chase. The borated polyethylene shielding about the failed horn is removed. The utilities connected to the failed horn are disconnected by hand or using long-reach tools. The marble and steel module shielding are remotely removed from the module. Multiple top shield blocks are removed from the cell using the bridge crane. Then the sliding shield door is remotely opened from the control room. The bridge crane remotely lifts the module and horn and transports them to the cell, placing the module on alignment feet located on corbels inside the cell. The marble and steel shielding are returned to the module inside the cell. Then top shielding can be placed around the module, the shield door is closed and the shielding above the chase is returned.

After all the shielding is properly returned, personnel access to the Target Hall can be granted, and the failed horn can be removed from the module. This is accomplished by locating the translating cart under the failed horn in the cell and then elevating the platform until the horn's weight is fully supported. Using a long-reach tool through openings in the shielding, the connections between the failed horn and module are released, similar what has proven successful with NuMI. With the horn disconnected from the module, the elevating platform is lowered. With personnel out of the Target Hall, the sliding shield door is remotely opened and the translating cart is rolled out with the failed horn on the elevating platform. The bridge crane is used to pick up the failed horn and place it into the shield cask, and the shield cask is capped with the shield lid.

The replacement horn is transported onto the elevating platform on the translating cart. The translating cart is remotely rolled back into the cell and the sliding shield door is closed.

The shield cask with the failed horn can be transported to the Target Service Building by rolling on rails through the connection hallway in preparation to place the failed horn in the morgue. With the failed horn out of the Target Hall, personnel can safely access the work cell and use long-reach tools to connect the replacement horn to the module. The module and replacement horn are now ready to be returned to the chase and personnel must leave the Target Hall. The shielding above the chase and work cell are removed along with the marble and steel shielding in the module. Then the sliding shield door is opened. The bridge crane transports the module with replacement horn to the chase, and the marble and steel shielding can be returned.

The cell's removable shield blocks are then returned, and the shield door is shut. With all the shielding in place, personnel access is allowed. The technicians can enter the Target Hall and connect the horn utilities by hand or using a long-reach tool. Once the utilities are connected, the horn's alignment can be checked and adjusted if needed. Then the borated polyethylene shielding above the horn can be returned. With all the shielding in place and the horn functioning properly, the facility can return to operation.

The work cell conceptual design provides a basic method for horn replacement while also providing a backup for target replacement if the in-chase system fails. This concept is not capable of quickly replacing the horn or target if the situation arises. However, this concept's minimal size and limited use of expensive equipment results in a very cost-effective solution.

The specifications for a remotely operated crane can be driven by either regulatory requirements or operational or mission requirements. Facility safety assessments will determine issues such as whether airborne contaminants are a concern if a crane failure were to occur, or whether significant radiation exposures to personnel or the public could result. These types of situations might cause the crane to be considered to be a Credited Engineered Control, which would impose higher design and operational standards. If that type of environment or risk is not applicable, then operational or mission requirements could also impose these higher crane standards. This would be the case if the risk to the Project were such that if a load was dropped or a crane failure occurred with a suspended radioactive load, then the consequences would be extremely severe in terms of personnel safety or recovery time and expense.

In general, cranes used in radiation environments have features that are driven by requirements in one or more of these areas:

1. Being able to support and hold a load during and after a defined seismic event

2. Having dual load paths and redundant mechanisms to ensure loads cannot fall

3. Having features that allow recovery from a crane failure by being able to manually lower a load and move the crane to a safe area for repair

Table 3–11: Target Hall crane characteristics.

Feature	Value or Description
Capacity	50 tons in a true vertical lift configuration
Lift	50 ft
Speed	Creep modes for all axes of travel
Reeving	Double reeved, single-failure-proof with provisions to prevent "two-blocking"
Radiation Environment	Total Absorbed Dose: 10^4 rads - Maximum Dose Rate: 10^2 rads/hr
Hook Rotate Capability	Continuous
Hook	Supported by two independent drive systems
Auxiliary Hoist	5T capacity, 50ft lift, no powered hook rotate
Brakes	Shall restrain all loads without slip or overtravel
Electronics	All electronics, including axis drive amplifiers, control circuits, and memory devices shall be located outside the Target Hall
Load Sensing with Overload Alarm/Interlock	Capability required
Cable Slack Detector	Capability required
Video Cameras (by Others)	Mounts and cable accommodation required
Lights (by Crane Vendor)	Mounted on bridges
Variable-speed Control	Local pendant and wired remote from control room
Recoverability Features	Custom redundant drives and/or manual winch for bridge recovery

For LBNE, the use of the crane to lift a radioactive load will occur only after facility start-up has begun. After that point, crane usage will be intermittent, with potentially weeks or months between uses. With that type of usage, the probability of a seismic event occurring while holding a load becomes extremely small, so from this standpoint a fail-proof (ASME NOG-1) crane is not considered necessary. However, when dealing with unshielded radioactive loads, the incorporation of redundant emergency drive systems is desired to enable putting unshielded radioactive loads in a safe condition in the case of a crane drive failure. In addition, some custom provisions to prevent "two-blocking" and removing the crane electronics from the Target Hall (to avoid exposure to beam-on conditions) are recommended. These features and other crane specifications are listed in Table 3–11.

As a means of increasing facility efficiency and overall availability, it is recommended that a control room be set up in the personnel-accessible area adjacent to the Target Hall. The control room will provide operators an environment conducive to carrying out all remote operations required in the Target Hall. In addition, during beam-on operations, it could provide system monitoring functions if desired.

The size and shape of the remote handling control room is dependent upon the facility in which it is located, although an approximate footprint is 20 ft × 20 ft. It is recommended that the control room have a raised panel floor and adjustable lighting suitable for computer rooms.

With no personnel allowed in the Target Hall during most of the maintenance operations, a remote viewing system is essential. Rather than set up a portable system for each operation, the facility should be designed with this capability incorporated. The system would consist of a video control center located in the remote handling control room that can be accessed with the beam on. The system would allow remote operation of cameras and allow the display of any camera image on one or multiple video monitors. Recording of video images is an additional capability that can be considered for archival purposes or to serve as training aids.

CCD cameras have a limited radiation tolerance, approximately 10^3 rads total integrated energy, and if it weren't for the neutron radiation could potentially be left in the Target Hall during beam-on. However, the neutron exposure would render the cameras inoperable, so during remote operation, the cameras will be removed from the Target Hall and placed in a protected area. Given the relatively low background radiation levels expected in the Target Hall during maintenance operations, the high cost (>\$60,000 each) of radiation hardened tube cameras is not justified, so the CCD cameras will be considered disposable.

Having audio feedback is beneficial to operators performing remote operations, so a minimal audio system is also recommended and is part of the reference design. If communication is required between the control room and the Target Hall during beam-off or construction operations, an operator communications capability can also be included.

3.11.3.2   Target Service Building Remote Handling Facilities

The Morgue and Maintenance area of the Target Service Building at LBNE 20 is an area for short-term storage of spent components. In addition, it will serve as a maintenance area for in-beam components. These facilities are described in this section from the perspective of remote handling activities and equipment that will occupy this area. The building, including the cast-in-place concrete shielding for the morgue and maintenance cell, will be provided by Conventional Facilities (see Volume 5 of this CDR for construction details).

The Target Service Building will be constructed with thick concrete walls sized to reduce the dose rate external to the building (i.e., the residual dose rate from radioactive components being serviced/stored inside) to acceptable limits. Some pertinent characteristics of this facility include:

- Integrated truck bay for surface-level loading/unloading

- Overhead bridge crane accessing both a truck bay and morgue/maintneance areas

- Shielded storage and repair areas for activated components, referred to as the morgue

- Maintenance cell to allow repair or reconfiguration of window, baffle, target and horn components (not activated modules)

Figure 3–47 provides a plan view of the proposed Target Service Building at LBNE-20. It is a dual-level facility with a ground-level truck bay of approximately 1,500 ft^{2}and an elevated morgue maintenance level of approximately 14,000 ft^2. From a radiation protection perspective, the truck bay is expected to be open access for personnel, while the morgue will be limited access. Each level is covered with the same 50-ton overhead bridge crane. The Target Hall is connected through a large hallway and a labyrinth at the upstream end. As the Target Hall ventilation system must be separated from the Target Service Building, a sealed shield door/plug in this connection hallway is required during beam-on operations. A control room is provided in the service room areas to allow personnel a shielded location from which to control the morgue and Target Hall cranes during remote operations.

It is assumed that the morgue will be a radiation buffer area, which requires that radiation levels in personnel-accessible areas are less than 5 mR/hr. A calculation was made by Fermilab to determine the thickness required to reduce the radiation from an assumed unshielded dose rate of 1,100 R/hr to a shielded rate of 5 mR/hr. The result showed that 3 ft of concrete or 11 in of steel will be needed between the component and personnel in the facility or to the exterior of the building, if the morgue were constructed above ground. For the below-ground morgue concept, exterior wall thicknesses will be determined by civil construction rather than radiation protection requirements.

Groundwater activation is not a concern for components being handled at the Target Service Building because they will not have enough energy to activate the water. However, surface water contamination due to collection of activated dust and loose particles in a flood scenario will be a concern, and the morgue level will require a redundant sump system and back-up power generator.

The Target Service Building concept was configured to provide two years of storage space of spent components with the expectation that radioactive components could be moved to another longer term storage location during that time. If the morgue storage requirements increase (due to shorter than assumed component lifetimes), the building could be expanded to allow for more storage capacity in the future. The expected storage requirements for the morgue is shown in Table 3–12 Shielding requirements will be provided by estimated residual activity which will be based on 2.3-MW operations.

Because the horns are the largest components (with Horn 2 being somewhat larger than Horn 1), side-load storage cells were designed to accommodate one Horn 2. For the two-year storage space requirement, a total of six cells were allocated to the facility concept. It should

Table 3–12: Morgue storage requirements.

Component	Replacement Frequency at 708 kW, #/yr	Storage Quantity at 708 kW, 2 yrs	Replacement Frequency at 2.3 MW, #/yr	Storage Quantity at 2.3 MW, 10 yrs
Proton Window	0.2	0.4	0.5	5
Baffle	0.2	0.4	0.5	5
Target	1.5	3	5	25
Horn 1	0.5	1	0.5	5
Horn 2	0.5	1	0.5	5

be noted that the smaller size of baffles, windows, and targets may allow storage of multiple small components in a single cell. This will increase the storage capacity of the Morgue.

Spent components would be transported from the Target Hall to the Morgue/Maintenance area of the Target Service Building in a shielded steel transport cask. The cask thickness would be determined by crane capacity in the Target Service Building (50 ton) rather than the thickness required to reduce dose rates to a level that allows long-term direct human contact with the container. For horns, an estimated cask thickness is 4 in. Because hands-on contact may be limited, the casks must be able to be remotely loaded and unloaded. The casks and morgue cells will be side loaded, enabling the radioactive component to be transferred from one to the other largely under shielding. For NuMI and NOvA components, a system that achieves this has been already designed and used in operation.

Figure 3–50 shows a picture of the morgue/cask transfer system in place at C-0 Remote Handling Facility. The component in the cask is supported by a rolling cart and pushed/pulled by a serapid chain mechanism mounted to the back of the cask. Temporary shielding is set around the gap between the cask and the morgue when the morgue and cask doors are removed.

The cask and morgue doors are designed to be remotely operated using the building crane, as is the temporary shielding. The area above the morgue cells may be used for storage or for storage cell upgrade (to provide an additional 6 cells in a second layer). The above floor design reduces the possibility of water contamination issues due to flooding.

To separate the air volumes of the Target Hall and the Target Service Building, a Target Hall connecting hallway shield door/plug and air seal must be constructed. The door is expected to consist of a steel or concrete plug mounted on rails to allow motorized movement. The exterior side of the door/plug will be lined with galvanized steel sheet to form the air barrier The air seal at the edges of this barrier is conceived to be either double O-rings with toggle clamps or a double inflatable air diaphragm with passive clamps. An air monitoring station to monitor the air activation on the Target Hall side of the door will provide information needed prior to granting removal of the cover.

Figure 3–50: Photo of cask-to-morgue cell transfer system used at C-0 Remote Handling Facility

The conceptual design of the Target Service Building includes a shielded maintenance cell. The primary purposes of this cell are to exchange spent targets from the target handler (see section 3.11.3.4) and allow repair/autopsy of failed components. All module maintenance will be performed in the Target Hall work cell.

The maintenance cell is shown in Figure 3–51 as an alcove protruding from the morgue area of the facility. This layout provided maximum usable floor space in the main area of the morgue. It is equipped with an in-cell overhead bridge crane and multiple workstations. A remotely operated sliding door allows unattended equipment access to the cell via a rail system similar to that of the Target Hall work cell and morgue cells. The maintenance cell will allow both remote and hands-on operations to be performed, assuming radiation levels permit entry. Local shielding is provided by reconfigurable recycled steel blocks.

The maintenance cell was positioned such that the sliding door is at the extent of the morgue crane coverage to allow straightforward installation of this door. Because of the desire to minimize overall facility height, there is no section of the maintenance cell that provides overlapping crane coverage. Because of this, a powered cart is provided that translates components into and out of the cell. Or the same chain mechanism utilized by the casks to morgue transfer may be used here as well. This arrangement will also make installation of the in-cell crane more difficult as well as its removal should off-site repairs be required.
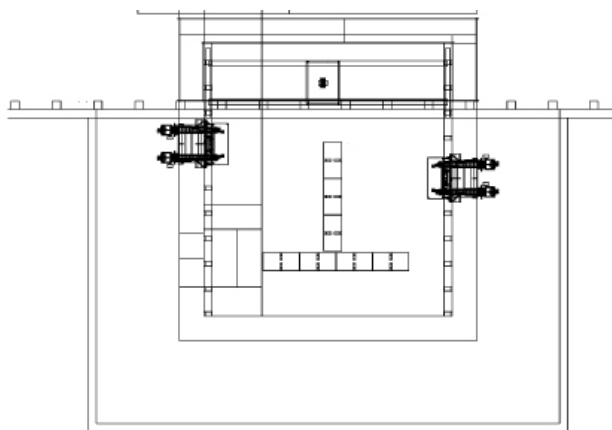
Figure 3–51: Target Service Building maintenance cell layout

There will be two separate cranes in the Target Service Building at LBNE-20: one each in the truck bay and the morgue (50 tons) and one in the maintenance cell (15 tons). The truck bay/morgue crane will provide similar functionality as the Target Hall crane, being used to remotely lift items coming from the Target Hall connection hallway and transport them into the maintenance cell for repair or dismantlement. It will also allow items to be remotely placed into the morgue storage area after cask transfer operations are performed outside the maintenance cell. However, unlike the Target Hall crane, the vast majority of radioactive component lifts will be done in a shielded configuration (side-load casks) that will allow at least brief hands-on access to the crane for recovery purposes. Therefore it should

be specified like the Target Hall crane, but without the recovery features (redundant drives). In addition, neutron radiation will not be an issue in the morgue, so the electronics on the morgue crane can be installed on the crane itself rather than in a remote location.

The crane for the maintenance cell will also be used for lifting activated, unshielded components on an infrequent basis. As with the morgue crane, radiation dose should not be a cost driver on this crane because the cell will not be used for long-term storage of activated components. The maintenance cell crane should have some recoverability features in case a failure occurs, but single-failure-proof design is not required. Since it will be remotely operated via pendant outside the cell, variable-speed functionality will be required along with hook rotate. On-board remote viewing will be needed because much of the cell will not be visible from the viewing windows.

Although most operations in the morgue area of the Target Service Building will be shielded, due to crane capacity limitations and gaps, the shielding may not be adequate to enable long hands-on access. Therfore it will be necessary to remotely operate the crane. A Target Service Building control room is recommended, which would provide operators a designated room with remote viewing capabilities along with crane control. This control room is located in the truck bay of the Target Service Building both for its convenience in personnel accessibility and its proximity to the end of the morgue area crane rails, which should simplify the required cabling. A shield window will be installed that allows direct viewing of the Target Hall and into the connecting hallway.

The Target Service Building video system will be similar to the Target Hall video system in that the morgue area crane bridge and storage area walls will be outfitted with cameras adequate to allow remote transport of items from the Target Hall to either the maintenance cell or the morgue storage area. As was the case in the Target Hall, radiation levels will permit the use of off-the-shelf CCD cameras.

3.11.3.3   Absorber Hall Remote Handling Facilities

The Absorber Hall remote handling facilities are similar in concept to those for the Target Hall in that they will include a bridge crane, cask system and long-reach tools to enable the replacement of the hadron monitor upstream of the hadron absorber. However, unlike in the Target Hall, replacement of components will not require a work cell and all hadron monitor replacement crane operations are planned to incorporate shielding that allows for some minimal hands-on access. In addition to hadron monitors, water-cooled absorber modules and steel shielding may fail, and some provisions must be made to allow replacement. Although the absorber components are designed to last the lifetime of the facility and will include redundant water-cooling lines, the consequences of complete failure are significant. Therefore, provisions will be made in the design of the Absorber Hall components and shielding to allow future replacement. However, because of the low probability of complete failure, design and

construction of remote handling equipment for absorber modules and water-cooled shielding will not be included in the LBNE project. If complete failure occurs during operation, a long downtime (6 months to 1 year) would then be required to design, build, develop procedures and safely replace the failed component(s).

The conceptual design of the Absorber Hall is shown in Figure 3–37. The hadron monitor and the absorber modules are located under steel and concrete shielding blocks. The hadron monitor is the furthest upstream component in the absorber assembly. Directly to the beam-right of the absorber assembly is an empty, shielded pit volume called the morgue. This morgue has been designed to accept three hadron monitors or absorber modules. In order to replace a hadron monitor, first, with shielding in place, utilities to the component must be disconnected by hand at the top of the absorber pile. After disconnecting utilities, using the crane and appropriate lifting fixtures, the top layer of shielding blocks are removed as necessary to uncover the hadron monitor shielding module. Although this step can be done remotely, it is expected that dose rates will be low enough (<300 mrem/hr) to allow limited hands-on access, if necessary. Next, a special open-top cask (called a "castle") is placed over the hadron monitor module. On the side of the castle, a special cask and monitor exchange system will be installed and readied for removing the spent hadron monitor (see Figure 3–52). The hadron monitor module is then drawn upward into the castle using the crane (during this step the monitor gas and signal lines are wound into a spool located within the cask. Once the hadron monitor is level with the side cask, the monitor is pulled from the castle into the side cask using a mechanism very similar to the one currently used for the NuMI hadron monitor exchange. Then the shutter doors on the side cask and castle can be closed and the cask containing the spent hadron monitor can be moved to a storage location (the side morgue) or out of the Absorber Hall as appropriate. The new monitor is installed in the reverse order and the top layer of shielding blocks is replaced. Finally, after a system check-out procedure, utilities can be re-connected and operation can be resumed.

There are no plans within the Project to provide support for removal of radioactive items from the Absorber Hall morgue to the surface. However, nothing in the Project plan precludes doing so in the future should it be necessary. Shielded casks could be built to shield radioactive components during transport, and the Absorber Hall bridge crane could be used to load and unload those casks.

The Absorber Hall bridge crane has a very similar function as the Target Hall bridge crane. This crane is actually located in the near-surface building (LBNE-30) above the Absorber Hall itself. The use of the crane to lift a radioactive load will occur only after facility start-up has begun. After that point, crane usage will be intermittent, with potentially weeks or months between uses. With that type of usage, the probability of a seismic event occurring while holding a load becomes extremely small, so from this standpoint a NOG-1 crane is not considered necessary. In addition, because the hadron monitor exchange system incorporates shielding casks (castle) at every step, recovery systems in case of crane failure are not necessary. A standard, industrial 30 ton bridge crane (with provisions to remove electronics from the Absorber Hall during beam operation) is sufficient. In addition, since true remote
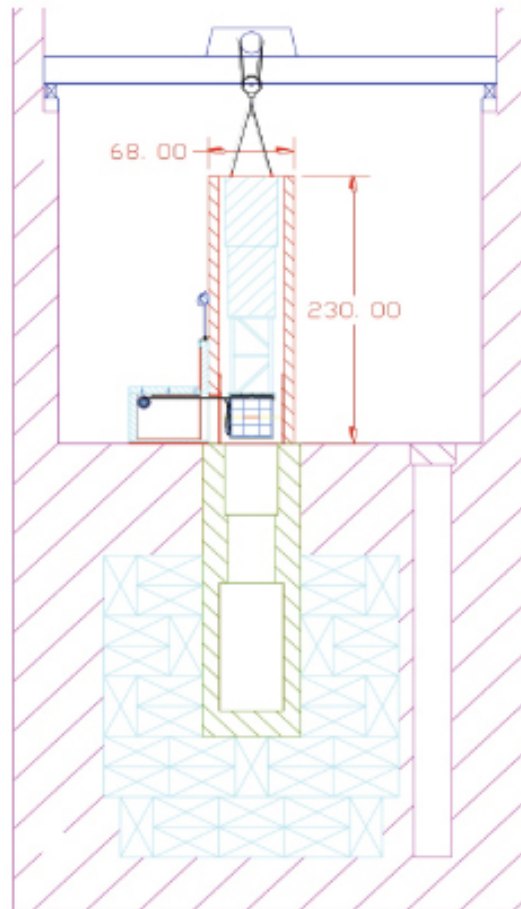
Figure 3–52: Absorber Hall beam view showing hadron-monitor replacement concept

operations using the crane are not planned for hadron monitor exchange, a control room for the Absorber Hall is not required.

The Absorber Hall video system will be a scaled down version of the Target Hall video system. Without a control room and limited remote handling needs, individual, re-locatable cameras and a portable video monitor cart similar to what NuMI uses at C-0 Remote Handling Facility and in the NuMI Target Hall should be sufficient.

3.11.3.4   Target Replacement Remote Handling System

Remote Systems equipment will primarily consist of master-slave manipulators, long-reach tools and remotely operated below-the-hook lifting fixtures. However, in order to enable rapid replacement of targets (desired due to the possible short lifetime of two to four months for targets at 2 MW beam power), a specialized system to replace the target will be designed. The system will speed replacement times by enabling extraction of the used target and insertion of the new target in situ in the target chase. This avoids the lengthy process of removing Horn 1 and its associated module and shielding in order to replace the target. This system will be stored, prepped and maintained in the Target Service Building. It is hoped that this system will enable target change-out times of less than three shifts (not including cool-down time).

Much of this portion of the CDR is based upon a conceptual design study performed by the Remote Systems Group at Oak Ridge National Laboratory. The final report of this study is referenced [38] and the applicable specifications and requirements recommended by that study are included in this section.

The target replacement remote handling system utilizes a central handling frame unit, shown in Figure 3–53. This device is lowered into the chase and roughly located (within 0.25 inch) in front of the Horn 1/target assembly by using a chase insertion frame (see Figure 3–54). When rough alignment is achieved, the handling frame uses a slide assembly and commercially available tooling mounts (pneumatically activated) to mount the target handler assembly to the Horn 1/target front mounting plate. Compliance is achieved via air-bag mounts under the slide assembly. The target handler assembly then utilizes a second slide assembly to move into position with the target mount plate and is gripped using the commercially available tooling mounts. After electrically operated wrenches release the three target mounting bolts, the target handler slide with the target attached can be extracted back into the handling frame unit (Figure 3–55). After disconnecting and retracting the alignment slide, the frame with failed target can be pulled out of the chase frame and the handling frame, and the failed target can be placed in a shielded cask for transport to the Target Service Building at LBNE-20. Using a second, identical handling frame already fitted with a new target, the process can be reversed to install the new target into Horn 1.
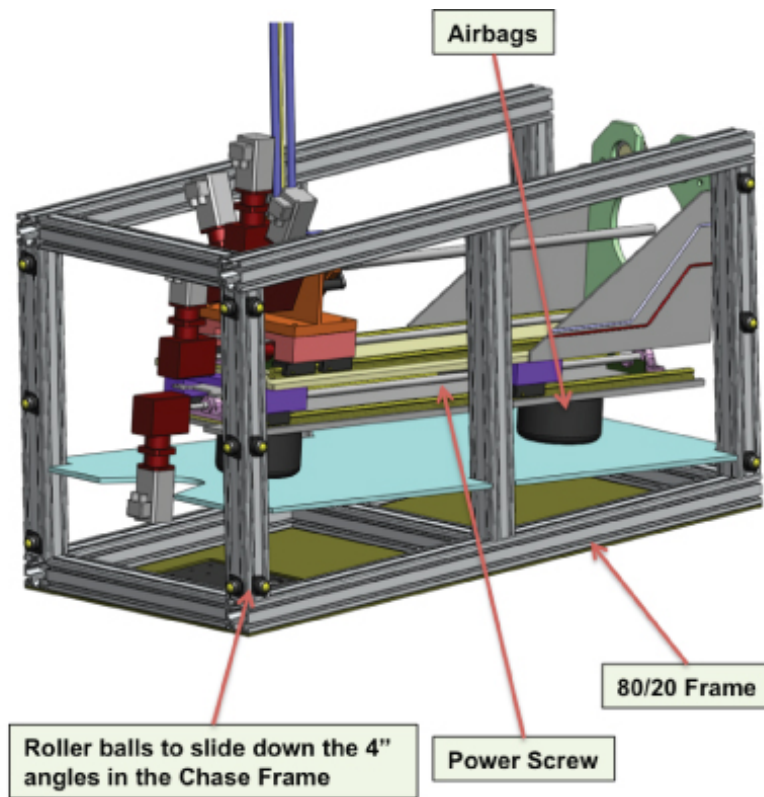
Figure 3–53: Target Handling frame concept
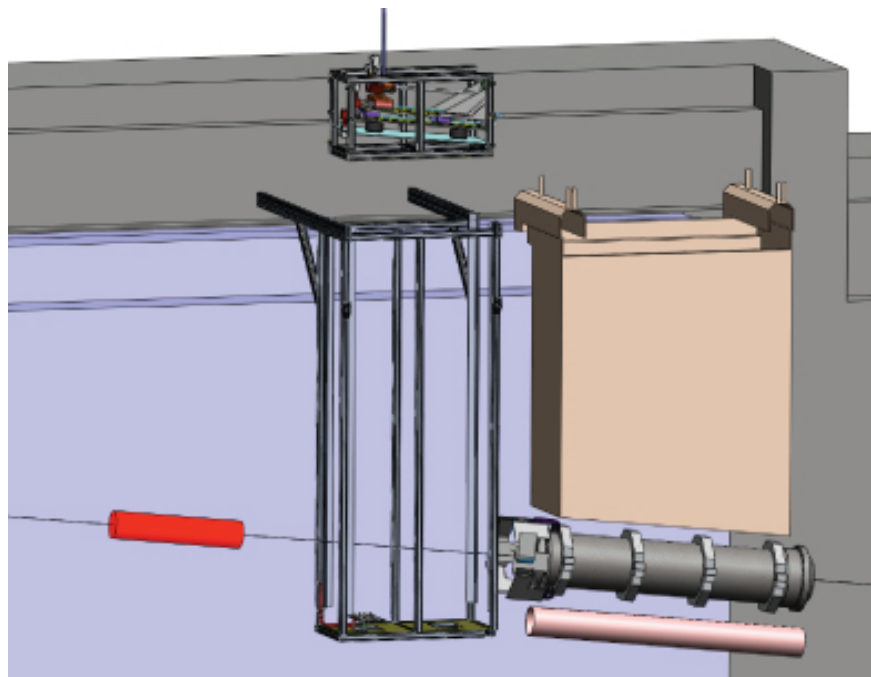
Figure 3–54: Target replacement system in the chase
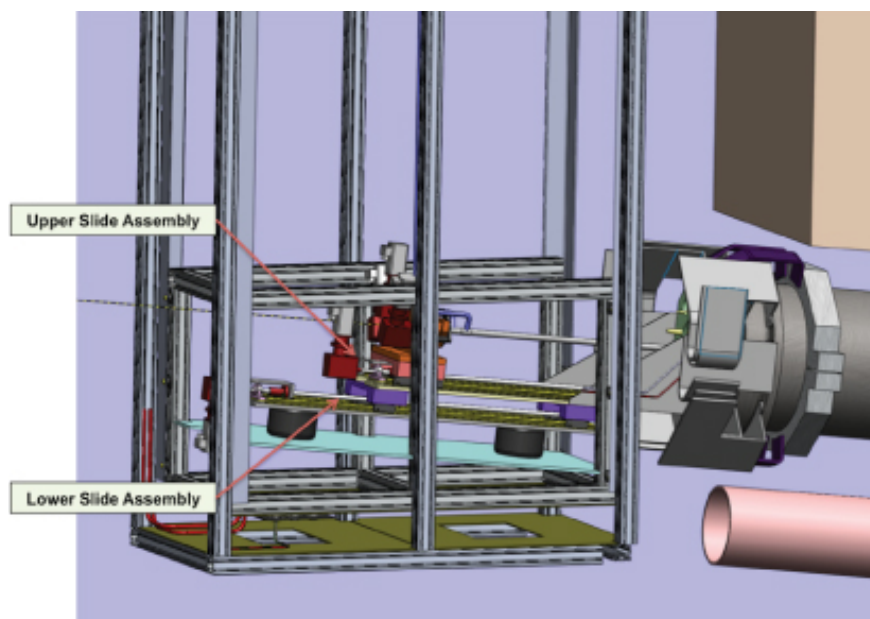
Figure 3–55: Target handling frame extracting failed target from Horn 1

This system allows the new target to be mounted into the handler frame in the Target Service Building before the access for replacement (while running beam). It can be aligned and go through dry runs of installing into a mock Horn 1 as well to ensure quick and accurate replacement activities. Likewise, the failed target can be removed from the handling frame in the Target Service Building (while running beam) and placed into the morgue storage area without interfering with beam operation.

The system will require vision systems, long-reach tools (for disconnecting utility and instrumentation lines), and quite a few mechanical sub-systems. A prototype target handling system will be built to help guide detailed design.

3.12   Modeling (WBS 130.02.03.12)

3.12.1   Introduction

This section describes the simulation of the neutrino beam and its effects on nearby materials using software models. The simulations use the MARS package, which is well documented and benchmarked [15] [39]. The MARS model of the reference design will describe the target, horns, decay pipe and absorber, as well as all of the shielding. In particular, MARS will be used for estimating:

- Beam-energy deposition in components, required for engineering considerations and estimating cooling capacities

- Prompt (beam-on) dose rates within halls outside of shields

- Residual dose rates from components within or outside shielding

- Radionuclide production in components, shielding and rock

3.12.2 Design Considerations

The level of detail in the model will follow the reference design as it evolves. The model already provides a basis for estimating the total thickness of shielding needed. Later, for example, as the block size and stacking pattern become set in the design, these details will be incorporated into the model. Thus, the effect of voids or cracks, which are small in a good design, will be studied at a later time. An estimate for the locations of excavated rock boundaries is needed for estimating tritium production and groundwater concentrations.

The composition of materials used in the MARS model needs to match that of the design materials to the known accuracy. The atomic mass fractions are usually sufficient for the simulations. Items to be modeled include rock, shielding materials and the materials incorporated into technical components. Components present in an engineering design or plan whose effect is negligible, e.g., bolts, will not be included.

3.12.3 Reference Design

A realistic MARS model has been built for the LBNE target, horns, target station and its shielding, decay pipe and tunnel shielding, and the hadron-absorber system. In the model as in the conceptual design, the proton beam is tilted down by 101 mrad, and the 25-m target station and decay channel follow this tilt while the hadron-absorber system is arranged horizontally. The hadron-absorber system includes an aluminum mask that protects the water cooling pipes, a 2.4-m long aluminum core followed by a 2.7-m long iron core surrounded massive iron shielding in a concrete shell, all in an 18-m long service building. Horn magnetic fields and all details of geometry and materials distributions are included in the model.

In the reference model, a 120-GeV proton beam hits a 0.96-m long cylindrical graphite target at an intensity of 1.6×10^{14} protons per pulse. A 60-GeV case is also being considered. We model in great detail both 708-kW and 2.3-MW normal operation (1.33-s repetition rate, 4.9×10^{13} and 1.6×10^{14} sec^{-1}, respectively) as well as an accident scenario. The latter is a 3.07-MJ beam accident ("target destroyed"), in which a proton beam interacts with 1-atm air (or helium) in the decay pipe and hits the absorber. Substantial modeling efforts are being conducted in the primary-beamline and baffle areas.

MARS is used to calculate energy deposition (peak values and total dynamic heat loads), integrated absorbed dose and residual activation in all the system components (target, horns, decay pipe, shielding, all the components of the hadron absorber, etc.), prompt-dose-equivalent distributions in and out of the service buildings, and radiation load on groundwater and air outside the shielding. These calculations will help in the design of optimal subsystems (target station, decay channel and hadron absorber) and will aid in the evaluation and minimization wherever possible of residual dose levels. They will also help optimize hands-on maintenance conditions, keep impact on the environment below the regulatory limits, and estimate and maximize wherever possible the component lifetime.

3.13   R&D Program

This section summarizes the R&D work on the components of the Neutrino Beam. There are detailed plans for ongoing and projected activities for the following areas:

- High-power target systems

- Horn systems that achieve high efficiency for focusing low-momentum pions

- Remote and automated target and horn removal and installation

As discussed in Section 3.3, at this time contract work has been funded to Rutherford Appleton Labs (UK) for target and and window designs suitable for both 708 kW and 2.3 MW operation [19], to IHEP for design work on the reference target design described in this document [20], and to Brookhaven for target-material irradiation studies. This work is expected to continue after CD-1.

4   System Integration (WBS 130.02.04)

4.1   Introduction

This chapter covers the System Integration activity of the LBNE Beamline subproject. The System Integration team's responsibilities can be broken into two major areas: first, the oversight of systems for Controls, Alignment and Interlocks, and second, coordination of interfaces between each of the systems of the Beamline subproject. The Controls, Alignment and Interlocks must function across the entire subproject and must therefore be properly supported by all the interfaces in addition to the relevant components. Interface coordination involves both achieving consensus as to the location and nature of each interface and the party responsible for it. The coordination activity must also ensure proper distribution of requirements and specifications so that all the needed components are accounted for, and that they will be constructed such that they will fit together properly during installation and operate successfully.

System Integration thus has the primary responsibility of facilitating good communication throughout the subproject in order to prevent deficiencies and scope-related problems, and for any that are introduced, to spot them early on and make sure they get corrected.

4.2   Controls (WBS 130.02.04.02)

4.2.1   Introduction

Any high-energy external beamline requires a robust control system to ensure proper operation. The control issues for a beamline like LBNE's are well understood. The control system must be able to

- reliably log data for every beam pulse (this implies a digitization with appropriate throughput)

- plot both real-time and logged data in strip-chart form and capture all operational information for the beamline devices in a database

- issue alarms for off-nominal conditions and provide power-supply controllers with ramping capability

- handle the so-called slow-control subsystems: water, vacuum and temperature

- provide environmental monitoring

- display information from the position and loss monitors along the beamline and provide an auto-tuning facility to keep the beam centered over its length without significant human intervention

The LBNE beamline consists of a large number of components, and the control system must have sufficient bandwidth to collect the necessary information from each component for each beam pulse.

The Accelerator Controls Network (ACNET) provides services for process control, monitoring, timing, save-and-restore and data logging for the Fermilab accelerator complex. Since the LBNE beamline is an extension of the accelerator complex, its control requirements will be supported via ACNET.

Given LBNE's very high beam power, 700 kW with a possible upgrade to 2.3 MW, the beam energy delivered per pulse, if misdirected, is sufficient to damage beamline components. This necessitates the use of a beam-permit system to verify a host of parameters about each beam pulse before it's extracted and to issue a "permit" if everything is in order. The beam-permit system must also be able to determine when a single bad pulse has been extracted and ensure that no further pulses are extracted until the problem is resolved. LBNE will use a system developed for NuMI that has also been used for several other Fermilab beamlines.

4.2.2   Reference Design

4.2.2.1   ACNET Controls

Controls for LBNE will be made up of standard Fermilab accelerator-control system interface and networking components. These include VME, HRM and PLC hardware with appropriate modules to provide control and monitoring of technical equipment along with commercial Ethernet switches and hubs for the networks. It should be noted that there are no plans to support the older CAMAC systems in the new LBNE areas. However, since it is unlikely that CAMAC will have been fully replaced in the MI by then, any LBNE equipment that might be installed in the MI-10/14 service buildings may be connected to ACNET via CAMAC.

ACNET services for LBNE will include connections to existing accelerator-timing systems (TCLK and MIBS from MI-8) and to the LBNE Beam-Permit System via fiber cables.

ACNET consoles provide the ability to monitor and control accelerator operations throughout the complex. This will include the LBNE beamline and technical components. While operations are typically directed via consoles in the Main Control Room remote consoles are available at a number of locations around the complex.

New controls for LBNE will be installed in seven locations (Beamline Service Building, Target Service Building, Target Hall Utility Room, Absorber Service Building, Absorber Hall, Near Detector Service Building and Near Detector Hall). LBNE user-interface displays will be configured to show the LBNE beamline as a single entity from the extraction kicker (described in Section 2.2) to LBNE target (described in Section 3.3).

4.2.2.2   Beam-Permit System

The LBNE Beam-Permit System works in two modes to prevent extraction of errant pulses that could cause damage: *current-pulse mode* to inhibit a faulty pulse from being extracted and *next-pulse mode* to prevent extraction of subsequent pulses in case of a problem.

In current-pulse mode, the beam permit system examines a few hundred parameters in the last few milliseconds before beam delivery to ensure everything is ready for the beam. All magnet power supplies are examined, and ramping to the flat-top level is checked. Beam positions of the circulating MI beam near the LBNE kicker will be examined to test the real-time orbit in the accelerator. Kicker charge level will also be checked to ensure that the desired extraction angle will be achieved. In addition, the beam-permit system will examine parameters of the MI radio frequency (RF) system to assure that the accelerating voltage is correct for nominal extraction. If anything wrong is sensed in any of the data, the kicker will be inhibited and the beam will be sent to the MI Beam Abort.

In next-pulse mode, the beam-permit system takes many measurements after a pulse has been delivered to ensure that it was delivered properly. Chief among these are measurements from the total and local loss monitors distributed along the beamline. These monitors are sensitive to losses on the order of one part in 10^4 and can sense an errant beam pulse immediately after its delivery. Other measurements are taken from the beam-position monitors near the target, which indicate the proper delivery of beam, and from an array of sensors reading out target data. In the case of an errant beam pulse, subsequent pulses are inhibited.

When the system is tripped in either mode, further delivery of the beam is inhibited until a control-room operator provides a manual reset. Repeated permit-system trips caused by beam losses escalate the authority level required to restart the beam; authority moves to beamline experts or safety personnel, depending on the circumstances.

The permit system has proven to be an excellent diagnostic for beamline and MI operations. If trips are kept at a low value, on the order of 5 to 10 per day, one can be reasonably sure that the beamline integrity is intact. After a down period, the permit system is used to check that the beamline is ready for re-establishment, and a single pulse is generally all that is required for start-up.

4.3 Radiation-Safety Interlock Systems (WBS 130.02.04.03)

4.3.1 Introduction

In this section we describe the philosophy, policies, procedures, design, fabrication, installation, checkout and commissioning for the Radiation Safety Interlock Systems (RSS), Radiation Monitors, Radiation Air Monitors, and Radiation Frisker Stations. Underlying all safety-system designs is a commitment to providing the necessary hardware, procedures, and knowledge to personnel to ensure their well-being. Inherent in each of these systems is the concept of redundancy.

The RSS systems are designed to protect personnel from exposure to particle beams. They are intended to prevent injury, serious overexposure or death from beam-on radiation, X-Rays or high-voltage/high-current power supplies. This includes the enclosure access-control interlocks, exclusion-area boundary gates, access keys and cores, emergency stop system, audio warning system, electrical-safety system, electrical-safety system interface units, the beamline critical-device-control contactors , critical-device controllers and associated interconnect cabling.

The Radiation Monitors are used to detect stray radiation during beamline operations. This includes Fermilab's "Chipmunk" radiation monitors (non-interlocked monitors so called because they emit an audible "chip" sound), multiplexing (mux) monitoring network, safety-system radiation-monitor interlock components and electronic berm components.

The Airborne Radiation Monitors are used to monitor the amount of radionuclides that are released to the environment during beam operations. This system includes the airborne-radiation monitors and the associated enclosure to house the components.

The Radiation Frisker Stations are used to survey personnel and materials being removed from the beamline, Target Hall and absorber enclosures. These include the portable and wall-mounted laboratory frisker and "wallflower" detectors and installation at the enclosure entry points.

4.3.2 Methods

The principal method employed by the interlock systems is to establish and maintain exclusion areas surrounding active accelerator areas, maintaining sufficient distance between beamline operating components and the closest point of approach. When potential exists for personnel to be within the defined exclusion area, the Radiation Safety Interlock System disables all operations that may create hazardous conditions.

Electrical-safety systems, a subset of the Radiation Safety Interlock System, have been developed to provide protection from high voltage, high current, and x-ray producing devices.

Another method is redundancy. All hardware is designed such that no single failure will result in the loss of protection. To accomplish this, two separate circuits are used to detect a given condition. For example, two separate switches monitor each door to detect its status. Each of these switches in turn is connected to a separate control circuit. Thus if one switch were to fail, the other would still operate, providing the necessary protection. An extension of the redundancy concept is used in the control of radiation-safety-system critical devices, i.e., one that prevents beam from entering an area. Two critical devices will be controlled by a single radiation-safety system.

Another key principle used in designing all safety systems, is the idea of "fail-safe" circuits. All circuits are designed in such a way that if a circuit fails, the failure would initiate a system shutdown, resulting in a safe condition. For example, if the cable that controls a device were cut, the device could not be enabled. In this way personnel are still safe. Since not all component failures can be detected by the interlock systems, functional testing in accordance with the Fermilab Radiological Control Manual (FRCM) [29] needs to be performed at periodic intervals and test results documented to ensure reliable operations.

"Search and secure," a walkthrough of an area in a predefined sequence by at least two qualified persons to ensure that the area is unoccupied, is perhaps the most important method to ensure radiation and electrical safety. This is required each time before beam or power supplies are enabled. The search sequence will be programmed into a Programmable Logic Controller (PLC) for the LBNE Radiation and Electrical-Safety systems. The order in which the interlocks are reset will be designed so as to ensure that no personnel are missed by the search team.

Once an area has been searched and secured, status displays on the outside of each access door and each section gate indicate to individuals that the area is interlocked and that access is forbidden to unauthorized personnel. Immediately before beam is brought into an area or power supplies are enabled, a prerecorded message consisting of a siren and verbal announcement will be played to allow personnel, which in the unlikely event of being missed on a search, have time to safely exit the area. Audio warning speakers will be located at approximately 125-foot increments. All doors to an area are locked and the keys to open

these doors are interlocked and guarded in the Main Control Room. Distribution of these keys is not taken lightly. Only authorized personnel are allowed access. The type of access determines the authorization level required for the individual.

4.3.3   Reference Design

The Radiation Safety Interlock Systems (RSS) for LBNE extends throughout the underground enclosures with the exception of the following areas, which are to remain accessible during LBNE beamline operations.

- LBNE Target Hall Power Supply and Utility Rooms

- LBNE Absorber Hall Access Shaft

- LBNE Below-Ground Absorber Hall Elevator Landing Area

- LBNE Absorber Sump and Pump Room and Instrumentation Room

- LBNE Near Detector Cavern and Access Shaft

Areas of exclusion during LBNE beam operations are divided into three separate areas. The primary beam enclosure is interlocked to the Booster RSS (not under LBNE control). The remaining exclusion areas, the Target Hall and absorber are interlocked to the LBNE RSS. The primary beam enclosure and Target Hall are contiguous with the decay-pipe region separating the Target Hall and absorber.

The LBNE RSS must be cleared for beam to be transmitted down the beamline. The state of the RSS is also an input to the LBNE Beam-Permit System. While not integral to the LBNE RSS, radiation "stack" monitors sample and record levels of activated air from the Pre-Target, Target Hall and absorber areas.

4.3.3.1   Critical-Device Controller

In support of LBNE operations, two critical devices will be utilized and controlled by the LBNE Critical Device Controller (CDC). This controller will be permitted when it is safe to extract MI beam into the LBNE beamline. The controller will be connected to the power supplies feeding two separate bend magnet strings, both of which are required for beam to be transported to the LBNE beamline. Should the controller detect a failure of either power supply not turning off, the controller will send a failure mode signal to the Booster RSS disabling any further beam to the MI.

4.3.3.2   Exclusion Areas

A new extraction pipe will be installed inside the MI enclosure connecting to the primary beam enclosure. The upstream section of the LBNE beamline, the beamline service building access point, LBNE 5, and the enclosure down to the upstream end of the Target Hall will be interlocked to the Booster CDC.

The Target Hall Complex will be interlocked as a separate enclosure allowing for work in the Target Hall while the upstream LBNE enclosure is interlocked in support of MI area operations.

The LBNE absorber is accessible from the LBNE 30 Service Building through the access shaft. The absorber will be interlocked as a separate enclosure.

It is expected that no more than two personnel will be required to satisfactorily search and secure areas in the domain of the LBNE RSS.

4.3.3.3   Electrical-Safety System

Electrical hazards from exposed conductors and connections will inevitably exist in the LBNE beamline from the point of extraction to the magnetic focusing horns. These hazards are typically associated with the beamline magnetic elements, introduced in Section 2.2, such as the extraction kickers, the Lambertsons, the dipole and quadrupole magnets and the focusing horns. The Electrical Safety System (ESS) extensions of the MI and LBNE RSS provide permitting inputs to associated power supplies in order to partially mitigate the hazard of exposed and otherwise unguarded conductors. The ESS connections will be available at the MI-10, LBNE 5 and Target Hall areas. Trim and correction-element conductors and connections are guarded and connection of their associated power supplies to an ESS is not necessary.

Accommodating access into the MI and LBNE is further provided by connection of selected supplies to the pulsed power feeder 96/97. This feeder is de-energized during MI access.

4.3.3.4   Radiation-Loss Monitoring

Fermilab has several radiation-monitoring devices available to detect beam losses. Although the radiation-shielding assessment has not been completed, we have identified some areas of concern. Given the shape of the beamline, one area is just downstream of the apex of the embankment. Excessive beam losses in this region could potentially lead to muons directed off-site. One of the radiation-monitoring devices, called a "Scarecrow," will be placed here. If

excessive beam losses are detected, the system will trip the LBNE Critical Device Controller (CDC) preventing further beam transport.

Non-interlocked Chipmunk monitors will be placed at various locations around the Target Hall and absorber areas to monitor for excessive radiation rates. Fermilab's MUX monitoring network will be extended into the LBNE area for recording of both interlocked and non-interlocked radiation-monitoring instruments.

4.3.3.5   Airborne-Radioactivity Monitors

Airborne Radiation Monitors are used to monitor the amount of radionuclides released to the environment during beam operations. Airborne activation results primarily from the direct interaction of primary and secondary particles with the air (or other gaseous medium). Dust, from natural erosion, wear or work on radioactive accelerator components is a secondary source, as is the emission of gaseous radioactivity from "hot" liquids in the radiation environment produced by the accelerator. Since the vast majority of the radioactive atoms produced are short-lived, delayed ventilation, with a delay time of one hour from production to exhaust, is used to reduce the radioactivity by roughly one order of magnitude at the air exhaust stack. Activation from the downstream LBNE primary beam, the Target Hall and the absorber areas will be monitored.

4.3.3.6   Enclosure Radiation Monitors

Radiation frisker stations are used to survey personnel and materials being removed from the primary beam, Target Hall and absorber enclosures. Fermilab has a standardized pair of instruments for frisking and determining a material's radioactive class. The laboratory standard frisker and wallflower detectors will be installed at each enclosure entry point. Emergency-exit locations will not be outfitted with frisker stations.

4.4   Alignment (WBS 130.02.04.04)

4.4.1   Introduction

This section summarizes the concepts, methodology, implementation and commissioning of the geodetic surveying (global positioning) efforts for determining the absolute positions of the LBNE beamline components at Fermilab and the underground site for the Far Detector at the Sanford Underground Laboratory. This information is critical to achieving proper aim

of the neutrino beam. From this information, the beam-orientation parameters are computed, as well as the alignment of the LBNE beamline and the Near Detectors.

4.4.2 Design Considerations

Clearly, directing the neutrino beam to intersect the Far Detector located at the Sanford Laboratory, 1,300 km distant from the source, is of paramount importance. Physics requirements, yet to be enumerated, drive the absolute and relative alignment tolerances.

The divergence (spatial spread orthogonal to the line of travel) of the neutrino beam at this distance is on the order of kilometers. The spectrum of neutrino energies varies with their offset from the beam's center line, higher-energy neutrinos closer to the center, lower-energy ones farther out. Lacking LBNE physics requirements at this time, LBNE will base its planning on NuMI's requirement for the energy spread. LBNE will require that the combined effect of all alignment errors must cause less than 2% change in any 1- GeV energy interval in predicting the Far-Detector energy spectrum (without oscillations) from the measured energy spectrum in the Near Site neutrino detector.

To accomplish this, and proportioning the baseline distances of LBNE (Batavia, IL to Lead, SD) to that of MINOS (Batavia, IL to Soudan, MN), the neutrino-beam center must be within $\pm$ 133 m from its ideal position at the Far Detector, corresponding to an angular error of $\pm$ 10^{-4} radians. Also scaling from the LBNE baseline length to that of MINOS, the primary beam must be pointed within $\pm$ 21 m from the center of the Far Detector, corresponding to an angular error of $\pm 1.6 \times 10^{-5}$ radians. Achieving this tolerance requires precise knowledge of the geometry of the neutrino beam. Table 4–1 lists absolute alignment-tolerance requirements for LBNE at one sigma. These are based on the tolerances used for the NuMI beam, with the exception of the Far Detector. The Far Detector tolerance is again proportioned using relative LBNE and MINOS baseline lengths. A Monte Carlo (PBEAM WMC) was used to calculate the effect of misalignments of each beamline element for the determination of the Far Detector spectrum (without oscillations) from the measured Near-Detector spectrum.

The requirement on the relative alignments of the beamline components and the target station components (target and horns) is that they be within $\pm$ 0.35 mm with the requirement based on NuMI experience. To accomplish this, high-accuracy local geodetic and underground networks will be established to support the installation and alignment of the primary-beam components, neutrino-beam devices and the Near Detectors.

Table 4–1: Alignment positioning tolerance requirements (1 sigma)

Primary beam components	±0.45 mm
Target position - each end	±0.5 mm
Horn 1 position - each end	±0.5 mm
Horn 2 position - each end	±0.5 mm
Decay pipe position	±20 mm
Downstream Hadron monitor	±25 mm
Muon monitors	±25 mm
Near Detectors	±25 mm
Far Detector	±21 m

4.4.3   Reference Design

4.4.3.1   Geodetic Determination of the Global Positions

The computation of the geometric parameters of the beam trajectory, expressed in terms of the azimuth and the slope of the vector joining the two sites, requires precise knowledge of the absolute positions of the two ends of the vector, at the near and far sites.

The geodetic orientation parameters of the beam, based on the absolute and relative positions of the target at Fermilab and the Far Detector at Sanford Lab, will be determined with GPS to a high level of accuracy in conjunction with the national Continuously Observed Reference Station (CORS) network. All other geodetic aspects related to the project, i.e., local geoid modeling, deflection from the vertical, differential tidal variations, plate tectonics, point velocities and precise azimuth determination, will be resolved and confirmed for quality assurance.

The development in the past decade of the CORS System led us to conclude that direct GPS observations of long baselines between survey monuments located at Fermilab and the Sanford Lab site, combined with CORS data, would provide the most precise and reliable results. Connections derived from two or more CORS stations will ensure unprecedented positional integrity without the expense of sending additional receivers and personnel into the field.

As a result of the ongoing collaboration, we will establish a Cooperative Agreement with the National Geodetic Survey (NGS) for determining the coordinates of several points belonging to the Fermilab and Sanford Lab networks in conjunction with the CORS system. In addition to the data analyzed at Fermilab, NGS will compute an independent solution and provide geodetic coordinates for the two sites using the adjacent CORS network.

The GPS observation campaign will follow the NGS specifications. Except for station occupa-

tion time, the specifications are similar to the High Accuracy Reference Network procedures regarding equipment setup, GPS-receiver controls, weather-data collection, and documentation. During three days of observations and using four dual-frequency receivers, three sessions will collect 9-10 hours of data at each site, staggering the observation start times in order to observe the complete satellite constellation orbital period of 12 hours.

The network for determining accurately the coordinates for the Fermilab-Sanford Lab baseline is formed by four CORS stations and the two primary LBNE survey monuments: 66589 at Fermilab, the closest to the designed LBNE Target Hall, and a new monument near Sanford Lab's Yates access shaft, for which the most GPS observation data will be collected. From the CORS stations adjacent to the main Fermilab-Sanford Lab baseline, four were selected, two on each side of the vector in a balanced manner. Figure 4–1 shows a map of the Midwest CORS stations with the proposed network superimposed.
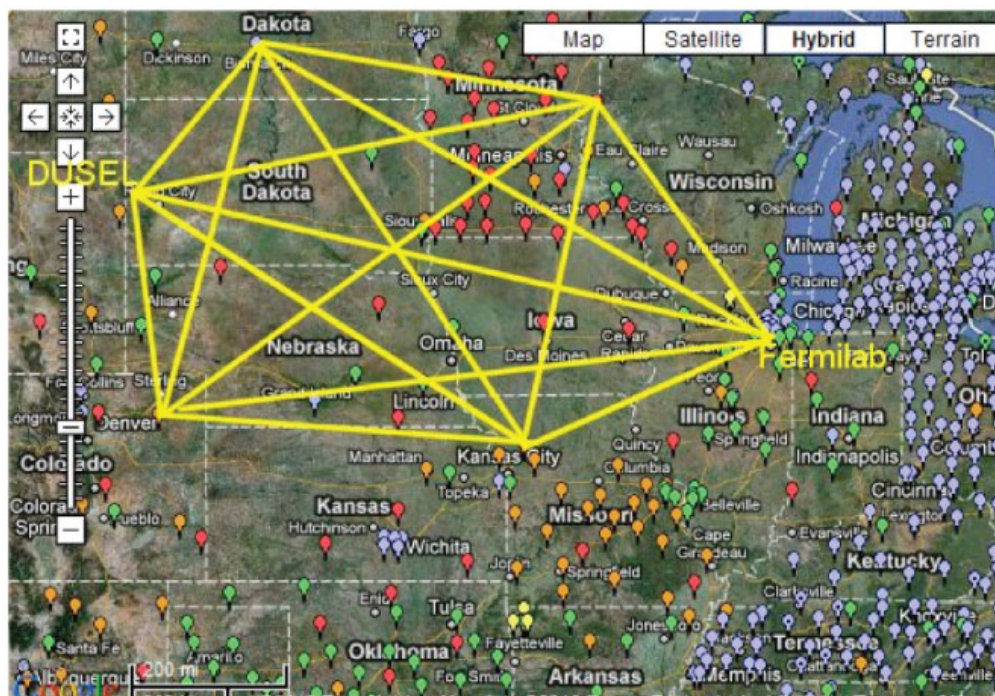

Figure 4–1: GPS network tying Fermilab and Sanford Lab to the CORS system.

The vector solutions for the network will be processed by combining the GPS data collected by Fermilab with the data collected by the CORS stations that are made available for retrieval via the Internet. To improve the accuracy of the baseline GPS-vector computations, the satellites' precise orbits, made available by NGS, will be used. Observed meteorological data will also be used for modeling the tropospheric effect on the GPS signal propagation.

A minimal-constraint, least-squares adjustment will be performed, consisting of 72 observations (24 vectors). Simulations and past experience from NuMI show the standard deviations of the adjusted coordinates to be in the millimeters range in all three coordinates (longi-

tude/latitude 1–3 mm, ellipsoid height 7–10 mm) at 95% confidence level. As a measure of internal consistency, the *RMS* of the residuals of the adjustment were 2 mm in both latitude and longitude and 6 mm in height as shown in Figure 4–2 *a* and *b*.

The high quality of this network will be further confirmed by computing standard deviations for the spatial distances and height differences for all adjusted vectors using variance-covariance propagation. Past experience from NuMI shows that standard deviations for the spatial distances are less than 5 mm (this includes lines across the network). The height differences have standard deviations of 10–15 mm.
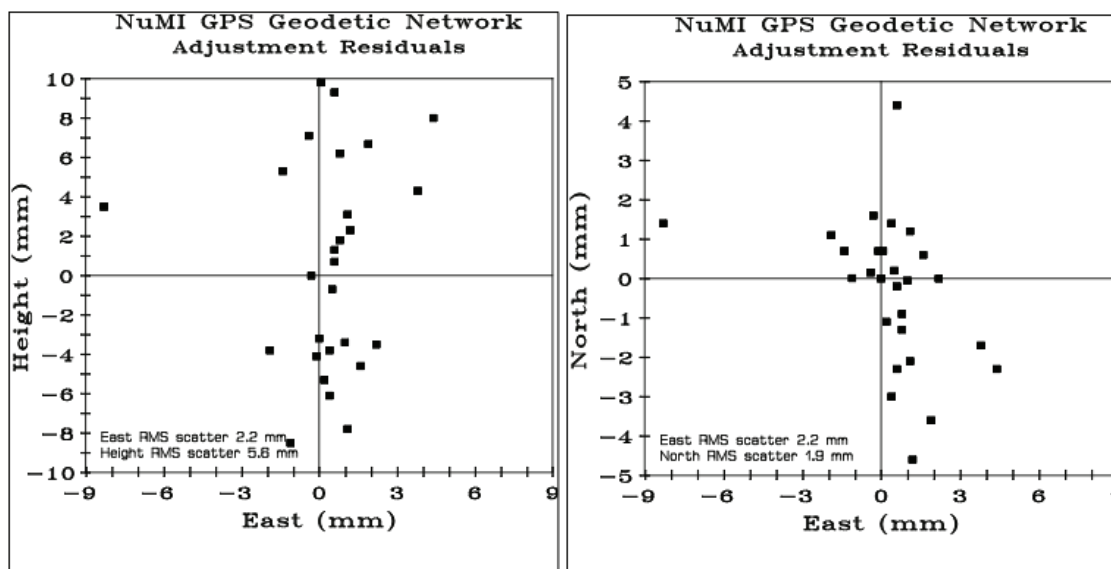

Figure 4–2: Residuals in latitude/longitude (left) and residuals in height (right)

Past experience from NuMI shows that a comparison between the two sets of results, computed independently by Fermilab and NGS, indicated differences on the mm level for the longitude and latitude and amounting up to 10 mm in height. These differences can be explained by the fact that the computations were performed independently in two reference frames: (International Terrestrial Reference Frame (ITRF96) and North American Datum (NAD 83), and the computations did not account for temporal tidal variations. The NAD 83 reference frame is defined such that the North American tectonic plate does not move as a whole relative to it. On the other hand, relative to the ITRF, even points located on the rigid part of the North American tectonic plate move continuously at rates ranging from 9 to 21 mm/year in the United States.

The proposed method for determining the location at the 4850-level of the Sanford Lab with respect to the geodetic coordinates system established at the surface is through inertial-survey techniques. Based on past experience from NuMI, Fermilab will contract The Department of Geomatics Engineering from the University of Calgary to perform a survey through the Yates and Ross shafts using a HG Honeywell 2001 Inertial Navigation System

(INS) unit. Given the large divergence of the neutrino beam, the only requirement will be that the *RMS* be below 1 meter.

The inertial-survey technique makes use of an Inertial Measuring Unit (IMU) composed of three accelerometers and three gyroscopes to output specific forces and respective angular velocities from the orthogonal sensor triads. The outputs are used in a dead-reckoning method which after initialization provides 3D geodetic coordinates at a high data rate. The accuracy of the results depends not only on the quality of the hardware, but also on the method used to estimate systematic errors inherently present in the sensors.

After the calibration of the inertial system, multiple determinations will be performed by running the unit, which will be rigidly attached in the center of the elevator car, through the access shafts between the surface and the 4850L. For NuMI, the comparison between the runs showed an agreement of 0.040 m in height and longitude and about 1 m in latitude. Although it met the given requirements, the latitude discrepancy was most likely caused by an initial azimuth misalignment between the IMU system and the surface geodetic-control system, which LBNE will correct by additional observations.

The geodetic coordinates provided by the tie to the CORS national network and the updated location of the 4850L at the Sanford Laboratory provided by the inertial-system survey will be used for the final computation of the geometric parameters of the beam trajectory.

4.4.3.2   Primary Surface Geodetic Network at Fermilab

The geodetic reference for supporting the construction and positioning of the LBNE project is derived from a high-accuracy local surface network. The existing Fermilab/MI master control network, which has a relative positional accuracy better than 2 mm, includes the monuments surveyed during the CORS tie campaign, described earlier in section 4.4.3.1, and will be supplemented with six geodetic monuments, providing densification around the tunnel access shafts. Figure 4–3 shows a simplified version of the network geometry.

The LBNE absolute-positioning-tolerance requirements call for extensive combined GPS, terrestrial and astronomic surveys. The computations will be performed in the NAD 83 system, which uses the Geodetic Reference System (GRS 80), which consists of a global reference ellipsoid. Simulations and past experience from NuMI show that minimal-constraint least-squares adjustment consisting of more than 410 observations will yield absolute error ellipses in the mm range at the 95% confidence level.

Comparison between computational models shows differences up to 5 mm, consistent with the expected values. Furthermore, this is also an indication that there are no local gravity anomalies (local variations in the gravity field) not modeled by the national model for this area, at least at this level of sensitivity. The LBNE beamline falls in the 1.5-mm range of those

Figure 4–3: Fermilab LBNE surface geodetic network.

differences, well within the estimated accuracy for the local or the national geoid models. The national geoid model was considered sufficient to cover the tolerance requirements for the project. As a result, the Geoid93 and Deflec93 provided by NGS were used in our geodetic computations.

4.4.3.3　High-Accuracy Underground Control Network

The final primary-beam trajectory is of crucial importance to LBNE. To minimize the relative errors between the beamline components, target and horn-alignment and to provide dynamic monitoring of their relative positions, a high-accuracy underground control network with strict tolerances will be implemented. Establishment of relative component positions to ± 0.35 mm (1σ) throughout the extraction enclosure, transfer tunnels and Target Hall is expected.

Network simulations of different models have led to an optimized design of the number (six) and locations of vertical sight risers. This is sufficient to provide azimuthal constraints and to control the scale of the network.

The configuration of the underground network is limited by the geometry of the tunnels and halls. Studies and past experience with NuMI have led to a configuration based on chains of polygons. In order to improve the isotropy of the network and compensate for the weaknesses caused by the poor ratio between the sides of polygons, additional measurements spanning adjacent polygons are added. Redundant observations are needed to ensure quality and uniformity of accuracy. In order to improve the overall spatial geometry, the network will alternate monuments permanently embedded in the enclosure's floor with those rigidly

attached to walls.

The underground control network will be measured with the Laser Tracker and processed as a 3D trilateration network (distances derived from Laser Tracker observations) and constrained to the vertical datum provided by precision underground levelling. Other types of observations include Mekometer distances, precision angles, and gyro-azimuths measured over long underground baselines, which provide additional information to control the scale in the underground environment, to study the behavior of the network during adjustment and to check the azimuth of the adjusted coordinates.

In simulations and past experience from NuMI, relative errors between control points have remained below ± 0.35 mm at the 95% confidence level throughout the network. Figure 4–4 show the distribution of the standardized observation residuals for the Pre-Target tunnel/Target Hall (on the left) and for the MINOS near detector networks (on the right).
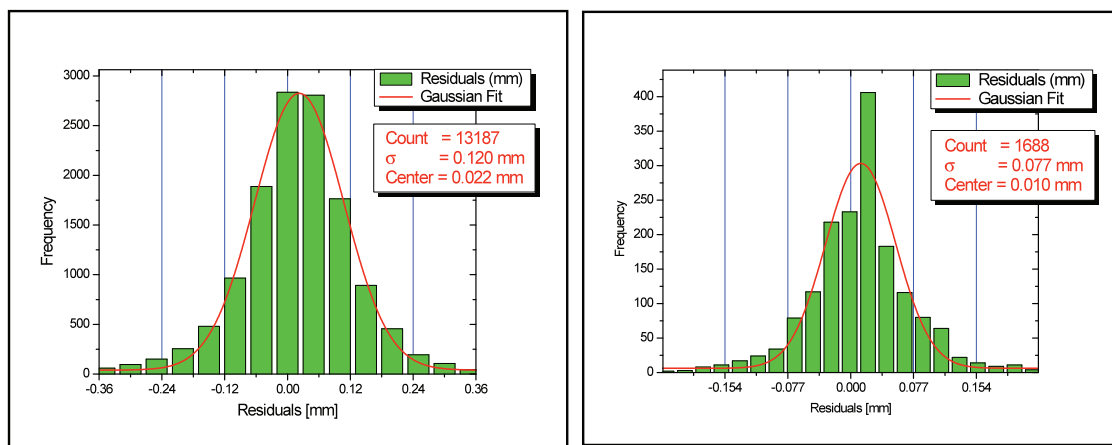

Figure 4–4: Distribution observation residuals for the Pre-Target tunnel and Target Hall in MINOS (left) and the Near Detector Hall in MINOS (right)

4.5 Installation Coordination (WBS 130.02.04.05)

This activity provides the management oversight of the day-to-day activities taking place in the installation areas and the framework for sequencing and scheduling the installation tasks. Therefore its role is primarily the *coordination* of installation activities and will be led by an Installation Coordinator. The technical responsibility for the design, fabrication and installation of each element of the Beamline subproject resides in its appropriate subsystem.

Each area (e.g., Target Area, absorber and so on) will have a Floor Manager whose job it is to oversee the overall installation activity taking place in the area and to supervise the daily activities of task managers who are leading the work crews in each area. Floor Managers will report directly to the Installation Coordinator.

During installation, a regular end-of-week installation meeting will be held with the Installation Coordinator and Deputy, the Floor Managers from all areas, and the ES&H Manager to review the progress of the week and discuss issues that have arisen.

In an additional weekly meeting, the Floor Managers will meet with the L3 and L4 managers to review progress, relate information from the previous installation meeting and discuss the tasks being considered for the upcoming time periods. This discussion will include lab and project management and ES&H representatives. It is expected that as issues arise which impact cost and schedule, they will be discussed if not resolved.

Daily "toolbox" meetings for everyone working in the areas will be held to outline the activities of the day and discuss any specific issues or concerns.

References

[1] Particle Physics Project Prioritization Panel, "US Particle Physics: Scientific Opportunities; A Strategic Plan for the Next Ten Years," 2008. `http://science.energy.gov/~/media/hep/pdf/files/pdfs/p5_report_06022008.pdf`.

[2] LBNE Science Collaboration, LBNE Case Study Report, Liquid Argon TPC Far Detector, Draft Version 1.2, October 2, 2011.

[3] T. Akiri *et al.*, "The 2010 Interim Report of the Long-Baseline Neutrino Experiment Collaboration Physics Working Groups." arXiv:1110.6249.

[4] LBNE Project Office, "LBNE Project Management Plan," tech. rep., FNAL, 2011. LBNE Doc 2453.

[5] "Alternatives Analysis." LBNE Project Management Team - LBNE Doc 4382, 2012.

[6] I. Kourbanis, "MI Beam Power for Different Energies," tech. rep., 2010. LBNE Doc 3716 `http://beamdocs.fnal.gov/AD-public/DocDB/ShowDocument?docid=3716`.

[7] "Accelerator Performance Charts." `http://www-%bd.fnal.gov/pplot/index.html`.

[8] "Neutrino Beamline Requirements Documentation," tech. rep. LBNE Doc 4835 `http://lbne2-docdb.fnal.gov:8080/cgi-bin/ShowDocument?docid=4835&version=2`.

[9] "Methodical Accelerator Design (MAD)." CERN - Accelerator Beam Physics Group `http://mad.home.cern.ch/mad/`.

[10] D.Harding. Magnet Test Facility measurement database private communication (Fermilab AD) .

[11] V. Bocean (Fermilab PPD/Alignment) private communication.

[12] Fermilab, "Fermilab ES&H Manual ." `http://esh.fnal.gov/xms/FESHM`.

[13] "Fermilab Engineering Manual, v07/10," tech. rep., 2010. `http://www.fnal.gov/directorate/documents/FNAL_Engineering_Manual.pdf`.

[14] I.Baishev, A.Drozhdin, N.Mokhov, and X.Yang, "STRUCT Program User's Reference Manual," 1994. SSC Doc: SSCL–MAN–0034 `http://www-ap.fnal.gov/users/drozhdin/`.

[15] N. Mokhov and S. Striganov, "MARS15 Overview, Hadronic Shower Simulation Workshop AIP Proceedings 896," tech. rep., 2007. Fermilab-Conf-07-008-AD.

[16] "NuMI Technical Design Handbook, Sec. 4.4," tech. rep., 2003. `http://www-numi.fnal.gov/numwork/tdh/tdh_index.html`.

[17] V.Zarucheisky *et al.*, "NOvA Target Hall Baffle Specification," 2010.

[18] M.Martens, J.Hylen, and K.Anderson, "Target and Horn Configuration for the NOvA Experiment," tech. rep., 2009. `http://www.fnal.gov/directorate/documents/FNAL_Engineering_Manual.pdf`.

[19] C.Densham *et al.*, "Conceptual Design Study of the LBNE Target and Beam Window," tech. rep., 2010. LBNE Doc 2400.

[20] V.Garkusha *et al.*, "700 kW target design study - IHEP 2009 Accord report," tech. rep., 2010. LBNE Doc 2423.

[21] N.Simos *et al.*, "Long Baseline Neutrino Experiment (LBNE) Target Material Radiation Damage from Energetic Protons of the Brookhaven Linear Isotope Production (BLIP) Facility," tech. rep., 2012. LBNE Doc 5724.

[22] B.Lundberg, "Specifications for Beam Simulations," tech. rep., 2009. LBNE Doc 2161.

[23] "NuMI Technical Design Handbook, Sec. 4.2.4," tech. rep., 2003.

[24] N.Mokhov, "The Mars Code System User's Guide," tech. rep., 2009. Fermilab-FN-628.

[25] J. Goodman, *Mechanics Applied to Engineering.* Longman, Green and Company, London, 1889.

[26] N.Mokhov *et al.*, "LBNE Target Station, Decay Volume and Hadron Absorber: Radiation and Thermal Analysis Modeling," tech. rep., 2011. LBNE Doc 2241.

[27] "ANSYS Engineering Simulation." `http://www.ansys.com`.

[28] E.Rivera, "NuMI Hadron Absorber Finite Element Analysis for NOvA Beam Energy'," tech. rep., 2010.

[29] "Fermilab Radiological Control Manual, and references therein," tech. rep. /url-http://esh.fnal.gov/xms/FRCM.

[30] D. Reitzner and K. Vaziri, "LBNE Groundwater Shielding Requirements for Shallow and Deep Beam," tech. rep., Fermilab. LBNE Doc 4052 `http://lbne2-docdb.fnal.gov:8080/0040/004052/004/ShieldingRequirementsGroundwater5.docx`.

[31] N. Mokhov, "LBNE Absorber MARS Studies." LBNE Doc 2205 `http://lbne2-docdb.fnal.gov:8080/0022/002205/001/LBNE_ABS_norm_mokhov_031610.pdf`.

[32] N. Mokhov, "Muon Range-out at LBNE." LBNE Doc 4199 `http://lbne2-docdb.fnal.gov:8080/0041/004199/001/LBNE_range_out_mokhov_082411.ppt`.

[33] "LBL Consultant Report on NuMI Tritium in Beampipe Shielding," tech. rep. LBNE Doc 2533.

[34] N. Mokhov, "Target Chase MARS Calculations." LBNE Doc 3216 `http://lbne2-docdb.fnal.gov:8080/0032/003216/001/LBNE-doc-3216-mokhov-120810.pdf`.

[35] D. Reitzner, "LBNE Dose at Site Boundary." LBNE Doc 4128 `http://lbne2-docdb.fnal.gov:8080/0041/004128/002/skyshine_on_axis_MI10_revisited.pptx`.

[36] P. Hurh, "LBNE Remote Handling Component List and Shielding Calculations," 2012.

[37] V.Graves, A.Carroll, and T.Burgess, "Conceptual Design of the Remote Handling Facilities for the Long-Baseline Neutrino Experiment," tech. rep., 2010. ORNL/TM-2010/125, LBNE DocDB 2483.

[38] V.Graves, A.Carroll, and T.Burgess, "Conceptual design of the target handling system for the long-basline neutrino experiment," tech. rep., 2010. ORNL/TM-2010/00, LBNE DocDB 2627.

[39] N. Mokhov, "Recent MARS15 Developments," tech. rep., 2010. Fermilab-Conf-10-518-APC.